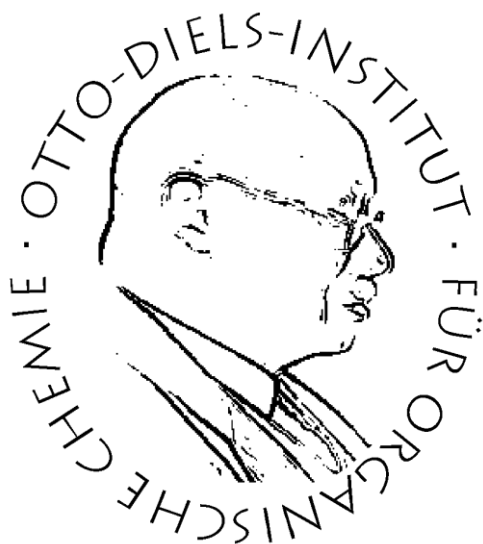


**Sweet switches: Azobenzene glycosides as photosensitive
lectin inhibitors in solution and on surfaces**



Dissertation

in fulfillment of the requirements for the degree “Dr. rer. nat.”
of the Faculty of Mathematics and Natural Sciences
at University of Kiel

submitted in English by

Vijayanand Chandrasekaran, M.Sc

Kiel 2013

First referee: Prof. Dr. Thisbe K. Lindhorst

Second referee: Prof. Dr. Ulrich Lüning

Date of oral examination: 09-07-2013

Approved for publication: 11-07-2013

Signed: Prof. Dr. Wolfgang. J. Duschl, Dean

Die vorliegende Arbeit wurde unter Anleitung von
Prof. Dr. Thisbe K. Lindhorst
am Otto Diels-Institut für Organische Chemie
der Christian-Albrechts-Universität zu Kiel
im Zeitraum von November 2008 bis Juli 2013 angefertigt.

Frau. Prof. Dr. Thisbe K. Lindhorst danke ich für die Überlassung des Themas, die zahlreichen Diskussionen und ihr stetes Interesse am Verlauf der Arbeit.

Declaration

The research work embodied in this thesis has been carried out under the supervision of Prof. Dr. Thisbe K. Lindhorst at the Institute of Organic Chemistry, University of Kiel, Germany. This work is original and has not been submitted either partially or wholly as part of a doctoral degree to another examining body. This thesis has been prepared subject to the Rules of Good Scientific Practice of the German Research Foundation.

Vijayanand Chandrasekaran

Contents

Abstract	V
Zusammenfassung	VI
Abbreviations	VII
1 Introduction	1
1.1 Carbohydrate-protein interactions	2
1.2 Multivalency	4
1.3 Bacterial adhesion	6
2. Photoswitches	9
2.1 Photoswitchable molecules	9
2.2 Azobenzene isomerization	13
2.3 Azobenzene derivatives in biological chemistry	15
2.4 Azobenzene derivatives in glycobiology	18
3. Synthesis and properties of azobenzene glycoconjugates in solution	20
3.1 <i>Synthesis and testing of the first azobenzene mannobioside as photoswitchable ligand for the bacterial lectin FimH</i>	21
V. Chandrasekaran, K. Kolbe, F. Beiroth, T. K. Lindhorst*	
<i>Beilstein J. Org. Chem.</i> 2013 , 9, 223-233.	

3.2	Sweet switches: Synthesis and photochemical properties of azobenzene glycosides	45
	V. Chandrasekaran, E. Johannes, H. Kobarg, F. D. Sönnichsen, T. K. Lindhorst*	
	<i>Chem. Eur. J. manuscript in preparation.</i>	
3.3	Sweet switches: Azobenzene glycoconjugates by click chemistry	78
	V. Chandrasekaran, T. K. Lindhorst*	
	<i>Chem. Commun.</i> 2012 , <i>48</i> , 7519-7521.	
3.4	UV-Vis spectroscopy of azobenzene glycosides in the presence of bacteria	113
	 <i>Inhibition of bacterial adhesion to live human cells: Activity and cytotoxicity of synthetic mannosides</i>	
	118	
	M. Hartmann, H. Papavlassopoulos, V. Chandrasekaran, C. Grabosch, F. Beiroth, T. K. Lindhorst*, C. Röhl*	
	<i>FEBS Lett.</i> 2012 , <i>586</i> , 1459-1465.	
4	Preparation and applications of azobenzene glycosides on surfaces	143
4.1	Monitoring of trans→cis isomerization of azobenzene glyco-SAMs on gold surfaces using IRRAS	144
	V. Chandrasekaran, K. Kathirvel, H. Jacob, F. Tuczec, T. K. Lindhorst*	
	<i>J. Colloid Interface Sci. manuscript in preparation.</i>	

4.2	<i>Photosensitive glyconanoparticles: A new tool to switch carbohydrate-protein interactions</i>	176
	V. Chandrasekaran, M. B. Thygesen, K. J. Jensen, T. K. Lindhorst * <i>Chem. Eur. J. manuscript in preparation.</i>	
5	Azobenzene glycoconjugates for conjugation with anti-freeze proteins	219
6	Resume	228
	Appendix	
	References	233
	Permissions for reprinting of Figures	239
	Acknowledgement	249
	Curriculum Vitae	251

All experimental data of interest, the corresponding compound numbers and references are described in the respective articles, manuscript or in the supplementary materials. A separate experimental part has not been given in this thesis. However, references for the introduction can be found in appendix.

Abstract

The glycocalyx of eukaryotic cells plays a crucial role in many biochemical communication processes. The molecular mechanisms underlying these processes are difficult to investigate and are still not fully understood. For example, non-covalent interactions between carbohydrate ligands and their lectin receptors are accompanied by conformational changes between the interacting partners. Such changes might reflect a principal conformational control of carbohydrate-protein interactions, which has received only little attention until to date. Hence, the central focus of this thesis is to synthesize photoswitchable glycomimetics and investigate the role of light-induced conformational changes in carbohydrate recognition. Photoinduced changes in glycoconjugates have been accomplished already earlier by introduction of a photoswitchable unit, namely azobenzene. $E \rightarrow Z$ isomerization of azobenzenes have been utilised in photocontrolling biomolecules like nucleic acids and peptides. Thus azobenzene glycoconjugates are principal target molecules of our research. Photoirradiation of azobenzene glycosides at ~ 365 nm induces $E \rightarrow Z$ isomerization leading to a certain E/Z ratio in the photostationary state (PSS). The special features of azobenzene glycoconjugates featuring an $E \rightarrow Z \rightarrow E$ isomerization option in solution will eventually allow us to utilise this type of molecules with α -D-mannose-specific lectins, such as the bacterial lectin FimH. In addition, azobenzene glycosides can be attached to different scaffolds or immobilised on surfaces to test as well as switch bacterial adhesion (Fig. 1).

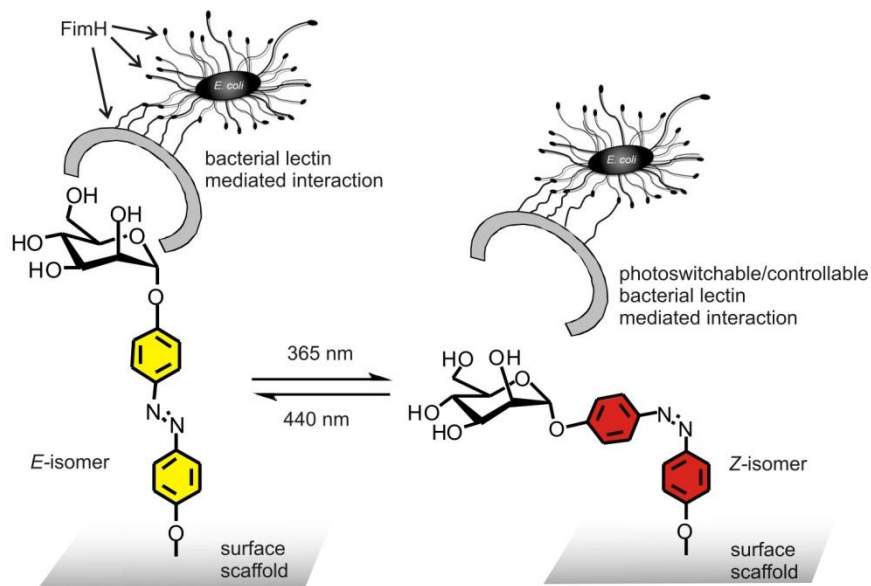


Figure 1: Vision of photoswitchable bacterial adhesion employing $E \rightarrow Z$ isomerization of azobenzene glycosides.

In this context, a new class of azobenzene glycosides were synthesized and their photochromic properties were studied in solution by ^1H NMR and UV-Vis spectroscopy and they were tested as inhibitors for type 1 fimbriae-mediated bacterial adhesion. To mimic the cell surface glycocalyx, azobenzene glycosides were immobilised on gold surfaces to form photoswitchable glyco-SAMs. Photoisomerization was performed on the gold surface and monitored by IRRAS and UV-Vis spectroscopy. To get insight in the conformational control of carbohydrate recognition in a multivalence context, photosensitive glyconanoparticles were also prepared and binding efficiency of different isomers was tested with the lectin ConA.

Zusammenfassung

Die Glykokalyx von eukaryontischen Zellen spielt eine entscheidende Rolle in vielen biologischen Kommunikationsprozessen. Die molekularen Mechanismen, die diesen Prozessen unterliegen, sind schwer zu untersuchen und bisher immer noch nicht vollständig verstanden. Beispielsweise gehen nicht-kovalente Wechselwirkungen zwischen Kohlenhydratliganden und deren Lektinrezeptoren immer mit Konformationsänderungen der beteiligten Interaktionspartner einher. Solche Änderungen weisen auf eine prinzipielle Konformationskontrolle von Kohlenhydrat-Protein-Wechselwirkungen hin, der bislang nur wenig Aufmerksamkeit geschenkt wurde. Daher liegt der Schwerpunkt der hier vorliegenden Arbeit in der Synthese von photoschaltbaren Glykomimetika und der Untersuchung lichtinduzierter Konformationsänderungen in Kohlenhydraterkennungsprozessen. Die Untersuchung photoinduzierter Änderungen in Glykokonjugaten wurde durch die Einführung einer photoschaltbaren Einheit möglich, dem Azobenzol. Die $E \rightarrow Z$ -Isomerisierung von Azobenzolen wurde bereits zur Photokontrolle von Biomolekülen wie Nukleinsäuren und Peptiden genutzt. Daher sind Azobenzolglykokonjugate von großem Interesse für die Forschung. Die Bestrahlung von Azobenzolglykosiden mit einer Wellenlänge von ~ 365 nm induziert eine $E \rightarrow Z$ Isomerisierung, was zu einem bestimmten $E \rightarrow Z$ -Verhältnis im photostationären Zustand (PSS) führt. Diese speziellen Eigenschaften von Azobenzolglykokonjugaten, besonders die Möglichkeit von einer $E \rightarrow Z \rightarrow E$ -Isomerisierung in Lösung, könnte es ermöglichen, diese Moleküle als Testsysteme zur Untersuchung α -D-Mannose-spezifischer Lektine (wie zum Beispiel dem bakteriellen Lektin FimH) zu nutzen. Des Weiteren können die erhaltenen Azobenzolglykoside zu verschiedenen Derivaten funktionalisiert oder auf Oberflächen wie Gold immobilisiert werden, um bakterielle Adhäsion FimH zu testen und zu schalten (Abb. 1).

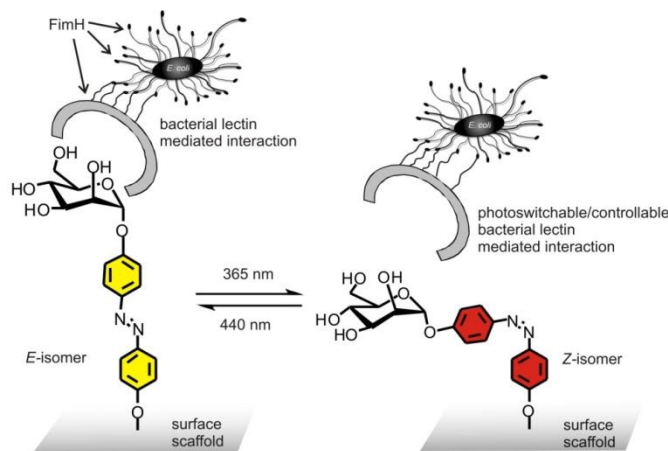


Abbildung 1: Die Vision schaltbarer bakterieller Adhäsion durch $E \rightarrow Z$ -Isomerisierung von Azobenzolglykosiden.

In diesem Zusammenhang wurde eine neue Klasse von Azobenzolglykosiden synthetisiert. Deren photochrome Eigenschaften wurden in Lösung mittels $^1\text{H-NMR}$ - und UV-Vis-Spektroskopie untersucht. Sie wurden außerdem als Inhibitoren für die Typ-1-Fimbrien- vermittelte bakterielle Adhäsion getestet. Um die glycosylierte Zelloberfläche zu mimikrieren wurden photoschaltbare Glyko-SAMs durch Immobilisierung von Azobenzolglykosiden auf einer Goldoberfläche hergestellt. Die Photoisomerisierung wurde auf den Goldoberflächen durchgeführt und mittels IRRAS sowie UV-Vis-Spektroskopie verfolgt. Um einen Einblick in die konformative Kontrolle von Kohlenhydrat-Erkennungsprozessen in einem multivalenten Kontext zu bekommen, wurden auch lichtempfindliche Glykonanopartikel synthetisiert. Dabei wurden die Bindungseffizienzen der zwei verschiedenen Isomere mit dem Lektin ConA getestet.

Abbreviations

Ac	Acetyl
atm.	Atmosphere
ATR	Attenuated total reflection
CCA	α -cyano-4-hydroxycinnamic acid
CRD	Carbohydrate Recognition Domain
Cy	Cyclohexane
DBU	1,8-Diazobicyclo[5.4.0.]undec-7-en
DEAD	Diethylazodicarboxylate
DIAD	Diisopropylazodicarboxylate
DIC	<i>N,N'</i> -Diisopropylcarbodiimide
DLS	Dynamic light scattering
DMF	Dimethylformamide
DMSO	Dimethylsulfoxide
ESI	Electrospray ionization
Et	Ethyl
Glc	Glucose
GFP	Green fluorescent protein
HATU	(<i>O</i> -(7-azabenzotriazol-1-yl)- <i>N,N,N',N'</i> -tetramethyluronium-hexafluorophosphate)
mg	Milligram

MALDI	Matrix-Assisted Laser Desorption Ionisation
Man	Mannose
Me	Methyl
MeMan	Methyl- α -D-mannoside
min	Minutes
NMR	Nuclear Magnetic Resonance
PEG	Polyethyleneglycol
<i>p</i> NPMan	<i>p</i> -Nitrophenylmannoside
PSS	Photostationary states
PTSA	<i>p</i> -Toluenesulfonic acid
RT	Room Temperature
R_f	Retention factor
SAM	Self-assembled Monolayer
TBDMS	<i>tert</i> -Butyldimethylsilyl
THF	Tetrahydrofuran
UV-Vis	Ultraviolet and Visible

1. Introduction

Carbohydrates are one of the most important fundamental classes of biomolecules next to proteins and nucleic acids. These are body's ideal fuel for many biological functions by providing the energy required for muscles and the molecular diversity for information exchange. Carbohydrates are composed of one or more sugar units, the simplest form is the monosaccharide. In monosaccharides, the hydroxyl group at the anomeric position can undergo a glycosylation reaction, a process in which carbohydrates as glycosyl donors are attached to other carbohydrates or non-carbohydrate molecules as the glycosyl acceptors. The resulting glycosidic bond be α - or β - configured. On the cell surface, carbohydrates are covalently linked to other biomolecules like proteins (glycoproteins, proteoglycans) or lipids (glycolipids, gangliosides) and thus exist in the form of glycoconjugates.^[1] Specific interactions of these glycoconjugates with proteins are of high crucial importance for biological recognition events like cell adhesion, cell communication and receptor binding. Glycoconjugate interactions occurring on the cell surfaces are not fully understood until today. Thus, studying the complexity of structure, function and biological relevance of carbohydrates on the cell surface is the central focus of glycobiological research.

Each eukaryotic cell surface is covered by complex carbohydrates, forming a layer that is called "glycocalyx". Glycocalyx constituents are arranged on cell surfaces in a diverse and heterogeneous manner (Fig. 1.1).^[2]

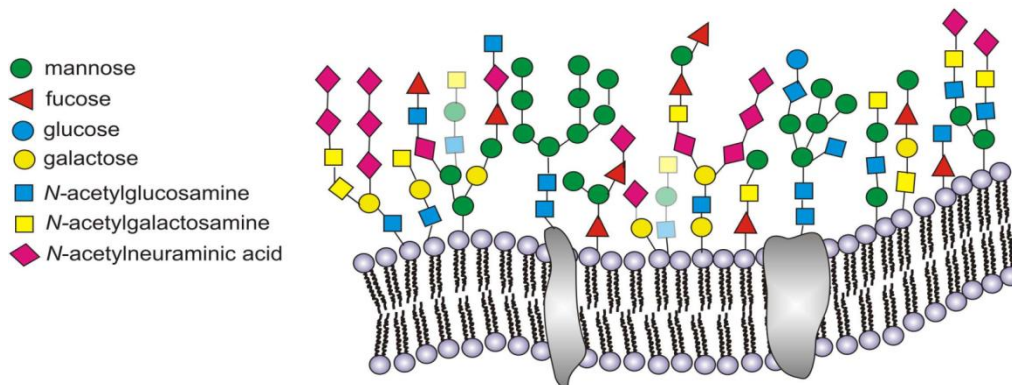


Figure 1.1: Schematic representation of different carbohydrates on the cell surface.

Each cell has its own glycocalyx characteristics and specific glycosylation pattern.^[3] The quality of the glycocalyx distinguishes disease cells and healthy cells and plays a crucial role in many biological processes.

An especially interesting example for the specific type of glycosylation of cells is the blood group antigens. A small structural variation in the terminal saccharide unit of a blood group glycoconjugate results in four different types of blood groups namely A, B, AB and O (Fig. 1.2).^[4] In blood group A, B or AB the galactose moiety is glycosylated with *N*-acetylgalactosamine or a galactose moiety, respectively whereas in blood group O, the terminal end of galactose is not further glycosylated.

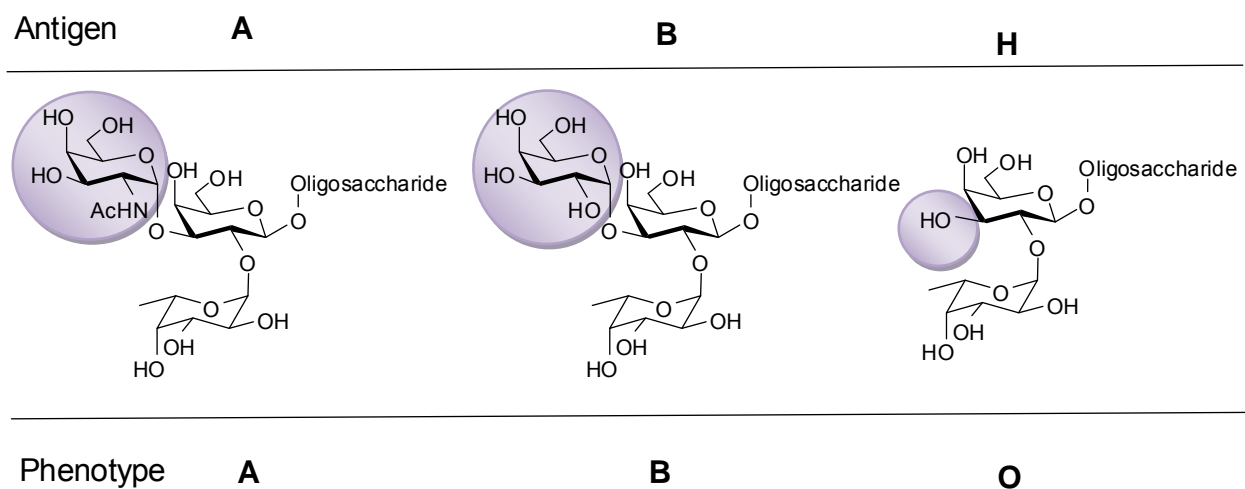


Figure 1.2: Presentation of different carbohydrate antigens in various blood groups.

1.1 Carbohydrate-protein interactions

Proteins that bind certain carbohydrates specifically are called “lectins”. The first lectin was discovered in plants and later found in other organisms like bacteria, viruses, and animals as well as humans. Lectins contain one or more binding sites for specific non-covalent complexation of carbohydrate ligands. Lectins are non-immunogenic in origin

and have no enzymatic function.^[5-6] Some of the most common monosaccharides that are recognized by lectins are D-glucose, D-galactose, D-mannose, *N*-acetylglucosamine, *N*-Acetylgalactosamine, L-fucose and *N*-Acetylneuraminic acid (Fig. 1.3).^[7]

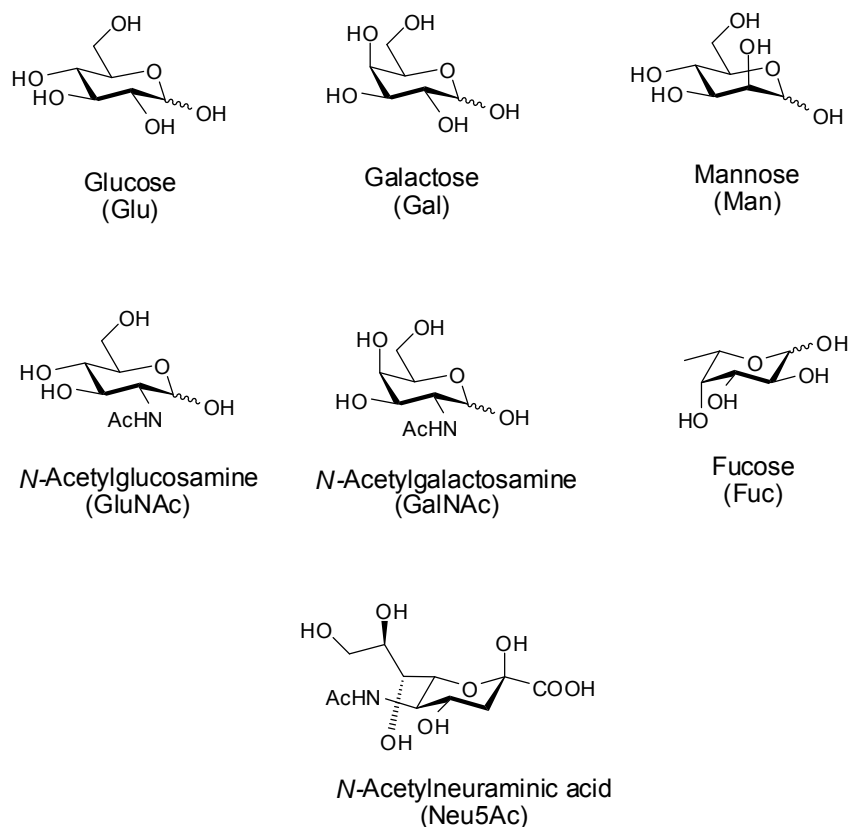


Figure 1.3: Examples of some monosaccharide structures that are recognized by lectins.

Carbohydrate-protein interactions are strongly governed by hydrogen bonds, which are often mediated via water molecules, tight metal coordination with Ca^{2+} or Mn^{2+} ions, respectively, van der Waals and hydrophobic interactions.^[8] Based on the amino acid sequence and 3D structure of lectins, the most important classes of lectins have been defined as C-type, S-type, and P-type. C-type lectins binds to carbohydrates in a Ca^{2+} -dependent manner. S-type lectins selectively bind to galactose and *N*-acetylgalactosamine, P-type lectins binds to mannose-6-phosphate receptors.^[9]

1.2 Multivalency

Multivalent interactions play a decisive role in biological processes like cell adhesion, cell-cell signaling, attachment of viruses to host cells, etc.^[16-17] Monovalent carbohydrate ligands bind weakly to their binding partners with a binding constant in millimolar to micromolar range. By multivalency, stronger binding is achieved by multiple interactions between carbohydrates and proteins, resulting in an overall high avidity.^[10-12] “Affinity” refers to the strength of monovalent receptor-ligand interactions, whereas “avidity” refers to the strength of association resulting from many weak interactions.^[2] To explain the concept of multivalency effects in carbohydrate-protein interactions the first synthetic multivalent oligosaccharide mimetic was reported in 1978 by Y. C. Lee and co-workers.^[13-14] They found that, a linear increase in number of carbohydrate ligands leads to a logarithmically increased avidity to the receptor protein, an effect that was called “cluster glycoside effect”.

For example, multivalent interactions of a virus to its receptor on the host cell surface leads to stable adhesion (Fig. 1.4a). Since the virus has multiple binding sites, its affinity to the host cell ligands can be effectively increased (Fig. 1.4b). In analogy, multivalent ligands have enormous potential in inhibiting and fighting viruses effectively compared to the respective monovalent ligand (Fig. 1.4c).^[15]

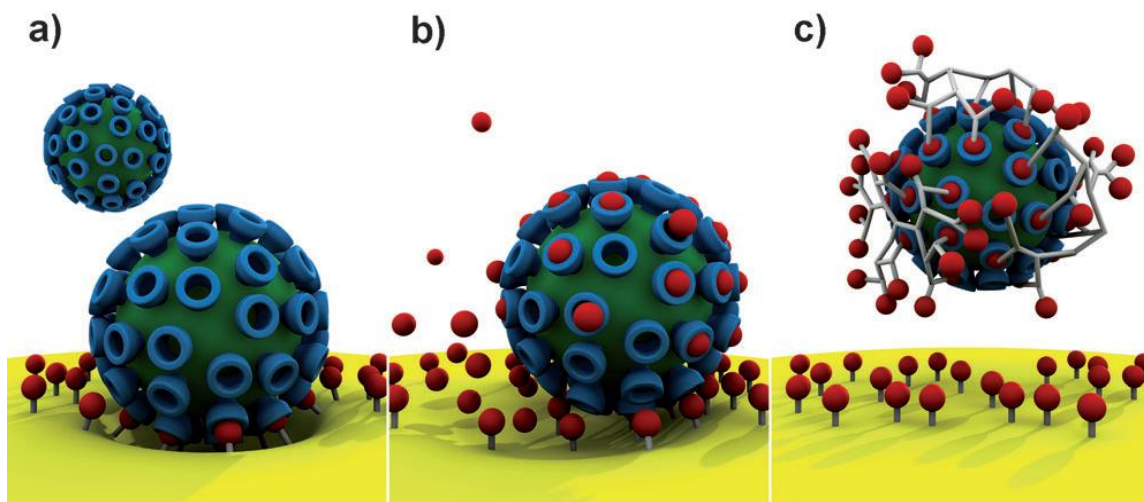


Figure 1.4: a) Multivalent binding of virus to cell surface; b) inhibition by monovalent ligands; c) inhibition by multivalent ligands, more effective than by the monovalent ligands. Adapted with permission from ref. 15. Copyright John Wiley and Sons.

Understanding multivalency effects occurring in natural systems is yet another challenge. There are different possible mechanisms which explain the multivalency effect and some of the relevant mechanisms are mentioned below (Fig. 1.5). In one approach, the strength of multivalent receptor-ligand interactions is stronger than the analogous monodentate receptor-ligand interaction (Fig 1.5a). In another approach, multivalency is enhanced by the secondary binding site along with the primary binding site on the target protein (Fig 1.5b). In the last approach, the strength of multivalent interactions is largely increased due to their ability to cluster their receptors (Fig 1.5c).^[18] Thus, multivalent ligands can exhibit a variety of different activities based on different binding modes.^[19]

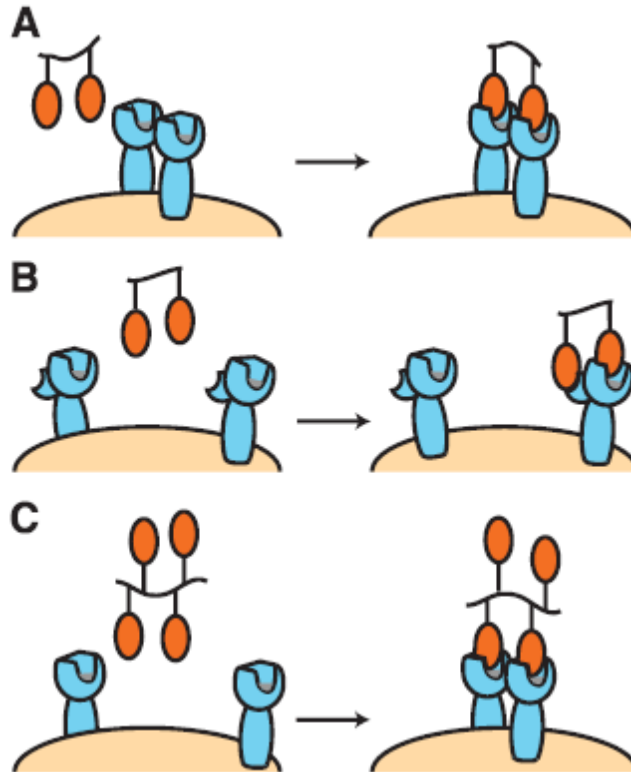


Figure 1.5: Examples for different binding modes in multivalency (organe – carbohydrate; blue – receptor). (a) chelate effect; (b) interaction with primary and secondary binding site of receptor; (c) receptor clustering.^[19]

1.3 Bacterial adhesion

Bacterial infections are usually initiated by adhesion and colonization of bacteria to the host cell surface. For example, adhesion of uropathogenic *Escherichia coli* (UPEC) bacteria to the carbohydrate receptors on the bladder epithelium can cause urinary tract infection and inflammation.^[20] To accomplish adhesion, bacteria utilize adhesive organelles called fimbriae. Fimbriae are hair-like structures with a length between 0.1-2 μm and a width of $\sim 7\text{nm}$ and are expressed on the surface of bacteria (Fig. 1.6a).^[21-22] Mannose-specific bacterial adhesion is mediated by a lectin called FimH that is located at the tips of type 1 fimbriae. The protein FimH consists of two domains, a lectin domain called carbohydrate recognition domain (CRD) and a pilin domain which is required for fimbriae assembly (Fig. 1.6b).^[23-24]

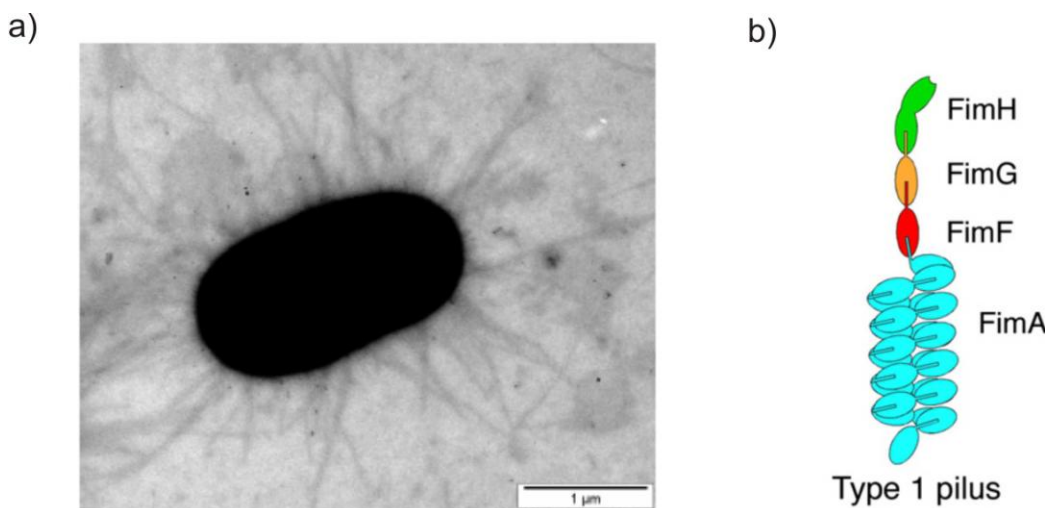


Figure 1.6: (a) Transmission electron micrograph (TEM) image of type 1 fimbriated *E. coli* bacteria. Adapted with permission from ref. 22. Copyright John Wiley and Sons; (b) cartoon of lectin subunit with FimH at the fimbrial tip. Adapted with permission from ref. 23. Copyright Elsevier.

In order to inhibit and to understand type 1 fimbriae-mediated bacterial adhesion, several mannosidic glycomimetics were synthesized and investigated as ligands of FimH.^[22, 25-28] It is known from X-ray studies that the bacterial lectin FimH binds to α -D-mannosyl units (glycone part) with the aglycone part sticking out of the carbohydrate binding site.^[21, 29-31] The entrance of the FimH carbohydrate binding site is flanked by two aromatic tyrosine residues, Tyr48 and Tyr137 forming the so called “tyrosine

gate”.^[24] This hydrophobic gate at the entrance of the FimH carbohydrate recognition domain facilitates π - π interactions with the synthetic mannosidic ligands holding an aromatic aglycon, which in turn increases its affinity for FimH.^[32-33] For example *p*-nitrophenyl α -D-mannoside shows greater inhibitory potency than methyl α -D-mannoside. Inhibition of bacterial adhesion by designed antagonists can be employed in the context of a specific antiadhesive therapy.^[34] Eventually antiadhesives could become therapeutics against infections like urinary tract infections.^[32, 34-35]

1.4 Glycomimetics

In order to understand the molecular details of carbohydrate-protein interactions occurring on the cell surface and its biological functions, an ultimate requirement is the isolation of the involved carbohydrate ligands from natural sources. However, to get them in required quantity in high purity for study their functions in detail is highly demanding. For this, one has to rely on the synthetic approach where a synthetic chemist also plays an important role in making interesting glycomimetics to unravel the involved biochemical processes. Designing glycomimetics is an approach of making carbohydrate molecules according to the naturally occurring carbohydrate ligands with various alterations.^[36-38] These glycomimetics are useful tools with structural features which facilitate the understanding of binding specificity and other fundamental properties of carbohydrate-protein interactions, paving the way to important biochemical answers.^[19]

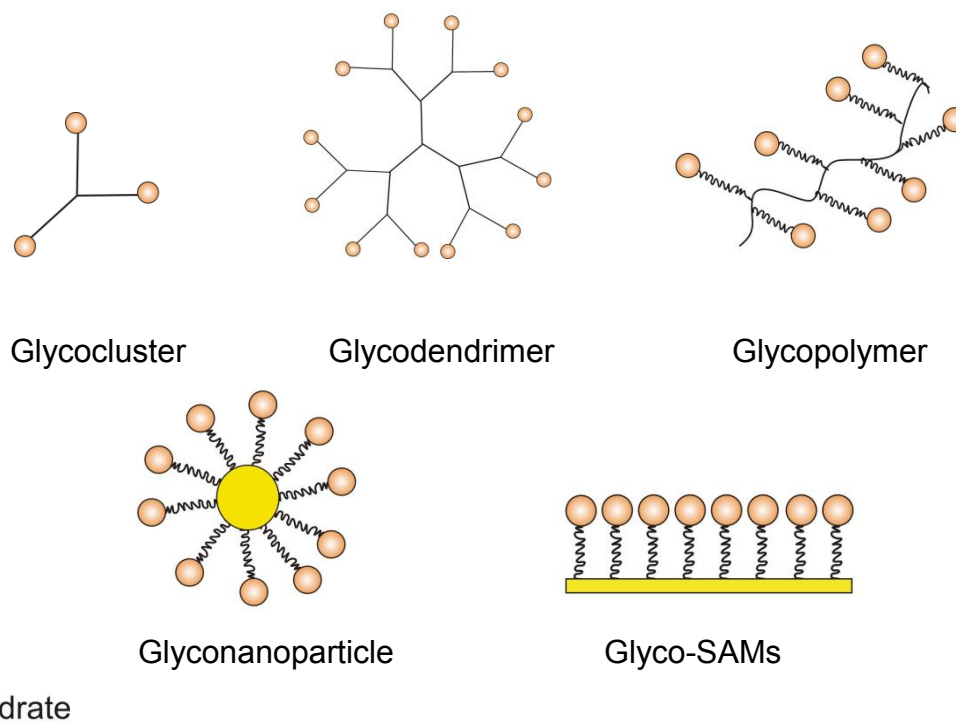


Figure 1.7: Different types of multivalent glycomimetics.

A considerable amount of monovalent and multivalent glycomimetics have been synthesized and reviewed.^[11, 28, 39-45] For example, some of the multivalent glycomimetics are glyocluster, glycodendrimers, glycopolymers, glyconanoparticels and glyco-SAMs (Fig. 1.7).^[46-48] To mimic the glycosylated cell surface, various carbohydrates can be immobilized on artificial surface leading to so called “glycoarrays” that are used in glycobiology. For example, carbohydrate derivatives with an alkyl unit with terminal thiol group will form a self-assembled monolayer (SAMs) on a gold surface to obtain “glyco-SAMs”.^[27, 49]

2. Photoswitches

2.1 Photoswitchable molecules

Nature, possesses perfectly designed biomolecules in all living organisms. Scientists try to understand the profound principles by making those biomolecules in a synthetic way. An elegant example found in nature is a photoswitchable biomolecule that is involved in the vision process, rhodopsin system (Fig. 2.1).^[50] When retinal is linked with the protein opsin, a light-induced isomerization (*cis* to *trans* isomerization) process leads to a conformational change in the opsin structure. This triggers a cascade of events leading to signal transduction along the optical nerve to the brain, and we receive them as visual signals.

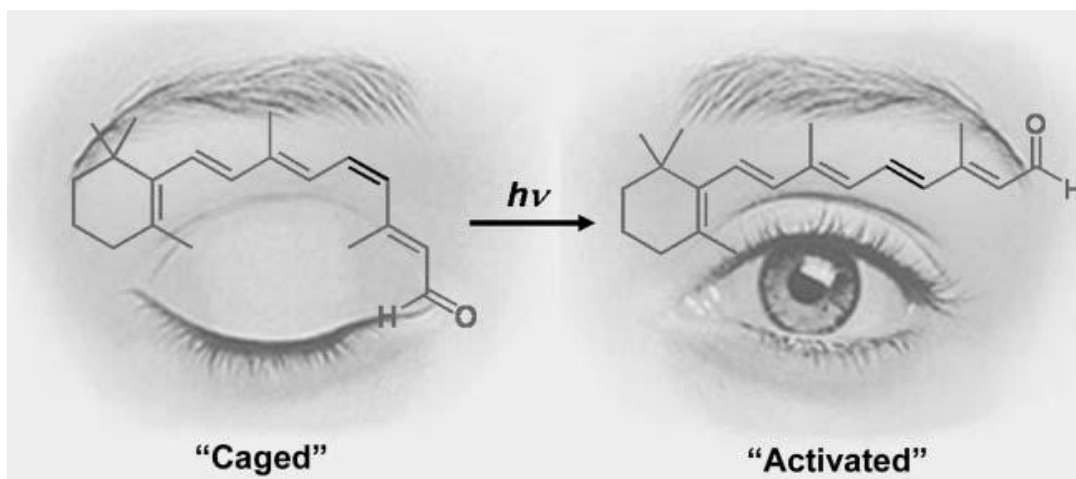


Figure 2.1: *Cis-trans* isomerization in rhodopsin triggers a cascade of events leading to signal transduction along the optical nerve to the brain, and we receive them as visual signals.^[51]

The term “photochromism” derives from the Greek words “phos” and “chroma”, which means light and color, indicating a photoinduced change in colour. The word photochromism was introduced in the early 1950s to indicate the photoinduced change in color of certain compounds. Undoubtedly, synthetic photoswitchable molecules have been inspired by those photo-responsive systems found in nature. Eventually, organic chemists have demonstrated some profound effects of photoswitchability by synthesizing photoswitchable molecules as inhibitors, which provided an indirect approach to gain understanding on changes of spatial and temporal control of

biomolecular structure and their functional differences between two isomeric states as a function of light.^[52-54]

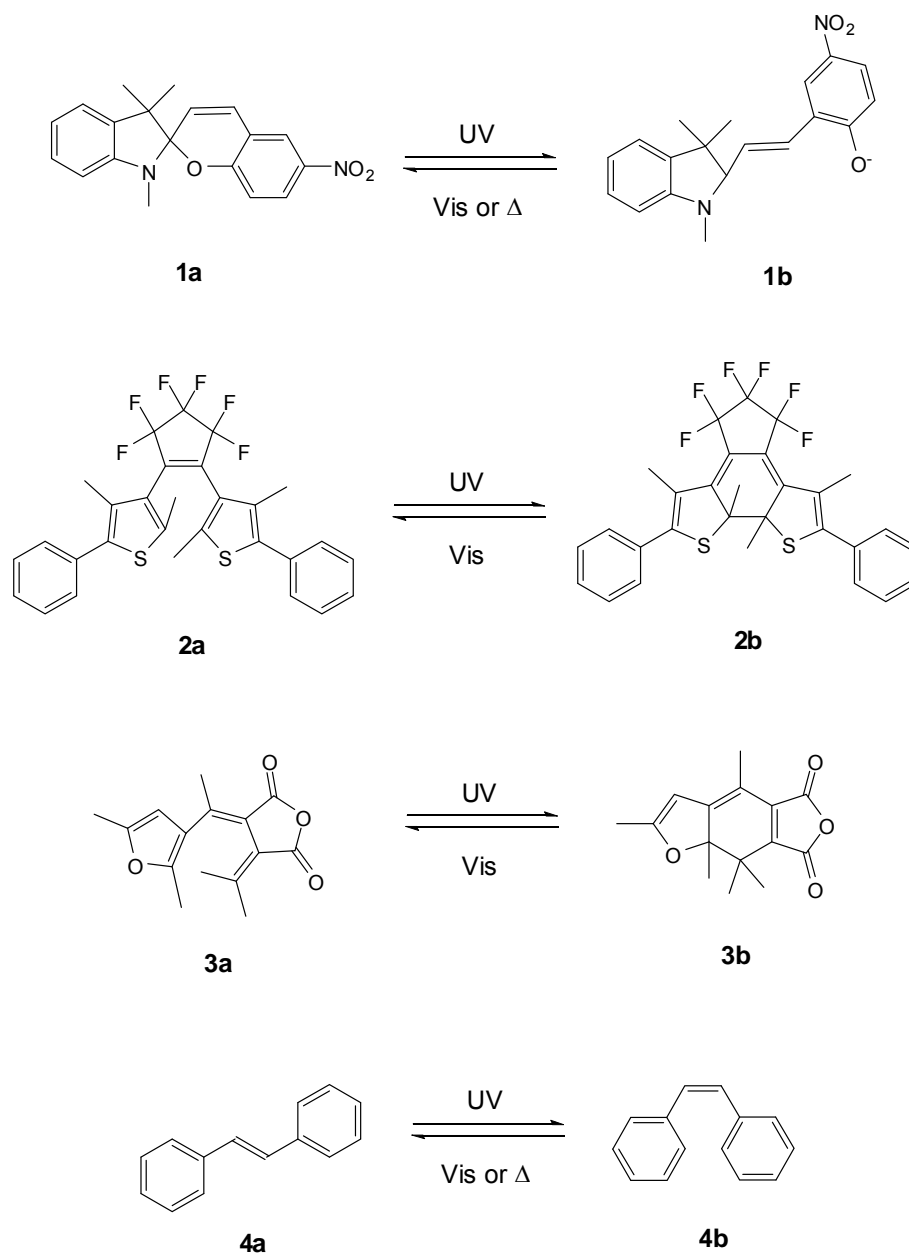


Figure 2.2: The photoinduced and thermal transformations of representative photochromic compounds.

Photochromic transformations are unimolecular reactions with a unique property of interconversion of two isomers, which involves either ring closing and opening reaction (coloration and decoloration) or *trans* → *cis* and *cis* → *trans* isomerization (Fig. 2.2).

In many cases, upon absorption of ultraviolet (UV) light the colourless closed isomer changes to a coloured open isomer, irradiation with visible light can reverse the molecule to its original colorless form. For example, spiropyran **1a** ring-opens to the merocyanine **1b** upon ultraviolet irradiation. The photogenerated coloured isomer **1b** eventually reverts to the initial state **1a** after thermal ring closing or by visible irradiation.^[55-56] Similarly, diarylethene generates two isomers **2a** and **2b**, using ring closing and ring opening photoreactions. The ring closing reaction of **2a** gives isomer **2b** by a cyclization reaction when irradiated with UV light, however unlike spiropyran the photogenerated isomer **2b** is thermally stable and the reverse reaction to the original state is only possible by exposing the compound to visible light irradiation.^[54, 57-58] As similar kind of ring opening and closing photochromic properties can also be seen in fulgides (e.g. **3a** and **3b**).^[59-60]

Alternative to ring opening and closing reactions, photoinduced *cis-trans* isomerization of stilbene and azobenzene can also be used to implement photochromic transformations. The transformation from the *trans* to the *cis* form can be effected by irradiation with UV light of appropriate wavelength, the reverse *cis* → *trans* isomerization process is achieved by visible light. Stilbene (1,2-diphenylethylene) was derived from the Greek word *stilbos*, which means shining. Stilbenes have two isomeric forms the stable *trans*-stilbene (**4a**) which is not sterically hindered and the less stable *cis*-stilbene (**4b**) which is sterically hindered. Resveratrol (3,4',5-trihydroxy-*trans*-stilbene) is a promising natural product found in grapes and in red wine. The anticancer activity of resveratrol was first studied by Jang *et al.*^[61] Oxidative stress is a preliminary step in the appearance and development of cardiovascular diseases, which decrease the bioavailability of nitric oxide (NO) in endothelium vessels, leading to endothelial dysfunction. One of the mechanisms involved by resveratrol and some stilbene derivatives in curing endothelial dysfunction by maintaining sufficient nitric oxide bioavailability in vascular endothelium during oxidative stress.^[62-63]

Another interesting example for a *cis* → *trans* isomerization process is azobenzene. Azobenzene was first described by Krollpfeiffer et.al in 1934.^[64] Photoinduced reversible isomerization to turn the *trans* into the *cis* isomer of azobenzene results in different chemical and physical properties, change in dipole moment (*trans* ~ 0 D; *cis* ~3 D) and change of distance between end to end carbon in the 4- and 4' position of azobenzene (Fig 2.3).^[65] Irradiation of *trans*-azobenzene **5a** with UV light of appropriate wavelength results in the formation of the *cis*-isomer **5b**. The photo-generated *cis* isomer reverts to its original *trans*-isomer either thermally or by irradiation with visible light. Further details of azobenzene and its potential application in biological context are described in chapter 2.2.

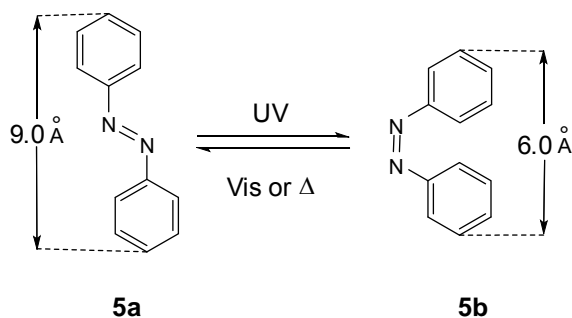


Figure 2.3: *cis-trans* isomerization of azobenzene

2.2 Azobenzene isomerization

Azobenzene, unarguably represents one of the most important organic compounds with a wide range of applications. Although azobenzenes are known since the 18th century and have been widely used in dye industry,^[66] over the past decades considerable attention has been spent on its light-triggered switching properties in the area of polymers,^[67-69] molecular switches,^[70] protein modification,^[71-72] drug delivery,^[73] magnetic resonance imaging,^[74] etc. Making synthetic analogues of this molecule is a challenge to synthetic chemists.

Azobenzene can be regarded as a derivative of diazene (HN=NH) group, where both hydrogen atoms are replaced by phenyl groups. The classical methods involved in the synthesis of azobenzenes are “azo coupling reaction”, coupling of diazonium salts with activated aromatic compounds, “Mills reaction”, reaction between aromatic nitroso derivatives with anilines and several other methods for the preparation of azobenzene derivatives have been reported.^[75-76]

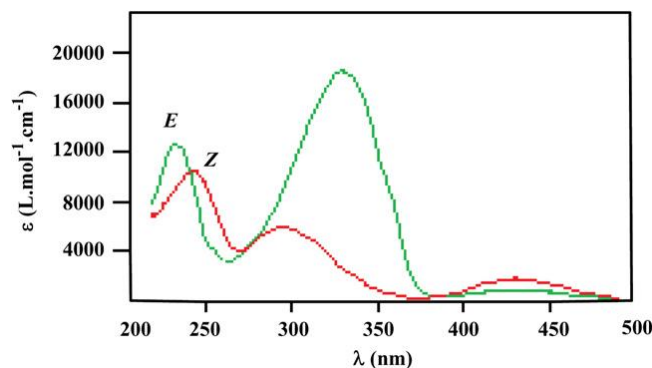


Figure 2.4: UV-Vis spectra of *trans*- (*E*-) and *cis*- (*Z*-) azobenzene in ethanol. Adapted with permission from ref. 75. Copyright Elsevier.

The *trans*- or *E*- isomer, respectively is thermodynamically more stable than the *cis*- or *Z*- isomer. A typical UV-visible absorption spectrum for *trans*- and *cis*- isomers of azobenzene are shown in Fig 2.4. For the *trans*- isomer, the absorption band around ~350 nm arises due to the π - π^* transition. After irradiation with visible light of

appropriate wavelength, formation of the *cis*- isomer can be observed by increase in absorption at ~440 nm due to the n- π^* transition. Depending on the substitution pattern of a azobenzene derivatives, absorption maxima and kinetic of back isomerization will differ greatly.^[77] The mechanism underlying in the isomerization of azobenzene from *trans* \rightarrow *cis* has always been subject of interest and four different mechanistic pathways are proposed in the literature (Fig. 2.5).^[78-80]

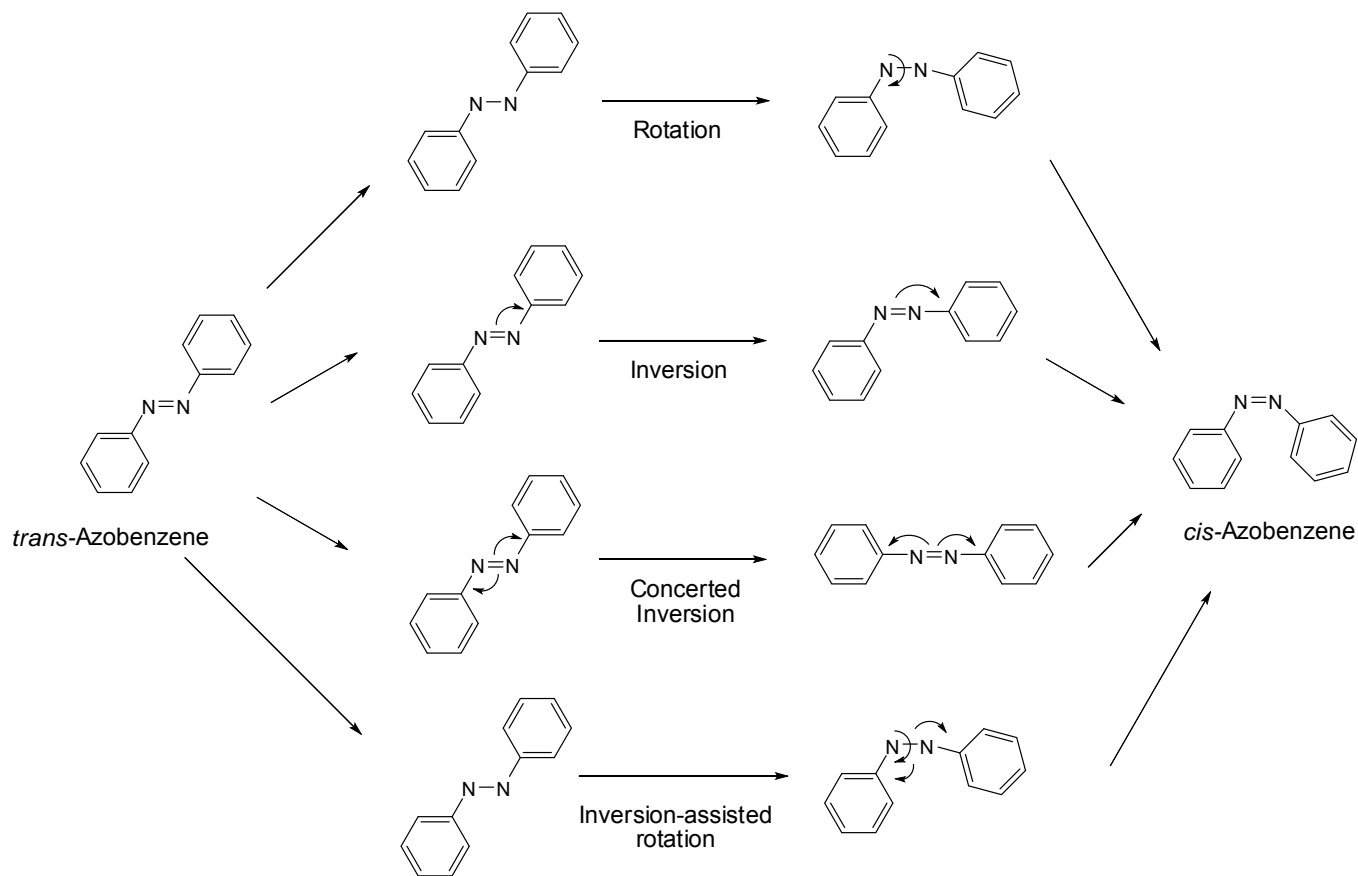


Figure 2.5: Different possible pathways for azobenzene photoisomerization.^[80]

Among the photochromic molecules, azobenzenes have been extensively studied for their unique photoisomerization and their role in controlling the functions of biomolecules like protein and nucleic acids.^[43, 74, 81-85]

2.3 Azobenzene derivatives in biological chemistry

2.3.1 Azobenzene in nucleic acid

Nucleic acids are large biomolecules found in all living organisms. Hybridization between two complementary DNA strands is a unique property of nucleic acids underlying biological functions such as transcription or posttranscriptional gene silencing (siRNA). Reversible photocontrol of nucleic acid activity has been achieved using photoswitchable molecular glue, which are known in literature.^{[51],[86]} For example, naphthyridine carbamate dimer (NCD) was integrated into photoswitchable molecular glue (NCDA) by incorporating azobenzene between two base-recognizing naphthyridine derivatives (Fig 2.6). NCDA in the *cis*-configuration induces the formation of dsDNA from two single stranded DNA structure (ssDNA), whereas in the *trans*-configuration dissociation of double stranded DNA structure (dsDNA) was observed, favouring ssDNA (Fig 2.6).^[87] Thus, introduction of azobenzene enables the control of hybridization and dehybridization of DNA by an external light stimulus.

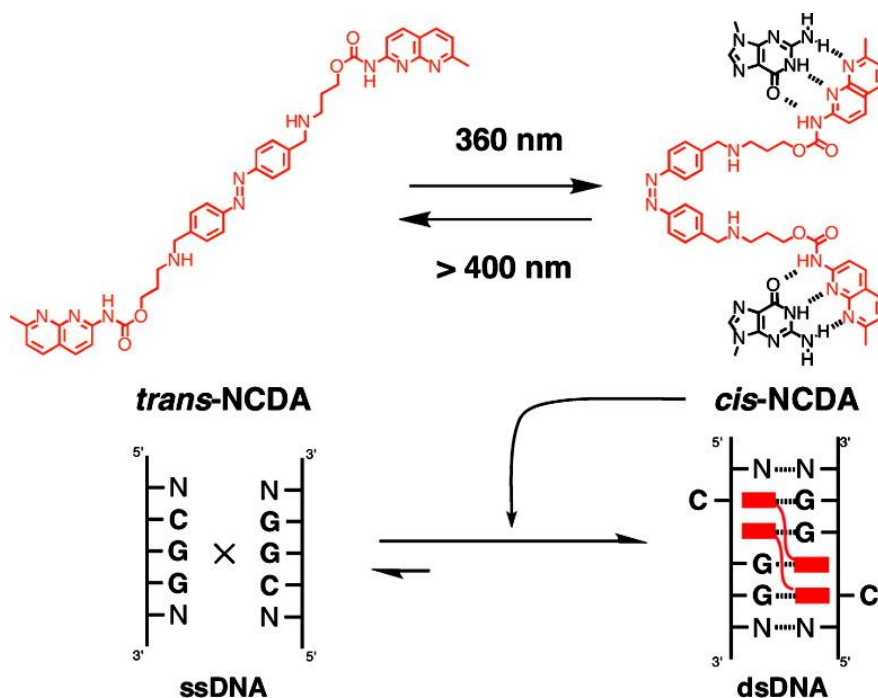


Figure 2.6: Photocontrol of DNA hybridization and dehybridization by photoswitchable molecular glue (NCDA). The *trans*-isomer favours single stranded-DNA structure (ssDNA), whereas *cis*-isomer favours hybridization resulting in double-stranded DNA (dsDNA). Adapted with permission from ref. 87. Copyright American Chemical Society.

2.3.2 Azobenzene in Proteins/Peptides

Reversible photocontrol of protein structure and its functions have also been studied using photoswitchable azobenzene derivatives.^[72, 88] For example, Wooley et al. have shown that incorporation of an azobenzene functional group into a peptide chain allows control of helicity.^[89-92] A key principle in their approach was to utilize the thiol active iodoacetamide functionalized azobenzene derivative with a very short linker between the azobenzene and the peptide (Fig. 2.7). Incorporation of an iodoacetamide-azobenzene derivative to the thiol moiety of a cystine residue of the peptide favours effective switching of the peptide backbone. More importantly, distance between two cystine residues and length of the crosslinkers determines the protein's structure and its activity. For example, *trans*-configuration of the azobenzene cross-linker attached at *i, i + 11*, spaced Cys residues stabilized the helical structure and in the *cis*-configuration leads to a distorted helical structure, due to the shorter end-to-end distance of the crosslinker (Fig. 2.8)

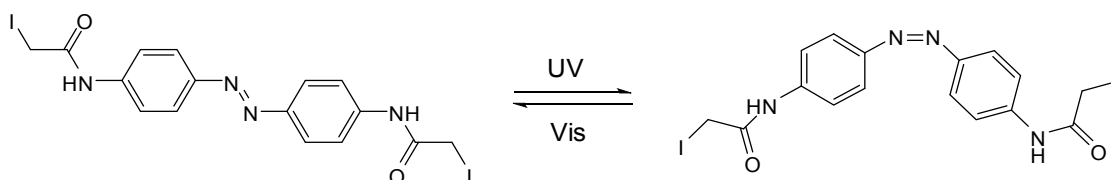


Figure 2.7: Azobenzene derivative with short linker (ethylene spacer) for effective *cis* → *trans* isomerization on the peptide backbone.

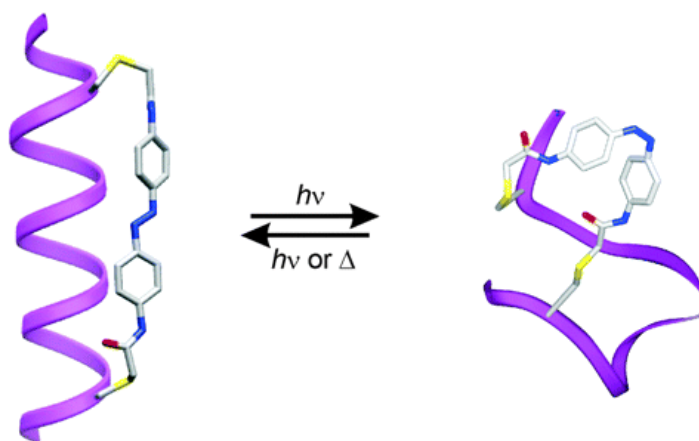


Figure 2.8: Photoisomerization of the crosslinker from *trans* → *cis* isomer leads to destabilization of the helix. Adapted with permission from ref. 91. Copyright American Chemical Society.

2.3.3 Azobenzene in neurobiology

Also the function of ion channels can be changed by photoisomerization of azobenzene derivatives. Ion channels play an important role in neural activities and their functions are influenced by ligand, voltage and temperature. Azobenzene-based photoswitchable ion channels are used since 1970s as a means to control neural activity artificially.^[93]

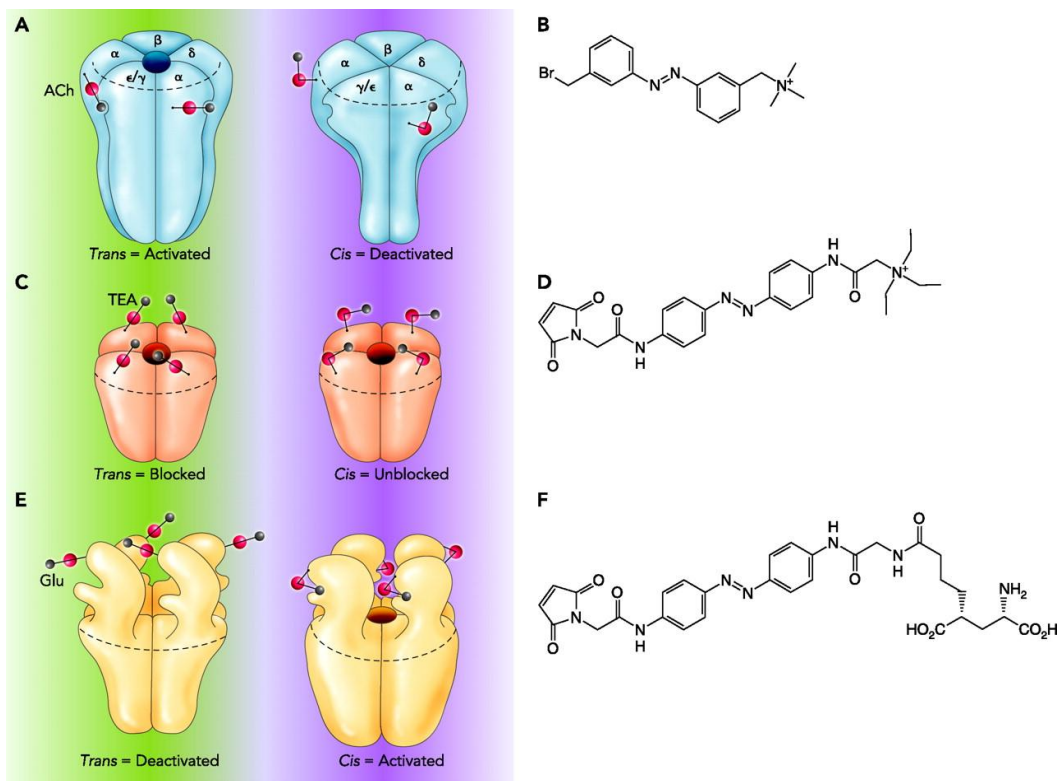


Figure 2.9: Light induced switching of ion channels and its receptors using photoswitchable ligands.

(A) optical control of the nicotinic acetylcholine receptor (nAChR) of the neuromuscular junction is achieved by attaching a choline agonist group via a photoisomerizable tether (red) near the two allosteric sites of the receptor; The receptor is activated with azobenzene derivative (compound B) in *trans*-conformation and deactivated in *cis*-conformation; C) in SPARK, the active site (pore) of the voltage-dependent K⁺ channel Shaker is reversibly blocked with azobenzene derivative (compound D) in *trans*-conformation and unblocked in *cis*-conformation; (E) in LiGluR, the photoisomerizable tethered glutamate agonist MAG (compound F) is attached to each of the four allosteric sites in the receptor. The receptor is deactivated with azobenzene in *trans*-conformation and activated in *cis*-conformation. (Figure adapted from the journal "physiology").^[94]

3-(α -Bromomethyl)-3'-[α -(trimethylammonium) methylazobenzene bromide (QBr) (Fig 2.9A, 2.9B) was the first photochromic compound to be nanoengineered with the nicotinic acetylcholine receptor of the neuromuscular junction which was pioneered by Erlanger *et al.*^[95] The receptor was activated by the *trans* conformation of the azobenzene whereas deactivated in *cis* conformation of azobenzene.

Later several groups reported the structure-based design of the ion channel gramicidin.^[96-97] Trauner and colleagues further extended photocontrol of ion channels using azobenzene modification. Maleimide-linked azobenzene quaternary ammonium salts (Fig 2.9C, 2.9D) was used as synthetic photoisomerizable azobenzene derivatives that regulated the K⁺ ion channel (SPARK), in which the channel is blocked in *trans*-configuration of the azobenzene moiety and retaining the blocker in *cis*-configuration.^[98] The same group extended their work in ionotropic glutamate receptor (iGluR) by attaching a photoisomerizable maleimide-linked azobenzene glutamate derivative, in which the receptor is deactivated in the *trans*-configuration and activated in the *cis*-configuration (Fig 2.9E, 2.9F).^[99] Lately, they also studied the photocontrol of neural activity *in vivo* with in zebrafish.^[100]

2.4 Azobenzene derivatives in glycobiology

Although, azobenzene photoswitches are greatly utilized in protein and nucleic acid chemistry, azobenzene has rarely been utilized in carbohydrate chemistry particularly in a biological context.^{[75],[85]} It has become evident that spatial distribution of glycoconjugates and the conformational characteristics of the glycocalyx plays a crucial role in biological processes involving carbohydrates. However, a systematic investigation of conformational changes and the impact of ligand orientation in carbohydrate-protein interactions has been less explored until today.^[43, 85] In order to investigate the importance of spatial distribution and orientation of carbohydrates as ligands of their receptors, azobenzene glycosides became principal targets for our research. *E/Z* isomerization of azobenzene glycosides results in substantial

conformational changes of the attached carbohydrate moieties and thus this isomerization process can be used to alter the orientation of carbohydrate ligands.

This thesis describes the synthesis of various azobenzene glycosides, their photocromic properties in solution and their interaction with live *E. coli* bacteria and human cells (chapter 3). Also, functionalization of azobenzene glycosides on gold surfaces and their interaction with lectins will be explained (chapter 4). In addition, modification of type I antifreeze proteins (AFP) by photoswitchable azobenzene glycosides is described briefly in this thesis (chapter 5).

3. Synthesis and properties of azobenzene glycoconjugates in solution.

For any relevant application of azobenzene glycoconjugates, their photochemical properties have to meet the requirements for biological testing. Only few examples of azobenzene glycoconjugates are known in literature and no systematic investigation of their photochromic properties has been published so far.^[72, 75] In view of this, we have designed and synthesized various photoswitchable azobenzene glycosides and studied their photophysical properties in solutions (chapter 3.2 and 3.3). In addition to this, *E* and *Z* isomers of azobenzene glycoside were tested as inhibitors of type 1 fimbriae-mediated bacterial adhesion of *E. coli* (chapter 3.1).

3.1 Synthesis and testing of the first azobenzene mannobioside as photoswitchable ligand for the bacterial lectin FimH.

Vijayanand Chandrasekaran, Katharina Kolbe, Femke Beiroth, Thisbe K. Lindhorst*

Beilstein J. Org. Chem. **2013**, *9*, 223-233.

In this full research paper, azobenzene mannobiosides and mannobiosides were synthesized, their photochromic properties were studied in solution and *E*- and *Z*-isomers were tested as inhibitors of type 1-fimbriated bacterial adhesion of *E. coli* (Fig 3.1). High yielding *E*→*Z* isomerization process and a long life time ($\tau_{1/2} = 178.5$ h) of the *Z*-isomer for the azobenzene mannobioside was observed. Biological testing results showed that both isomers have nearly the same inhibitory potency, which is in well agreement with computer-aided docking studies. This finding suggests that the same molecule can be immobilized and test the adhesion of *E. coli* on photoswitchable glycoarrays.

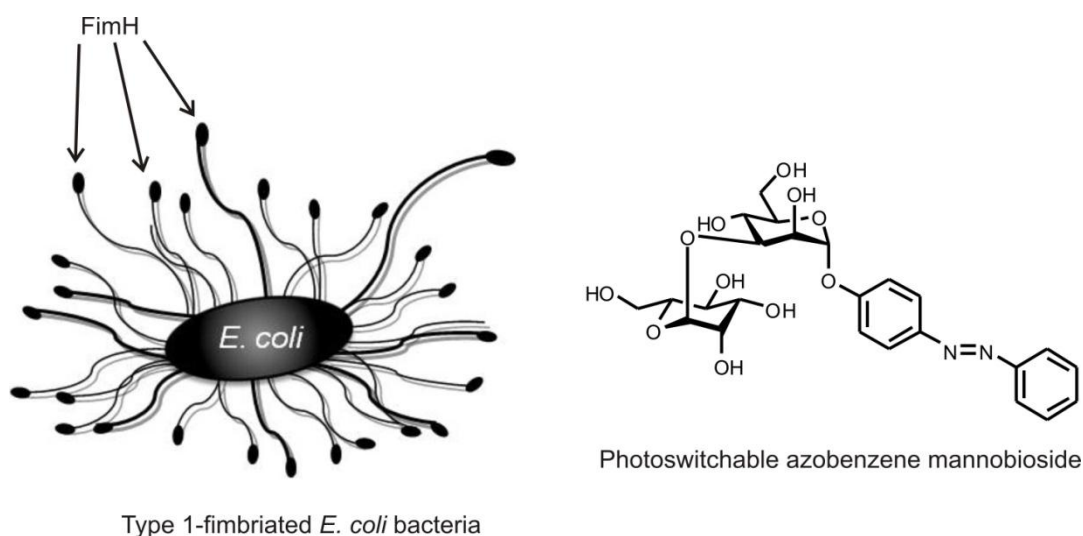


Figure 3.1: The depicted azobenzene mannobioside was tested as inhibitor of the bacterial lectin FimH.

In this project, F. Beiroth performed the molecular docking studies, K. Kolbe did the biological testing and I did the synthesis and studied the photochromic properties of azobenzene glycosides. All authors contributed in writing this article and supplementary material.

Synthesis and testing of the first azobenzene mannobioside as photoswitchable ligand for the bacterial lectin FimH

Vijayanand Chandrasekaran, Katharina Kolbe, Femke Beiroth
and Thisbe K. Lindhorst*

Full Research Paper

Open Access

Address:
Christiana Albertina University of Kiel, Otto Diels Institute of Organic
Chemistry, Otto-Hahn-Platz 3/4, D-24098 Kiel, Germany, Fax: +49
431 8807410

Email:
Thisbe K. Lindhorst* - tkind@oc.uni-kiel.de

* Corresponding author

Keywords:
azobenzene glycosides; bacterial adhesion; *E/Z* photoisomerisation;
FimH antagonists; mannobiosides; molecular switches; sweet
switches

Beilstein J. Org. Chem. **2013**, *9*, 223–233.
doi:10.3762/bjoc.9.26

Received: 08 November 2012
Accepted: 18 January 2013
Published: 01 February 2013

This article is part of the Thematic Series "Molecular switches and cages".

Guest Editor: D. Trauner

© 2013 Chandrasekaran et al; licensee Beilstein-Institut.
License and terms: see end of document.

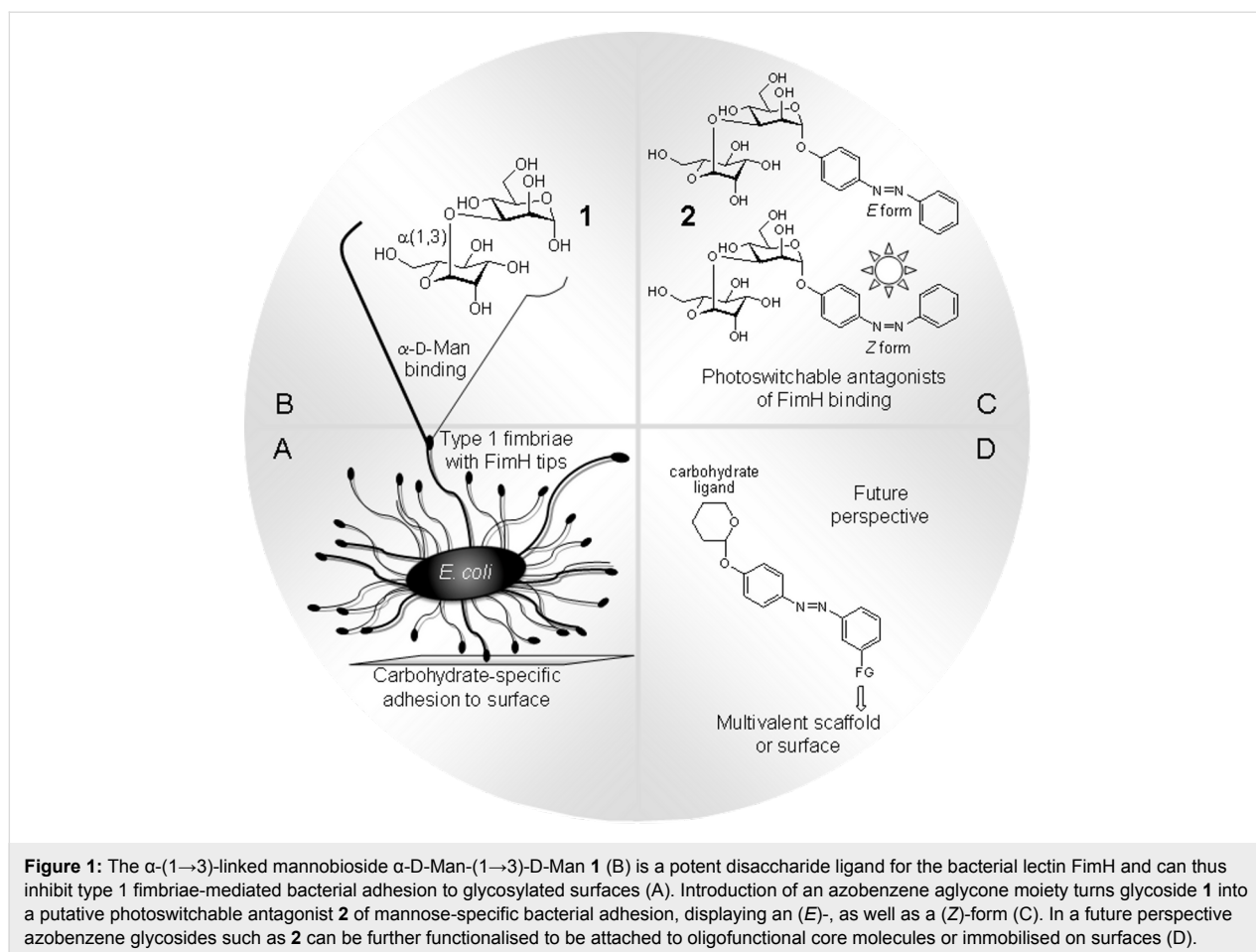
Abstract

In order to allow spatial and temporal control of carbohydrate-specific bacterial adhesion, it has become our goal to synthesise azobenzene mannobiosides as photoswitchable inhibitors of type 1 fimbriae-mediated adhesion of *E. coli*. An azobenzene mannobioside **2** was prepared and its photochromic properties were investigated. The *E*→*Z* isomerisation was found to be highly effective, yielding a long-lived (*Z*)-isomer. Both isomers, *E* and *Z*, show excellent water solubility and were tested as inhibitors of mannobioside-specific bacterial adhesion in solution. Their inhibitory potency was found to be equal and almost two orders of magnitude higher than that of the standard inhibitor methyl mannobioside. These findings could be rationalised on the basis of computer-aided docking studies. The properties of the new azobenzene mannobioside have qualified this glycoside to be eventually employed on solid support, in order to fabricate photoswitchable adhesive surfaces.

Introduction

Adhesion of bacteria to surfaces can be a severe problem both in vivo and in vitro. Hence, inhibition of bacterial adhesion by powerful antagonists is highly desirable, however, ideally on demand, that is, in a specific and spatially as well as temporally resolved way. Often bacterial adhesion depends on the inter-

action of adhesive organelles called fimbriae. They project from the surface of bacteria and contain lectin domains to attach to certain carbohydrate ligands of a glycosylated surface such as the glycocalyx of eukaryotic target cells (Figure 1A) [1-4]. This offers the possibility to inhibit bacterial adhesion by designed



antagonists of the respective carbohydrate-specific bacterial lectins [5]. In order to expand the scope of carbohydrate-based antiadhesives, it has become our goal to make photoswitchable ligands of bacterial lectins to allow blocking of bacterial adhesion in a photocontrolled manner.

One of the best-known fimbriae are the type 1 fimbriae of uropathogenic *E. coli* (UPEC), which comprise the α -D-mannosyl-specific lectin FimH at the tip of the fimbrial shaft. FimH antagonists are currently considered as new therapeutics for the treatment of urinary tract infections [6]. The carbohydrate specificity of FimH has been investigated in great detail [7] and its structure is well-known from several X-ray studies [8–11]. It has turned out that the 1,3-linked mannobioside α -D-Man-(1 \rightarrow 3)-D-Man (**1**, Figure 1B) is an ideal disaccharide ligand for FimH [3,12]. All other isomeric mannobiosides do not bind favourably to FimH. Therefore, we have designed the respective azobenzene mannobioside **2** (Figure 1C) in order to make a photoswitchable FimH antagonist available. Photoirradiation of azobenzene glycosides at \sim 365 nm effects *E* \rightarrow *Z* isomerisation of the N=N double bond, and thermal relaxation or irradiation at \sim 450 nm leads to *Z* \rightarrow *E* back isomerisation

[13,14]. In the case that the *E* \rightarrow *Z* isomerisation process is high-yielding and the lifetime of the (*Z*)-form of the azobenzene glycoside is long enough, it can be employed in bacterial adhesion assays independently from the more stable (*E*)-isomer. Eventually, this type of azobenzene mannobioside can be further functionalised to be attached to various supports such as oligofunctional core molecules [15] or surfaces, to achieve switchable adhesive surfaces in continuation of our work on glycoarrays [16–18] (Figure 1D).

In this account, we describe the synthesis of the azobenzene mannobioside **2** as well as of mannoside **6**, investigation of their photochromic properties, and testing of mannobioside **2** as an inhibitor of type 1 fimbriae-mediated bacterial adhesion. Interpretation of the test results was supported by computer-aided docking studies.

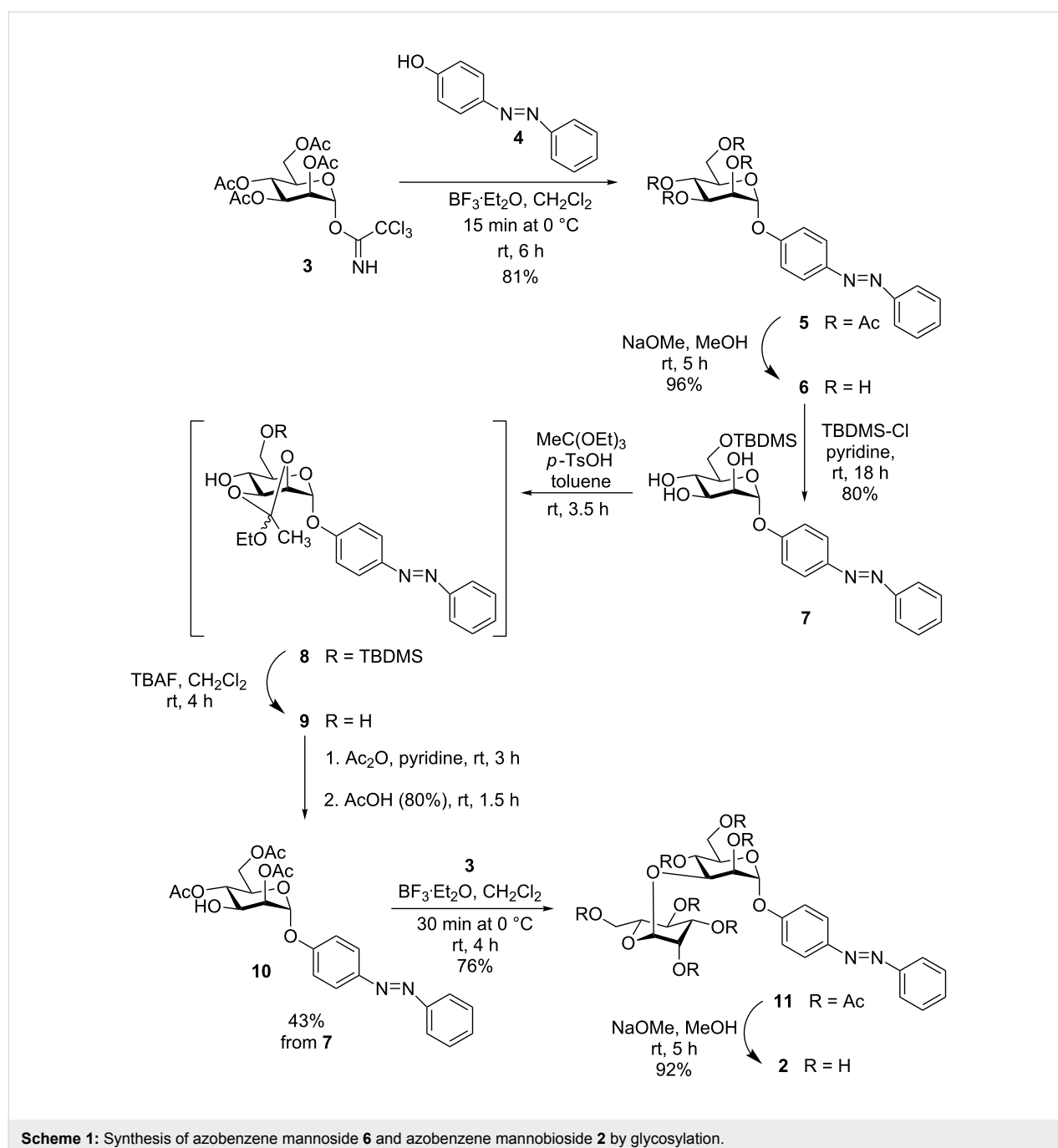
Results

Synthesis of azobenzene mannobioside **2**

For the preparation of azobenzene mannobioside **2**, the azobenzene mannoside **6** was prepared first. Thus, mannosylation of the hydroxy-functionalised azobenzene **4** by using the mannosyl

trichloroacetimidate **3** [19] led to the respective azobenzene α -mannosides **5** in 81% yield (Scheme 1). Treatment of **5** under Zemplén conditions [20] furnished the deprotected mannoside **6** in a basically quantitative reaction. Then, a standard protecting-group strategy was employed to allow the synthesis of the 3-OH unprotected mannoside **10**, which is a key intermediate serving as the glycosyl acceptor in the following disaccharide synthesis. First, regioselective protection of the primary 6-hydroxy group in **6** was accomplished by using TBDMS chloride in pyridine to yield **7**. Then, triethylorthoacetate was employed to make the

orthoester **8**, which, without intermediate purification steps, could be carried on in a sequence of silyl ether-deprotection leading to the intermediate **9**, acetylation of the 4- and 6-hydroxy groups, and then acid-mediated regioselective ring opening of the 2,3-orthoester in the same pot to yield the free 3-OH azobenzene mannoside **10** in an overall yield of 43%. Thus, the required protecting group pattern was obtained in a highly efficient way, based on the regioselective opening of orthoacetates to yield a vicinal arrangement of equatorial OH and axial O-acetyl groups [21,22]. The acetylation pattern was



clearly confirmed by ^1H NMR spectroscopy showing the expected downfield shift for the H-3 signal resonating at 4.32 ppm (H-2: 5.30 ppm, H-4: 5.17 ppm).

Next, glycosylation of the key intermediate **10** by using the mannosyl donor **3** gave the desired mannoside **11** in 76% yield. Finally, removal of the *O*-acetyl groups according to Zemplén led to the unprotected 1,3-linked target mannoside $\alpha\text{-D-Man-(1}\rightarrow\text{3)-D-Man}$ (**2**).

With the two azobenzene glycosides **6** and **2** at hand, their solubility and photochromic properties were then investigated and compared. Mannoside **6** showed only poor solubility in most organic solvents, except for DMSO. Unfortunately, it was also not soluble in water, or in water/DMSO mixtures, which would allow biological testing. Mannoside **2**, on the other hand, showed good solubility in polar organic solvents as well as in pure water. Thus, it was amenable to biological testing in aqueous buffer.

E→*Z* photoisomerisation of azobenzene mannoside **6** was studied in DMSO, while isomerisation of azobenzene mannoside **2** was performed in water. Photoirradiation was carried out in the dark at room temperature by employing a 365 nm LED. Photostationary states (PSS) were reached after 10 minutes of irradiation for both compounds. *E*→*Z* isomerisation was observed by both ^1H NMR and UV–vis spectroscopy. The *E/Z* ratios of the ground state (GS) as well as of the photostationary state were determined on the basis of the integration of the anomeric H-1 protons in the ^1H NMR spectrum. Half-life were determined by UV–vis spectroscopic observation of the thermal *Z*→*E* relaxation process (Supporting Information File 1). The respective data are collected in Table 1.

Fortunately, the mannoside **2** is ideally suited for biological testing as it is soluble in water and aqueous buffer, respectively. Photoirradiation of the (*E*)-isomer leads to almost quantitative

isomerisation, and the life time of the resulting (*Z*)-isomer is long enough to test this isomer independently from the more stable (*E*)-form.

Biological testing of azobenzene mannoside **2**

As a test system for mannose-specific bacterial adhesion, fluorescent GFP-transfected *E. coli* bacteria (pPKL1162) [23] were employed and tested on a mannan-coated polystyrene microtiter plate surface. In this setup the amount of bacterial adhesion correlates with fluorescence intensity and can be quantified by using a standard microtiter plate reader. For inhibition of bacterial adhesion, two sets of serially diluted solutions of **2** were prepared to inhibit adhesion of fluorescing *E. coli* to the mannan surface. In one case, a stock solution of (*E*)-**2** was serially diluted, in the second case, this stock solution of (*E*)-**2** was irradiated for 15 minutes to obtain the pure (*Z*)-**2** isomer for subsequent serial dilution. The effect of both isomers as inhibitors of mannose-specific bacterial adhesion was then measured in a concentration-dependent way. From the testing results sigmoidal inhibition curves were obtained (Supporting Information File 1) from which IC_{50} values for every individual inhibitor were deduced. The IC_{50} value reflects the concentration at which a compound inhibits 50% of bacterial adhesion to a mannan-coated surface. The determined IC_{50} values were referenced to the inhibitory potency of methyl $\alpha\text{-D-mannoside}$ (MeMan) and *p*-nitrophenyl $\alpha\text{-D-mannoside}$ (*p*NPMan), respectively, each tested on the same plate. Thus, relative inhibitory potencies (RIP values) were obtained, which allow comparison of inhibitory potencies of different inhibitors, even when they were not tested in the same experiment. The testing results collected in Table 2 show that the inhibitory power of mannoside **2** is roughly the same, regardless of whether its (*E*)- or (*Z*)-form was employed. Inspection of their relative inhibitory potencies reveals that both isomers of **2** are equally potent inhibitors of type 1 fimbriae-mediated bacterial adhesion, similar to the power of the well-known mannoside *p*NPMan.

Table 1: Characterisation of the (*E*)- and (*Z*)-isomers of azobenzene glycosides **6** and **2**.

azobenzene glycoside	<i>E/Z</i> ^a (GS)	<i>E/Z</i> ^a (PSS)	H-1 (ppm) (<i>E</i>)-isomer	H-1 (ppm) (<i>Z</i>)-isomer	UV–vis absorption maxima (nm) $\lambda_{\text{max}}(\text{E}), \lambda_{\text{max}}(\text{Z})$	half-life, $\tau_{1/2}$ (h)
6	99:1	3:97	5.54 ^b	5.34 ^b	347, 440 ^c	89
2	95:5	4:96	5.65 ^d	5.52 ^d	339, 429 ^e	178.5

^aaccording to the integration ratio of H-1(*E*) and H-1(*Z*) in the ^1H NMR spectrum;

^b10 mM concentration in DMSO-*d*₆;

^c50 μM concentration in DMSO;

^d8 mM concentration in D₂O;

^e65 μM concentration in H₂O.

Table 2: Inhibition of adhesion of *E. coli* to a mannan-coated surface. The inhibitory potencies of (*E*)- and (*Z*)-**2** are compared to the standard inhibitors MeMan and *p*NPMan.^a

	MeMan	<i>p</i> NPMan	(<i>E</i>)- 2	(<i>Z</i>)- 2
IC ₅₀ ± SD (mM)	5.205 ± 0.416		0.064 ± 0.018	0.073 ± 0.001
		0.073 ± 0.003	0.078 ± 0.006	0.084 ± 0.002
RIP (MeMan) ± SD	IP ≡ 1		81 ± 25	71 ± 1
RIP (<i>p</i> NPMan) ± SD		IP ≡ 1	0.94 ± 0.07	0.87 ± 0.02

^aAverage values from duplicate results; SD: standard deviation (from one assay); RIP: relative inhibitory potency referenced to either MeMan or *p*NPMan, each tested on the same microtiter plate.

In order to support the interpretation of the obtained test results, binding of (*E*)-**2** and (*Z*)-**2** to the bacterial lectin FimH was investigated by computer-aided docking studies to get an idea of their interactions with the carbohydrate-recognition domain (CRD) of the lectin.

Docking of azobenzene mannoside **2** into the carbohydrate binding site of FimH

To visualise complexation of the (*E*)- and (*Z*)-isomers of azobenzene mannoside **2** within the CRD of FimH FlexX [24-26], flexible docking and consensus scoring [27,28], as implemented in Sybyl 6.9 [29], was employed. Docking was based on two different X-ray structures of FimH. They differ in the conformation of the so-called tyrosine gate at the entrance of the CRD, formed by the side chains of Y48 and Y137. One structure is crystallised in an “open-gate” conformation [9], another in the “closed-gate” conformation [10]. Affinity of any FimH ligand is improved when it exerts favourable interactions with the tyrosine gate of FimH. Thus, this substructure is an important feature of the rim of the carbohydrate binding site of this lectin.

Before minimisation of the ligands, the bond angle of the N=N double bond of the azobenzene moiety was manually set as 180° for (*E*)-**2** and as 90° for (*Z*)-**2** [30]. Then docking was performed holding the FimH CRD fixed whereas the ligands were allowed to change their conformations under the influence of the force field. A FlexX scoring value has been attributed to each of the 30 obtained conformations (Table 3). This value correlates with the binding affinity of the ligand for the FimH CRD, more negative values suggesting higher binding affinity than less negative ones.

Docking gave very similar results for both isomers of mannoside **2**, (*E*)-**2** and (*Z*)-**2**. Scoring values based on the open-

Table 3: FlexX scoring values for the (*E*)- and the (*Z*)-isomer of **2** based on two different crystal structures in comparison to MeMan and *p*NPMan.

Ligand	“open-gate” structure [9]	“closed-gate” structure [10]
MeMan	-22.5	-23.3
<i>p</i> NPMan	-24.9	-27.4
(<i>E</i>)- 2	-28.8	-20.4
(<i>Z</i>)- 2	-28.7	-21.6

gate structure of FimH are almost equal (−28.8 and −28.7), and also the scoring values obtained with the closed-gate structure do not differ significantly (−20.4 and −21.6). Interestingly, the predictions for *p*NPMan and also MeMan are the opposite, suggesting better binding to the closed-gate conformation of FimH, as described earlier [31]. Representative snapshots as depicted in Figure 2 show that both isomers have the terminal mannoside complexed within the CRD of the lectin, as expected, and furthermore, that in both cases the azobenzene moiety exerts effective interactions with the tyrosine gate involving both benzene rings.

Regardless of whether the (*E*)- or the (*Z*)-form of **2** is complexed with FimH, favourable π - π interactions can be formed between the azobenzene moiety and the tyrosine gate at the entrance of the CRD, though in different ways. The only difference that is seen is that, apparently, the interactions of mannoside **2** with the open-gate conformation of FimH are advantageous over those with the closed-gate form. From the bioassay in solution phase it can certainly not be decided, which conformation the bacterial lectin adopts to interact with compound **2**; however, our test results confirm that both isomers of the azobenzene mannoside **2** have the same power as inhibitors of FimH-mediated bacterial adhesion.

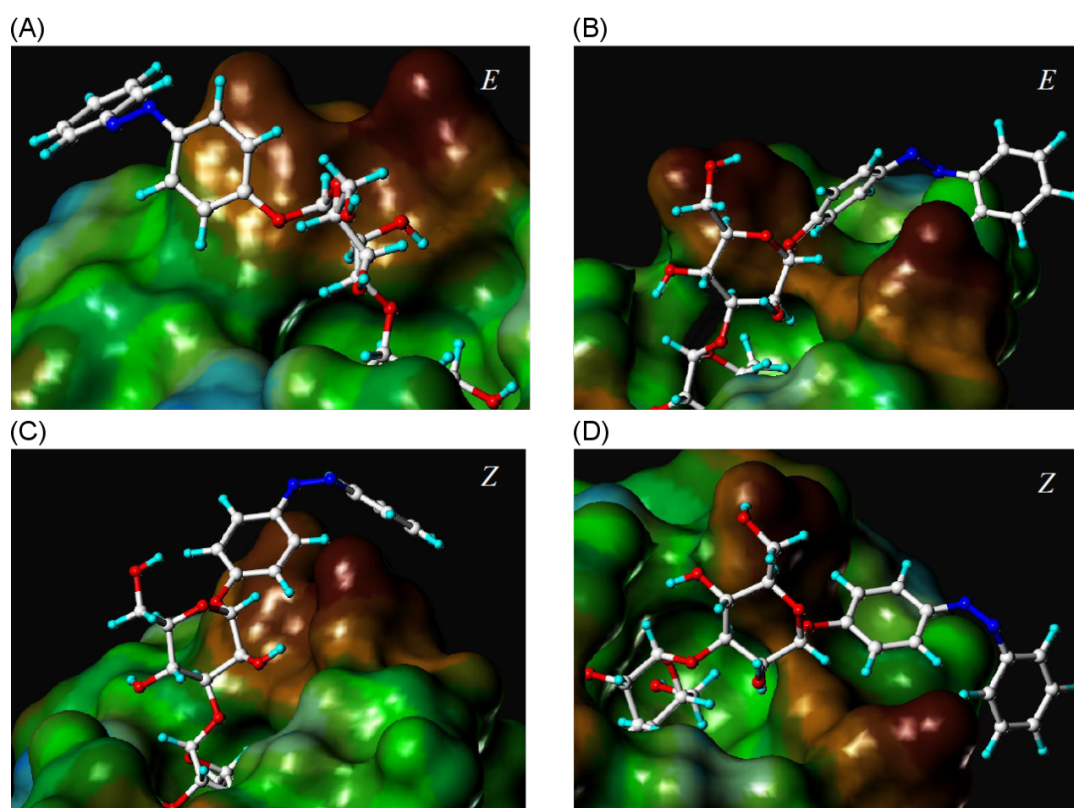


Figure 2: Connolly [32,33] descriptions of the FimH CRD with the docked azobenzene mannobioside **2**. Top: (*E*)-isomer (A, closed-gate; B, open-gate conformation). Bottom: (*Z*)-isomer (C, closed-gate; D, open-gate conformation).

Discussion

The azobenzene mannobioside **2** was selected as a photoswitchable inhibitor of the bacterial lectin FimH based on earlier findings about the inhibitory potency of several mannobiosides [34,35]. Its synthesis was straightforward and high-yielding. It has very convenient photochromic properties as the *E*→*Z* isomerisation is almost quantitative and the resulting (*Z*)-isomer is especially long-lived. Both isomers are very well water-soluble and could be independently tested as inhibitors of mannose-specific bacterial adhesion and showed an equal and high inhibitory potency in the range of the well-known high-affinity inhibitor *p*-nitrophenyl α -D-mannoside (*p*NPMan). This result can be rationalised by computer docking, showing that regardless of the configuration of the N=N double bond of the azobenzene moiety in **2**, favourable interactions can be formed with the tyrosine gate of the FimH CRD. While the terminal mannose portion is complexed in the carbohydrate binding site, the first mannose does not add significantly to the affinity and this is in accordance with other studies on the complexation of oligosaccharides by FimH [11]. However, this

mannose ring acts as a spacer moiety, sticking out straight from the CRD and placing the azobenzene portion in an orientation that allows flexible interactions with the tyrosine gate at the entrance of the carbohydrate binding site of the lectin.

Apparently, the affinity of **2** to the open-gate form of FimH is higher than to the closed-gate conformation, a finding that differs from many other docked FimH ligands. Here, the higher affinity for the open-gate FimH can be explained by strong π - π stacking of the first aromatic ring of the azobenzene unit with the tyrosine gate.

As both isomers of **2** interact equally well with FimH, they can't be used to switch type 1 fimbriae-mediated bacterial adhesion in solution. On the other hand, the obtained results support the idea to immobilise the azobenzene mannobioside on a solid support to photocontrol the adhesive properties of the resulting surface. In this approach the azobenzene N=N double bond can be used as a hinge region to bend down the terminal mannose moiety of the compound, which is critical for specific bacterial

adhesion. Thus, upon *E*→*Z* isomerisation, the ligand will no longer be available for the interaction with the FimH-terminated type 1 fimbriae that mediate adhesion. In this approach, the second mannose moiety of the mannoside is important both to mediate hydrophilicity and to intensify the steric effect that photoswitching has on the exposition of the terminal mannoside.

Conclusion

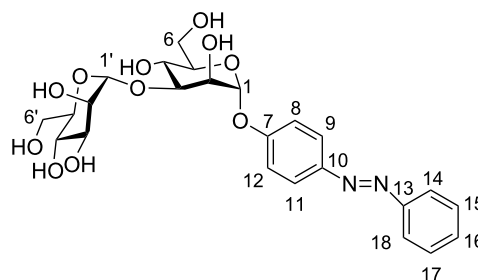
The azobenzene mannosides presented herein resemble a structure quite similar to biaryl mannosides, which have been introduced lately and shown to be of medical relevance as FimH antagonists [6]. Thus, our novel “sweet switches” [15] appear to be highly promising FimH ligands, with the additional feature of a photoswitchable moiety. The biomedical potential of azobenzene glycosides seems even higher when their favourable physiological properties are considered, such as low toxicity [36] and receptor specificity of the azobenzene aglycon [37]. It will be our next goal to employ derivatives of azobenzene mannoside **2** for immobilisation to test the photoswitching of adhesion on surfaces.

Experimental

Materials and general methods

p-Hydroxyazobenzene was purchased from Sigma Aldrich and used without further purification. Moisture-sensitive reactions were carried out under nitrogen in dry glassware. Thin-layer chromatography was performed on silica-gel plates (GF 254, Merck). Detection was effected by UV and/or charring with 10% sulfuric acid in EtOH followed by heat treatment at ~180 °C. Flash chromatography was performed on silica gel 60 (Merck, 230–400 mesh, particle size 0.040–0.063 mm) by using distilled solvents. Optical rotations were measured with a Perkin-Elmer 241 polarimeter (sodium D-line: 589 nm, length of cell: 1 dm) in the solvents indicated. ¹H and ¹³C NMR spectra were recorded on Bruker DRX-500 and AV-600 spectrometers at 300 K. Chemical shifts are reported relative to internal tetramethylsilane ($\delta = 0.00$ ppm) or D₂O ($\delta = 4.76$ ppm). Full assignment of the peaks was achieved with the aid of 2D NMR techniques (¹H/¹H COSY and ¹H/¹³C HSQC). IR spectra were measured with a Perkin Elmer FT-IR Paragon 1000 (ATR) spectrometer. ESI mass spectra were recorded on an Esquire-LC instrument from Bruker Daltonics. MALDI-TOF mass spectra were recorded on a Bruker Biflex III instrument with 19 kV acceleration voltage, and 2,5-dihydroxybenzoic acid (DHB) was used as the matrix. UV–vis absorption spectra were performed on Perkin-Elmer Lambda-241 or Varian Cary-5000 at a temperature of 18 ± 1 °C. Photoirradiation was carried out by using a LED (emitting 365 nm light) from the Nichia Corporation (NC4U133A) with a FWHM of 9 nm and an optical power output (P_0) ~ 1 W.

For NMR assignments the following numbering was used:



(*E*)-*p*-(Phenylazo)phenyl 2,3,4,6-tetra-*O*-acetyl- α -D-mannopyranoside (5**).** To a solution of the mannosyl donor **3** (5.00 g, 10.2 mmol) and *p*-hydroxyazobenzene (**4**, 2.01 g, 10.2 mmol) in dry CH₂Cl₂ (100 mL) BF₃·etherate (1.88 mL, 15.2 mmol) was added at 0 °C under N₂ atmosphere, and the reaction mixture was stirred at this temperature for 15 min. Then, stirring was continued at rt for about 6 h, and then the reaction was quenched by the addition of satd. aq. NaHCO₃ solution (50 mL). The phases were separated, the aqueous phase was extracted with CH₂Cl₂ (2 × 150 mL), and the combined organic phases were dried over MgSO₄. This was filtered, and the filtrate was concentrated under reduced pressure. Purification of the crude product by column chromatography (cyclohexane/ethyl acetate, 3:1) gave the title glycoside **5** as an orange crystalline solid (4.33 g, 8.19 mmol, 81%). Mp 53–55 °C; *R*_f 0.35 (cyclohexane/ethyl acetate 2:1); [α]_D²⁰ +0.86 (*c* 0.9, DMSO); ¹H NMR (500 MHz, CDCl₃) δ 7.92 (d, *J* = 9.0 Hz, 2H, H-9, H-11), 7.89 (d, *J* = 8.5 Hz, 2H, H-14, H-18), 7.53–7.45 (m, 3H, H-15, H-16, H-17), 7.23 (d, *J* = 9.0 Hz, 2H, H-8, H-12), 5.62 (d, *J*_{1,2} = 1.8 Hz, 1H, H-1), 5.58 (dd, *J*_{2,3} = 3.6 Hz, *J*_{3,4} = 10.1, 1H, H-3), 5.49 (dd, *J*_{1,2} = 1.8 Hz, *J*_{2,3} = 3.6 Hz, 1H, H-2), 5.39 (dd~t, *J*_{3,4} = *J*_{4,5} = 10.0 Hz, 1H, H-4), 4.30 (dd, *J*_{5,6a} = 5.4 Hz, *J*_{6a,6b} = 12.0 Hz, 1H, H-6a), 4.14–4.07 (m, 2H, H-5, H-6b), 2.21, 2.06, 2.05, 2.03 (each s, each 3H, 4 OAc); ¹³C NMR (125 MHz, CDCl₃) δ 170.5, 169.9, 169.9, 169.7 (4 C=O), 157.6 (C-7), 152.6 (C-13), 148.4 (C-10), 130.8 (C-16), 128.9 (C-15, C-17), 124.6 (C-9, C-11), 123.1 (C-14, 18), 116.8 (C-8, C-12), 95.7 (C-1), 69.4 (C-5), 69.3 (C-2), 68.8 (C-3), 65.9 (C-4), 62.1 (C-6), 20.9, 20.7, 20.7, 20.6 (4 COCH₃); IR (ATR) $\tilde{\nu}$: 2929, 1743, 1598, 1496, 1366, 1209, 1029 cm⁻¹; ESIMS (*m/z*): [M + Na]⁺ calcd for C₂₆H₂₈N₂O₁₀, 551.5; found, 551.1.

(*E*)-*p*-(Phenylazo)phenyl α -D-mannopyranoside (6**).** To a solution of the acetyl-protected glycoside **5** (600 mg, 1.14 mmol) in dry MeOH (6 mL), a catalytic amount of solid NaOMe was added under N₂ atmosphere, and the reaction mixture was stirred for 5 h at rt. Then it was neutralized with Amberlite IR 120 ion-exchange resin and filtered. The filtrate was evaporated under reduced pressure to yield the deprotected

mannoside **6** as a pale yellow solid (393 mg, 1.09 mmol, 96%). Mp 183–185 °C; R_f 0.34 (ethyl acetate/MeOH 4:1); $[\alpha]_D^{20} +1.40$ (c 1.0, DMSO); $^1\text{H NMR}$ (500 MHz, DMSO- d_6) δ 7.86 (d, $J = 8.7$ Hz, 2H, H-9, H-11), 7.82 (d, $J = 7.7$ Hz, 2H, H-14, H-18), 7.53–7.45 (m, 3H, H-15, H-16, H-17), 7.26 (d, $J = 8.7$ Hz, 2H, H-8, H-12), 5.53 (bs, 1H, H-1), 3.89 (dd-bs, 1H, H-2), 3.73 (dd, $J_{3,4} = 9.2$ Hz, $J_{3,2} = 3.0$ Hz, 1H, H-3), 3.58–3.47 (m, 3H, H-6a, H-4, H-6b), 3.38 (m_c, 1H, H-5); $^{13}\text{C NMR}$ (125 MHz, DMSO- d_6) δ 158.9 (C-7), 155.5 (C-13), 151.9 (C-10), 130.9 (C-16), 129.4 (C-15, C-17), 124.3 (C-9, C-11), 122.3 (C-14, C-18), 117.1 (C-8, C-12), 98.7 (C-1), 75.2 (C-5), 70.6 (C-3), 69.9 (C-2), 66.6 (C-4), 60.9 (C-6); UV, λ_{max} : 347 nm; $\epsilon = 25907 \pm 529 \text{ L} \times \text{mol}^{-1} \times \text{cm}^{-1}$; IR (ATR) $\tilde{\nu}$: 3337, 2920, 1599, 1584, 1496, 1227 cm^{-1} ; MALDI-TOFMS (m/z): $[\text{M} + \text{H}]^+$ calcd for 361.36; found, 361.21; anal. calcd for $\text{C}_{18}\text{H}_{20}\text{N}_2\text{O}_6$: C, 59.99; H, 5.59; N, 7.77; found: C, 61.07; H, 5.80; N, 8.07.

NMR spectroscopic data for (Z)-6. $^1\text{H NMR}$ (500 MHz, DMSO- d_6) δ 7.32 (t, $J = 7.8$ Hz, 2H, H-15, H-17), 7.18 (t, $J = 7.4$ Hz, 1H, H-16), 6.97 (d, $J = 8.9$ Hz, 2H, H-9, H-11), 6.82 (dd, $J = 8.2$ Hz, $J = 6.7$ Hz, 4H, H-8, H-12, H-14, H-18), 5.32 (d, $J_{1,2} = 1.6$ Hz, 1H, H-1), 3.77 (dd, $J_{2,3} = 3.1$ Hz, $J_{1,2} = 1.9$ Hz, 1H, H-2), 3.62 (dd, $J_{3,4} = 9.3$ Hz, $J_{3,2} = 3.3$ Hz, 1H, H-3), 3.52 (dd, $J_{5,6a} = 2.1$ Hz, $J_{6a,6b} = 11.8$ Hz, 1H, H-6a), 3.48–3.36 (m, 2H, H-4, H-6b), 3.31 (ddd, $J_{4,5} = 9.4$ Hz, $J_{5,6a} = 5.8$ Hz, $J_{5,6b} = 2.1$ Hz, 1H, H-5); $^{13}\text{C NMR}$ (125 MHz, DMSO- d_6) δ 155.4 (C-7), 153.8 (C-13), 147.3 (C-10), 129.1 (C-15, C-17), 127.0 (C-16), 122.5 (C-8, C-12), 119.4 (C-14, C-18), 116.7 (C-9, C-11), 98.7 (C-1), 74.8 (C-5), 70.3 (C-3), 69.7 (C-2), 66.3 (C-4), 60.7 (C-6); UV, λ_{max} : 440 nm, $\epsilon = 2635 \pm 76 \text{ L} \times \text{mol}^{-1} \times \text{cm}^{-1}$.

(E)-p-(Phenylazo)phenyl 6-O-tert-butylidimethylsilyl- α -D-mannopyranoside (7). To a solution of the azobenzene mannoside **6** (3.00 g, 8.33 mmol) in pyridine (30.0 mL) *tert*-butylidimethylchlorosilane (1.38 g, 9.17 mmol) was added and the reaction mixture was stirred at rt for 18 h, after which TLC showed complete consumption of the starting material. The reaction was quenched with MeOH (2.0 mL) and further diluted with ethyl acetate (150 mL). Then it was washed with satd. aq. NaHCO_3 solution (30 mL) and the aqueous phase extracted with ethyl acetate (2 \times 50 mL). The combined organic phases were dried over MgSO_4 and filtered, and the filtrate concentrated under reduced pressure to obtain the crude product. Purification by flash column chromatography ($\text{CH}_2\text{Cl}_2/\text{MeOH}$ 3:7) gave the title compound as a dark orange solid (3.16 g, 6.66 mmol, 80%). Mp 74 °C; R_f 0.59 ($\text{CH}_2\text{Cl}_2/\text{MeOH}$ 7:1); $[\alpha]_D^{20} +73$ (c 0.97, MeOH); $^1\text{H NMR}$ (500 MHz, MeOH- d_4) δ 7.94–7.88 (m, 4H, H-9, H-11, H-14, H-18), 7.57–7.49 (m, 3H, H-15, H-16, H-17), 7.30 (d, $J = 9.0$ Hz, 2H, H-8, H-12), 5.62 (d,

$J_{1,2} = 1.7$ Hz, 1H, H-1), 4.08 (dd, $J_{1,2} = 1.8$ Hz, $J_{2,3} = 3.4$ Hz, 1H, H-2), 3.98 (dd, $J_{5,6a} = 1.8$ Hz, $J_{6a,6b} = 11.2$ Hz, 1H, H-6a), 3.94 (dd, $J_{2,3} = 3.5$ Hz, $J_{3,4} = 9.1$ Hz, 1H, H-3), 3.82 (dd, $J_{5,6b} = 6.5$ Hz, $J_{6a,6b} = 11.3$ Hz, 1H, H-6b), 3.71 (t, $J = 9.4$ Hz, 1H, H-4), 3.65 (m_c, 1H, H-5), 0.83 (s, 9H, *tert*-butyl), 0.04, 0.05 (each s, each 3H, 2 Si- CH_3) ppm; $^{13}\text{C NMR}$ (125 MHz, MeOH- d_4) δ 160.4 (C-7), 154.1 (C-13), 149.18 (C-10), 131.8 (C-16), 130.2 (C-15), 125.5 (C-17), 123.6 (C-9), 118.2 (C-11), 100.0 (C-1), 76.2 (C-5), 72.3 (C-2), 71.7 (C-3), 68.6 (C-4), 64.4 (C-6), 26.4 (C(CH_3)₃), 19.1 (C(CH_3)₃), -5.13 (2 Si- CH_3) ppm; IR (ATR) $\tilde{\nu}$: 3337, 2928, 1599, 1498, 1229, 1006, 685 cm^{-1} ; ESIMS (m/z): $[\text{M} + \text{Na}]^+$ calcd for $\text{C}_{24}\text{H}_{34}\text{N}_2\text{O}_6\text{Si}$, 497.1; found, 497.2;.

(E)-p-(Phenylazo)phenyl 6-O-tert-butylidimethylsilyl-2,3-O-(ethylorthoacetyl)- α -D-mannopyranoside (8). To a solution of mannoside **7** (500 mg, 1.05 mmol) in toluene (8.0 mL), triethylorthoacetate (773 μL , 4.22 mmol) and a catalytic amount of *p*-toluenesulfonic acid were added at rt, and the reaction mixture was stirred for 3.5 h, after which TLC showed complete consumption of the starting material. Then, it was neutralised with triethylamine (100 μL), and the solution was diluted with water (10 mL). It was extracted with toluene (2 \times 20 mL), and the extract was concentrated under reduced pressure to get crude **8** (600 mg) as a red viscous syrup, which was used in the next reaction step without further purification.

(E)-p-(Phenylazo)phenyl 2,3-O-(ethylorthoacetyl)- α -D-mannopyranoside (9). The crude intermediate **8** (600 mg) was dissolved in CH_2Cl_2 (6.0 mL), tetrabutylammonium fluoride (1 M solution in THF, 1.68 mL) was added, and the reaction mixture was stirred at rt for 4 h, after which TLC showed complete consumption of the starting material. Then, it was concentrated under reduced pressure to obtain crude **9** as a dark red viscous syrup (594 mg), which was used in the next reaction step without further purification.

(E)-p-(Phenylazo)phenyl 2,4,6-tri-O-acetyl- α -D-mannopyranoside (10). The crude orthoester-protected mannoside **9** (594 mg) was dissolved in pyridine (2.5 mL), and acetic anhydride (1.26 mL) was added for O-acetylation. The reaction mixture was stirred at rt for 3 h. Then, pyridine was removed under reduced pressure, and the residue was dissolved in ethyl acetate (20 mL) and washed with satd. aq. NaHCO_3 solution (10 mL). The aqueous phase was extracted with ethyl acetate (2 \times 25 mL), the combined organic phases were dried over Na_2SO_4 and filtered, and the filtrate concentrated was under reduced pressure to obtain a syrupy intermediate. It was dissolved in 80% acetic acid (2.5 mL), and the mixture was stirred at rt for 1.5 h to effect regioselective cleavage of the orthoester. Then, ethyl acetate (50 mL) was added and the

organic layer was washed with water (5 mL) and dried over MgSO_4 . It was filtered, and the filtrate was evaporated to obtain the crude product, which purified by column chromatography (cyclohexane/ethyl acetate 2:1) to yield the free 3-OH title mannoside **10** as a bright orange solid (220 mg, 0.453 mmol, 43% over three steps). Mp 144–146 °C; R_f 0.21 (cyclohexane/ethyl acetate); $[\alpha]^{20}_D +70$ (c 0.96, CH_2Cl_2); ^1H NMR (500 MHz, CDCl_3) δ 7.92 (d, $J = 8.9$ Hz, 2H, H-9, H-11), 7.89 (d, $J = 7.9$ Hz, 2H, H-14, H-18), 7.53–7.44 (m, 3H, H-15, H-16, H-17), 7.19 (d, $J = 8.9$ Hz, 2H, H-8, H-12), 5.69 (d, $J_{1,2} = 1.4$ Hz, 1H, H-1), 5.30 (dd, $J_{1,2} = 1.7$ Hz, $J_{2,3} = 3.8$ Hz, 1H, H-2), 5.17 (t, $J = 10.0$ Hz, 1H, H-4), 4.32 (m, 2H, H-3, H-6a), 4.11 (dd, $J_{5,6b} = 2.2$ Hz, $J_{6a,6b} = 12.4$ Hz, 1H, H-6b), 4.05 (m_c, 1H, H-5), 2.23, 2.15, 2.03 (each s, each 3H, 3 OAc), 1.62 (bs, OH) ppm; ^{13}C NMR (150 MHz, CDCl_3) δ 171.3, 170.6, 170.4 (3 COCH_3), 157.7 (C-7), 152.6 (C-13), 148.3 (C-10), 130.8 (C-16), 129.1 (C-15, C-17), 124.6 (C-9, C-11), 122.7 (C-14, C-18), 116.7 (C-8, C-12), 95.42 (C-1), 71.99 (C-2), 69.14 (C-5), 69.04 (C-4), 68.47 (C-3), 62.15 (C-6), 20.97, 20.91, 20.69 (3 COCH_3) ppm; IR (ATR) $\tilde{\nu}$: 3453, 2961, 1737, 1228, 1023, 798 cm^{-1} ; ESIMS (m/z): $[\text{M} + \text{H}]^+$ calcd for $\text{C}_{24}\text{H}_{26}\text{N}_2\text{O}_9$, 509.1; found, 509.2.

(E)-p-(Phenylazo)phenyl 3-O-(2,3,4,6-tetra-O-acetyl- α -D-mannopyranosyl)-2,4,6-tri-O-acetyl- α -D-mannopyranoside (11). The 3-OH unprotected mannoside **10** (50 mg, 103 μmol) and the mannosyl donor **3** (101 mg, 206 μmol) were dissolved in dry CH_2Cl_2 (10 mL), and the mixture was cooled to -10 °C under N_2 atmosphere. To this ice-cooled solution BF_3 ·etherate (13 μL , 108 μmol) was added and the mixture was stirred at 0 °C for about 30 min. Then, the reaction mixture was allowed to warm to rt and stirred for another 4 h. The reaction mixture was then quenched by the addition of a catalytic amount of solid NaHCO_3 and concentrated under reduced pressure to obtain the crude product as a dark reddish-brown syrup. Purification by column chromatography (CH_2Cl_2 /ethyl acetate 8:2) gave the acetyl-protected mannoside **11** as a pale yellow solid (64 mg, 78 μmol , 76%). Mp 84–85 °C; R_f 0.57 (CH_2Cl_2 /ethyl acetate 8:2); $[\alpha]^{20}_D +103$ (c 0.86, CH_2Cl_2); ^1H NMR (500 MHz, CDCl_3) δ 7.92 (d, $J = 9.0$ Hz, 2H, H-9, H-11), 7.89 (d, $J = 7.1$ Hz, 2H, H-14, H-18), 7.46–7.38 (m, 3H, H-15, H-16, H-17), 7.18 (d, $J = 9.0$ Hz, 2H, H-8, H-12), 5.65 (d, $J_{1,2} = 1.7$ Hz, 1H, H-1), 5.46 (dd, $J_{1,2} = 1.8$ Hz, $J_{2,3} = 3.5$ Hz, 1H, H-2), 5.40 (t, $J = 10.1$ Hz, 1H, H-4'), 5.30 (m_c, 1H, H-3'), 5.26 (m_c, 1H, H-4), 5.09 (d, $J_{1,2} = 1.7$ Hz, 1H, H-1'), 5.06 (dd, $J_{1,2} = 1.9$ Hz, $J_{2,3} = 2.9$ Hz, 1H, H-2'), 4.41 (dd, $J_{2,3} = 3.5$ Hz, $J_{3,4} = 9.9$ Hz, 1H, H-3), 4.30 (dd, $J_{5,6b} = 6.3$ Hz, $J_{6a,6b} = 12.7$ Hz, 1H, H-6a), 4.24 (dd, $J_{5',6b'} = 5.8$ Hz, $J_{6a',6b'} = 12.3$ Hz, 1H, H-6a'), 4.14–4.10 (m, H-5', H-6b), 4.08 (dd, $J_{5,6a} = 2.4$ Hz, $J_{6a,6b} = 12.3$ Hz, 1H, H-6b), 3.99 (ddd, $J_{4,5} = 10.2$ Hz, $J_{5,6a} = 2.3$ Hz, $J_{6a,6b} = 5.8$ Hz, 1H, H-5), 2.20, 2.09, 2.08, 2.03, 2.00, 1.97,

1.94 (each s, each 3H, 7 OAc) ppm; ^{13}C NMR (125 MHz, CDCl_3) δ 170.6, 170.5, 170.4, 170.0, 169.9, 169.8, 169.6 (7 COCH_3), 157.4 (C-7), 152.6 (C-13), 148.4 (C-10), 130.8 (C-16), 129.1 (C-15, C-17), 124.6 (C-9, C-11), 122.71 (C-14, C-18) 116.7 (C-8, C-12), 99.1 (C-1'), 95.6 (C-1), 74.8 (C-3), 70.8 (C-2), 69.9 (C-2'), 69.9, 69.6 (C-5, C-5'), 68.3 (C-4), 67.4 (C-4'), 65.9 (C-3'), 62.5, 62.7 (C-6, C-6'), 20.9, 20.8, 20.7, 20.7, 20.6, 20.6 (7 COCH_3) ppm; IR (ATR) $\tilde{\nu}$: 1743, 1213, 1032, 838 cm^{-1} ; ESIMS (m/z): $[\text{M} + \text{Na}]^+$ calcd for $\text{C}_{38}\text{H}_{44}\text{N}_2\text{O}_{18}$, 839.3; found, 839.2.

(E)-p-(Phenylazo)phenyl 3-O-(α -D-mannopyranosyl)- α -D-mannopyranoside (2). The acetyl-protected disaccharide **11** (50 mg, 61.2 μmol) was dissolved in dry MeOH (2 mL) and a catalytic amount of solid NaOMe was added under N_2 atmosphere. The reaction mixture was stirred for 5 h at rt, and then it was neutralized with Amberlite IR 120 ion-exchange resin. It was then filtered and thoroughly washed with MeOH (2 \times 20 mL), and the filtrate was evaporated to obtain the crude product, which after purification by flash column chromatography (CH_2Cl_2 /methanol 9:1) gave the final mannoside **2** as a pale yellow solid (29.3 mg, 56.1 μmol , 92%). Mp 107–109 °C; R_f 0.08 (CH_2Cl_2 /MeOH 9:1); $[\alpha]^{20}_D +18.4$ (c 0.48, MeOH); ^1H NMR (500 MHz, D_2O) δ 7.81 (d, $J = 8.2$ Hz, 2H, H-9, H-11), 7.75 (d, $J = 7.4$ Hz, 2H, H-14, H-18), 7.53–7.49 (m, 3H, H-15, H-16, H-17), 7.24 (d, $J = 8.3$ Hz, 2H, H-8, H-12), 5.65 (s, 1H, H-1), 5.16 (s, 1H, H-1'), 4.29 (m_c, 1H, H-2), 4.14 (dd, $J_{2,3} = 3.1$ Hz, $J_{3,4} = 10.3$ Hz, 1H, H-3'), 4.06 (m_c, 1H, H-2'), 3.89–3.81 (m, 3H, H-3, H-4, H-4'), 3.79–3.62 (m, 6H, H-6a, H-6b, H-5, H-5', H-6a', H-6b') ppm; ^{13}C NMR (125 MHz, D_2O) δ 158.2 (C-7), 151.3 (C-13), 148.2 (C-10), 131.4 (C-16), 129.6 (C-15, C-17), 124.4 (C-9, C-11), 122.2 (C-14, C-18), 117.3 (C-8, C-12), 102.4 (C-1'), 97.8 (C-1), 77.9 (C-3'), 73.8 (C-5), 73.5 (C-3), 70.5 (C-4'), 70.1 (C-2'), 69.5 (C-2), 66.9 (C-5'), 65.9 (C-4), 61.1 (C-6), 60.6 (C-6') ppm; IR (ATR) $\tilde{\nu}$: 3318, 2927, 1599, 1231, 1007, 685 cm^{-1} ; MALDI-TOFMS (m/z): $[\text{M} + \text{Na}]^+$ calcd for $\text{C}_{24}\text{H}_{30}\text{N}_2\text{O}_{11}$, 545.18; found, 545.17; UV, λ_{max} : 339 nm, $\epsilon = 14776 \pm 729 \text{ L} \times \text{mol}^{-1} \times \text{cm}^{-1}$; anal. calcd for $\text{C}_{24}\text{H}_{30}\text{N}_2\text{O}_{11} \times 1.1 \text{ H}_2\text{O}$: C, 52.11; H, 6.09; N, 5.07; found: C, 52.04; H, 5.79; N, 5.06.

NMR-spectroscopic data for (Z)-2. ^1H NMR (500 MHz, D_2O) δ 7.32 (t, $J = 7.1$ Hz, 2H, H-15, H-17), 7.24 (t, 1H, H-16), 7.00 (dd, $J = 1.9$ Hz, $J = 8.9$ Hz, 2H, H-9, H-11), 6.95 (dd, $J = 1.9$ Hz, $J = 8.9$ Hz, 2H, H-8, H-12), 6.91 (dd, $J = 1.3$ Hz, $J = 7.8$ Hz, 2H, H-14, H-18), 5.52 (s, 1H, H-1), 5.12 (s, 1H, H-1'), 4.22 (m_c, 1H, H-2), 4.07 (m_c, 1H, H-3'), 4.03 (dd, $J_{1,2} = 1.7$ Hz, $J_{2,3} = 3.2$ Hz, 1H, H-2'), 3.85–3.82 (m, 2H, H-3, H-4), 3.79–3.59 (m, 7H, H-4', H-6a, H-6b, H-5, H-5', H-6a', H-6b') ppm; ^{13}C NMR (125 MHz, D_2O) δ 155.3 (C-7), 153.5 (C-13), 146.9 (C-10), 129.2 (C-15, C-17), 128.2 (C-16), 123.4 (C-8,

C-12), 120.3 (C-14, C-18), 116.9 (C-9, C-11), 102.4 (C-1'), 97.8 (C-1), 77.8 (C-3'), 73.7 (C-5), 73.4 (C-3), 70.4 (C-4'), 70.1 (C-2'), 69.4 (C-2), 66.8 (C-5'), 65.9 (C-4), 61.0 (C-6), 60.6 (C-6') ppm; UV, λ_{max} : 429 nm, $\epsilon = 1699 \pm 68 \text{ L} \times \text{mol}^{-1} \times \text{cm}^{-1}$.

Supporting Information

Supporting Information File 1

Photoisomerization studies, UV-vis spectra, NMR spectra, bioassay and docking results.

[<http://www.beilstein-journals.org/bjoc/content/supplementary/1860-5397-9-26-S1.pdf>]

Acknowledgements

Financial support by the DFG (collaborative network SFB677) and FCI (Fonds der Chemischen Industrie) is gratefully acknowledged. We thank Max Britz for technical assistance.

References

- Ohlsen, K.; Oelschlaeger, T. A.; Hacker, J.; Khan, A. S. *Top. Curr. Chem.* **2009**, *288*, 17–65. doi:10.1007/128_2008_10
- Klemm, P.; Schembri, M. A. *Int. J. Med. Microbiol.* **2000**, *290*, 27–35. doi:10.1016/S1438-4221(00)80102-2
- Mulvey, M. A. *Cell. Microbiol.* **2002**, *4*, 257–271. doi:10.1046/j.1462-5822.2002.00193.x
- Kau, A. L.; Hunstad, D. A.; Hultgren, S. J. *Curr. Opin. Microbiol.* **2005**, *8*, 54–59. doi:10.1016/j.mib.2004.12.001
- Hartmann, M.; Lindhorst, T. K. *Eur. J. Org. Chem.* **2011**, 3583–3609. doi:10.1002/ejoc.201100407
See for a review.
- Scharenberg, M.; Schwardt, O.; Rabbani, S.; Ernst, B. *J. Med. Chem.* **2012**, *55*, 9810–9816. doi:10.1021/jm3010338
- Knight, S. D.; Bouckaert, J. *Top. Curr. Chem.* **2009**, *288*, 67–107. doi:10.1007/128_2008_13
- Choudhury, D.; Thompson, A.; Stojanoff, V.; Langerman, S.; Pinkner, J.; Hultgren, S. J.; Knight, S. D. *Science* **1999**, *285*, 1061–1066. doi:10.1126/science.285.5430.1061
- Hung, C.-S.; Bouckaert, J.; Hung, D.; Pinkner, J.; Widberg, C.; Defusco, A.; Auguste, C. G.; Strouse, R.; Langermann, S.; Waksman, G.; Hultgren, S. J. *Mol. Microbiol.* **2002**, *44*, 903–918. doi:10.1046/j.1365-2958.2002.02915.x
- Bouckaert, J.; Berglund, J.; Schembri, M.; Genst, E. D.; Cools, L.; Wuhler, M.; Hung, C.-S.; Pinkner, J.; Slättegård, R.; Zavalov, A.; Choudhury, D.; Langermann, S.; Hultgren, S. J.; Wyns, L.; Klemm, P.; Oscarson, S.; Knight, S. D.; Greve, H. D. *Mol. Microbiol.* **2005**, *55*, 441–455. doi:10.1111/j.1365-2958.2004.04415.x
- Wellens, A.; Garofalo, C.; Nguyen, H.; Van Gerven, N.; Slättegård, R.; Hernalsteens, J. P.; Wyns, L.; Oscarson, S.; De Greve, H.; Hultgren, S.; Bouckaert, J. *PLoS One* **2008**, *3*, e2040. doi:10.1371/journal.pone.0002040
- Dubber, M.; Sperling, O.; Lindhorst, T. K. *Org. Biomol. Chem.* **2006**, *4*, 3901–3912. doi:10.1039/b610741a
- Russew, M.-M.; Hecht, S. *Adv. Mater.* **2010**, *22*, 3348–3360. doi:10.1002/adma.200904102
- Kramer, R. H.; Fortin, D. L.; Trauner, D. *Curr. Opin. Neurobiol.* **2009**, *19*, 544–552. doi:10.1016/j.conb.2009.09.004
- Chandrasekaran, V.; Lindhorst, T. K. *Chem. Commun.* **2012**, *48*, 7519–7521. doi:10.1039/c2cc33542e
- Weissenborn, M. J.; Castangia, R.; Wehner, J. W.; Šardžik, R.; Lindhorst, T. K.; Flitsch, S. *Chem. Commun.* **2012**, 4444–4446. doi:10.1039/c2cc30844d
- Grabosch, C.; Kolbe, K.; Lindhorst, T. K. *ChemBioChem* **2012**, *13*, 1874–1879. doi:10.1002/cbic.201200365
- Wehner, J. W.; Weissenborn, M. J.; Hartmann, M.; Gray, C. J.; Šardžik, R.; Eysers, C. E.; Flitsch, S. L.; Lindhorst, T. K. *Org. Biomol. Chem.* **2012**, *10*, 8919–8926. doi:10.1039/c2ob26118a
- Jung, K.-H.; Hoch, M.; Schmidt, R. R. *Liebigs Ann. Chem.* **1989**, 1099–1106. doi:10.1002/jlac.198919890276
- Zemplén, G.; Pacsu, E. *Ber. Dtsch. Chem. Ges. B* **1929**, *62*, 1613–1614. doi:10.1002/cber.19290620640
- Lindhorst, T. K.; Bruegge, K.; Fuchs, A.; Sperling, O. *Beilstein J. Org. Chem.* **2010**, *6*, 801–809. doi:10.3762/bjoc.6.90
- Oscarson, S.; Tidén, A.-K. *Carbohydr. Res.* **1993**, *247*, 323–328. doi:10.1016/0008-6215(93)84266-9
- Hartmann, M.; Horst, A. K.; Klemm, P.; Lindhorst, T. K. *Chem. Commun.* **2010**, *46*, 330–332. doi:10.1039/b922525k
- Rarey, M.; Kramer, B.; Lengauer, T.; Klebe, G. *J. Mol. Biol.* **1996**, *261*, 470–489. doi:10.1006/jmbi.1996.0477
- Rarey, M.; Kramer, B.; Lengauer, T. *J. Comput.-Aided Mol. Des.* **1997**, *11*, 369–384. doi:10.1023/A:1007913026166
- Kramer, B.; Rarey, M.; Lengauer, T. *Proteins: Struct., Funct., Genet.* **1999**, *37*, 228–241. doi:10.1002/(SICI)1097-0134(19991101)37:2<228::AID-PROT8>3.0.CO;2-8
- Clark, R. D.; Strizhev, A.; Leonard, J. M.; Blake, J. F.; Matthew, J. B. *J. Mol. Graphics Modell.* **2002**, *20*, 281–295. doi:10.1016/S1093-3263(01)00125-5
- Charifson, P. S.; Corkery, J. J.; Murcko, M. A.; Walters, W. P. *J. Med. Chem.* **1999**, *42*, 5100–5109. doi:10.1021/jm990352k
- SYBYL, Version 6.9; Tripos, Inc.: St. Louis, MO.
- Dokić, J.; Gothe, M.; Wirth, J.; Peters, M. V.; Schwarz, J.; Hecht, S.; Saalfrank, P. *J. Phys. Chem. A* **2009**, *113*, 6763–6773. doi:10.1021/jp9021344
- Sperling, O.; Fuchs, A.; Lindhorst, T. K. *Org. Biomol. Chem.* **2006**, *4*, 3913–3922. doi:10.1039/b610745a
- Connolly, M. L. *Science* **1983**, *221*, 709–713. doi:10.1126/science.6879170
- Connolly, M. L. *J. Appl. Crystallogr.* **1983**, *16*, 548. doi:10.1107/S0021889883010985
- Sharon, N. *FEBS Lett.* **1987**, *217*, 145–157. doi:10.1016/0014-5793(87)80654-3
- Lindhorst, T. K. Ligands for FimH. In *Synthesis and Biological Applications of Glycoconjugates*; Renaudet, O.; Spinelli, N., Eds.; Bentham Science e-Books, 2011; pp 12–35.
- Hartmann, M.; Papavlassopoulos, H.; Chandrasekaran, V.; Grabosch, C.; Beiroth, F.; Lindhorst, T. K.; Röhl, C. *FEBS Lett.* **2012**, *586*, 1459–1465. doi:10.1016/j.febslet.2012.03.059
- García-Amorós, J.; Díaz-Lobo, M.; Nonell, S.; Velasco, D. *Angew. Chem., Int. Ed.* **2012**, *51*, 12820–12823. doi:10.1002/anie.201207602

License and Terms

This is an Open Access article under the terms of the Creative Commons Attribution License (<http://creativecommons.org/licenses/by/2.0>), which permits unrestricted use, distribution, and reproduction in any medium, provided the original work is properly cited.

The license is subject to the *Beilstein Journal of Organic Chemistry* terms and conditions: (<http://www.beilstein-journals.org/bjoc>)

The definitive version of this article is the electronic one which can be found at:
[doi:10.3762/bjoc.9.26](https://doi.org/10.3762/bjoc.9.26)

Supporting Information

for

Synthesis and testing of the first azobenzene mannobioside as photoswitchable ligand for the bacterial lectin FimH

Vijayanand Chandrasekaran, Katharina Kolbe, Femke Beiroth and Thisbe K. Lindhorst*

Address: Christiana Albertina University of Kiel, Otto Diels Institute of Organic Chemistry,
Otto-Hahn-Platz 3/4, D-24098 Kiel, Germany, Fax: +49 431 8807410

E-mail: Thisbe K. Lindhorst - tklind@oc.uni-kiel.de

*Corresponding author

Photoisomerization studies, UV–vis spectra, NMR spectra, bioassay and docking results

Table of contents

1. Data of photoisomerisation	S2
UV–vis spectra of thermal (<i>Z</i>)- 6 →(<i>E</i>)- 6 relaxation.....	S2
UV–vis spectra of thermal (<i>Z</i>)- 2 →(<i>E</i>)- 2 relaxation.....	S3
¹ H and ¹³ C NMR spectra of (<i>E</i>)- 6 and (<i>Z</i>)- 6	S4
¹ H and ¹³ C NMR spectra of (<i>E</i>)- 2 and (<i>Z</i>)- 2	S5
2. Bioassays	S6
3. Docking studies	S8
4. References	S12

1. Data of photoisomerization

Photoirradiation experiments were carried out at room temperature by using 365 nm LED lights (Product Number: NC4U133A) from Nichia Corporation (NJSE107) with power dissipation 1.4 W and luminous flux 44 [lm]. Photoisomerization experiments with compound **6** were performed in DMSO and with compound **2** in water. Upon irradiation, the photostationary state (PSS) was within 10 min for both compounds, as observed by UV-vis spectroscopy. The $E \rightarrow Z$ isomerisation process is reflected by a decrease of the $\pi-\pi^*$ transition and an increase in the $n-\pi^*$ transition band.

The kinetics of the $Z \rightarrow E$ relaxation process was determined by UV-vis spectroscopy in the dark. For determination of the rate constants, a graph of $\ln(A_\infty - A_t)$ was plotted as a function of time; where A_∞ is the absorbance of the $\pi-\pi^*$ transition at infinitive time and A_t is the absorbance at time t after the relaxation process was started. The negative slope k of the linear plot is the rate constant of the $Z \rightarrow E$ relaxation process. The half life $\tau_{1/2}$ as $\tau_{1/2} = \ln 2/k$.

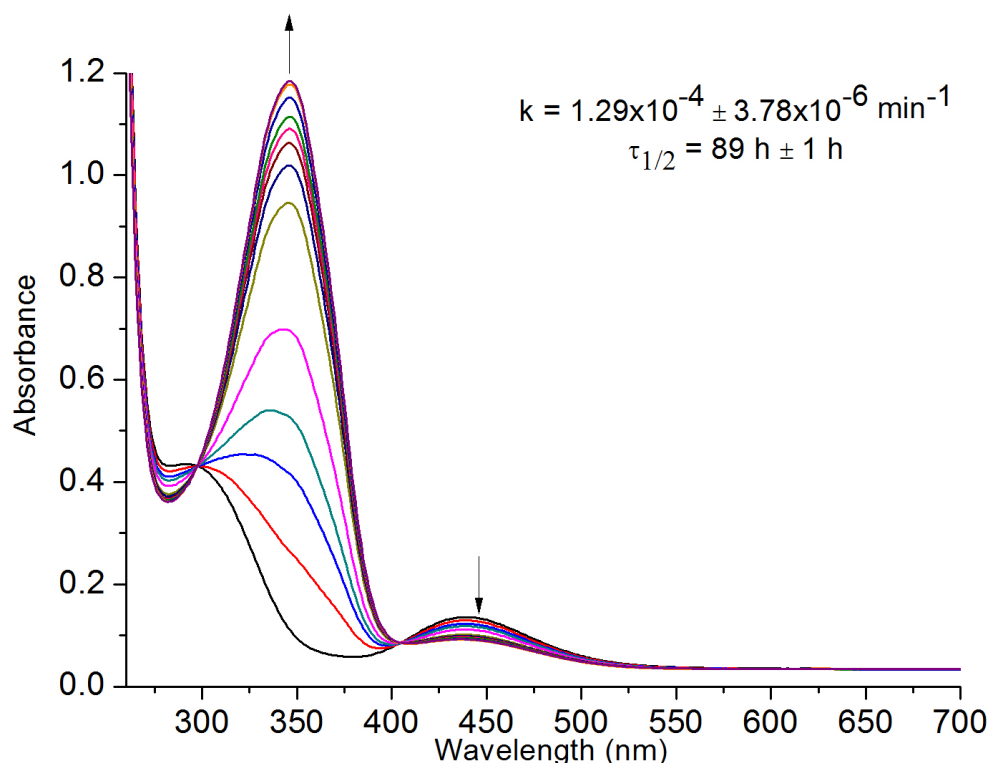


Figure S1: UV-vis spectra of thermal $Z \rightarrow E$ relaxation of mannoside **6** in DMSO (50 μM) at 18 ± 1 °C.

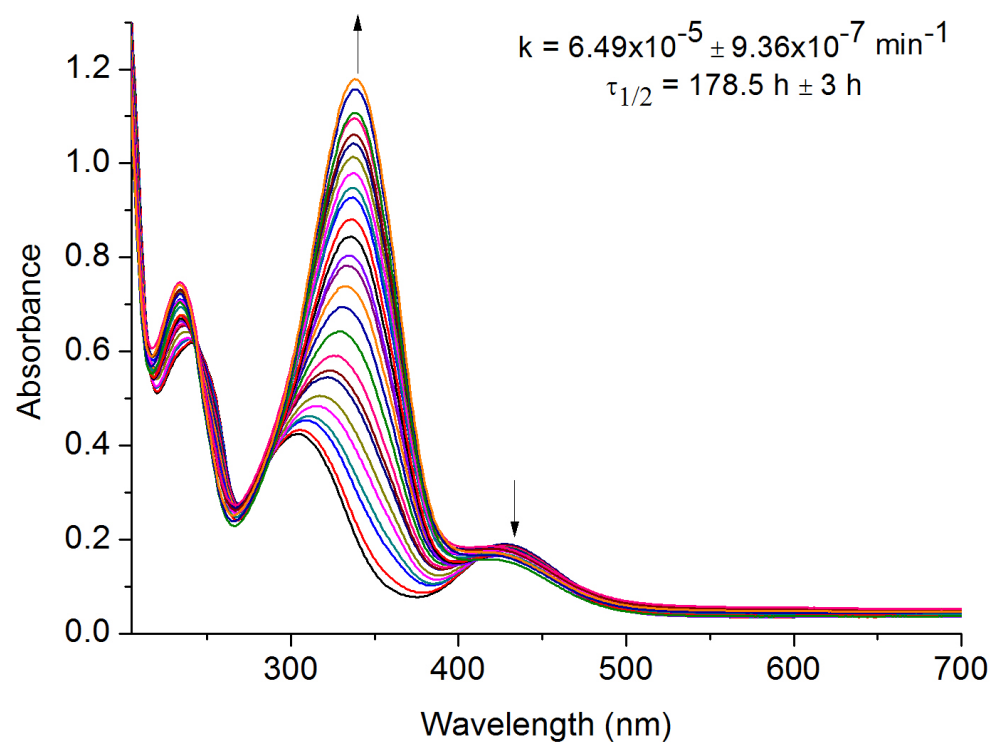


Figure S2: UV-vis spectra of thermal $Z \rightarrow E$ relaxation of the mannobioside **2** in water (65 μM) at 18 ± 1 $^{\circ}\text{C}$.

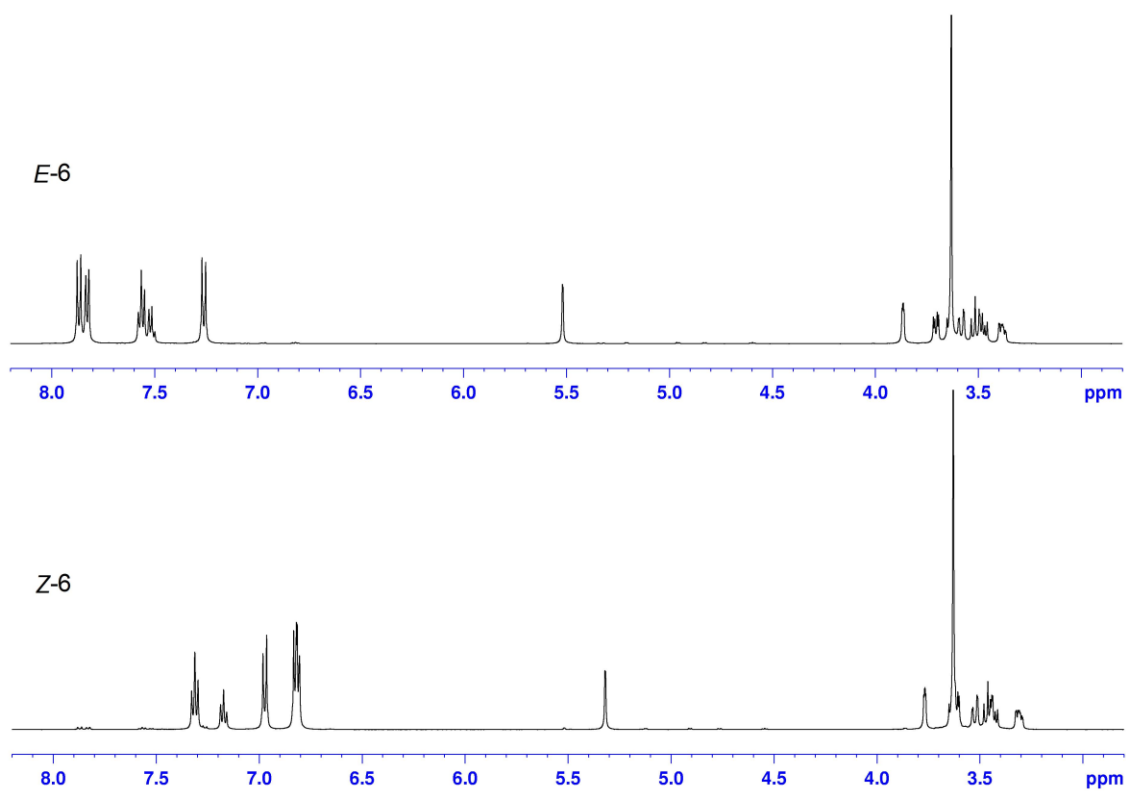


Figure S3: ¹H NMR spectra of (*E*)-**6** and (*Z*)-**6** in DMSO-*d*₆ (500 MHz).

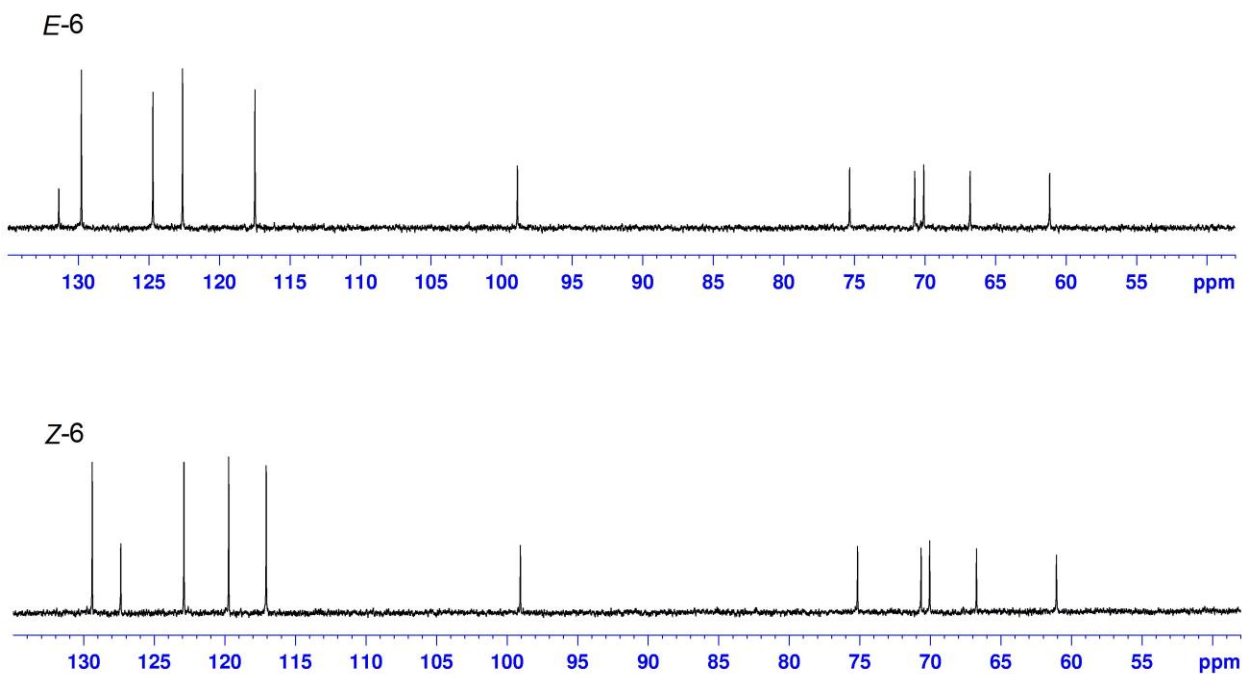


Figure S4: ¹³C NMR spectra of (*E*)-**6** and (*Z*)-**6** in DMSO-*d*₆ (125 MHz).

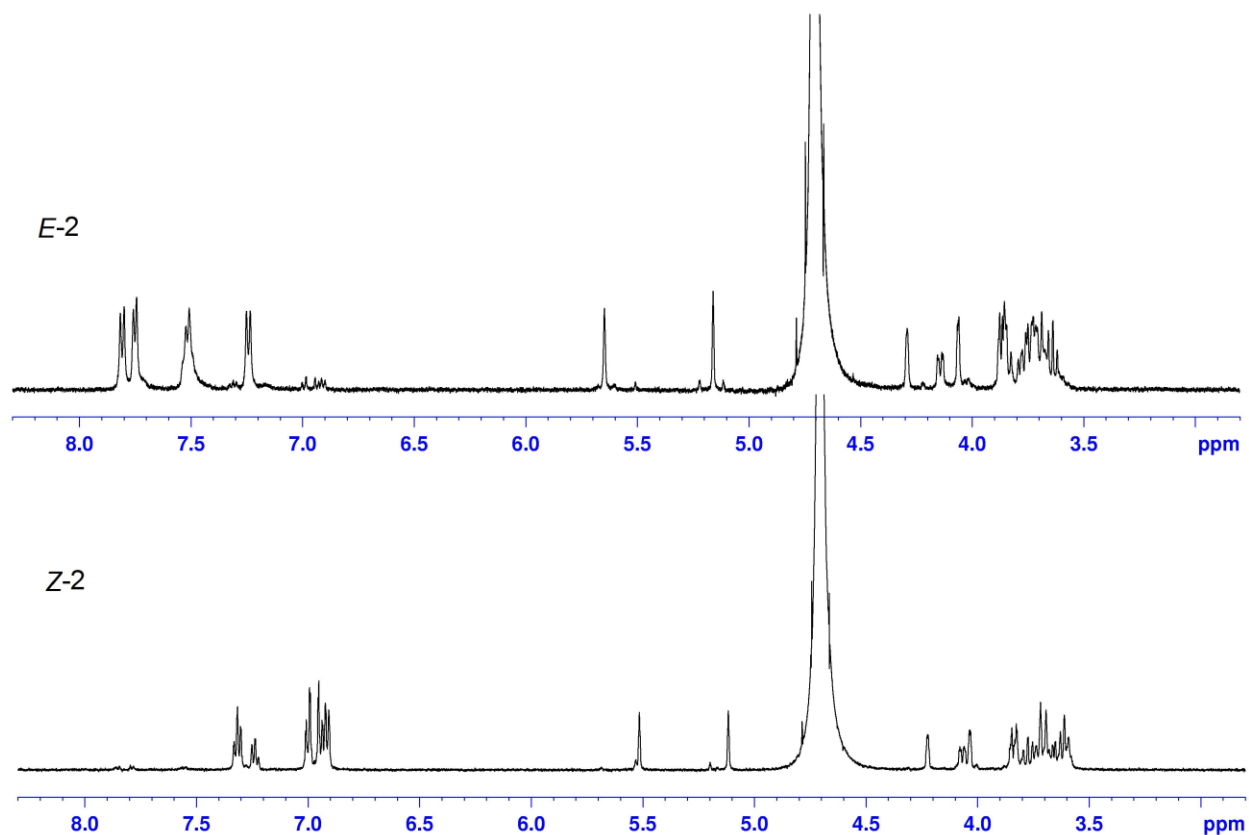


Figure S5: ¹H NMR spectra of (*E*)-**2** and (*Z*)-**2** in D₂O (500 MHz).

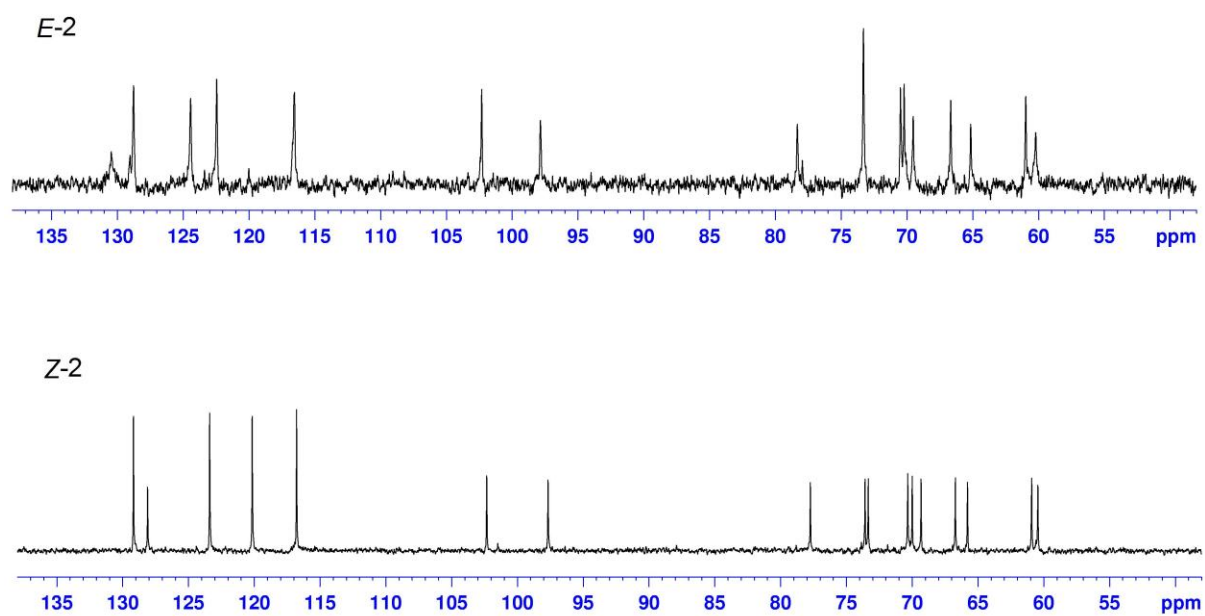


Figure S6: ¹³C NMR spectra of (*E*)-**2** and (*Z*)-**2** in D₂O (125 MHz).

2. Bioassays

Media and buffer solutions: Carbonate buffer solution (pH 9.6): sodium carbonate (1.59 g) and sodium hydrogen carbonate (2.52 g) were dissolved in double-distilled water (1.00 L). PBS buffer solution (pH 7.2): sodium chloride (8.00 g), potassium chloride (200 mg), sodium hydrogen phosphate dihydrate (1.44 g) and potassium dihydrogenphosphate (200 mg) were dissolved in double-distilled water (1.00 L). PBST buffer solution (pH 7.2): PBS buffer + 0.05% v/v Tween® 20. LB medium: tryptone (10.0 g), sodium chloride (10.0 g) and yeast extract (5.00 g) were dissolved in distilled, deionised water (1.00 L); after autoclaving, ampicillin (100 mg) and chloramphenicol (50.0 mg) were added. pH values were adjusted by using 0.1 M HCl or 0.1 M NaOH.

Cultivation of bacteria: *E. coli* bacteria (strain pPKL1162) [1] were grown on LB medium overnight at 37 °C in a sterilized tube. After centrifugation and washing with PBS buffer (2 × 2.00 mL) the bacteria pellet was suspended to a concentration of 2.00 mg/mL in PBS buffer.

GFP assay: The published assay [2] was adapted and modified as follows: Black (nunc Maxisorp) plates were treated with a solution of mannan from *Saccharomyces cerevisiae* (1.2 mg/mL in carbonate buffer, pH 9.5; 100 µL/well) and allowed to dry at 37 °C overnight. The plates were washed with PBST (3 × 150 µL/well). Before use the wells were blocked with BSA (5% in PBS, 120 µL/well) for 2 h at 37 °C and then washed with PBST (3 × 150 µL/well). Serial dilutions of the examined inhibitor mannobioside **2** ((*E*)- or (*Z*)-configured, respectively) were prepared in the plates (50 µL/well). The bacteria suspension (2 mg bacteria/mL, 50 µL/well) was added and the plates were agitated (80 rpm) and incubated for 1 h at 37 °C. After washing with PBS (2 × 150 µL) the wells were filled with PBS (100 µL/well) and the fluorescence intensity (485 nm/535 nm) was determined.

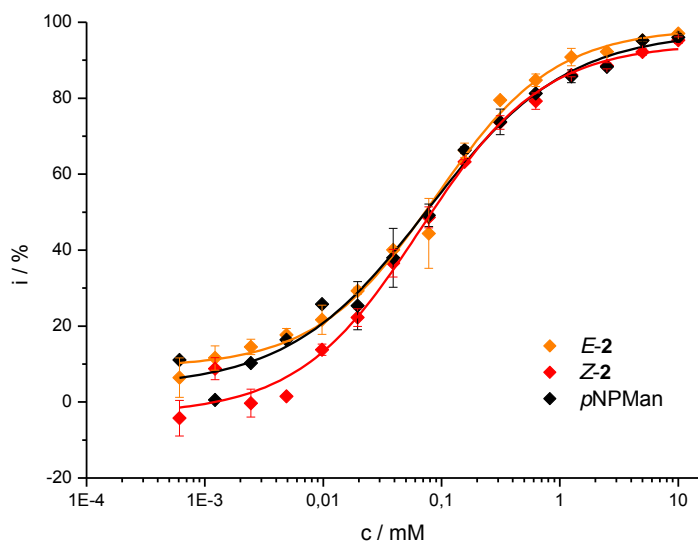


Figure S7: Inhibition curves obtained in inhibition of adhesion of *E. coli* to a mannan-coated surface. The isomers (*E*)- and (*Z*)-**2** were tested on one microtiter plate together with pNPMAN. The sigmoidal concentration–response curves were fitted by nonlinear regression.

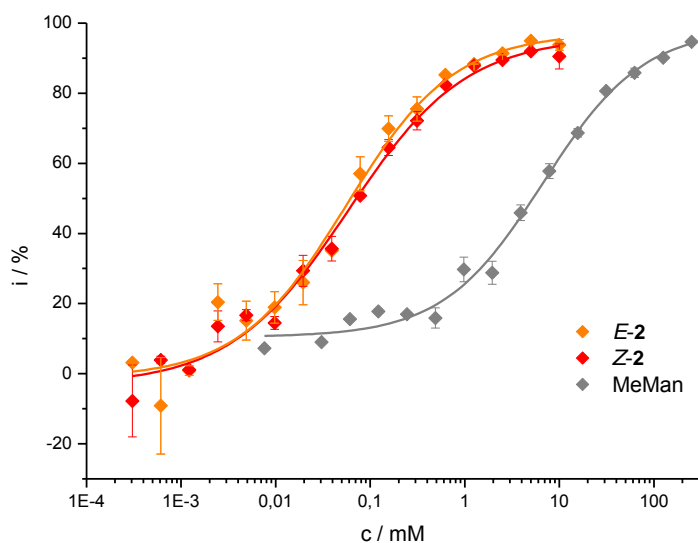


Figure S8: Inhibition curves obtained in inhibition of adhesion of *E. coli* to a mannan-coated surface. The isomers (*E*)- and (*Z*)-**2** were tested on one microtiter plate together with MeMan. The sigmoidal concentration–response curves were fitted by nonlinear regression.

3. Docking studies

Computer-aided docking was performed by using FlexX flexible docking and consensus scoring, as implemented in Sybyl 6.9 [3] as described previously [4]. Docking was based on two published X-ray structures of the bacterial lectin FimH [5] (1KLF (open-gate) and 1UWF (closed-gate structure)). The torsion angle of the azobenzene moiety was manually set up to 180° for the (*E*)- and to 90° for the (*Z*)-isomer and then the structures were minimized by using the Tripos force field and Gasteiger–Hückel charges. Thirty conformations and FlexX scoring values were obtained for each ligand and listed in Tables S1–S4.

Table S1: Scoring values for docking of *E*-configured azobenzene mannobioside **2** into the closed-gate structure of FimH.

No.	Total Score	Match Score	Lipo Score	Ambig Score	Clash Score	Rot Score	RMS Value	Simil. Index	#Match	Avg. Volume	Max. Volume	Frag. No.
1	-20.362	-25.378	-12.299	-8.232	1.947	18.200	0.000	-1.000	9	0.045	0.666	1
2	-19.480	-28.399	-10.811	-8.923	5.053	18.200	5.165	-1.000	10	0.193	2.362	1
3	-18.806	-23.699	-12.232	-8.767	2.292	18.200	0.816	-1.000	8	0.049	0.840	1
4	-18.641	-25.472	-11.712	-8.529	3.472	18.200	0.563	-1.000	10	0.127	1.369	1
5	-18.416	-24.813	-11.531	-8.295	2.622	18.200	0.825	-1.000	9	0.053	0.710	1
6	-18.401	-25.638	-10.708	-7.968	2.313	18.200	1.574	-1.000	9	0.072	1.215	1
7	-18.063	-23.870	-11.586	-9.123	2.917	18.200	0.904	-1.000	9	0.099	1.916	1
8	-18.047	-28.399	-9.790	-8.512	5.053	18.200	4.341	-1.000	10	0.193	2.362	1
9	-17.876	-28.399	-9.822	-8.309	5.053	18.200	4.908	-1.000	10	0.193	2.362	1
10	-17.872	-28.399	-9.817	-8.309	5.053	18.200	4.922	-1.000	10	0.193	2.362	1
11	-17.859	-28.399	-9.810	-8.306	5.056	18.200	4.911	-1.000	10	0.193	2.362	1
12	-17.832	-27.788	-10.267	-8.836	5.459	18.200	3.758	-1.000	10	0.237	2.362	1
13	-17.800	-28.928	-7.061	-8.124	2.714	18.200	3.619	-1.000	14	0.096	1.580	1
14	-17.744	-27.788	-9.883	-9.132	5.459	18.200	3.807	-1.000	10	0.237	2.362	1
15	-17.676	-28.399	-9.579	-8.351	5.053	18.200	4.356	-1.000	10	0.193	2.362	1
16	-17.563	-29.810	-5.148	-7.249	1.044	18.200	7.255	-1.000	10	0.067	1.818	1
17	-17.563	-29.810	-5.148	-7.249	1.044	18.200	7.015	-1.000	10	0.067	1.818	1
18	-17.563	-29.810	-5.148	-7.249	1.044	18.200	5.507	-1.000	10	0.067	1.818	1
19	-17.563	-29.810	-5.148	-7.249	1.044	18.200	6.413	-1.000	10	0.067	1.818	1
20	-17.563	-29.810	-5.148	-7.249	1.044	18.200	7.271	-1.000	10	0.067	1.818	1
21	-17.563	-29.810	-5.148	-7.249	1.044	18.200	7.057	-1.000	10	0.067	1.818	1
22	-17.563	-29.810	-5.148	-7.249	1.044	18.200	5.813	-1.000	10	0.067	1.818	1
23	-17.563	-29.810	-5.148	-7.249	1.044	18.200	5.763	-1.000	10	0.067	1.818	1
24	-17.563	-29.810	-5.148	-7.249	1.044	18.200	7.050	-1.000	10	0.067	1.818	1
25	-17.563	-29.810	-5.148	-7.249	1.044	18.200	6.432	-1.000	10	0.067	1.818	1
26	-17.563	-29.810	-5.148	-7.249	1.044	18.200	7.000	-1.000	10	0.067	1.818	1
27	-17.563	-29.810	-5.148	-7.249	1.044	18.200	6.404	-1.000	10	0.067	1.818	1
28	-17.563	-29.810	-5.148	-7.249	1.044	18.200	5.785	-1.000	10	0.067	1.818	1
29	-17.563	-29.810	-5.148	-7.249	1.044	18.200	5.823	-1.000	10	0.067	1.818	1
30	-17.563	-29.810	-5.148	-7.249	1.044	18.200	7.052	-1.000	10	0.067	1.818	1

Table S2: Scoring values for docking of *E*-configured azobenzene mannobioside **2** into the open-gate structure of FimH.

No.	Total Score	Match Score	Lipo Score	Ambig Score	Clash Score	Rot Score	RMS Value	Simil. Index	#Match	Avg. Volume	Max. Volume	Frag. No.
1	-28.809	-34.291	-10.848	-9.010	1.740	18.200	0.000	-1.000	16	0.040	0.577	1
2	-28.340	-34.839	-11.028	-9.298	3.224	18.200	0.553	-1.000	17	0.112	1.245	1
3	-28.331	-34.037	-10.560	-9.118	1.784	18.200	0.312	-1.000	17	0.042	0.600	1
4	-28.006	-34.637	-11.348	-8.848	3.227	18.200	0.451	-1.000	16	0.115	1.271	1
5	-27.439	-34.726	-12.221	-9.279	5.186	18.200	0.753	-1.000	19	0.188	1.635	1
6	-27.439	-34.726	-12.221	-9.279	5.186	18.200	0.754	-1.000	19	0.188	1.635	1
7	-27.310	-34.110	-12.764	-9.021	4.986	18.200	0.973	-1.000	19	0.195	1.803	1
8	-27.310	-34.110	-12.764	-9.021	4.986	18.200	0.977	-1.000	19	0.195	1.803	1
9	-27.105	-34.470	-11.724	-9.320	4.810	18.200	0.821	-1.000	19	0.174	1.591	1
10	-27.105	-34.470	-11.724	-9.320	4.810	18.200	0.820	-1.000	19	0.174	1.591	1
11	-26.932	-33.398	-9.896	-9.136	1.898	18.200	0.692	-1.000	18	0.050	0.357	1
12	-26.374	-32.093	-11.116	-9.247	2.482	18.200	2.173	-1.000	14	0.103	2.432	1
13	-26.374	-32.093	-11.116	-9.247	2.482	18.200	2.178	-1.000	14	0.103	2.432	1
14	-26.027	-32.323	-11.843	-9.705	4.243	18.200	0.715	-1.000	19	0.154	1.414	1
15	-25.828	-32.093	-10.673	-9.376	2.713	18.200	2.142	-1.000	14	0.109	2.432	1
16	-25.656	-31.832	-11.030	-9.314	2.920	18.200	2.217	-1.000	14	0.121	2.499	1
17	-25.269	-32.753	-9.472	-9.062	2.417	18.200	0.774	-1.000	17	0.062	0.408	1
18	-25.180	-32.257	-12.177	-9.206	4.860	18.200	2.309	-1.000	16	0.210	1.894	1
19	-25.136	-36.193	-4.934	-8.667	1.058	18.200	6.207	-1.000	15	0.020	0.233	1
20	-25.028	-36.127	-4.994	-8.590	1.083	18.200	6.155	-1.000	15	0.021	0.239	1
21	-24.949	-36.035	-5.107	-8.583	1.175	18.200	6.188	-1.000	15	0.021	0.233	1
22	-24.836	-31.393	-10.343	-9.182	2.482	18.200	2.013	-1.000	13	0.103	2.432	1
23	-24.836	-31.393	-10.343	-9.182	2.482	18.200	2.010	-1.000	13	0.103	2.432	1
24	-24.666	-31.393	-10.173	-9.182	2.482	18.200	2.012	-1.000	13	0.103	2.432	1
25	-24.666	-31.393	-10.173	-9.182	2.482	18.200	2.007	-1.000	13	0.103	2.432	1
26	-24.462	-32.257	-11.944	-9.259	5.397	18.200	2.333	-1.000	16	0.240	1.894	1
27	-24.379	-28.723	-10.438	-9.887	1.068	18.200	0.784	-1.000	17	0.042	0.743	1
28	-24.110	-31.788	-9.435	-9.119	2.631	18.200	0.894	-1.000	16	0.075	0.833	1
29	-24.097	-31.488	-8.155	-8.762	0.709	18.200	1.267	-1.000	19	0.010	0.155	1
30	-24.059	-32.062	-11.949	-9.376	5.727	18.200	2.277	-1.000	16	0.264	1.894	1

Table S3: Scoring values for docking of Z-configured azobenzene mannoside **2** into the closed-gate structure of FimH.

No.	Total Score	Match-Score	Lipo-Score	Ambig-Score	Clash-Score	Rot-Score	RMS-Value	Simil.-Index	#Match	Avg. Volume	Max. Volume	Frag.No.
1	-21.629	-32.441	-6.000	-8.104	1.316	18.200	0.000	-1.000	16	0.023	0.368	1
2	-21.028	-31.583	-6.370	-8.124	1.449	18.200	0.562	-1.000	14	0.027	0.373	1
3	-20.667	-29.688	-8.669	-7.905	1.996	18.200	1.280	-1.000	15	0.069	1.365	1
4	-20.367	-29.176	-8.595	-8.544	2.347	18.200	1.314	-1.000	15	0.091	1.397	1
5	-20.343	-27.224	-11.410	-7.122	1.813	18.200	3.973	-1.000	9	0.036	0.505	1
6	-20.294	-30.810	-8.664	-7.539	3.119	18.200	2.711	-1.000	15	0.103	1.239	1
7	-19.913	-28.876	-9.322	-6.770	1.454	18.200	4.235	-1.000	12	0.029	0.272	1
8	-19.572	-31.351	-5.484	-7.834	1.497	18.200	1.277	-1.000	13	0.029	0.433	1
9	-19.433	-31.283	-5.756	-7.819	1.824	18.200	1.265	-1.000	13	0.036	0.436	1
10	-19.289	-31.357	-6.031	-8.700	3.198	18.200	0.913	-1.000	13	0.124	1.623	1
11	-19.261	-30.218	-8.659	-7.725	3.742	18.200	2.711	-1.000	14	0.144	1.726	1
12	-19.256	-28.248	-9.447	-6.788	1.627	18.200	4.389	-1.000	11	0.034	0.392	1
13	-19.074	-29.401	-8.115	-7.754	2.596	18.200	1.463	-1.000	15	0.085	1.293	1
14	-19.073	-30.200	-7.072	-6.499	1.098	18.200	2.802	-1.000	15	0.017	0.213	1
15	-19.073	-30.200	-7.072	-6.499	1.098	18.200	2.726	-1.000	15	0.017	0.213	1
16	-18.928	-28.939	-8.841	-6.950	2.203	18.200	3.917	-1.000	12	0.070	0.948	1
17	-18.657	-29.088	-7.827	-7.390	2.048	18.200	3.044	-1.000	13	0.050	0.699	1
18	-18.636	-29.088	-7.806	-7.390	2.048	18.200	3.025	-1.000	13	0.050	0.699	1
19	-18.544	-29.238	-6.309	-7.606	1.010	18.200	2.447	-1.000	13	0.018	0.163	1
20	-18.544	-29.238	-6.309	-7.606	1.010	18.200	2.536	-1.000	13	0.018	0.163	1
21	-18.532	-29.157	-10.540	-6.618	4.184	18.200	2.877	-1.000	11	0.190	2.247	1
22	-18.369	-27.137	-9.210	-7.423	1.801	18.200	2.706	-1.000	10	0.040	0.506	1
23	-18.219	-28.909	-7.796	-7.162	2.048	18.200	2.076	-1.000	12	0.048	0.699	1
24	-18.171	-28.909	-7.796	-7.113	2.048	18.200	2.070	-1.000	12	0.048	0.699	1
25	-18.063	-29.804	-6.325	-6.930	1.396	18.200	2.757	-1.000	13	0.025	0.214	1
26	-18.046	-29.467	-6.656	-6.676	1.153	18.200	3.441	-1.000	13	0.018	0.197	1
27	-18.046	-29.467	-6.656	-6.676	1.153	18.200	3.375	-1.000	13	0.018	0.197	1
28	-18.012	-30.467	-6.022	-7.753	2.630	18.200	1.721	-1.000	15	0.117	2.095	1
29	-17.962	-28.449	-8.869	-6.443	2.198	18.200	4.259	-1.000	10	0.052	0.496	1
30	-17.885	-28.909	-7.796	-6.828	2.048	18.200	2.666	-1.000	12	0.048	0.699	1

Table S4: Scoring values for docking of Z-configured azobenzene mannoside **2** into the open-gate structure of FimH.

No.	Total Score	Match Score	Lipo Score	Ambig Score	Clash Score	Rot Score	RMS Value	Simil. Index	#Match	Avg. Volume	Max. Volume	Frag. No.
1	-28.675	-36.178	-11.041	-10.107	5.052	18.200	0.000	-1.000	18	0.183	1.604	1
2	-28.101	-35.957	-11.911	-9.699	5.866	18.200	0.607	-1.000	18	0.278	1.895	1
3	-27.461	-34.986	-8.537	-9.270	1.733	18.200	1.984	-1.000	18	0.026	0.176	1
4	-27.338	-35.333	-8.159	-9.387	1.942	18.200	1.135	-1.000	18	0.047	0.658	1
5	-27.337	-36.098	-8.771	-8.701	2.633	18.200	1.827	-1.000	20	0.066	0.866	1
6	-27.336	-35.422	-8.846	-8.652	1.984	18.200	1.153	-1.000	20	0.035	0.296	1
7	-27.311	-33.089	-11.891	-9.269	3.338	18.200	1.173	-1.000	17	0.081	1.103	1
8	-26.980	-35.283	-8.233	-9.112	2.049	18.200	1.206	-1.000	17	0.044	0.567	1
9	-26.805	-32.947	-13.663	-9.641	5.846	18.200	1.635	-1.000	15	0.208	1.668	1
10	-26.779	-34.867	-8.583	-8.989	2.060	18.200	1.235	-1.000	18	0.035	0.245	1
11	-26.656	-33.244	-15.330	-9.986	8.304	18.200	1.338	-1.000	17	0.356	2.058	1
12	-26.549	-34.269	-8.961	-9.240	2.320	18.200	1.353	-1.000	17	0.054	0.507	1
13	-26.548	-34.518	-8.751	-8.639	1.760	18.200	1.811	-1.000	17	0.034	0.440	1
14	-26.414	-34.527	-8.636	-8.612	1.762	18.200	1.871	-1.000	17	0.034	0.434	1
15	-26.242	-34.448	-8.513	-8.706	1.825	18.200	1.241	-1.000	17	0.031	0.238	1
16	-26.226	-35.056	-8.329	-8.324	1.884	18.200	3.890	-1.000	17	0.033	0.275	1
17	-26.110	-32.411	-11.442	-8.774	2.917	18.200	1.181	-1.000	17	0.062	0.811	1
18	-26.072	-32.609	-14.988	-10.020	7.946	18.200	1.378	-1.000	16	0.304	1.790	1
19	-25.929	-34.907	-7.597	-9.245	2.220	18.200	1.221	-1.000	18	0.052	0.746	1
20	-25.737	-32.637	-10.894	-9.386	3.580	18.200	1.833	-1.000	16	0.086	0.998	1
21	-25.682	-33.273	-8.441	-8.614	1.047	18.200	4.184	-1.000	18	0.022	0.502	1
22	-25.442	-34.053	-8.308	-8.537	1.857	18.200	2.812	-1.000	16	0.038	0.535	1
23	-25.332	-30.941	-12.878	-10.138	5.025	18.200	1.361	-1.000	15	0.188	1.812	1
24	-25.318	-31.356	-10.634	-8.341	1.414	18.200	1.356	-1.000	19	0.019	0.134	1
25	-25.303	-33.041	-8.315	-8.586	1.039	18.200	2.651	-1.000	17	0.021	0.455	1
26	-25.300	-33.035	-8.317	-8.586	1.038	18.200	2.671	-1.000	17	0.021	0.455	1
27	-25.285	-32.073	-9.889	-9.078	2.155	18.200	2.017	-1.000	13	0.070	1.488	1
28	-25.264	-33.053	-8.295	-8.647	1.131	18.200	4.224	-1.000	17	0.022	0.485	1
29	-25.254	-32.748	-10.455	-9.964	4.313	18.200	1.356	-1.000	14	0.207	1.668	1
30	-25.249	-34.097	-10.945	-8.911	5.104	18.200	1.892	-1.000	16	0.160	1.519	1

4. References

- [1] a) Reisner, A.; Haagensen, J. A. J.; Schembri, M. A.; Zechner, E. L.; Molin, S., *Mol. Microbiol.*, **2003**, *48*, 933-946; b) The GFP-tagged strain pPKL1162 was constructed in the Klemm group by introduction of the plasmid pPKL174 into strain SAR18; pPKL174 contains the fim gene cluster, which is required for type 1 fimbriae assembly and expression. The chromosome of strain SAR18 from the Reisner group contains the GFP gene, controlled by a constitutive promoter.
- [2] Hartmann, M.; Horst, A. K.; Klemm, P.; Lindhorst, T. K., *Chem. Commun.* **2010**, *46*, 330-332.
- [3] Tripos, Inc., SYBYL 6.9, 1699 South Hanley Road, St. Louis, MO 63144-2319.
- [4] Grabosch, C.; Hartmann, M.; Schmidt-Lassen, J.; Lindhorst, T. K. *ChemBioChem* **2011**, *12*, 1066-1074.
- [5] a) Hung, C. S.; Bouckaert, J.; Hung, D.; Pinkner, J., Widberg, C.; Defusco, A.; Auguste, C. G.; Strouse, R.; Langermann, S.; Waksman, G.; Hultgren, S. J. *Mol. Microbiol.* **2002**, *44*, 903-915.; b) Bouckaert, J.; Berglund, J.; Schembri, M.; De Genst, E.; Cools, L.; Wuhrer, M.; Hung, C. S.; Pinkner, J.; Slättegård, R.; Zavialov, A.; Choudhury, D.; Langermann, S.; Hultgren, S. J.; Wyns, L.; Klemm, P.; Oscarson, S.; Knight, S. D.; De Greve, H. *Mol. Microbiol.* **2005**, *55*, 441-455.

3.2 Sweet switches: Synthesis and photochemical properties of azobenzene glycosides.

Vijayanand Chandrasekaran, Eugen Johannes, Hauke Kobarg, Frank D. Sönnichsen, Thisbe K. Lindhorst*

Chem. Eur. J, to be submitted.

Before exploring azobenzene glycoconjugates in biochemical applications it is essential to have knowledge about their photochromic properties in solution. Although few examples of carbohydrates conjugated to azobenzene are known, the systematic investigations of their photochemical properties has not been published yet.

In this manuscript, a series of azobenzene glycosides was synthesized. All the compounds were varied with regard to the anomeric configuration (α or β , mannose or glucose, respectively), then configuration of the carbohydrates at C-2 and different substituents on the azobenzene moiety (Fig 4.1.2). Photochromic properties for the photoswitchable glycoconjugates were studied, compared and discussed.

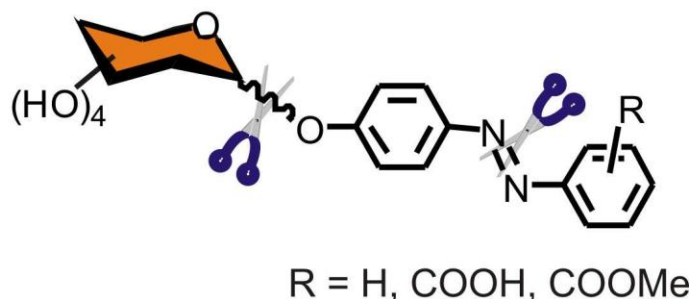


Figure 3.2: Retrosynthetic cuts for the preparation of different azobenzene glycosides. All are varied with regard to anomeric configuration (α or β , mannose or glucose, respectively) and substituent at the azobenzene moiety.

In this project, E. Johannes synthesized the azobenzene α -D-glucosides (4-6), H. Kobarg synthesized compound 29 and I synthesized all azobenzene α -D-mannosides (1-3) and β -D-glucosides (7-9, 26 and 27). I and T. K. Lindhorst wrote the manuscript and supporting information.

Sweet switches: Synthesis and photochemical properties of azobenzene glycosides

Vijayanand Chandrasekaran,^[a] Eugen Johannes,^[a] Hauke Kobarg,^[a] Frank D. Sönnichsen^[a] and Thisbe K. Lindhorst^{*[a]}

Abstract: A series of photoswitchable azobenzene glycosides were synthesized and their photochemical properties studied. These

photoswitchable carbohydrates can be used as a model system to understand the conformational behaviour/role in protein bindings.

Keywords: glycosides • azobenzene • photoisomerization • functional glycoconjugates

Introduction

“Sweet switches” are carbohydrate derivatives that can be reversibly shifted between two structurally different states in order to control their function. Such functional saccharides are envisioned to serve as molecular tools to study the details of carbohydrate recognition in a biochemical context. For example, switching the orientation of carbohydrate epitopes within an array of glycans allows to study the consequences of carbohydrate orientation on surfaces in essential biological processes such as carbohydrate-protein interactions^[1, 2] and cell adhesion.

Our minimalistic “sweet switch” design for structure-function studies comprises a selected saccharide covalently linked to a photoactive compound. For the latter, we select the azobenzene moiety, as it is well known to serve as a reliable photoresponsive unit, permitting to switch (an attached glycoside) between two independently addressable states.^[3] Irradiation of the planar and more stable *E*-azobenzene form with UV light (λ 365 nm) effects transition to the bent *Z*-isomer. Thus, *E/Z* isomerization of the azobenzene unit effects a considerable change in the spatial orientation of the conjugated sugar moiety. By exposure to visible light ($\lambda > 440$ nm) or by thermal equilibration, the azobenzene *Z*-isomer relaxes back to the *E*-form according to a half life $\tau_{1/2}$ which

is an individual parameter of a specific azobenzene derivative (Figure 1).

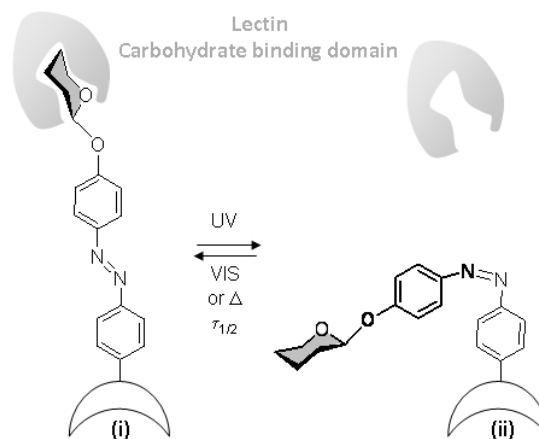


Figure 1. *E/Z* Isomerization of azobenzene glycosides leads to a significant change in orientation of the ligated carbohydrate moiety and can thus effect essential biological processes connected to carbohydrate recognition: (i) lectin binding; (ii) no lectin binding.

[a] V. Chandrasekaran, E. Johannes, H. Kobarg, Prof. Dr. F. D. Sönnichsen, Prof. Dr. Th. K. Lindhorst
Otto Diels Institute of Organic Chemistry
Christiana Albertina University of Kiel
Otto-Hahn-Platz 3/4, 24098 Kiel, Germany.
Fax: (+)49 431-880-7140
E-mail: tkind@oc.uni-kiel.de

Supporting information for this article is available on the WWW under <http://www.chemeurj.org/>.

Whereas in nucleic acid and protein chemistry the azobenzene unit has been frequently used as photoswitchable unit,^[4] only few examples of carbohydrate-azobenzene conjugates are known and no systematic investigation of their photochromic properties has been published so far.^[5-7] In addition, carbohydrates have mostly been conjugated to the azobenzene sub-structure by peptide coupling, and only rarely glycosidically linked azobenzene derivatives have been prepared.^[8-10] In azobenzene glycosides, the azobenzene unit is *O*-glycosidically attached to the relevant carbohydrate. Here, in order

to validate this class of sweet switches for biochemical applications, a series of different azobenzene glycosides was synthesized and their photochromic properties compared. Azobenzene glycosides were varied with regard to configuration at C-2 of the carbohydrate ring (mannose or glucose, respectively), the anomeric configuration (α or β , respectively), and a substituent at the azobenzene moiety. Accordingly, nine azobenzene glycosides (Figure 2) were selected as target molecules for this study and their *E/Z* isomerization investigated.

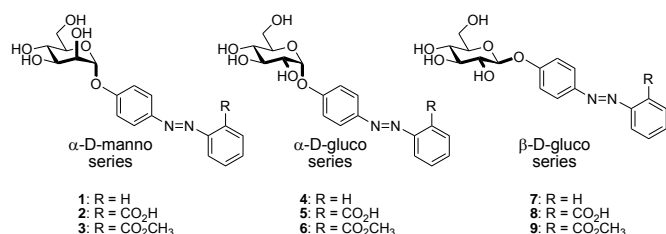


Figure 2. Target azobenzene glycosides: Structural characteristics were systematically varied to study their effect on the photochromic properties of the respective glycoside.

Preparation of azobenzene glycosides can be rather straightforward. Just one or two retrosynthetic cuts, respectively, are required for their synthesis (Figure 3). Either glycosylation of the hydroxylated azobenzene aglycon furnishes the target glycoside in one step; or first an appropriate glycosidic aniline is prepared and then condensation with a nitrosoarene completes the synthetic route (Mills reaction).^[11]

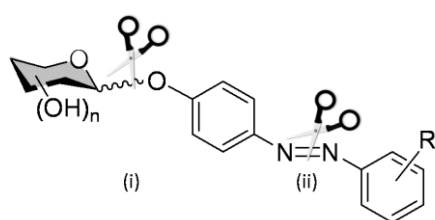
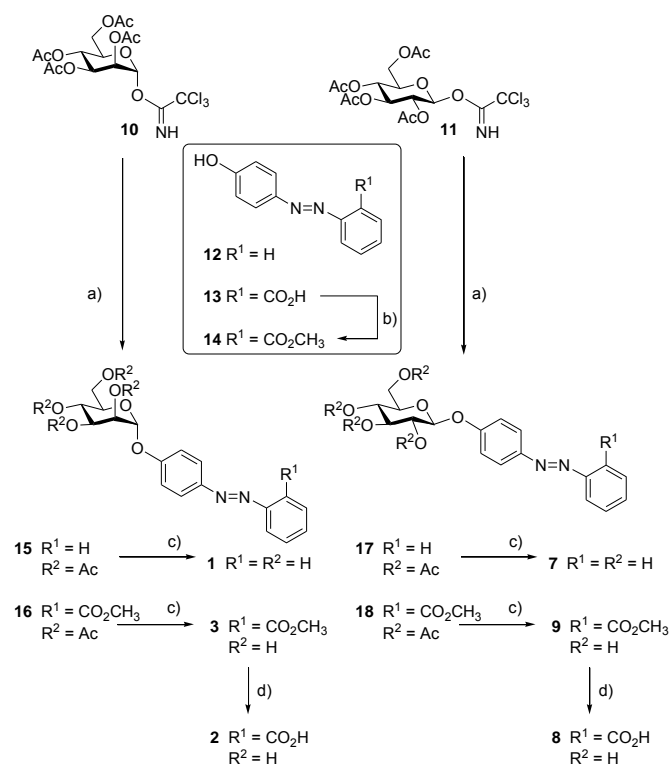


Figure 3. One or two retrosynthetic cuts, respectively, are required to approach azobenzene glycosides: (i) glycosylation and/or (ii) condensation of anilines and nitrosoarenes.

Results and Discussion

Synthesis of azobenzene glycosides: owing to our long standing interest in α -mannoside-specific proteins such as the bacterial lectin FimH, we started with the preparation α -D-mannosides (**1-3**, Figure 2). Glycosides of the 1,2-*trans*-type such as the α -D-mannosides can be obtained from the appropriate azobenzene alcohol employing an *O*-acylated glycosyl donor in a stereospecific glycosylation reaction. The neighbouring group participation of the 2-*O*-acyl group of the sugar ring ensures the stereospecific course of the glycosylation reaction. Thus, for the synthesis of azobenzene α -D-mannosides, *O*-acetylated mannosyl trichloroacetimidate **10**^[12, 13] was used as a starting material (Scheme 1). According to Schmidt's procedure,^[14, 15] Lewis acid catalyzed reaction of **10** with the commercially available 4-hydroxyazobenzene **12** gave the α -configured mannoside **15** and its deprotection under Zemplén conditions^[16] gave the target mannoside **1**. It turned out that this mannoside has a rather limited solubility in water and is therefore not suitable for biological tests.

Thus, we aimed at introducing a carboxy group as substituent on the azobenzene aglycone in order to improve water solubility. The carboxy-substituted azobenzene derivative **13**, *o*-(*p*-hydroxyphenylazo)benzoic acid (HABA), is commercially available. For glycosylation, it was converted into its methyl ester **14** and then Lewis acid-promoted reaction with the glycosyl donor **10**, as before, led to the α -mannoside **16** in high yield. Zemplén deacetylation,^[16] converted **16** into the methyl ester **3** and treatment with LiOH in a subsequent step delivered the unprotected *o*'-carboxy-substituted azobenzene glycoside **2**. Interestingly, the water solubility of the methyl ester **3** was better than that of the carboxylic acid **2**. Thus, azobenzene mannoside **3** is the best candidate for testing photoswitching in aqueous solution in this series of azobenzene mannosides, e.g. to investigate binding to mannose-specific lectins.

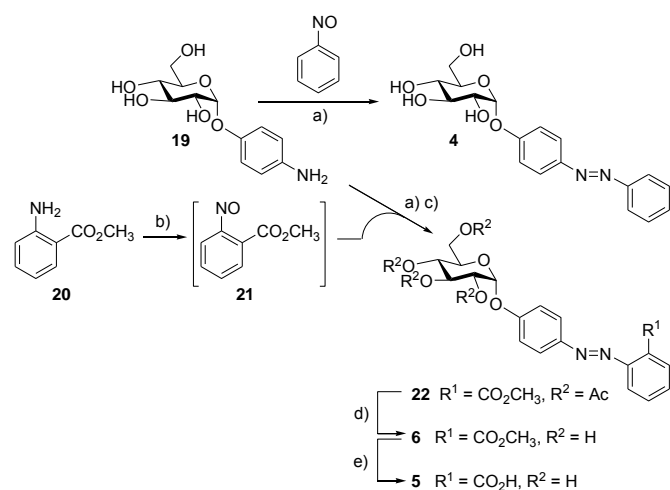


Scheme 1. Synthesis of azobenzene glycosides **1-3** and **7-9**. (a) $\text{BF}_3 \cdot \text{Et}_2\text{O}$, CH_2Cl_2 , RT, overnight, **15** (with **12**: 81%), **16** (with **14**: 84%), **17** (with **12**: 73%), **18** (with **14**: 79%); (b) MeOH/HCl , reflux, 5 h, 85%; (c) NaOMe , MeOH , RT, overnight, **1** (92%), **3** (89%), **7** (90%), **9** (83%); (d) LiOH , $\text{THF}-\text{H}_2\text{O}$ (2:1), RT, overnight, **2** (93%), **8** (91%).

In full analogy to the synthesis of the α -mannosides **1-3**, the 1,2-*trans*-type β -glucosides **7-9** were obtained employing the glucosyl donor **11** (Scheme 1).^[14, 17] Overall, the synthesis of the first two sets of azobenzene glycosides, **1-3** and **7-9** required only a handful of high-yielding steps furnishing the final products as coloured crystalline compounds.

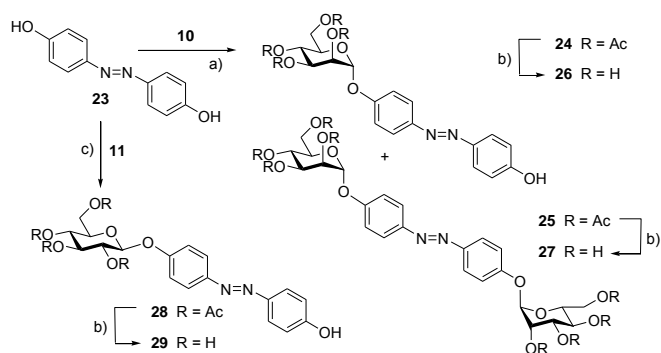
In order to compare the influence of the anomeric configuration on *E/Z* isomerization of an azobenzene glycoside, the series of β -D-glucosides was then supplemented by the α -D-glucosides **4-6**. These glucosides are representatives of the 1,2-*cis*-glycoside type, and therefore more difficult to synthesize stereoselectively. A number of methods providing a stereospecific access to α -glucosides have been introduced, however, require a more or less high number of synthetic steps. We therefore refrained from a glycosylation approach for the synthesis of **4-6**. Instead the synthesis was started with *p*-aminophenyl α -D-glucoside **19** which can be obtained by

catalytic reduction of commercially available *p*-nitrophenyl α -D-glucoside in a quantitative reaction.^[18, 19] In a second step, the amine **19** was submitted to condensation with the respective nitrosoarenes (Scheme 2). Acid-catalyzed condensation with nitrosobenzene delivered the unprotected target glucoside **4** in high yield. Likewise, target glucoside **5** was derived from condensation of **19** with the nitrosobenzene derivative **21**, which was obtained from its carboxylic acid ester **20**^[20] and employed in situ. In order to facilitate purification of the condensation product, it was submitted to *O*-acetylation with acetic anhydride in pyridine to yield glucoside **22**, which could be easily purified. De-*O*-acetylation of pure **22** according to Zemplén^[19] furnished the methoxycarbonyl-substituted glucoside **6** and saponification of **6** with LiOH gave the carboxylic acid derivative **5**.



Scheme 2. Synthesis of azobenzene glycosides **4**, **5** and **6**. (a) Acetic acid, RT, overnight, 96%; (b) oxone, CH₂Cl₂-H₂O (16:20), RT, 20 h; (c) pyridine, acetic anhydride, RT, overnight, 89%; (d) NaOMe, MeOH, RT, overnight, 96%; (e) LiOH, THF-H₂O (2:1), RT, 18 h, 95%.

In addition to the nine target azobenzene glycosides **1-9**, we were interested in mannosides **26** and **27** (Scheme 3) as these two compounds are promising antagonists of the mannose-specific bacterial lectin FimH.^[21, 22] The glycosyl acceptor diol **23** was obtained according to the literature,^[23] and a subsequent glycosylation using the mannosyl donor **10** gave a mixture of the mono- and bis-glycosylated azobenzene mannosides **24** and **25** in 37% and 31% yield, respectively, after separation by column chromatography. De-*O*-acetylation led to the OH-free target glycosides **26** and **27** in high yield. The bis-glycosylated glycoside **27** is a symmetrical molecule, which displays one signal set for both mannosyl moieties in its NMR spectra. For comparison of the photochromic properties of the mono-glycosylated azobenzene alcohol **26** (*vide infra*), the respective glucoside **29** was also prepared in analogy to the synthesis of **26** (Scheme 3).



Scheme 3. Synthesis of azobenzene glycoside **26** and **27**. (a) BF₃-Et₂O, CH₂Cl₂, RT, overnight, **24** (37%), **25** (31%); (b) NaOMe, MeOH, RT, overnight, **26** (88%), **27** (93%), **29** (89%); (c) and **28** (31%).

Photoisomerization studies: With this collection of new azobenzene glycosides in hand, *E*→*Z* photoisomerization was studied by ¹H NMR spectroscopy, and kinetics of the relaxation process (*Z*→*E*) were determined by UV-Vis spectroscopy. To allow for a comparison of the photochromic properties of the investigated azobenzene glycosides, all photoisomerization experiments were performed in DMSO. Photostationary states (PSS) were reached after irradiation at 365 nm for ~30 min. In the ¹H NMR spectra, *E* and *Z* isomers were easily distinguished and quantified by integration, as they display well separated chemical shift for the aromatic protons or the anomeric H-1 of the sugar ring (Table 1). Half lives $\tau_{1/2}$ of thermal *Z*→*E* isomerisation were determined by UV-Vis spectroscopy employing 50 μ M solutions in DMSO (shown for azobenzene mannoside **1** in Figure 4; for other glycosides see Supporting Information).

While in the ground state (GS) all investigated azobenzene glycosides are nearly 100% *E*-configured. *E/Z* ratios in the PSS obtained after irradiation of a sample at 365 nm vary significantly among the 12 investigated glycosides. Unsubstituted azobenzene glycosides **1**, **4**, and **7**, as well as the bivalent mannoside **27** could be isomerized almost quantitatively (Table 2) with long-lived *Z*-isomers having half lives $\tau_{1/2}$ of up to over 90 h. A comparison of the unsubstituted azobenzene glycosides **1**, **4**, **7** shows that in this row, neither the anomeric linkage nor the configuration of the 2-substituent of the sugar ring significantly influences the PSS. On the other hand, irradiation of the azobenzene glycosides bearing a substituent at the azobenzene aglycon resulted in larger *E/Z* ratios. In the extreme cases of the carboxy-substituted glycosides **2** and **5** irradiation led to *E/Z* ratios of 85/15 and 76/24, respectively. However, the carboxy-substituted analogue of the β -glucoside series, **8**, shows a *E/Z* ratio of ~40/60 after irradiation, thus differed significantly from **2** and **5**. Here, the β -glycosidic linkage makes a difference! Comparison of the methoxycarbonyl-substituted azobenzene glycosides leads to the conclusion, the configuration of the 2-hydroxyl group is significant. While glucosides **6** and **9** have *E/Z* ratios of ~40/60 in the PPS, the analogous mannoside **3** showed 10/90. Half lives of the *ortho*'-substituted azobenzene glycosides vary between 2 and 5 h. Thus in these cases the *Z*-isomers are much shorter lived than in case of the non substituted azobenzene glycosides **1**, **4**, and **7**.

The bis-glycosylated azobenzene **27** showed photochromic properties similar to the unsubstituted azobenzene glycosides. However, for the *para*'-OH-substituted azobenzene mannoside **26** *E*→*Z* photoisomerization could not be observed in the NMR.

Table 1. Chemical shifts (DMSO-D₆ at 500 MHz) of anomeric protons (H-1) in ppm of *E*- and *Z*-configured azobenzene glycosides. Integration of H-1 signals was used to determine *E/Z* ratios in the PSS.

H-1	1	2	3	4	5	6	7	8	9	27
<i>E</i>	5.53	5.53	5.53	5.55	5.57	5.57	5.04	4.99	5.00	5.51
<i>Z</i>	5.32	5.30	5.31	5.35	5.34	5.35	4.80	4.78	4.80	5.34

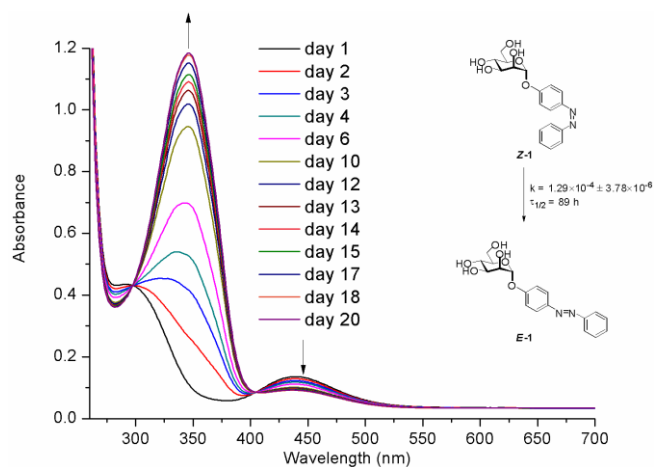


Figure 4. Series of UV-Vis spectra monitoring the thermal *Z*→*E* relaxation of *Z*-azobenzene glycoside **1** in DMSO: Absorption peaks due to *n*→ π^* transition are decreasing and absorption due to π → π^* transition simultaneously increases.

Table 2. Photochromic properties of synthesized azobenzene glycosides.

Azobenzene glycoside	Substituent	GS <i>E/Z</i> ratios ^[a] (ϵ) ^[b]	PSS <i>E/Z</i> ratios ^[a] (ϵ) ^[b]	UV-Vis absorption maxima [nm] $\lambda_{\max}(E), \lambda_{\max}(Z)$	half life ($\tau_{1/2}$) [h] ^[c]
1 (α -man)	H	99:1 (25907)	3:97 (2635)	347, 440	89
2 (α -man)	ortho'-CO ₂ H	99:1 (29362)	85:15 (3106)	341, 423	2
3 (α -man)	ortho'-CO ₂ Me	98:2 (21694)	10:90 (3452)	345, 426	5
4 (α -glc)	H	99:1 (15804)	2:98 (1712)	356, 439	36
5 (α -glc)	ortho'-CO ₂ H	98:2 (13715)	76:24 (1407)	341, 424	2.5
6 (α -glc)	ortho'-CO ₂ Me	99:1 (16943)	45:55 (1734)	345, 426	2
7 (β -glc)	H	98:2 (23274)	4:96 (1704)	347, 439	94
8 (β -glc)	ortho'-CO ₂ H	99:1 (28335)	41:59 (2521)	337, 425	4
9 (β -glc)	ortho'-CO ₂ Me	98:2 (18722)	39:61 (2071)	346, 425	5
26	α -Man para'-OH	99:1 (19804)	Fast kinetics	363, 480	–
27	α -Man para- α -Man	98:2 (18810)	5:95 (1395)	358, 446	24
29	β -Glu para'-OH	99:1 (17871)	Fast kinetics	362, 476	–

[a] *E/Z* ratios are based on the integrals of the respective anomeric protons H-1 in the ¹H NMR spectrum (10 mg samples in ~550 μ L DMSO-D₆, 500 MHz); [b] ϵ : extinction coefficient [$\text{mol} \times \text{L}^{-1} \times \text{cm}^{-1}$]; [c] $\tau_{1/2}$: half lives were determined by UV-Vis spectroscopy (50 μ M samples in DMSO).

Discussion of photochromic properties: The fact that isomerisation of the *para*'-OH-substituted azobenzene mannoside **26** was not observed is in line with reports from the literature, showing that *p*-hydroxy-substituted azobenzene derivatives are characterized by extremely fast kinetics of thermal relaxation of the *Z* isomer.^[24] The electron-donating effect of the OH-substituent lowers the barrier for thermal back isomerisation leading to relaxation times in the ms range. This feature is also emphasized by our observation that the *p*-OH-substituted azobenzene glycoside **29** behaves exactly the same as the analogous mannoside **26** (Table 2), regardless whether isomerisation is carried out in DMSO, EtOH, or water. Interestingly, fast isomerization dynamics can facilitate the use of sweet switches in applications, where fast information processing is required. Such hydroxy-substituted sweet switches are of great interest for all applications, where short-lived excited states and rapid relaxation are required, e.g. the study of biological regulatory processes.

Finally, carboxy- and methoxycarbonyl substitutions had significant effects on the isomerization behaviour of the investigated azobenzene glycosides in accordance with earlier observations made for differently substituted azobenzenes.^[25-27] It was suggested that substituents on the azobenzene sub-structure can alter the isomerization mechanism and as a consequence *E*→*Z* photoisomerization becomes less effective. In addition, it has been stated that formation of intramolecular hydrogen bonds can lead to fast *Z*→*E* thermal recovery.^[28] For the investigated azobenzene glycosides substitution, the PSS correlates with the half life $\tau_{1/2}$ of the *Z* isomer. Larger *E/Z* ratios parallel with shorter life times of the less stable *Z* isomer, suggesting that the barrier for thermal relaxation is lowered. While substitution effects could hardly be predicted, it is apparent, that the anomeric linkage of a glycoside can influence photoisomerisation behaviour (cf. **5** and **8**) as well as the configuration of the 2-OH group can be crucial (cf. **3** vs. **6** and **9**). Preliminary structural models suggest that the substituents installed in the *ortho*'-position of the azobenzene moiety can interact with the azo group, whereas interaction with the glycosidic aglycon is less likely. Future theoretical studies might help to reveal, which effects are caused by effects or protonation by a carboxy substituent.

Conclusion

The employed carboxy- and methoxycarbonyl-substituted azobenzene derivatives provide an option for immobilization of the respective glycosides, derived thereof, on surfaces or for other further modification and conjugation. This is of interest to eventually study the influence of *E/Z* isomerization within an array of azobenzene glycosides on carbohydrate-specific cell adhesion.

-
- [14] R. R. Schmidt, J. Michel, *Tetrahedron Lett.* **1984**, 25, 821-824.
- [15] K.-H. Jung, M. Hoch, R. R. Schmidt, *Liebigs Ann. Chem.* **1989**, 1099-1106.
- [16] G. Zemplén, E. Pascu, *Ber. dtsch. chem. Ges* **1929**, 62, 1613-1614.
- [17] J. Wegner, S. V. Ley, A. Kirschning, A.-L. Hansen, J. Montenegro Garcia, I. R. Baxendale, *Org. Lett.* **2012**, 14, 696-699.
- [18] Y. Huang, J. Hu, W. Kuang, Z. Wei, C. F. J. Faul, *Chem. Commun.* **2011**, 47, 5554-5556.
- [19] C.-H. Sung, L.-R. Kung, C.-S. Hsu, T.-F. Lin, R.-M. Ho, *Chem. Mater.* **2005**, 18, 352-359.
- [20] C. M. Crane, J. Kaiser, N. L. Ramsden, S. Lauw, F. Rohdich, W. Eisenreich, W. N. Hunter, A. Bacher, F. Diederich, *Angew. Chem.* **2006**, 118, 1082-1087; *Angew. Chem. Int. Ed.*, **2006**, 45, 1069-1074.
- [21] M. Dubber, O. Sperling, T. K. Lindhorst, *Org. Biomol. Chem.* **2006**, 4, 3901-3912.
- [22] M. A. Mulvey, *Cell. Microbiol.* **2002**, 4, 257-271.
- [23] W.-h. Wei, T. Tomohiro, M. Kodaka, H. Okuno, *J. Org. Chem.* **2000**, 65, 8979-8987.
- [24] J. Garcia-Amoros, A. Sanchez-Ferrer, W. A. Massad, S. Nonell, D. Velasco, *Phys. Chem. Chem. Phys.* **2010**, 12, 13238-13242.
- [25] H. M. D. Bandara, T. R. Friss, M. M. Enriquez, W. Isley, C. Incarvito, H. A. Frank, J. Gascon, S. C. Burdette, *J. Org. Chem.* **2010**, 75, 4817-4827.
- [26] B. R. Hsieh, D. Désilets, P. M. Kazmaier, *Dyes Pigm.* **1990**, 14, 165-189.
- [27] J. García-Amorós, W. A. Massad, S. Nonell, D. Velasco, *Org. Lett.* **2010**, 12, 3514-3517.
- [28] J. García-Amorós, D. Velasco, *Beilstein J. Org. Chem.* **2012**, 8, 1003-1017.

Received: ((will be filled in by the editorial staff))

Revised: ((will be filled in by the editorial staff))

Published online: ((will be filled in by the editorial staff))

Supporting Information

Synthesis and photochemical properties of novel azobenzene glycosides

Vijayanand Chandrasekaran, Eugen Johannes, Hauke Kobarg, Frank D.
Sönnichsen and Thisbe K. Lindhorst*

Contents

Analytical data for azobenzene glycosides

1.	¹H NMR spectra	S4
	¹ H NMR spectra of (<i>E</i>)- 1 and (<i>Z</i>)- 1	S5
	¹ H NMR spectra of (<i>E</i>)- 2 and (<i>Z</i>)- 2	S5
	¹ H NMR spectra of (<i>E</i>)- 3 and (<i>Z</i>)- 3	S6
	¹ H NMR spectra of (<i>E</i>)- 4 and (<i>Z</i>)- 4	S6
	¹ H NMR spectra of (<i>E</i>)- 5 and (<i>Z</i>)- 5	S7
	¹ H NMR spectra of (<i>E</i>)- 6 and (<i>Z</i>)- 6	S7
	¹ H NMR spectra of (<i>E</i>)- 7 and (<i>Z</i>)- 7	S8
	¹ H NMR spectra of (<i>E</i>)- 8 and (<i>Z</i>)- 8	S8
	¹ H NMR spectra of (<i>E</i>)- 9 and (<i>Z</i>)- 9	S9
	¹ H NMR spectra of (<i>E</i>)- 26 and (<i>Z</i>)- 26	S9
	¹ H NMR spectra of (<i>E</i>)- 27 and (<i>Z</i>)- 27	S10
	¹ H NMR spectra of (<i>E</i>)- 29 and (<i>Z</i>)- 29	S10
2.	¹³C NMR spectra	S11
	¹³ C NMR spectra of (<i>E</i>)- 1 and (<i>Z</i>)- 1	S12
	¹³ C NMR spectra of (<i>E</i>)- 2 and (<i>Z</i>)- 2	S12
	¹³ C NMR spectra of (<i>E</i>)- 3 and (<i>Z</i>)- 3	S13
	¹³ C NMR spectra of (<i>E</i>)- 4 and (<i>Z</i>)- 4	S13
	¹³ C NMR spectra of (<i>E</i>)- 5 and (<i>Z</i>)- 5	S14

¹³ C NMR spectra of (<i>E</i>)- 6 and (<i>Z</i>)- 6	S14
¹³ C NMR spectra of (<i>E</i>)- 7 and (<i>Z</i>)- 7	S15
¹³ C NMR spectra of (<i>E</i>)- 8 and (<i>Z</i>)- 8	S15
¹³ C NMR spectra of (<i>E</i>)- 9 and (<i>Z</i>)- 9	S16
¹³ C NMR spectra of (<i>E</i>)- 26 and (<i>Z</i>)- 26	S16
¹³ C NMR spectra of (<i>E</i>)- 27 and (<i>Z</i>)- 27	S17
¹³ C NMR spectra of (<i>E</i>)- 29 and (<i>Z</i>)- 29	S17
3. Determination of rate constants for $Z \rightarrow E$ relaxation by UV-Vis spectroscopy	S18
UV-vis spectra of thermal (<i>Z</i>)- 1 and (<i>E</i>)- 1	S19
UV-vis spectra of thermal (<i>Z</i>)- 2 and (<i>E</i>)- 2	S19
UV-vis spectra of thermal (<i>Z</i>)- 3 and (<i>E</i>)- 3	S20
UV-vis spectra of thermal (<i>Z</i>)- 4 and (<i>E</i>)- 4	S20
UV-vis spectra of thermal (<i>Z</i>)- 5 and (<i>E</i>)- 5	S21
UV-vis spectra of thermal (<i>Z</i>)- 6 and (<i>E</i>)- 6	S21
UV-vis spectra of thermal (<i>Z</i>)- 7 and (<i>E</i>)- 7	S22
UV-vis spectra of thermal (<i>Z</i>)- 8 and (<i>E</i>)- 8	S22
UV-vis spectra of thermal (<i>Z</i>)- 9 and (<i>E</i>)- 9	S23
UV-vis spectra of thermal (<i>Z</i>)- 27 and (<i>E</i>)- 27	S23

1. ^1H NMR spectra

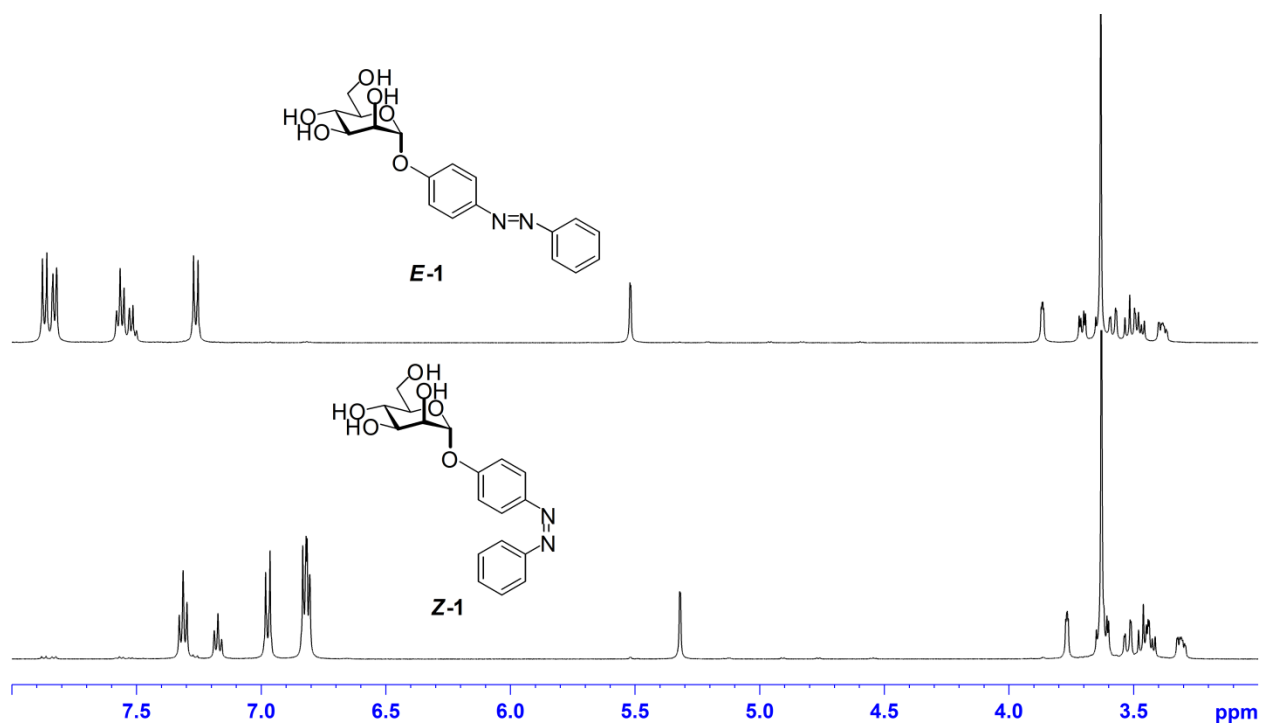


Figure S1. ^1H NMR (500 MHz, DMSO-D_6)

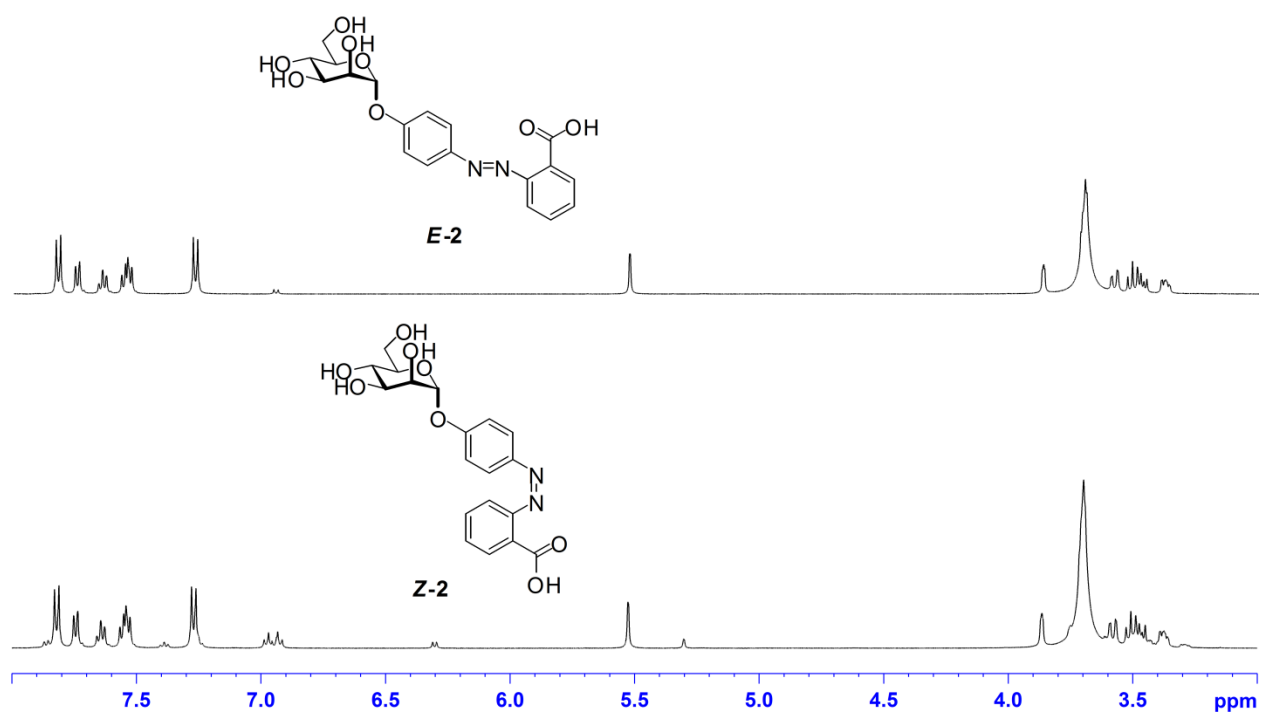


Figure S2. ^1H NMR (500 MHz, DMSO-D_6)

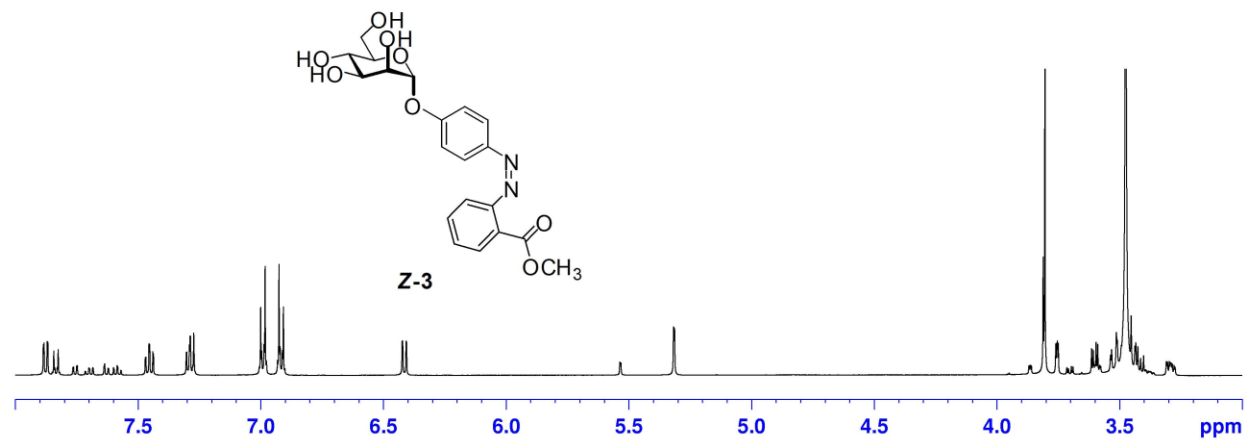
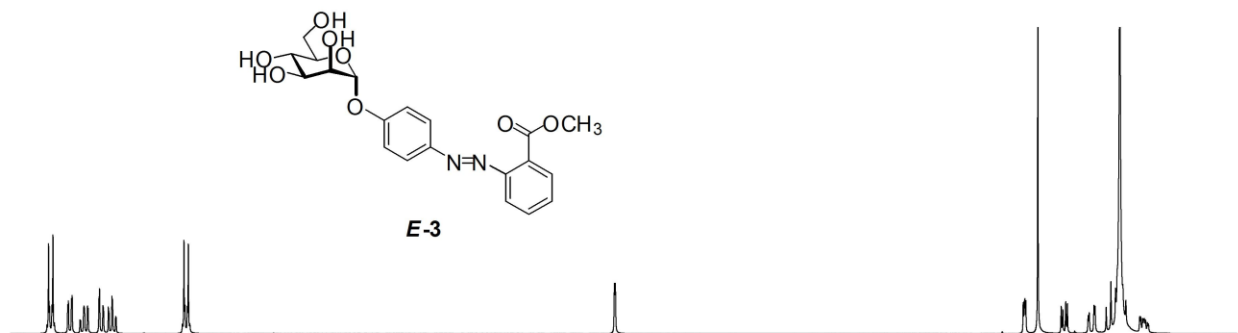


Figure S3. ^1H NMR (500 MHz, DMSO-D_6)

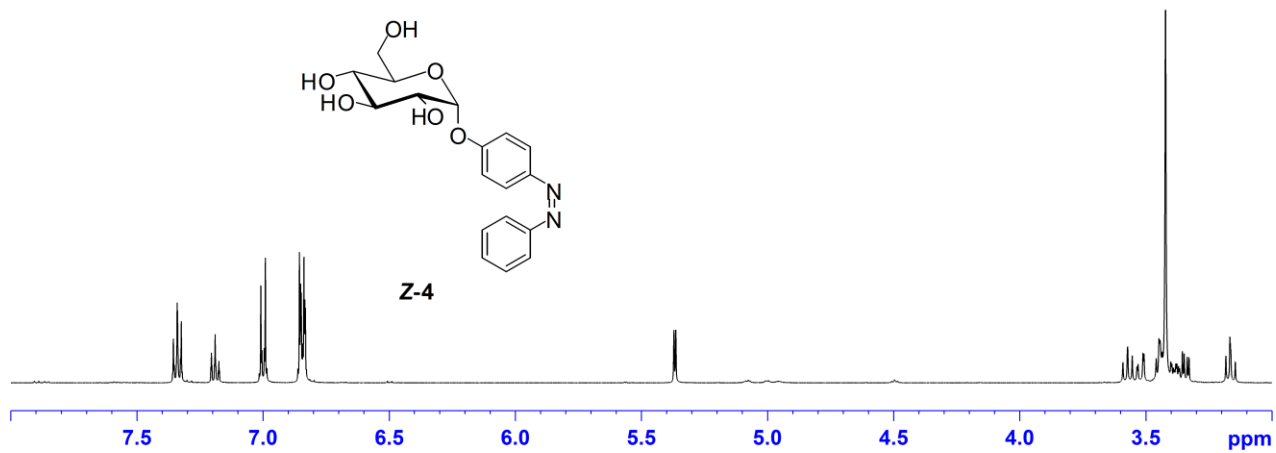
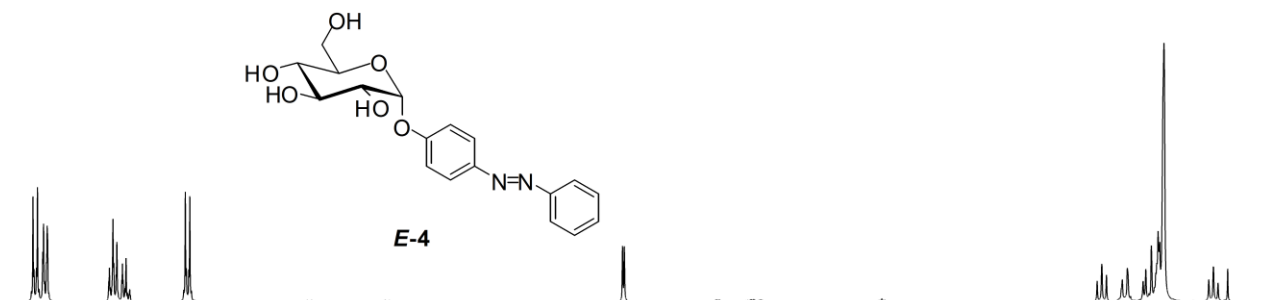


Figure S4. ^1H NMR (500 MHz, DMSO-D_6)

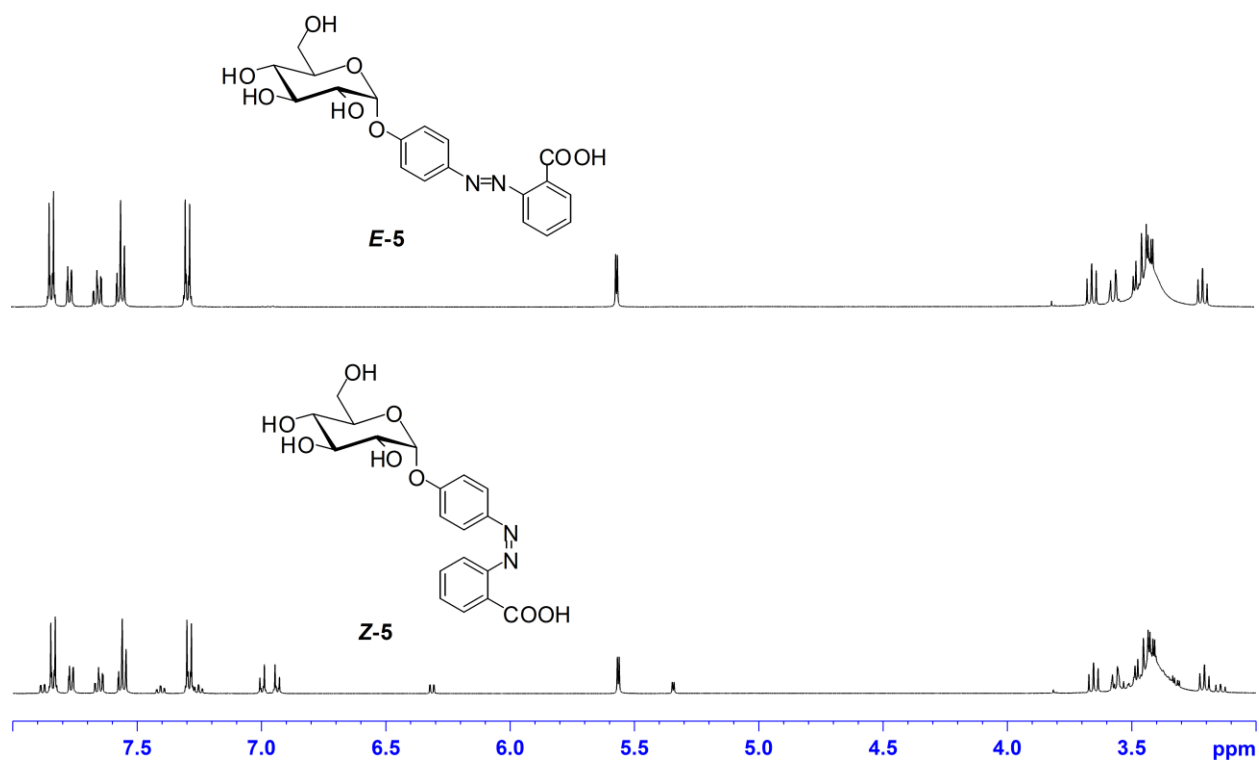


Figure S5. ^1H NMR (500 MHz, DMSO-D_6)

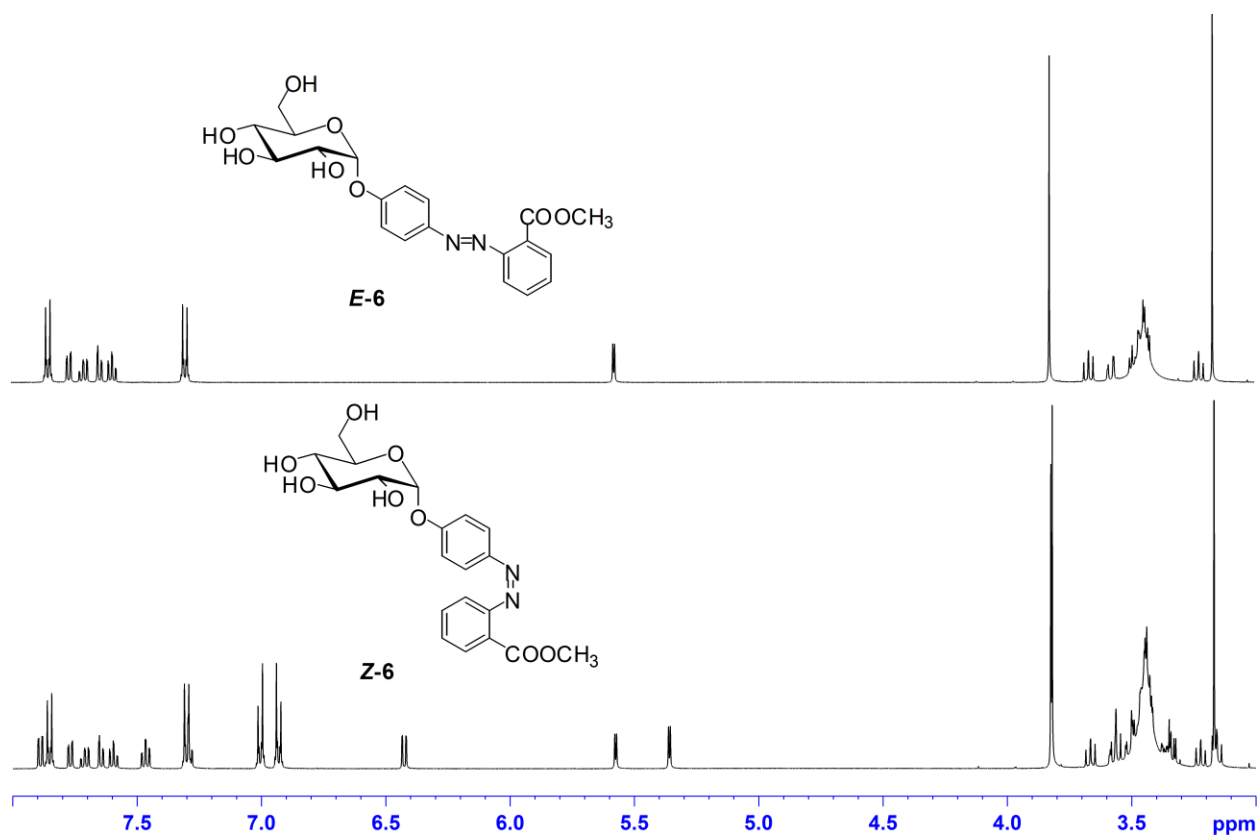


Figure S6. ^1H NMR (500 MHz, DMSO-D_6)

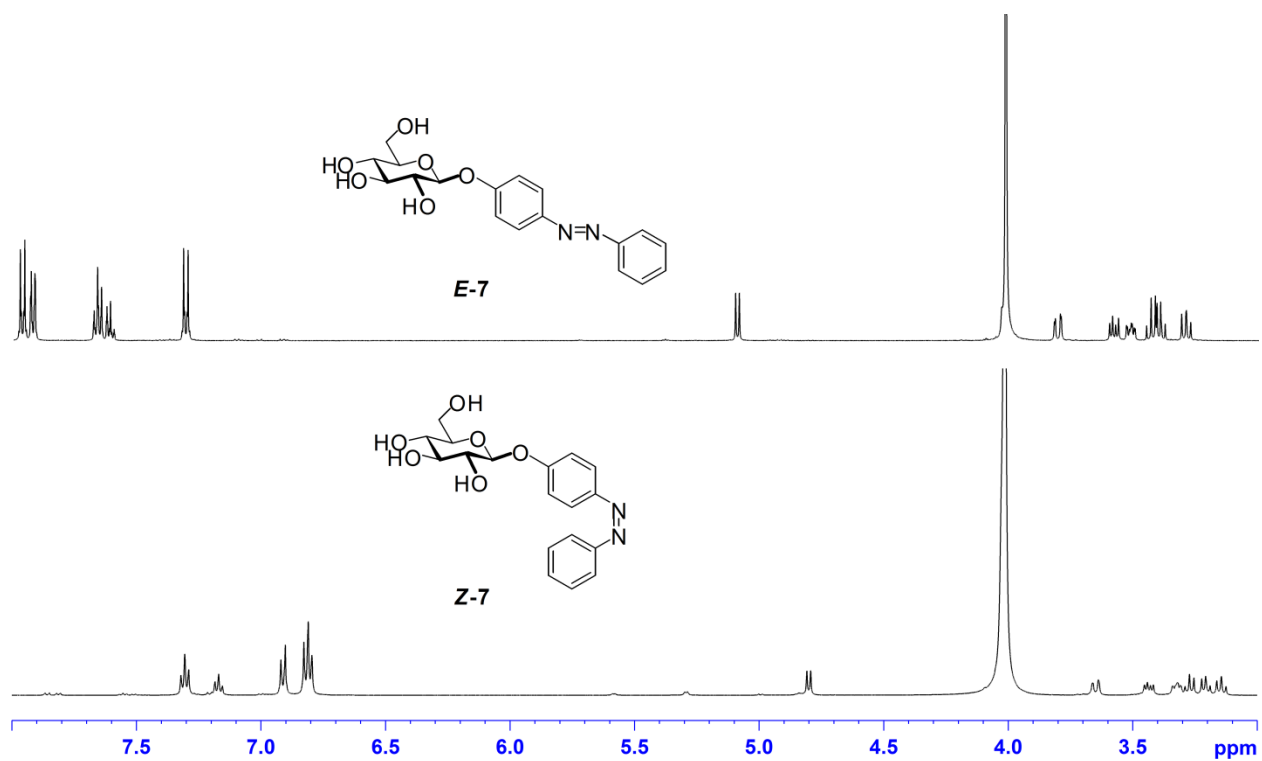


Figure S7. ^1H NMR (500 MHz, DMSO-D_6)

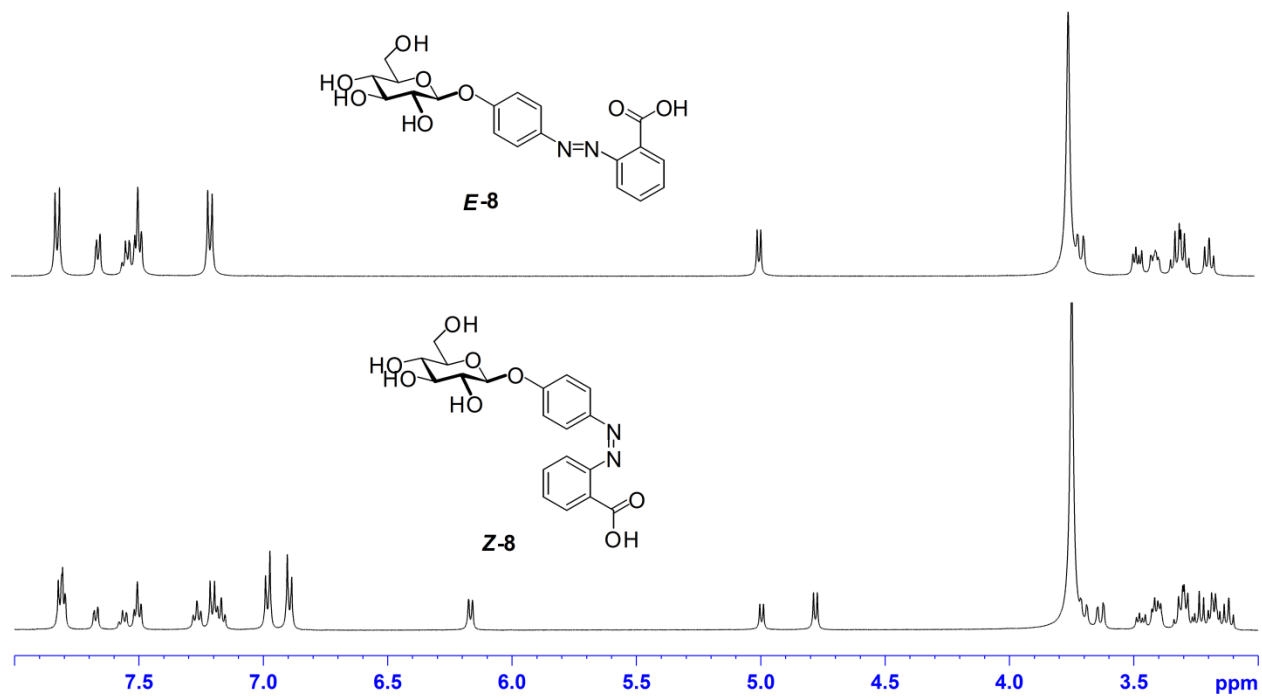


Figure S8. ^1H NMR (500 MHz, DMSO-D_6)

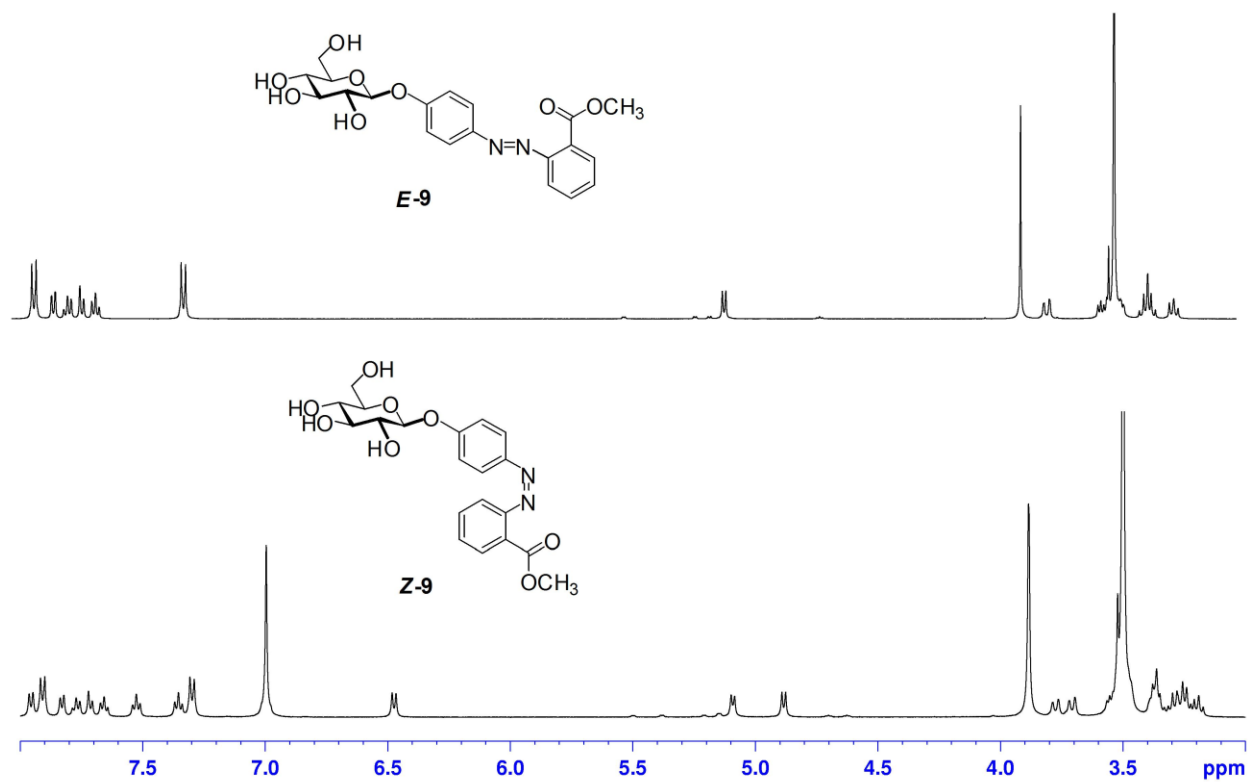


Figure S9. ^1H NMR (500 MHz, DMSO-D_6)

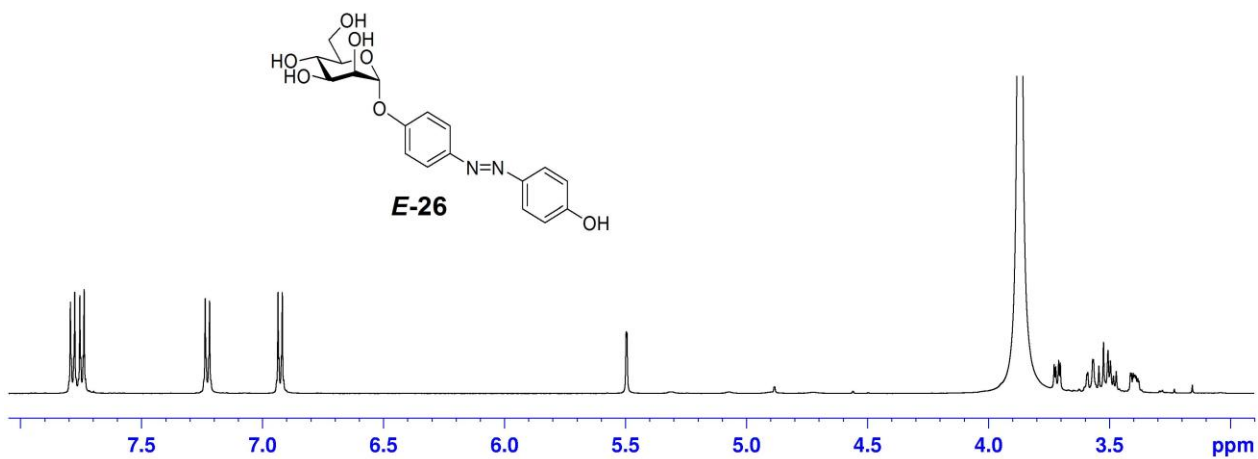


Figure S10. ^1H NMR (500 MHz, DMSO-D_6)

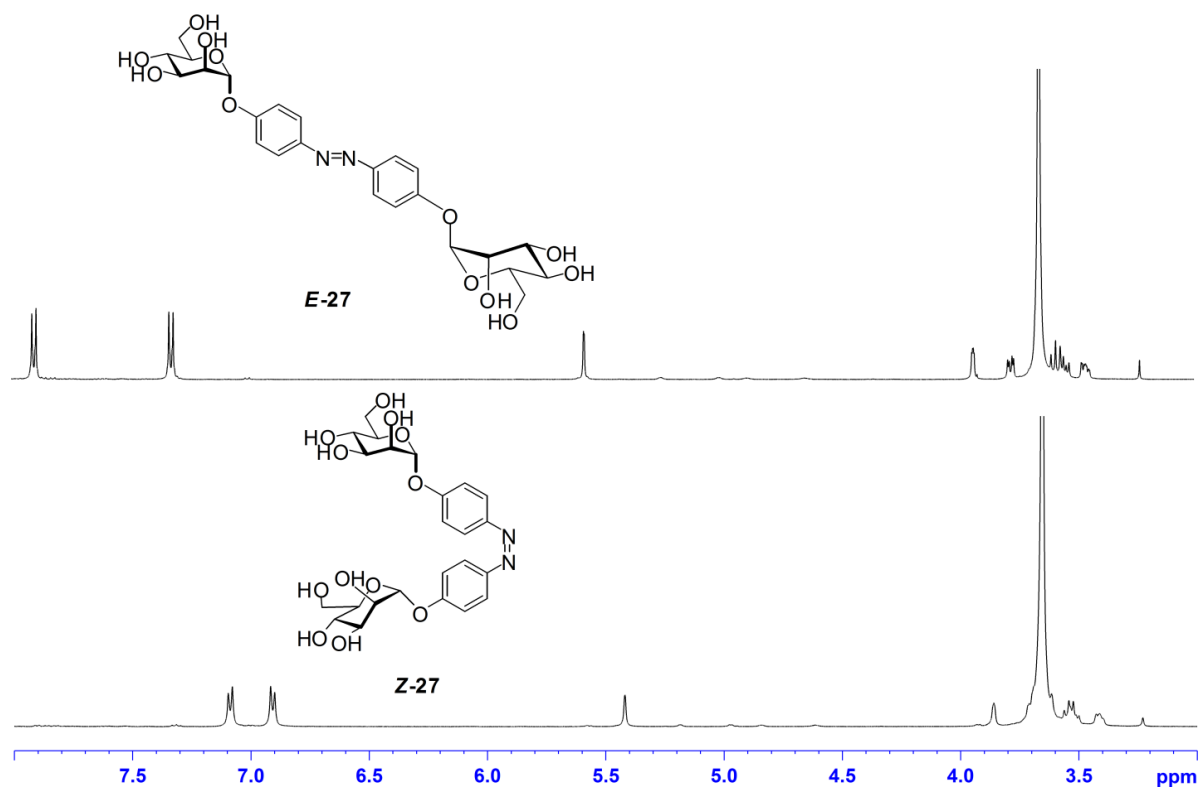


Figure S11. ^1H NMR (500 MHz, DMSO-D_6)

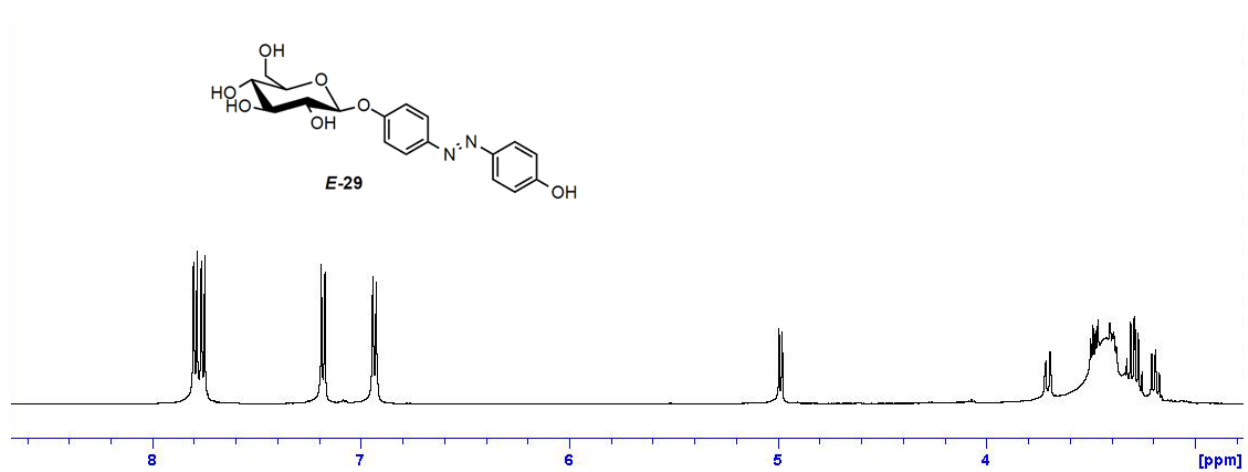


Figure S12. ^1H NMR (500 MHz, DMSO-D_6)

2. ^{13}C NMR Spectra

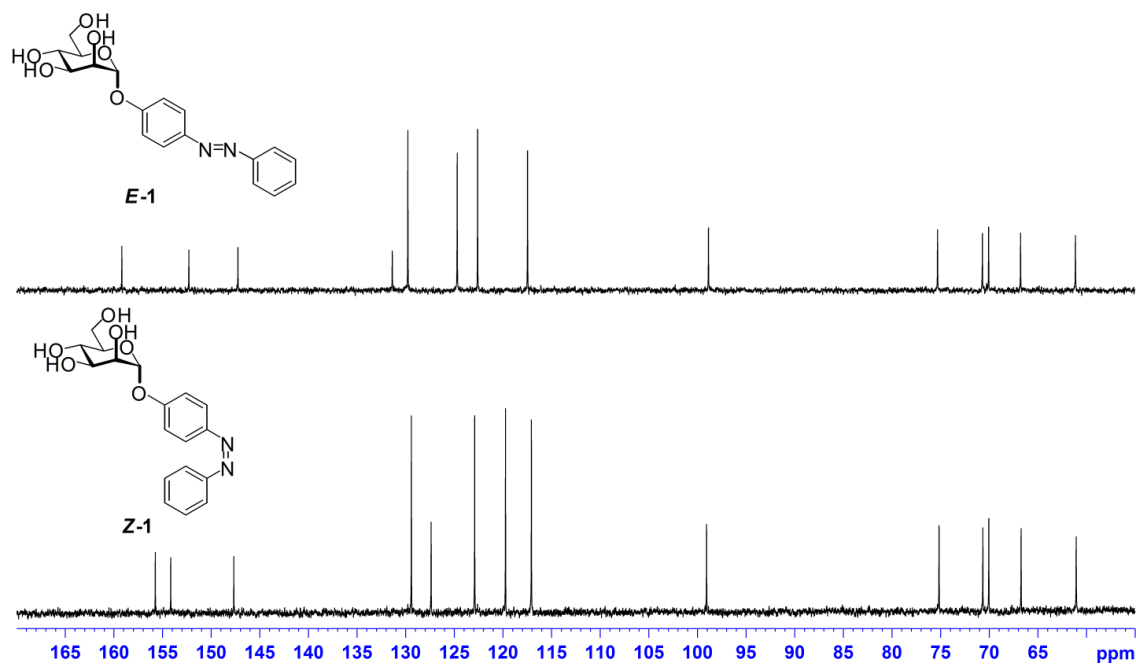


Figure S13. ^{13}C NMR (125 MHz, DMSO-D_6)

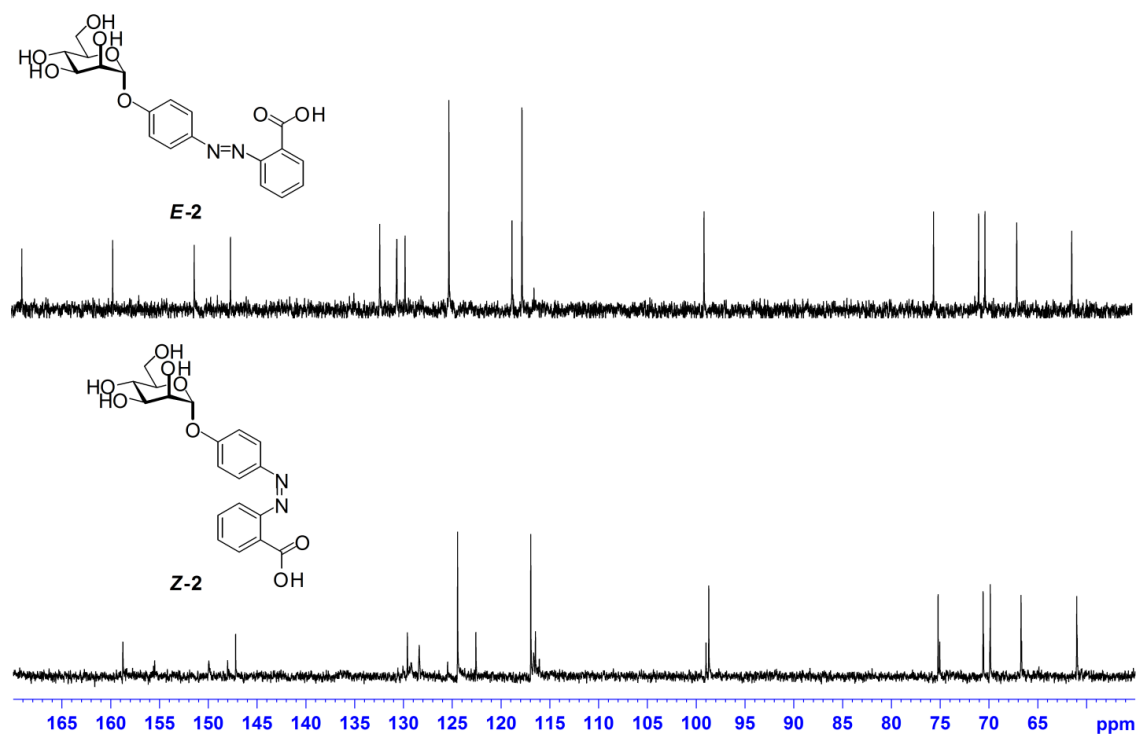


Figure S14. ^{13}C NMR (125 MHz, DMSO-D_6)

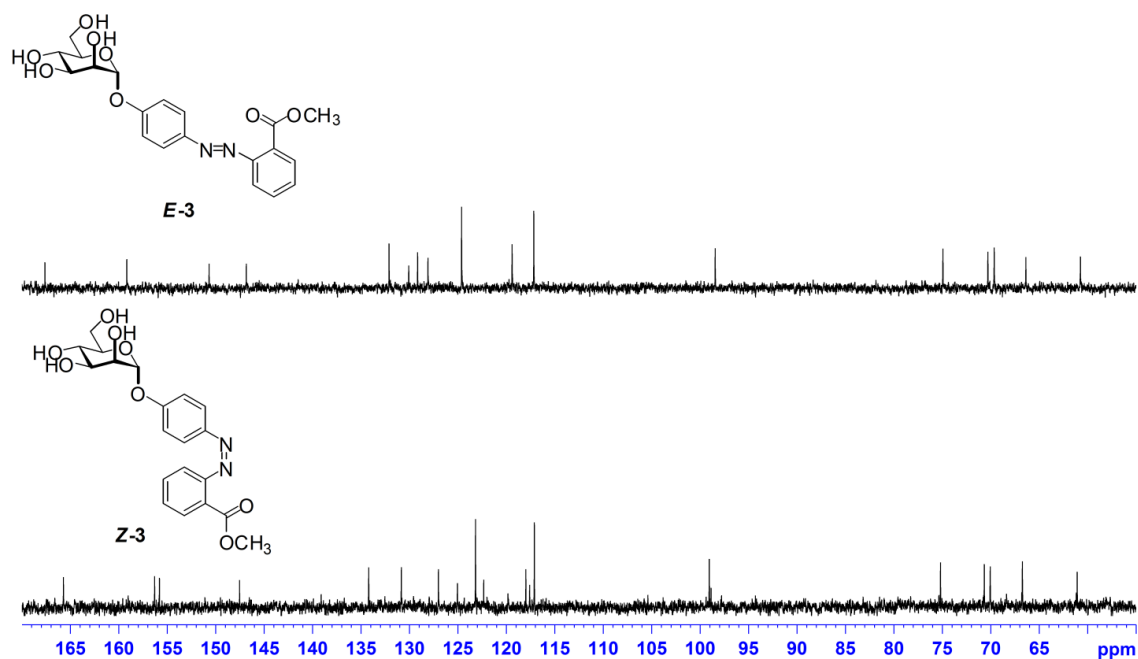


Figure S15. ^{13}C NMR (125 MHz, DMSO-D_6)

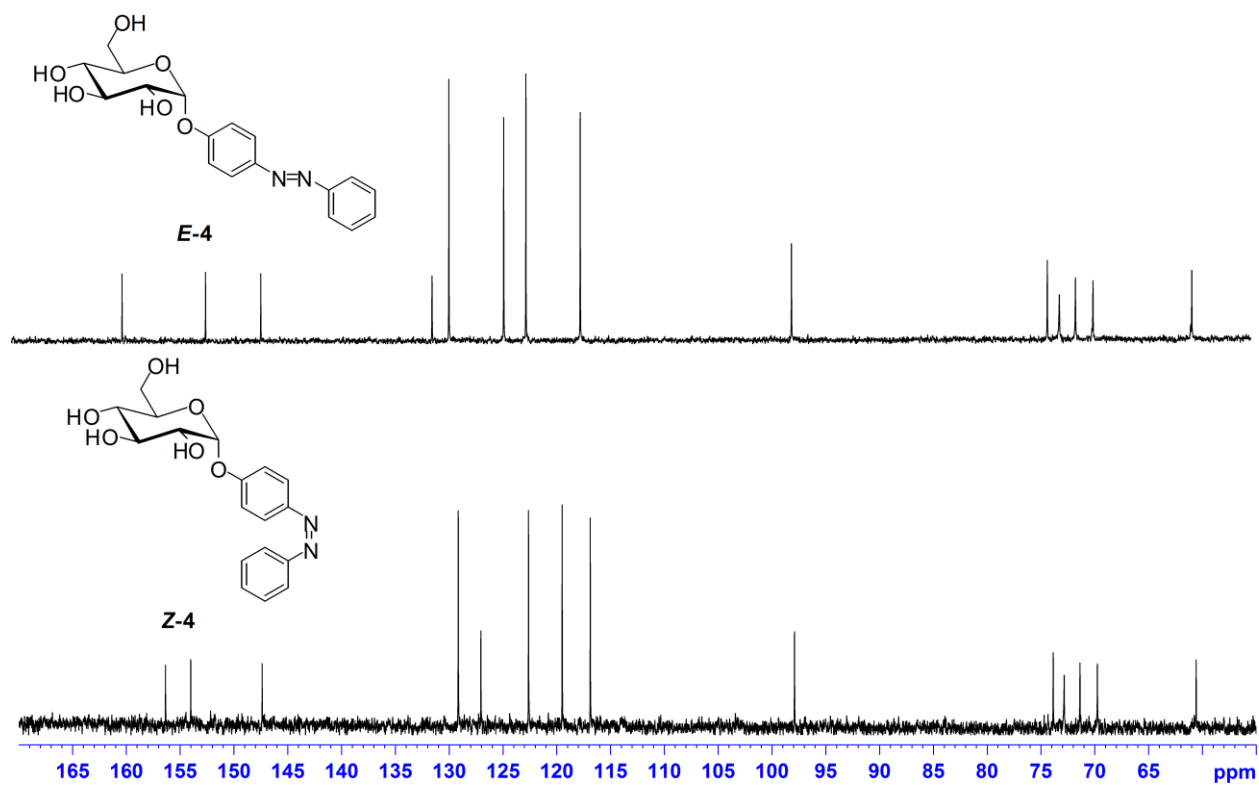


Figure S16. ^{13}C NMR (125 MHz, DMSO-D_6)

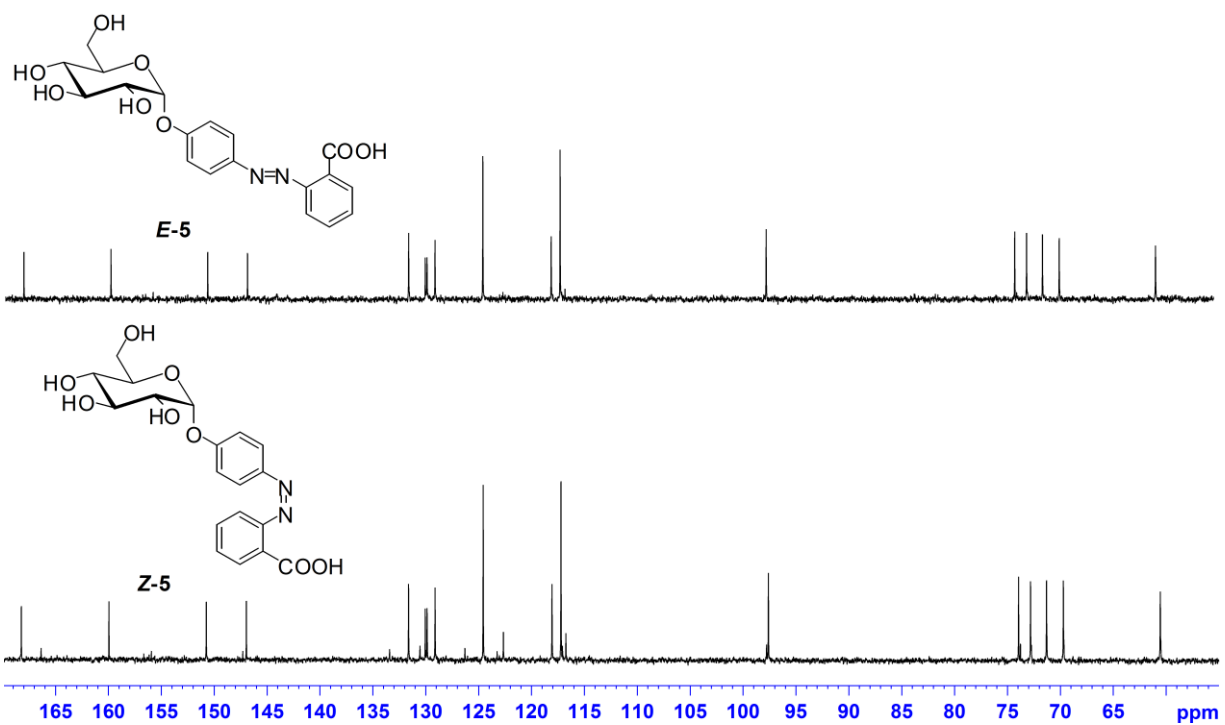


Figure S17. ^{13}C NMR (125 MHz, DMSO-D_6)

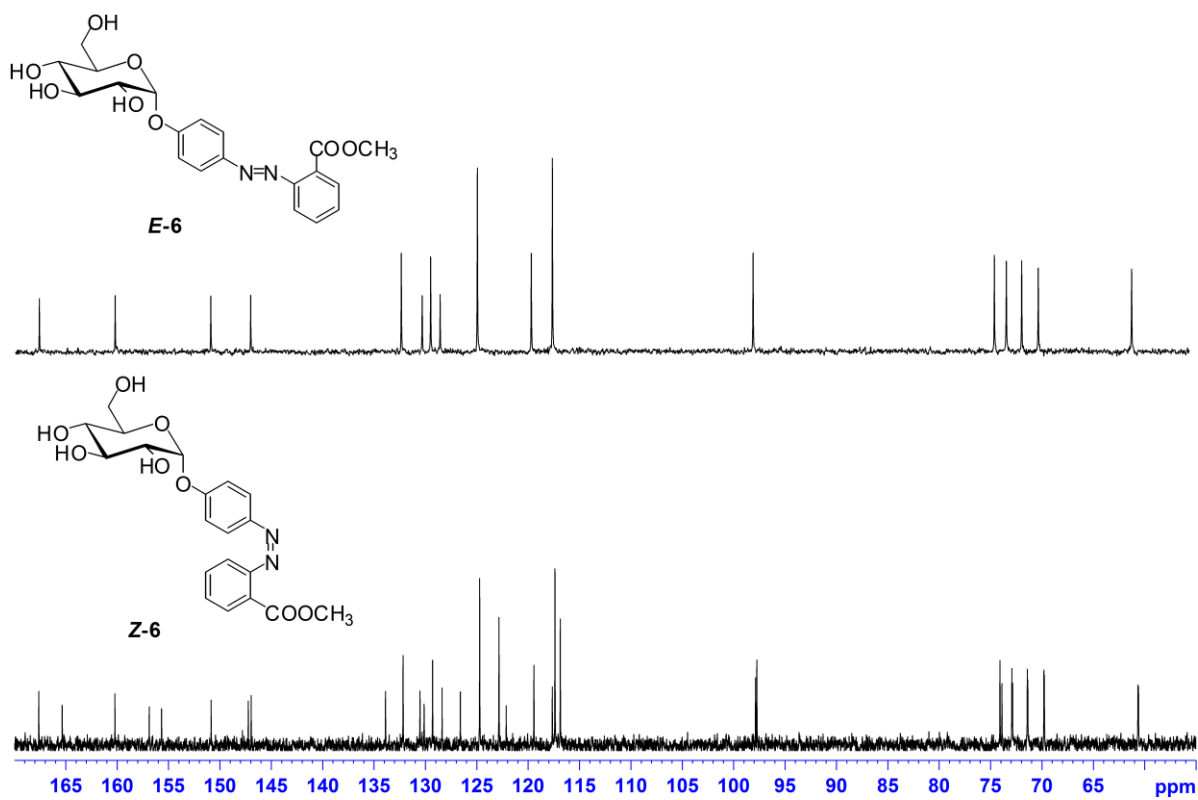


Figure S18. ^{13}C NMR (125 MHz, DMSO-D_6)

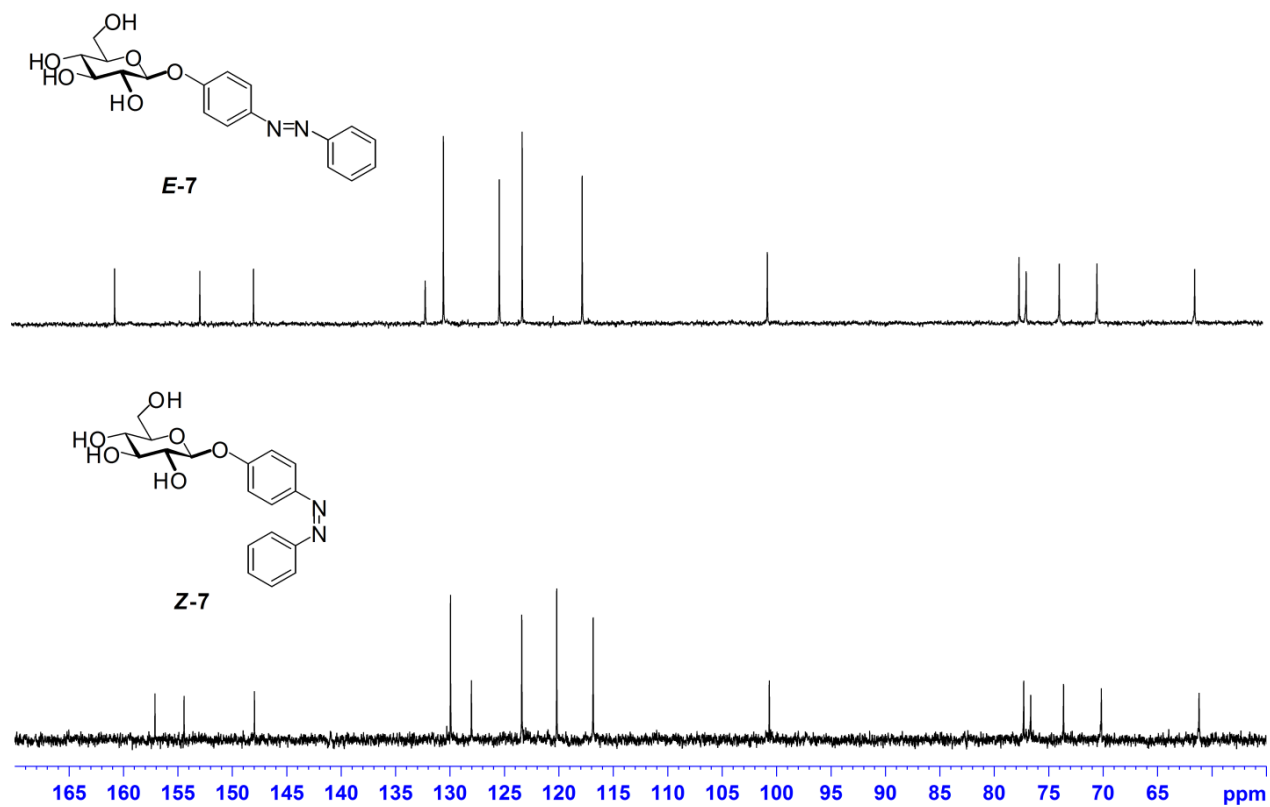


Figure S19. ^{13}C NMR (125 MHz, DMSO-D_6)

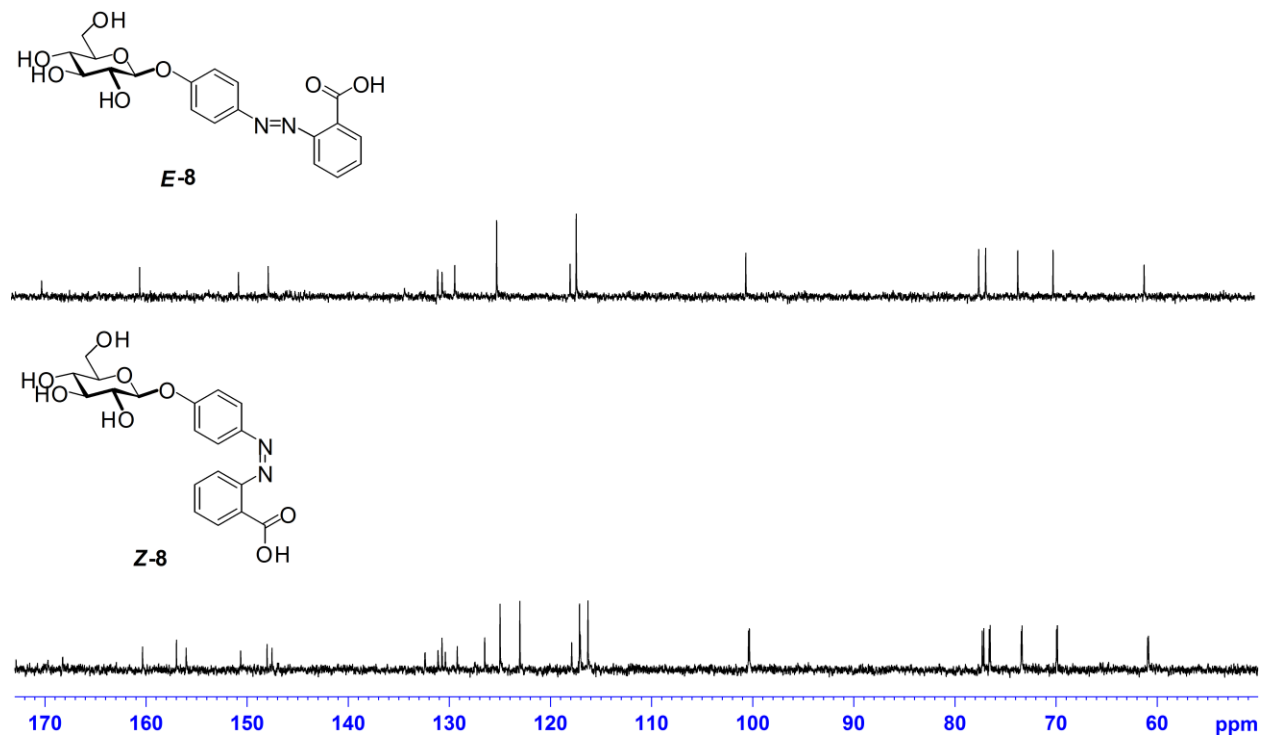


Figure S20. ^{13}C NMR (125 MHz, DMSO-D_6)

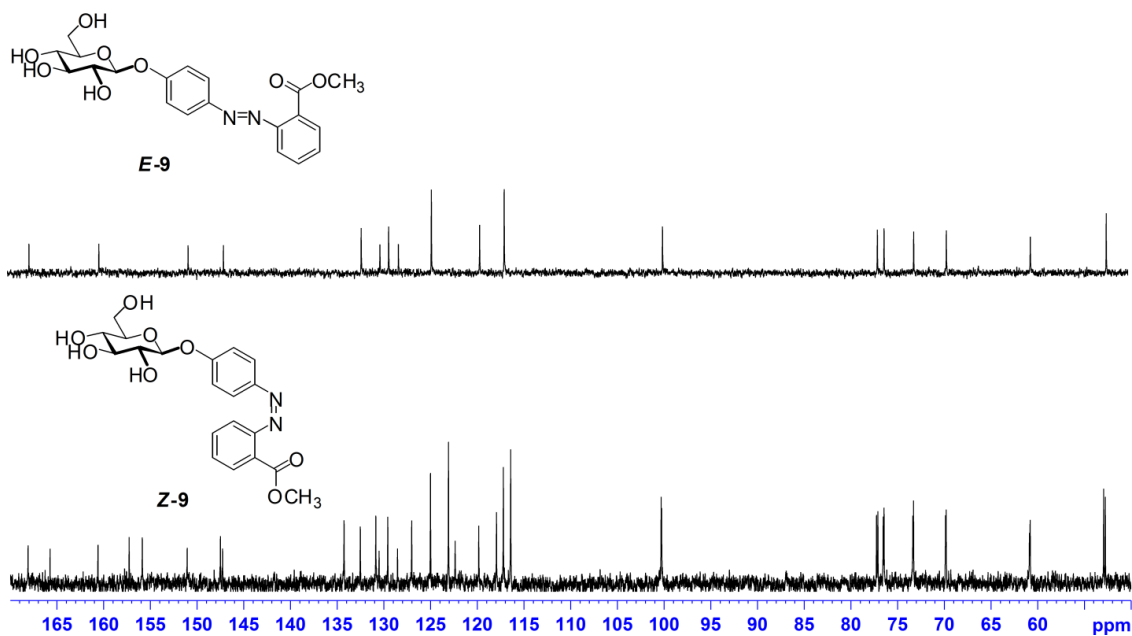


Figure S21. ^{13}C NMR (125 MHz, DMSO-D_6)

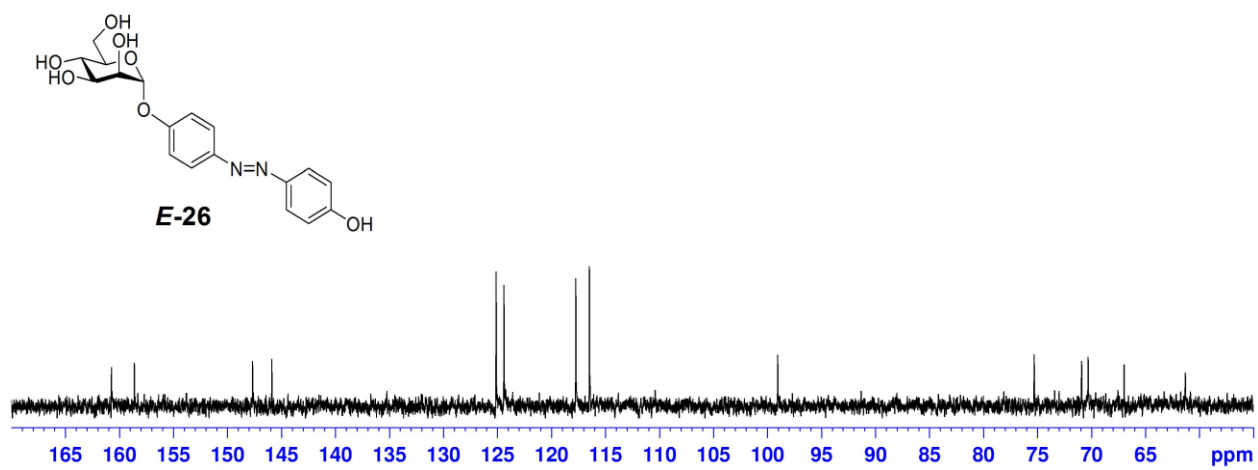


Figure S22. ^{13}C NMR (125 MHz, DMSO-D_6)

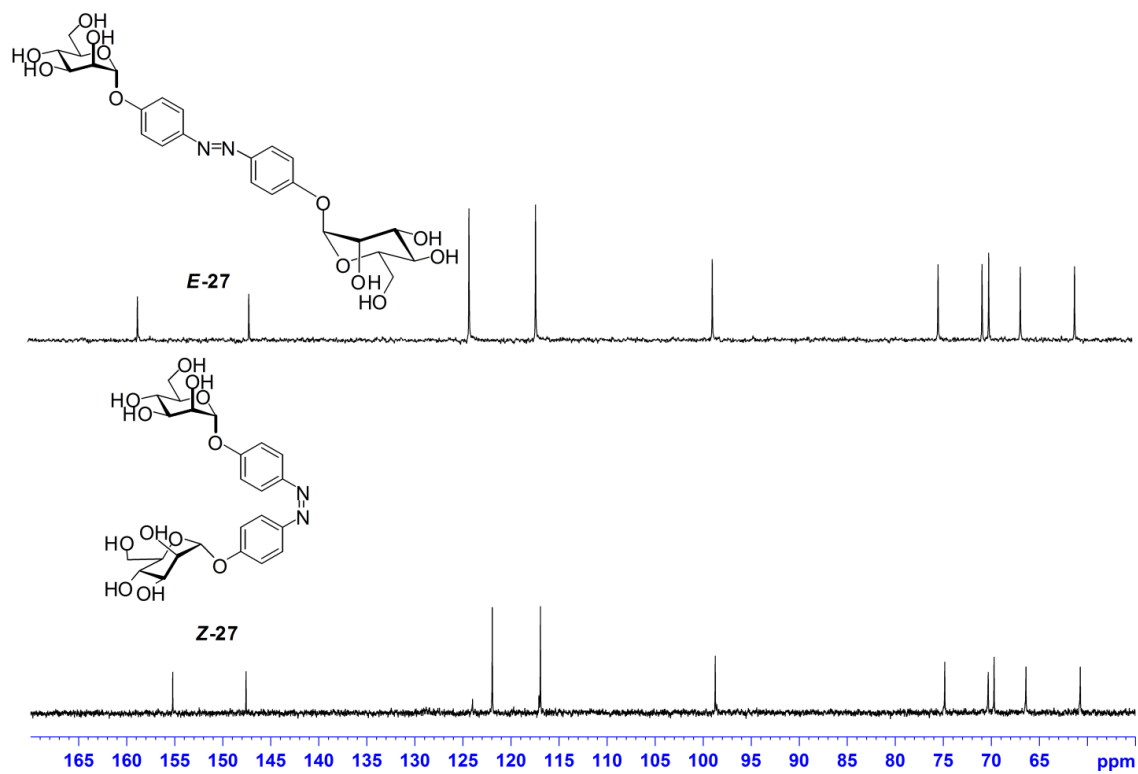


Figure S23. ^{13}C NMR (125 MHz, DMSO-D_6)

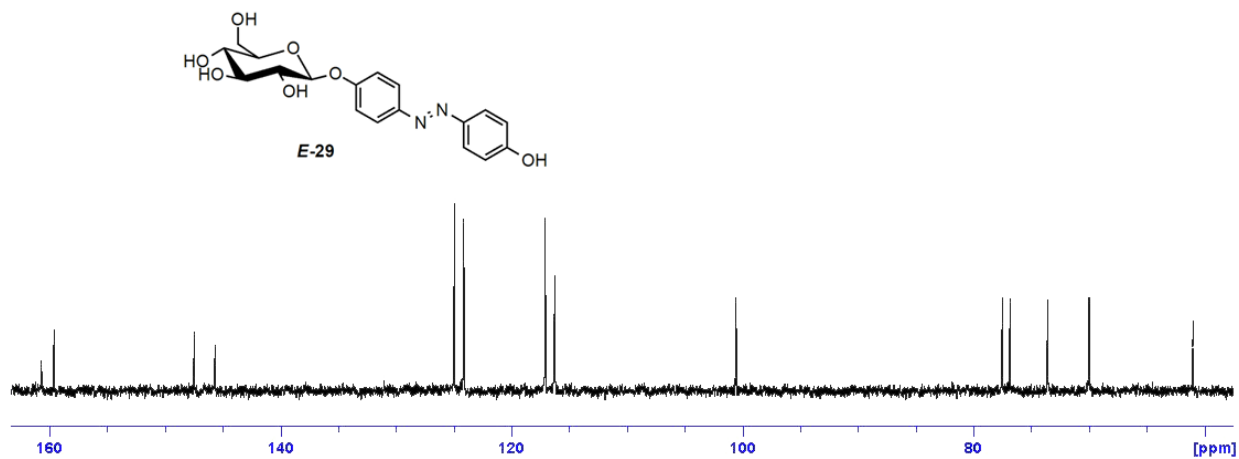


Figure S24. ^{13}C NMR (125 MHz, DMSO-D_6)

3. Determination of the rate constants for $Z \rightarrow E$ relaxation by UV-Vis spectroscopy

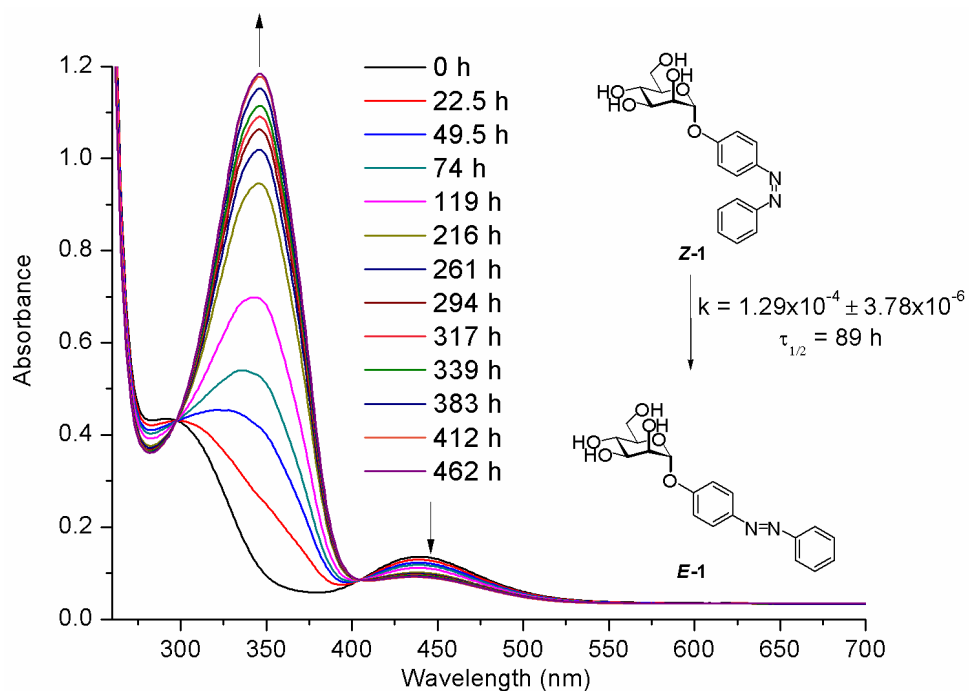


Figure S25: Thermal relaxation of Z-1 to E-1 in DMSO (50 μM) at 18 ± 1 $^{\circ}\text{C}$

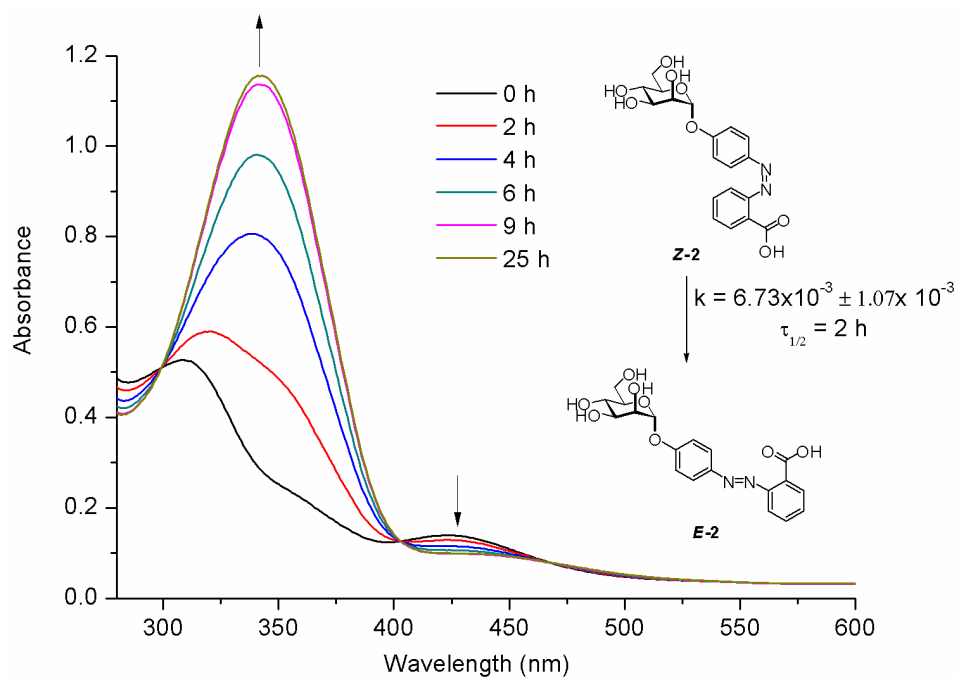


Figure S26: Thermal relaxation of Z-2 to E-2 in DMSO (50 μM) at 18 ± 1 $^{\circ}\text{C}$

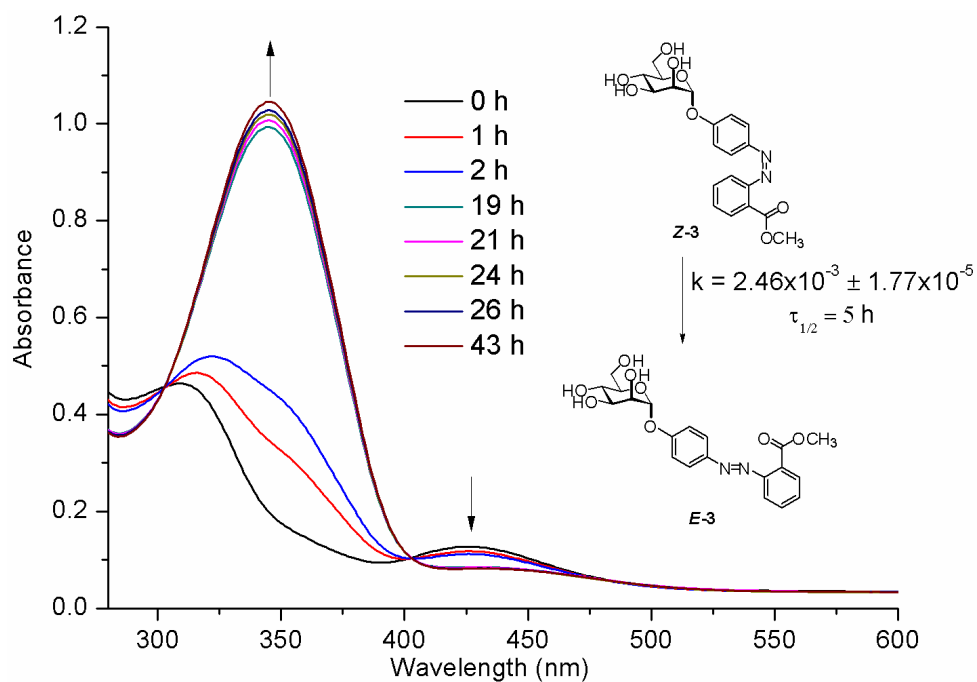


Figure S27: Thermal relaxation of Z-3 to E-3 in DMSO (50 μM) at 18±1 °C

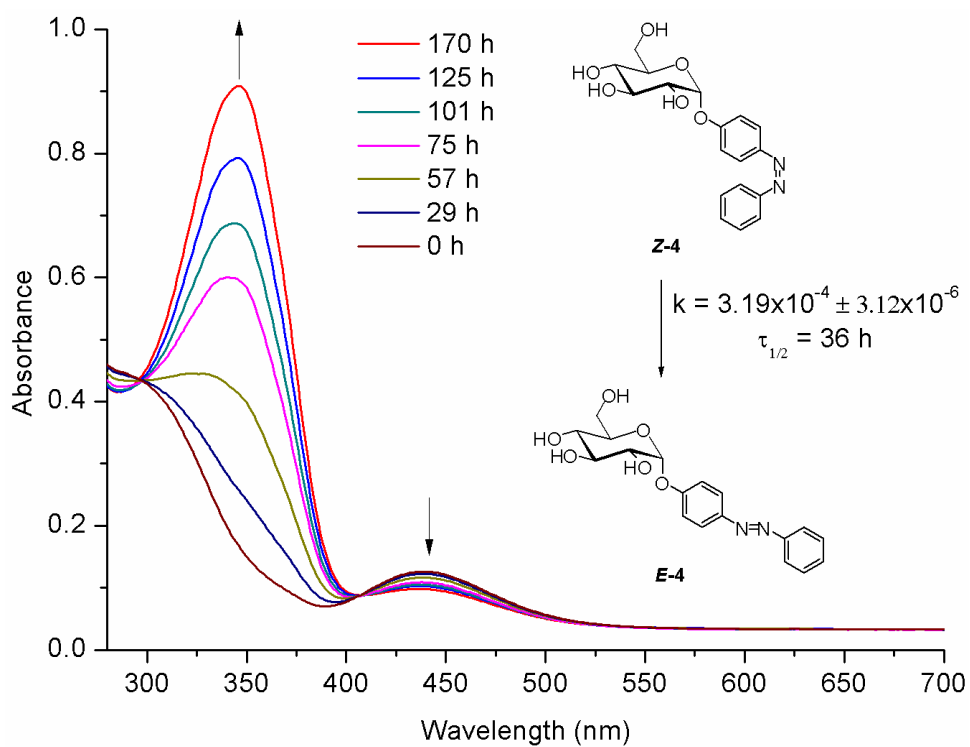


Figure S28: Thermal relaxation of Z-4 to E-4 in DMSO (50 μM) at 18±1 °C

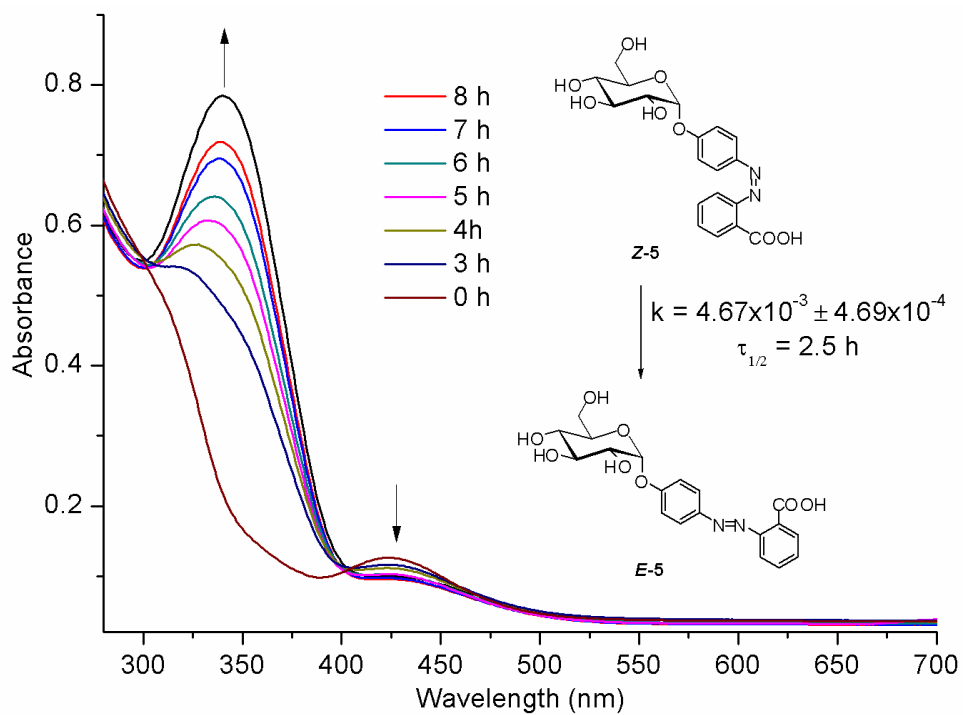


Figure S29: Thermal relaxation of Z-5 to E-5 in DMSO (50 μM) at 18±1 °C

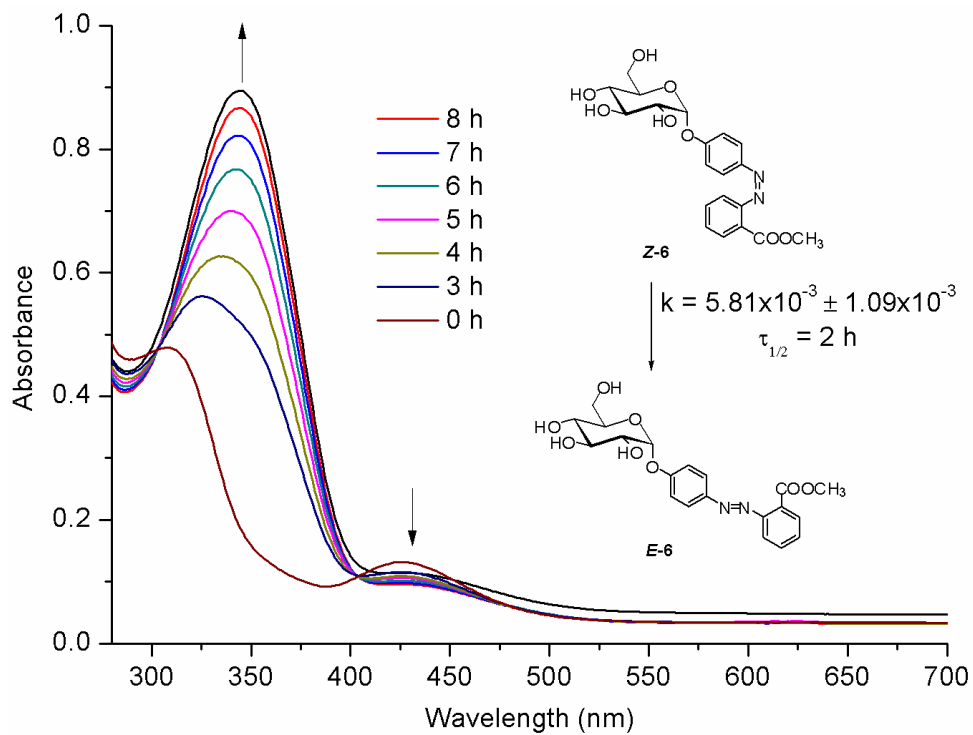


Figure S30: Thermal relaxation of Z-6 to E-6 in DMSO (50 μM) at 18±1 °C

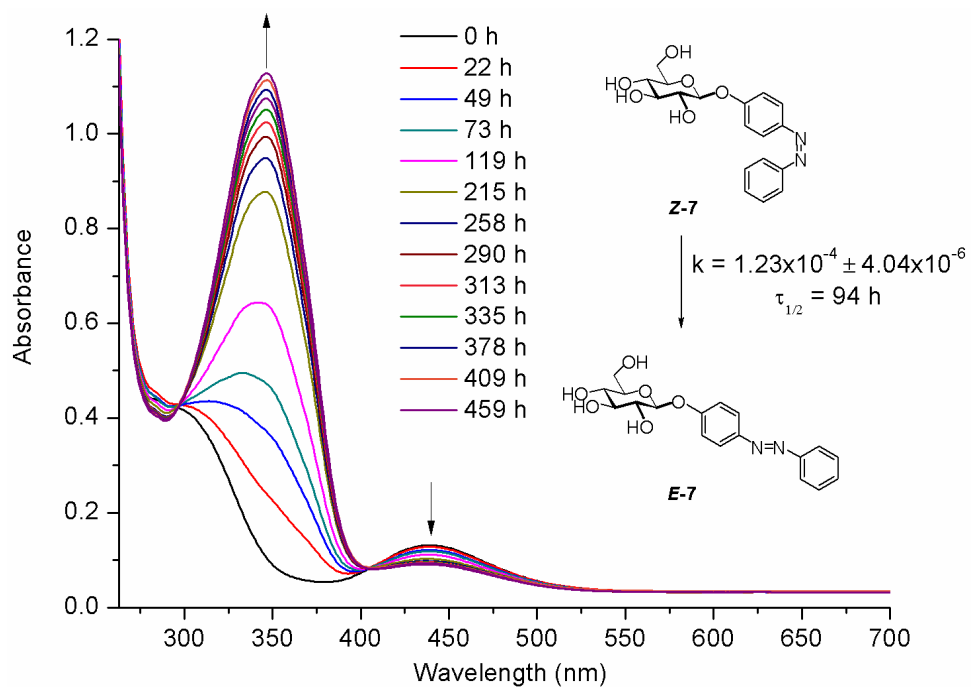


Figure S31: Thermal relaxation of *Z*-7 to *E*-7 in DMSO (50 μ M) at 18 ± 1 $^{\circ}$ C

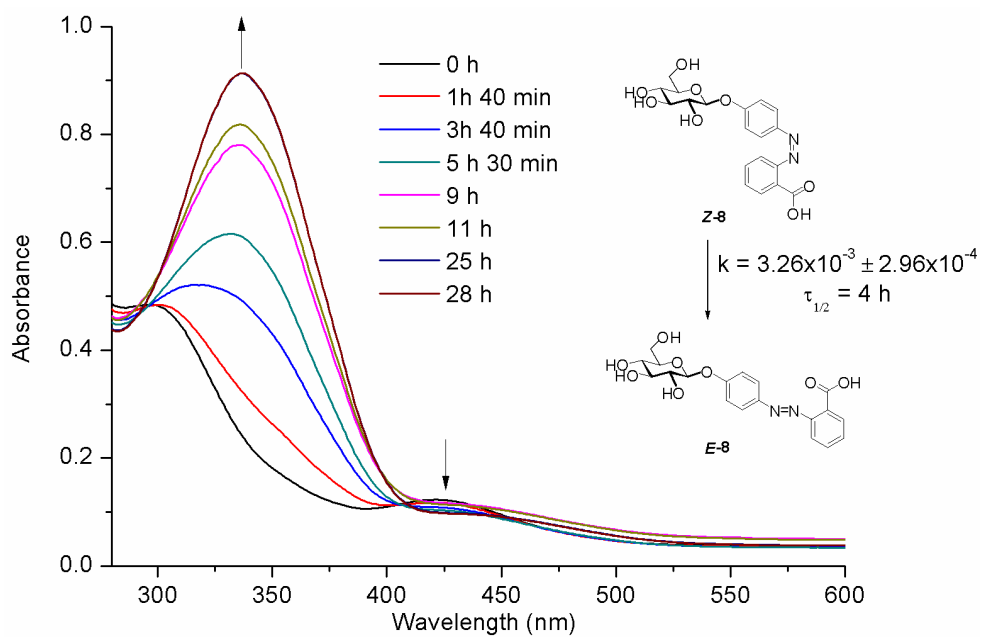


Figure S32: Thermal relaxation of *Z*-8 to *E*-8 in DMSO (50 μ M) at 18 ± 1 $^{\circ}$ C

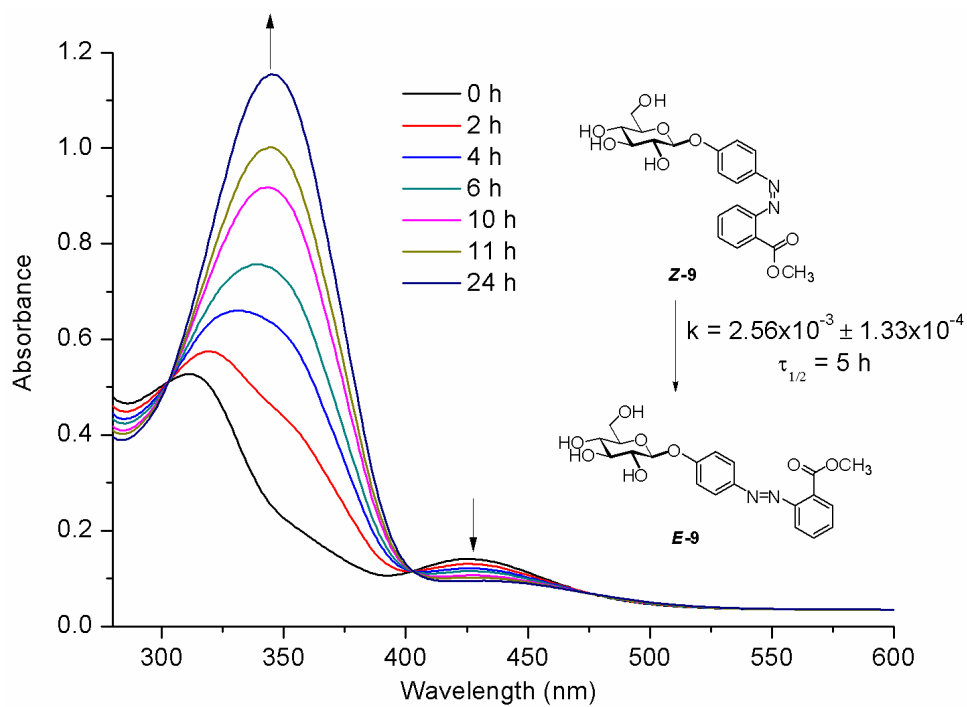


Figure S33: Thermal relaxation of *Z*-9 to *E*-9 in DMSO (50 μ M) at 18 ± 1 $^{\circ}$ C

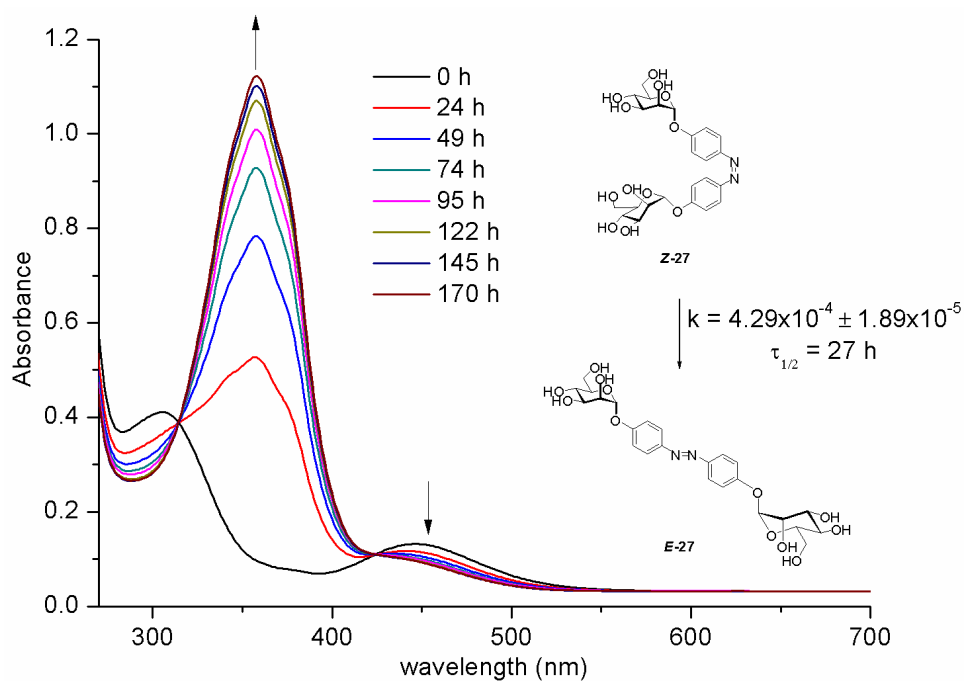


Figure S34: Thermal relaxation of *Z*-27 to *E*-27 in DMSO (50 μ M) at 18 ± 1 $^{\circ}$ C

3.3 Sweet switches: Azobenzene glycoconjugates by click chemistry

Vijayanand Chandrasekaran, Thisbe K. Lindhorst*

Chem. Commun. **2012**, 48, 7519-7521.

Multiple assembly of azobenzene glycoconjugates is of special interest because it allows the investigation of conformational aspects of multivalency effects in carbohydrate recognition. However, a systematic approach how the conformation will control the multivalent azobenzene glycoconjugates is less explored. In this communication, a series of mono-, di- and trivalent azobenzene glycoconjugates were synthesized via click chemistry and the photochromic properties were studied in solution. In future perspective, multivalent azobenzene glycoarrays will be formed on different surface scaffolds for biological testing. (Fig 3.3)

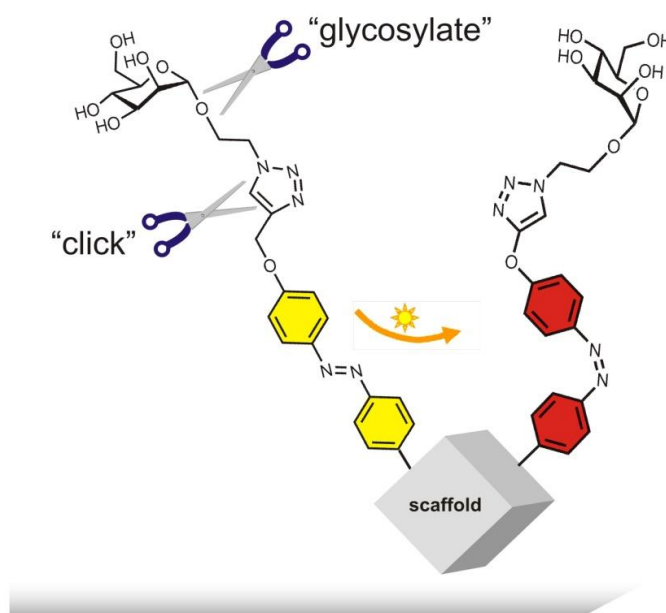


Figure 3.3: Schematic representation for the synthesis of multivalent photoswitchable glycoconjugates, which can be achieved by glycosylation and click chemistry reaction.

In this project, I did the synthesis, substance characterization and studied the photochromic properties of the prepared azobenzene glycosides. T. K. Lindhorst and I wrote the manuscript and the supplementary material part.

Cite this: *Chem. Commun.*, 2012, **48**, 7519–7521

www.rsc.org/chemcomm

Sweet switches: azobenzene glycoconjugates synthesized by click chemistry†

Vijayanand Chandrasekaran and Thisbe K. Lindhorst*

Received 16th May 2012, Accepted 1st June 2012

DOI: 10.1039/c2cc33542e

Azobenzene glycoconjugates can be switched between two isomeric states, *E* and *Z*, to change the spatial orientation of the conjugated carbohydrate ligands. Mono-, di- and trivalent azobenzene glycoconjugates were synthesized using click chemistry and their photochromic properties determined. Multivalency effects were observed in photoisomerisation.

Molecular recognition processes in biology are governed by the constitution and configuration of the interaction partners. Moreover, they are controlled and fine-tuned by conformational changes within the supramolecular environment of the biological system, such as a glycosylated cell surface.¹ In order to gain insight into conformational control of biological processes, photoswitchable bioprobes have become popular.² Typically, these are organic molecules that undergo a defined and reversible change between two sterically different states upon irradiation with light of an appropriate wavelength. Some of the best investigated molecular switches are azobenzenes that exist in a stable planar *E*-form and can be photoisomerised into a bent *Z*-isomer. Switching azobenzene conjugates between these two states effects a significant steric change within the molecule and alters the relative orientation of the conjugated bioprobes.

Azobenzene derivatives have been shown to be well-suited for biological applications³ and their two isomeric forms (*E* and *Z*) can be independently addressed in biological testing. However, to date, only few examples have been published where carbohydrates have been combined with an azobenzene photoswitch.⁴ It has been shown, though, that isomerisation of photoswitchable glycoconjugates changes their interactions with carbohydrate-recognizing proteins (lectins).^{5,6}

As azobenzene glycoconjugates are important target molecules for glycobiological research it is necessary to improve their synthesis and facilitate their application in various contexts. The multiple assembly (clustering) of azobenzene glycoconjugates is of special relevance because it allows the investigation of conformational aspects of multivalency effects in

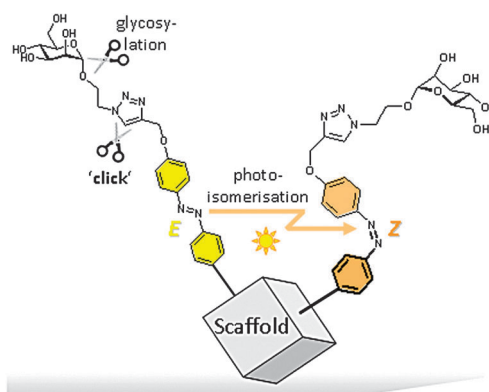


Fig. 1 The combination of glycosylation and click chemistry is a powerful method to create photoswitchable glycoconjugates of different valencies.

carbohydrate recognition.⁷ In the past small glycoclusters have proven to be very valuable tools for probing lectins.⁸ Here, it has been our goal to utilize the concept of “click chemistry”⁹ for the effective preparation of azobenzene glycosides and their di- and trivalent clustered analogues (*cf.* Fig. 1).

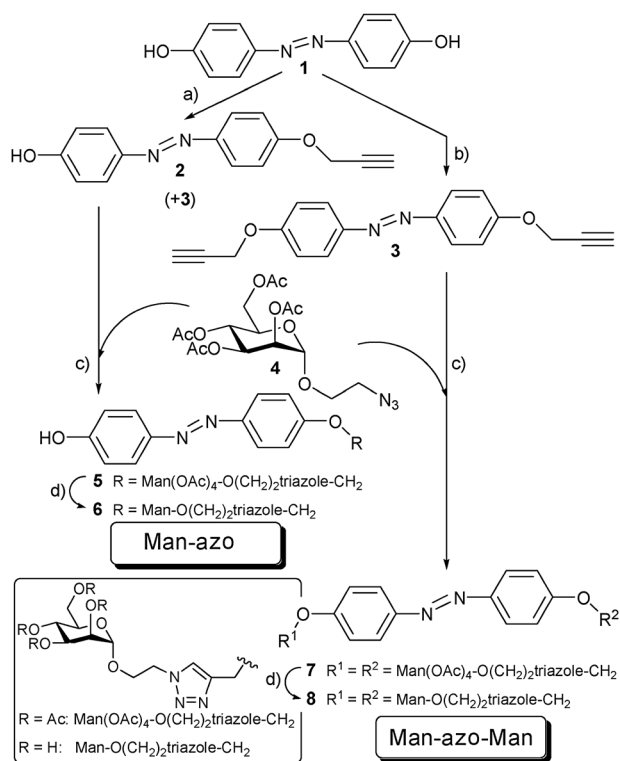
In order to employ click chemistry for the synthesis of photoswitchable glycoconjugates, the best approach is to use azobenzene propargyl ethers on the one hand and azido-functionalised carbohydrates on the other hand.

Firstly, ether-functionalised azobenzene derivatives are known for their favourable photochromic properties. Furthermore, the required azide-modified saccharides can be easily obtained in great variety. Owing to our long standing interest in mannose-specific lectins¹⁰ we have selected mannoside **4** (Scheme 1) as the prototype azide for the current study.

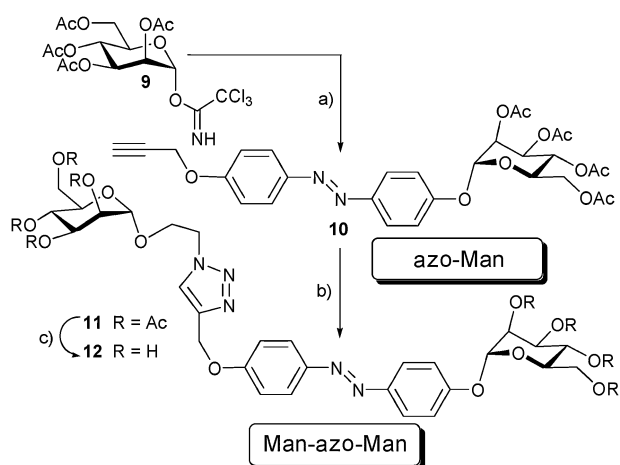
The synthetic routes leading to mono- as well as bis-glycosylated azobenzene glycoconjugates were both started from 4,4'-dihydroxyazobenzene (**1**, Scheme 1) which was prepared according to the literature.¹¹ Regioselective conversion into the mono-propargyl ether **2** was achieved in 35% yield with recovery of ~40% starting material. The same reaction using 5 equivalents of both propargyl bromide and potassium carbonate leads to the bis-propargyl ether **3** as the only product in 91% yield.¹² Both azobenzene propargyl ethers, **2** and **3**, were subjected to 1,3-dipolar cycloaddition under “click conditions”¹³ using the 2-azidoethyl mannoside **4**, which was easily obtained from D-mannose in three high-yield steps.¹⁴ The desired triazole derivatives **5** and **7**, respectively, were obtained in high yield.

Otto Diels Institute of Organic Chemistry, Christiana Albertina University of Kiel, Otto-Hahn-Platz 3-4, D-24098 Kiel, Germany.
E-mail: tkind@oc.uni-kiel.de; Fax: +49 431 880 7410;
Tel: +49 0431 880 2023

† Electronic supplementary information (ESI) available. See DOI: 10.1039/c2cc33542e



Scheme 1 Reaction conditions: (a) propargyl bromide (1.1 equiv.), K_2CO_3 (0.5 equiv.), 35% **2**, 7% **3**, 42% recovered **1**; (b) propargyl bromide (5 equiv.), K_2CO_3 (5 equiv.), 91%; (c) $Cu/CuSO_4$, $t-BuOH/H_2O$ (1 : 1), rt, 30 h, 89% (**5**), 83% (**7**); (d) NaOMe, MeOH, rt, overnight: 92% (**6**), 96% (**8**).



Scheme 2 Reaction conditions: (a) **2**, $BF_3 \cdot Et_2O$, CH_2Cl_2 , rt, 12 h, 88%; (b) **4**, $Cu/CuSO_4$, $t-BuOH/THF/H_2O$, 70 °C, 16 h, 82%; (c) NaOMe, MeOH, 93%.

De-*O*-acetylation under Zemplén conditions¹⁵ afforded the unprotected mono- and bis-glycosylated azobenzene conjugates **6** (Man-azo) and **8** (Man-azo-Man) in nearly quantitative yields.

Alternatively, bis-glycosylated azobenzene derivatives can be prepared by combination of a glycosylation and a cycloaddition step (Scheme 2). Accordingly, Lewis acid-promoted mannosylation of **2** with the mannosyl donor **9**¹⁶ gave the α -mannoside **10**, which upon reaction with the azide **4** under Cu(I) catalysis led to the triazole derivative **11** in 82% yield.

Zemplén deprotection afforded the OH-free bis-glycosylated azobenzene glycoconjugate **12**.

The two prepared conjugates of the “Man-azo-Man” type, **8** and **12**, differ in that **8** is a symmetrical compound as reflected in the 1H NMR spectrum, whereas **12** consists of two different fragments and displays two signal sets for the differently attached mannosidic moieties.

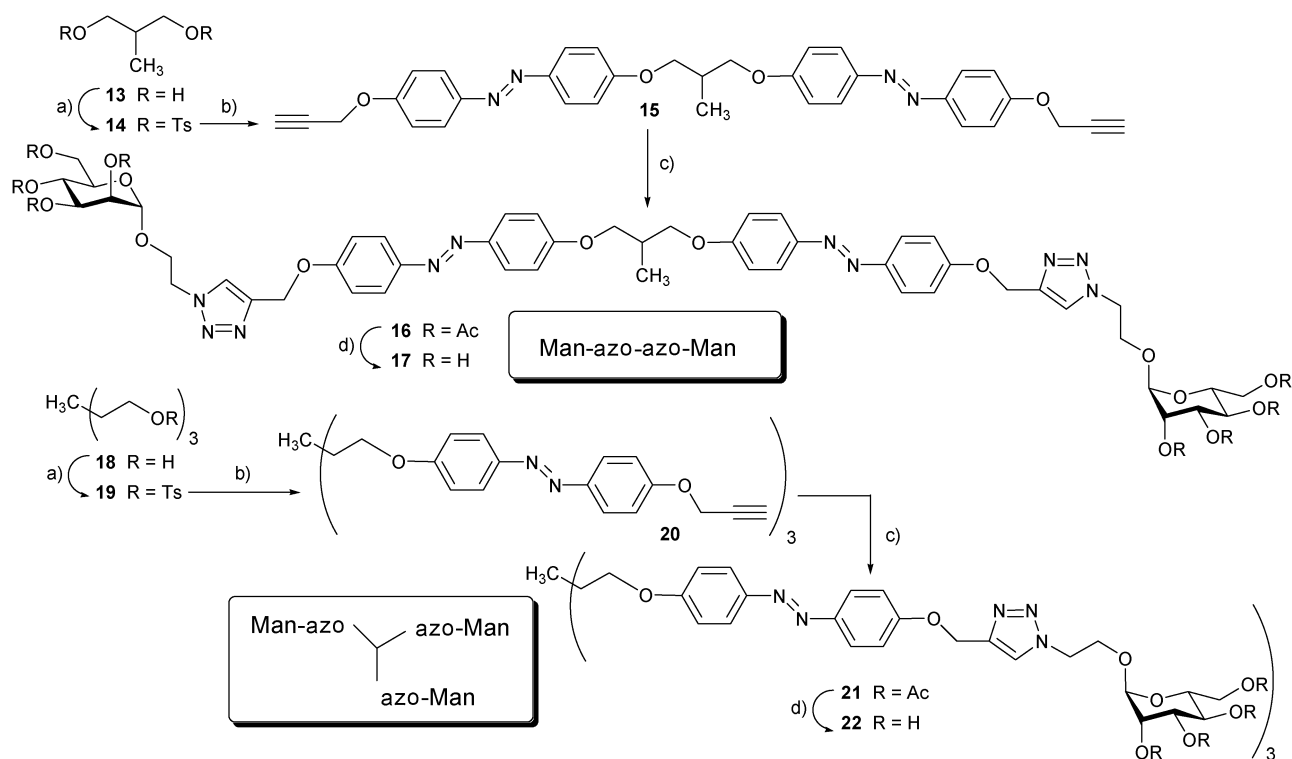
Next, clustering of glycoazobenzene moieties was investigated. As scaffolding core molecules, the diol **13** and the branched triol **14** were employed (Scheme 3). Our first attempt to use Mitsunobu conditions for the alkylation of these alcohols with the phenol **2** failed unexpectedly. Therefore, hydroxyl groups were activated by tosylation to subsequently undergo a classical nucleophilic substitution reaction. Reaction of the tosylates **14**¹⁷ and **19**¹⁸ using the azobenzene derivative **2** led to the desired di- and trivalent azobenzene alkynes **15** and **20**, respectively. They formed the starting materials for the subsequent click reaction with the azide **4** using a mixture of $CuSO_4$ and copper powder, leading to the triazole-linked glycoconjugates **16** and **21** in good yields. Again Zemplén deprotection occurred without any problem, furnishing the unprotected symmetric di- and trivalent azobenzene mannoside clusters **17** (Man-azo-azo-Man) and **22** ([Man-azo]₃).

The photochromic properties of mono-, di- and trivalent azobenzene glycoconjugates were tested next. In the ground state (GS) all azobenzene glycoconjugates, **6**, **8**, **12**, **17**, and **22**, existed in their *E*-configuration almost exclusively (Table 1).

Irradiation in DMSO solution for 30 min at 365 nm led to the respective photostationary states (PSS) with varying *E* : *Z* ratios, as determined by integration of the 1H NMR signals. The PSS *E* : *Z* ratios of the monovalent bis-glycosylated azobenzene glycoconjugates **8** and **12** are excellent (3 : 97 and 1 : 99, respectively) with long half lives allowing independent biological evaluation of both isomeric forms. For the monoglycosylated azobenzene alcohol **6** on the other hand, the PSS could not be determined by UV-VIS spectroscopy. This is presumably due to the extremely fast kinetics of thermal relaxation of the *Z* isomer, as has been described earlier for *p*-hydroxy-substituted azobenzene derivatives.¹⁹ The electron-donating effect of the OH-substituent lowers the barrier for thermal back isomerisation (Fig. 2) leading to relaxation times in the ms range. This feature makes such sweet switches interesting candidates for applications, where fast information processing is required.

Interestingly, photoisomerisation of the di- and trivalent azobenzenes was less effective than that in the case of **8** and **12**, leading to *E* : *Z* ratios in the PSS of 33 : 67 and 63 : 37, respectively. These ratios are averaged over an equilibrium mixture of *EE*, *EZ* and *ZZ* isomers for **17** having two azobenzene branches and a mixture of *EEE*, *EEZ*, *EZZ*, and *ZZZ* isoforms for **22** having three azobenzene branches (cf. 1H NMR spectra in the ESI†).

The photoswitching in this case is most likely influenced by electronic effects including intramolecular quenching processes such as excitonic coupling, which was also shown for azobenzene SAMs.²⁰ The di- and trivalent azobenzene clusters may easily adopt a conformation in which the azobenzene branches are stacked, leading to decay of the excited state before isomerisation takes place. In addition, nonradiative decay could be responsible for less effective photoisomerisation.



Scheme 3 Reaction conditions: (a) tosyl chloride, pyridine, 83% (**14**), quant. (**19**); (b) **2**, K_2CO_3 , DMF, 100 °C, 16 h, 74% (**15**), 65% (**20**); (c) Cu/CuSO₄·H₂O, *t*-BuOH/THF/H₂O (1 : 1 : 1), 70 °C, 48 h, 81% (**16**), 79% (**21**); (d) NaOMe, MeOH, rt, overnight, 91% (**17**), quant. (**22**).

Table 1 Photochromic properties of azobenzene glycoconjugates

Azobenzene glycoconjugate	<i>E</i> : <i>Z</i> ^a GS	<i>E</i> : <i>Z</i> ^a PSS	$\tau_{1/2}$ (h)
6 Man-azo	99 : 1	—	—
8 Man-azo-Man	98 : 2	3 : 97	14
12 Man-azo-Man	99 : 1	1 : 99	21.3
17 Man-(azo) ₂ -Man	99 : 1	33 : 67 ^b	15.5
22 (Man-azo) ₃	99 : 1	63 : 37 ^b	16

^a *E* : *Z* ratios were determined by ¹H-NMR spectroscopy (10 mg in 0.5–0.6 mL). ^b Averaged over all branches. GS: ground state; PSS: photostationary state; $\tau_{1/2}$: half life, determined by UV-VIS spectroscopy (cf. ESI).

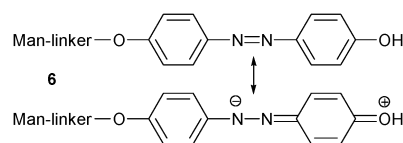


Fig. 2 Two resonance structures of **6** explaining fast *Z* → *E* relaxation.

The detailed kinetics of photoisomerisation of azobenzene clusters **17** and **22** will be determined in due course.

In conclusion, mono- and oligovalent azobenzene glycoconjugates with exciting photochromic properties have been made available employing click chemistry. Photoisomerisation of the di- and trivalent azobenzene clusters **17** and **22** is influenced by intramolecular effects leading to a mixture of isoforms. Multivalent glycoazobenzenes will be further investigated in advanced NMR studies and utilised for fabrication of photoswitchable multivalent glycoassemblies (arrays) for biological testing.

This work was supported by the DFG (Deutsche Forschungsgemeinschaft, SFB 677).

Notes and references

- S. Reitsma, D. W. Slaaf, H. Vink, M. A. M. J. van Zandvoort and M. G. A. oude Egbrink, *Pflugers Arch. Eur. J. Physiol.*, 2007, **454**, 345–359.
- M.-M. Russew and S. Hecht, *Adv. Mater.*, 2010, **22**, 3348–3360.
- A. A. Beharry and G. A. Woolley, *Chem. Soc. Rev.*, 2011, **40**, 4422–4437.
- F. Hamon, F. Djedaini-Pilard, F. Barbot and C. Len, *Tetrahedron*, 2009, **65**, 10105–10123.
- I. Willner and S. Rubin, *J. Am. Chem. Soc.*, 1992, **114**, 3151–3153.
- O. Srinivas, N. Mitra, A. Surolia and N. Jayaraman, *Glycobiology*, 2005, **15**, 861–873.
- M. Mammen, S.-K. Choi and G. M. Whitesides, *Angew. Chem., Int. Ed.*, 1998, **37**, 2754–2794.
- Y. M. Chabre and R. Roy, *Adv. Carbohydr. Chem. Biochem.*, 2010, **63**, 165–393.
- The concept of “click chemistry” has been described in: C. Kolb, M. G. Finn and K. B. Sharpless, *Angew. Chem., Int. Ed.*, 2001, **40**, 2004–2021.
- M. Hartmann and T. K. Lindhorst, *Eur. J. Org. Chem.*, 2011, 3583–3609.
- W. Wei, T. Tomohiro, M. Kodaka and H. Okuno, *J. Org. Chem.*, 2000, **65**, 8979–8987.
- J. M. Casas-Solvas, M. C. Martos-Maldonado and A. Vargas-Berenguel, *Tetrahedron*, 2008, **64**, 10919–10923.
- M. Meldal and C. W. Tornøe, *Chem. Rev.*, 2008, **108**, 2952–3015.
- A. Y. Chernyak, G. V. M. Sharma, L. O. Kononov, P. R. Krishna, A. B. Levinsky, N. K. Kochetkov and A. V. Rama Rao, *Carbohydr. Res.*, 1992, **223**, 303–309.
- G. Zemplén and E. Pascu, *Ber. Dtsch. Chem. Ges.*, 1929, **62**, 1613–1614.
- T. K. Lindhorst, S. Kötter, U. Krallmann-Wenzel and S. Ehlers, *J. Chem. Soc., Perkin Trans. 1*, 2001, 823–831.
- E. R. Nelson, M. Maienthal, L. A. Lane and A. A. Benderly, *J. Am. Chem. Soc.*, 1957, **79**, 3467–3469.
- L. Beaufort, L. Delaude and A. F. Noels, *Tetrahedron*, 2007, **63**, 7003–7008.
- J. Garcia-Amorós, A. Sánchez-Ferrer, W. A. Massad, S. Nonell and D. Velasco, *Phys. Chem. Chem. Phys.*, 2010, **12**, 13238–13242.
- C. Gahl, R. Schmidt, D. Brete, E. R. McNellis, W. Freyer, R. Carley, K. Reuter and M. Weinelt, *J. Am. Chem. Soc.*, 2010, **132**, 1831–1838.

Sweet switches: Azobenzene glycoconjugates by click chemistry

Supporting Information

Vijayanand Chandrasekaran and Thisbe K. Lindhorst*

Otto Diels Institute of Organic Chemistry, Christiana Albertina University of Kiel, Otto-Hahn-Platz 3-4, D-24098 Kiel, Germany. E-mail: tkind@oc.uni-kiel.de

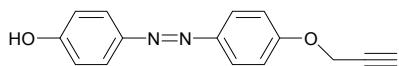
- 1. General methods**
- 2. Synthetic procedures**
- 3. Photochemistry of azobenzene glycoconjugates**
- 4. NMR spectra of azobenzene glycoconjugates**
- 5. References**

1. General methods

Thin layer chromatography was performed on silica gel plates (GF 254, Merck). Detection was effected by UV and subsequent charring with 10% sulphuric acid in EtOH followed by heat treatment at ~180 °C. Flash chromatography was performed on silica gel 60 (Merck, 230-400 mesh, particle size 0.040-0.063 mm) using distilled solvents. Optical rotations were measured with a Perkin-Elmer 241 polarimeter (sodium D-line: 589 nm, length of cell: 1 dm) in the solvents indicated. ¹H and ¹³C NMR spectra were recorded on Bruker DRX-500 and AV-600 spectrometers at 300 K. Chemical shifts are reported relative to internal tetramethylsilane ($\delta = 0.00$ ppm) or D₂O ($\delta = 4.76$ ppm). Full assignment of the peaks was achieved with the aid of 2D NMR techniques (¹H-¹H COSY and ¹H-¹³C HSQC). IR spectra were measured with a Perkin Elmer FT-IR Paragon 1000 (ATR) spectrometer. ESI mass spectra were recorded on a Esquire-LC instrument from Bruker Daltonics. MALDI-TOF mass spectra were recorded on a Bruker Biflex III instrument with 19 kV acceleration voltage. 2,5-Dihydroxybenzoic acid (DHB) was used as a matrix. Air/moisture sensitive reactions were carried out under nitrogen in dry glassware. UV-Vis absorption spectra were performed on Perkin-Elmer Lambda-241 and Varian Cary-5000 at a temperature of 18 ± 1 °C. Photoirradiation was carried out with a high pressure mercury lamp UV-P 250C from Panacol-Elosol. The bandpass filters were obtained from “Laser” components.

2. Synthetic procedures

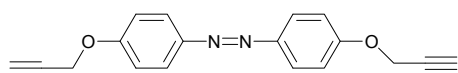
4-Hydroxy-4'-propargyloxy azobenzene (**2**):



A mixture of *p,p'*-dihydroxyazobenzene (**1**, 1.00 g, 4.67 mmol) and propargyl bromide (611 mg, 5.14 mmol, 1.1 equiv.) was added to acetone (50 mL) and stirred under nitrogen at room temperature for 30 min. K₂CO₃ (322 mg, 2.34 mmol, 0.5 equiv.) was added and then the reaction mixture was refluxed for 12 h. TLC (cyclohexane/ethyl acetate, 4:1) showed a mixture of 3 spots corresponding to compounds **1**, **2**, and **3**. After the solvent was evaporated under reduced pressure, the residue was dissolved in ethyl acetate (50 mL) and washed with water (50 mL),

dried over MgSO_4 , filtered and concentrated under reduced pressure. Purification by column chromatography on silica gel (cyclohexane/ethyl acetate, 4:1) gave the mono-substituted product **2** as a white solid (410 mg, 1.63 mmol, 35%) along with the disubstituted product **3** (100 mg, 0.34 mmol, 7%) and recovered **1** (420 mg, 1.96 mmol, 42%). R_f 0.20 (cyclohexane/ethyl acetate, 4:1); m.p. 134 °C; ^1H NMR (500 MHz, CD_3OD , 300 K, TMS): δ = 7.83 (d, J = 9.1 Hz, 2 aryl-H), 7.77 (d, J = 8.9 Hz, 2 aryl-H), 7.10 (d, J = 9.1 Hz, 2 aryl-H), 6.90 (d, J = 8.9 Hz, 2 aryl-H), 4.81 (d, J = 2.4 Hz, 2H, $\text{H-C}\equiv\text{C-CH}_2$), 2.98 (t, J = 2.4 Hz, 1H, $\text{H-C}\equiv\text{C-CH}_2$) ppm; ^{13}C NMR (125 MHz, CD_3OD , 300 K, TMS): δ = 161.6 (C_q , aryl-C), 160.9 (C_q , aryl-C), 148.8 (aryl-C), 147.5 (aryl-C), 125.6 (aryl-C), 124.9 (aryl-C), 116.7 (aryl-C), 116.3 (aryl-C), 79.5 ($\text{H-C}\equiv\text{C-CH}_2$), 77.1 ($\text{H-C}\equiv\text{C-CH}_2$), 56.9 ($\text{H-C}\equiv\text{C-CH}_2$), ppm; ESI MS calcd for $\text{C}_{15}\text{H}_{12}\text{N}_2\text{O}_2$: m/z 253.0898 $[\text{M}+1]^+$; found: m/z 253.0966 $[\text{M}+1]^+$; IR (ATR) 3264 ($\text{C}\equiv\text{C}$), 1588, 1504, 1270, 1024, 826, 676 cm^{-1} .

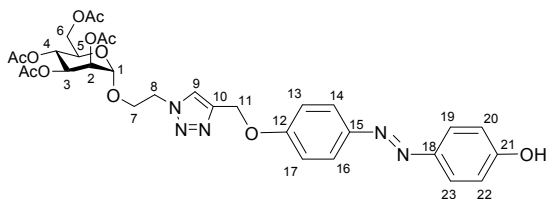
4,4'-Di-propargyloxy azobenzene (**3**):¹



A mixture of *p,p'*-dihydroxyazobenzene (**1**, 100 mg, 0.467 mmol) and propargyl bromide (278 mg, 2.34 mmol, 5.0 equiv.) was added to acetone (5 mL) and the reaction mixture stirred under nitrogen at room temperature for 30 min. Then, K_2CO_3 (322 mg, 2.34 mmol, 5 equiv.) was added and the reaction mixture was refluxed for 16 h. TLC (cyclohexane/ethyl acetate, 4:1) showed a spot-to-spot conversion of product **3**. After the solvent was evaporated under reduced pressure, the residue was dissolved in ethyl acetate (30 mL) and washed with water (10 mL), dried over MgSO_4 , filtered and concentrated under reduced pressure. Purification by column chromatography on silica gel (cyclohexane/ethyl acetate, 4:1) gave the disubstituted product **3** (123 mg, 0.42 mmol, 91%) as a yellow solid. R_f 0.45 (cyclohexane/ethyl acetate, 4:1); m.p. 191 °C; ^1H NMR (500 MHz, CDCl_3 , 300 K, TMS): δ = 8.22 (d, J = 9.2 Hz, 4 aryl-H), 7.05 (d, J = 9.2 Hz, 4 aryl-H), 4.79 (d, J = 2.4 Hz, 4H, 2 $\text{H-C}\equiv\text{C-CH}_2$), 2.58 (d, J = 2.4 Hz, 2H, 2 $\text{H-C}\equiv\text{C-CH}_2$) ppm; ^{13}C NMR (125 MHz, CDCl_3 , 300 K, TMS): δ = 162.3 (C_q , aryl-C), 142.2 (C_q , aryl-C), 125.8, 115.0 (aryl-C), 77.3 ($\text{H-C}\equiv\text{C-CH}_2$), 76.8 ($\text{H-C}\equiv\text{C-CH}_2$), 56.3 ($\text{H-C}\equiv\text{C-CH}_2$) ppm; ESI

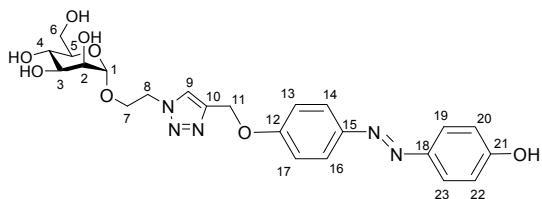
MS calcd for $C_{18}H_{14}N_2O_2$: m/z 290.1055 $[M+1]^+$; found: m/z 291.1055 $[M+1]^+$; IR (ATR): 3260 ($C\equiv CH$), 1587, 1493, 1245, 1020, 844, 663 cm^{-1} .

Click reaction: Acetylated monoglycosylated azobenzene glycoconjugate 5 (Man-a z o [OAc]₄):



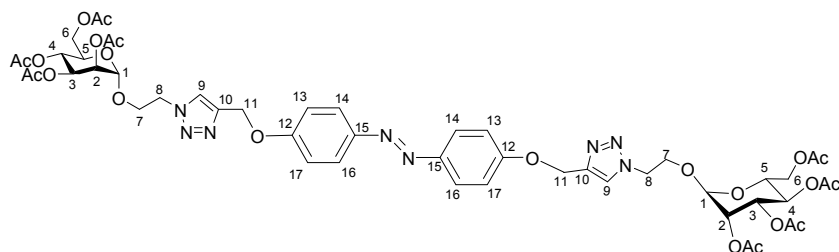
A mixture of *tert*-butanol and water (1:1, 3 mL) was added to a mixture of the azobenzene alcohol **2** (50 mg, 0.19 mmol, 1.0 equiv.), the mannoside **4**² (99.3 mg, 0.24 mmol, 1.2 equiv.), $CuSO_4 \times 5H_2O$ (3 mg) and Cu powder (30 mg). The reaction mixture was stirred at room temperature for 30 h. Then, TLC (cyclohexane/ethyl acetate, 1:4) showed complete consumption of **2**. Ethyl acetate (30 mL) was added, Cu removed by filtration over celite, and the filtrate was dried over $MgSO_4$. It was filtered and the filtrate concentrated under reduced pressure. Purification of crude product by column chromatography on silica gel (cyclohexane/ethyl acetate, 1:4) gave mannoside **5** as a reddish brown low melting solid (118 mg, 0.18 mmol, 89%). R_f 0.22 (cyclohexane/ethyl acetate, 1:4); $[\alpha]_D^{22} = +23$ ($c = 0.64$, CH_2Cl_2); m.p. 70-72 °C; 1H NMR (500 MHz, $CDCl_3$, 300 K, TMS): $\delta = 7.83-7.81$ (m, 3H, H-16, H-14, H-9), 7.78 (d, $J = 8.7$ Hz, 2H, H-19, H-23), 7.06 (d, $J = 8.9$ Hz, 2H, H-13, H-17), 6.94 (d, $J = 8.7$ Hz, 2H, H-20, H-22), 5.27 (s, 2H, H-11), 5.25-5.23 (m, 2H, H-3, H-4), 5.21 (m, 1H, H-2), 4.80 (d, $J = 1.4$ Hz, 1H, H-1), 4.63 (t, $J = 5.1$ Hz, 2H, H-8a, H-8b), 4.20 (dd, $J = 12.3, 5.3$ Hz, 1H, H-6a), 4.15 (m_c, 1H, H-7a), 4.06 (dd, $J = 12.34, 2.4$ Hz, 1H, H-6b), 3.89 (m_c, 1H, H-7b), 3.55 (ddd, $J = 9.4, 5.3, 2.3$ Hz, 1H, H-5), 2.14, 2.09, 2.00, 1.98 (each s, each 3H, 4 C(O)CH₃) ppm; ^{13}C NMR (125 MHz, $CDCl_3$, 300 K, TMS): $\delta = 170.7, 170.1, 170.0, 169.7$ (4 C=O), 160.1 (C-12), 158.4 (C-21), 147.4 (C-15), 146.9 (C-18), 144.0 (C-10), 124.6 (C-19, C-23), 124.3 (C-10, C-14, C-9), 115.8 (C-20, C-22), 115.0 (C-13, C-17), 97.5 (C-1), 69.2 (C-5, C-2), 68.9 (C-3), 66.2 (C-7), 65.7 (C-4), 62.3 (C-6), 61.9 (C-11), 49.9 (C-8), 20.8, 20.7, 20.7, 20.6 (4 COCH₃) ppm; ESI MS calcd for $C_{31}H_{35}N_5O_{12}$: m/z 692.228 $[M+Na]^+$; found: m/z 692.219 $[M+Na]^+$; IR (ATR) 3144, 1750, 1580, 1498, 1221, 1147, 850, 554 cm^{-1} .

Deprotection: Monoglycosylated azobenzene glycoconjugate 6 (Man- α z o):



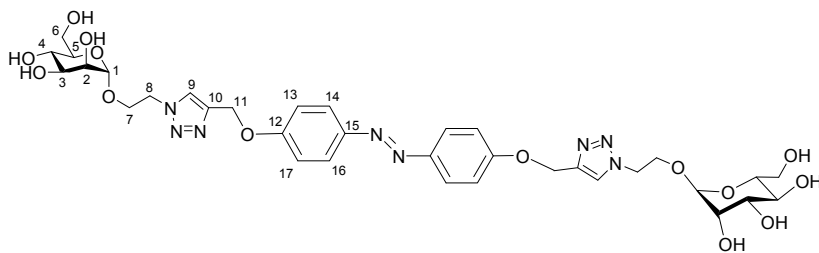
The acetyl-protected monovalent azobenzene glycoconjugate **5** (100 mg, 0.14 mmol) was dissolved in anhydrous methanol (5 mL) and a catalytic amount of solid NaOMe was added. The reaction mixture was stirred at room temperature overnight. Then, it was neutralized with Amberlite IR 120 ion exchange resin and filtered. The filtrate was evaporated to yield **6** as a dark orange syrup compound (71.8 mg, 0.143 mmol, 92%). R_f 0.28 ($\text{CH}_2\text{Cl}_2/\text{MeOH}$, 4:1); $[\alpha]_D^{22} = +15.6$ ($c = 1.03$, DMSO); $^1\text{H NMR}$ (500 MHz, CD_3OD , 300 K, TMS): $\delta = 8.13$ (s, 1H, H-9), 7.84 (d, $J = 8.9$ Hz, 2H, H-14, H-16), 7.77 (d, $J = 8.9$ Hz, 2H, H-19, H-23), 7.16 (d, $J = 9.0$ Hz, 2H, H-13, H-17), 6.90 (d, $J = 8.9$ Hz, 2H, H-20, H-22), 5.26 (s, 2H, H-11a, H-11b), 4.74 (d, $J = 1.5$ Hz, 1H, H-1), 4.66 (ddd, $J = 10.5, 7.2, 3.9$ Hz, 2H, H-8a, H-8b), 4.14 (ddd, $J = 10.5, 6.5, 3.8$ Hz, 1H, H-7a), 3.90 (ddd, $J = 10.6, 6.5, 3.3$ Hz, 1H, H-7b), 3.78 (dd, $J = 11.8, 2.3$ Hz, 1H, H-6a), 3.75 (dd, $J = 2.8, 1.8$ Hz, 1H, H-2), 3.66 (dd, $J = 11.8, 5.9$ Hz, 1H, H-6b), 3.61-3.56 (m, 2H, H-3, H-4), 3.23-3.24 (ddd~ m_c , 1H, H-5) ppm; $^{13}\text{C NMR}$ (125 MHz, CDCl_3 , 300 K, TMS): $\delta = 160.8$ (C-21), 160.5 (C-12), 146.9 (C-15), 145.7 (C-18), 142.7 (C-10), 125.5 (C-9), 124.9 (C-20, C-22), 124.4 (C-13, C-17), 116.3 (C-19, C-23), 115.7 (C-14, C-16), 100.3 (C-1), 74.7 (C-5), 71.3 (C-3), 70.5 (C-2), 67.3 (C-4), 65.4 (C-7), 61.9 (C-11), 61.6 (C-6), 49.9 (C-8) ppm; UV/Vis (DMSO) $\lambda_{\text{max}} = 364$ nm; $\epsilon = 25804 \pm 1109$ L x mol $^{-1}$ x cm $^{-1}$; MALDI-TOF MS calcd for $\text{C}_{23}\text{H}_{27}\text{N}_5\text{O}_8$: m/z 524.185 $[\text{M}+\text{Na}]^+$; found: m/z 524.176 $[\text{M}+\text{Na}]^+$.

Click reaction: Acetylated bisglycosylated azobenzene glycoconjugate **7 (Man- α z o-Man [OAc]₈):**



To a mixture of the azobenzene **3** (200 mg, 0.689 mmol), the mannoside **4**² (633 mg, 1.52 mmol, 2.2 equiv.), CuSO₄ x 5H₂O (12 mg) and Cu powder (100 mg) *tert*-butanol and water (1:1, 10 mL) were added. The reaction mixture was stirred at room temperature for 48 h. Then, TLC (CH₂Cl₂/MeOH, 4:1) showed complete consumption of **3**. The reaction was diluted with ethyl acetate (100 mL), Cu removed by filtration using celite, and the filtrate was dried over MgSO₄. It was filtered and the filtrate concentrated under reduced pressure. Purification of the crude by column chromatography on silica gel (CH₂Cl₂/MeOH, 4:1) gave product **7** as a crystalline pale yellow solid (643 mg, 0.572 mmol, 83%). R_f 0.24 (cyclohexane/ethyl acetate, 1:1); $[\alpha]_D^{22} = + 29.6$ ($c = 1.01$, CH₂Cl₂); m.p. 99-103 °C; ¹H NMR (500 MHz, CDCl₃, 300 K, TMS): $\delta = 7.87$ (d, $J = 9.0$ Hz, 4H, aryl-H), 7.79 (s, 2H, 2 H-9), 7.11 (d, $J = 9.1$ Hz, 4H, aryl-H), 5.30 (s, 4H, 2 H-11a, 2 H-11b), 5.24- 5.22 (m_c, 4H, 2 H-4, 2 H-3), 5.20-5.19 (m_c, 2H, 2 H-2), 4.80 (d, $J = 1.5$ Hz, 2H, 2 H-1), 4.62 (t, $J = 5.2$ Hz, 4H, 2 H-8a, 2 H-8b), 4.20 (dd, $J = 12.3, 5.4$ Hz, 2H, 2 H-6a), 4.14 (td, $J = 10.9, 5.4$ Hz, 2H, 2 H-7a), 4.04 (dd, $J = 12.3, 2.4$ Hz, 2H, 2 H-6b), 3.91-3.87 (m, 2H, 2 H-7b), 3.53 (ddd, $J = 9.7, 5.2, 2.4$ Hz, 2H, 2 H-5), 2.14, 2.09, 1.99, 1.98 (each s, each 6H, 8 C(O)CH₃) ppm; ¹³C NMR (125 MHz, CDCl₃, 300 K, TMS): $\delta = 170.6, 169.9, 169.9, 169.6$ (8 C(O)CH₃), 160.3 (2 C-12), 147.4 (2 C-15), 144.0 (2 C-10), 124.4 (2 C-14, 2 C-16), 124.3 (2 C-10, 2 C-14, 2 C-9), 115.1 (2 C-13, 2 C-17), 97.5 (2 C-1), 69.2 (2 C-5, 2 C-3), 68.8 (2 C-2), 66.2 (2 C-7), 65.7 (2 C-4), 62.2 (2 C-6), 62.1 (2 C-11), 49.8 (2 C-8), 20.8, 20.7, 20.7, 20.6 (8 COCH₃) ppm; ESI MS calcd for C₅₀H₆₀N₈O₂₂: m/z 1147.382 [M+Na]⁺; found: m/z 1147.373 [M+Na]⁺; IR (ATR) 2933, 1739, 1597, 1367, 1214, 1041, 841, 599 cm⁻¹.

Deprotection: Bisglycosylated azobenzene glycoconjugate 8 (Man- α z o-Man):



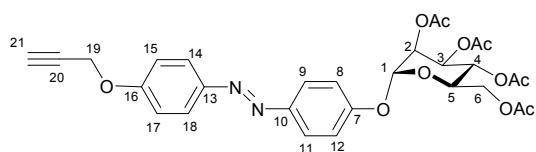
The acetyl-protected azobenzene glycoconjugate **7** (100 mg, 0.09 mmol) was dissolved in anhydrous methanol (3 mL) and a catalytic amount of solid NaOMe was added. The reaction mixture was stirred at room temperature overnight. Then, it was neutralized with Amberlite IR 120 ion exchange resin and filtered. The filtrate was evaporated to yield **8** (67 mg, 0.085 mmol, 96%) as a reddish brown solid. R_f 0.28 ($\text{CH}_2\text{Cl}_2/\text{MeOH}$, 3:7); $[\alpha]_D^{22} = +22$ ($c = 0.96$, DMSO); m.p. 170-171 °C; $^1\text{H NMR}$ (600 MHz, $\text{DMSO-}d_6$, 300 K, TMS): $\delta = 8.20$ (s, 2H, 2 H-9), 7.82 (d, $J = 8.9$ Hz, 4H, 2 H-14, 2 H-16), 7.20 (d, $J = 9.0$ Hz, 4H, 2 H-13, 2 H-17), 5.22 (s, 4H, 2 H-11a, 2 H-11b), 4.61 (d, $J = 1.2$ Hz, 2H, 2 H-1), 4.58 (dd, $J = 4.0, 6.3$ Hz, 4H, 2 H-8a, 2 H-8b), 4.53 (dd, $J = 6.6, 4.0$ Hz, 2H, 2 H-7a), 3.94 (ddd, $J = 10.7, 6.4, 4.0$ Hz, 2H, 2 H-7b), 3.78 (dd, $J = 11.6, 1.9$ Hz, 2H, 2 H-6a), 3.56-3.53 (m, 2H, 2 H-2), 3.40 (dd, $J = 11.7, 6.3$ Hz, 2H, 2 H-6b), 3.39-3.32 (m, 4H, 2 H-4, 2 H-3), 3.14-3.11 (mc, 2H, 2 H-5) ppm; $^{13}\text{C NMR}$ (150 MHz, $\text{DMSO-}d_6$, 300 K, TMS): $\delta = 160.6$ (2 C-12), 146.6 (2 C-15), 142.5 (2 C-10), 125.3 (2 C-9), 124.4 (2 C-14, 2 C-16), 115.6 (2 C-13, 2 C-17), 100.0 (2 C-1), 74.2 (2 C-5), 70.9 (2 C-3), 70.2 (2 C-2), 66.8 (2 C-4), 65.1 (2 C-7), 61.6 (2 C-11), 61.2 (2 C-6), 49.7 (2 C-8) ppm; UV/Vis (DMSO) $\lambda_{\text{max}} = 363$ nm; $\epsilon = 27858 \pm 902 \text{ L x mol}^{-1} \text{ x cm}^{-1}$; MALDI-TOF MS calcd for $\text{C}_{34}\text{H}_{44}\text{N}_8\text{O}_{14}$: m/z 811.297 $[\text{M}+\text{Na}]^+$; found: m/z 811.249 $[\text{M}+\text{Na}]^+$; IR (ATR) 2933, 1739, 1597, 1367, 1214, 1041, 841, 599 cm^{-1} .

After irradiation: Z-8:

$^1\text{H NMR}$ (600 MHz, $\text{DMSO-}d_6$, 300 K, TMS): $\delta = 8.18$ (s, 2H, 2 H-9'), 7.00 (d, $J = 8.9$ Hz, 4H, 2 H-13, 2 H-17), 6.87 (d, $J = 8.9$ Hz, 4H, 2 H-14, 2 H-16), 5.11 (s, 4H, 2 H-11a, 2 H-11b), 4.62 (bs, 2H, 2 H-1), 4.56-4.52 (m, 4H, 2 H-8a, 2 H-8b), 3.95 (ddd, $J = 10.7, 6.3, 4.1$ Hz, 2H, 2 H-7a), 3.79 (ddd, $J = 10.9, 6.7, 4.0$ Hz, 2H, 2 H-7b), 3.61 (dd, $J = 9.9, 5.7$ Hz, 2H, 2 H-6a), 3.53 (bs, 2H, 2 H-2), 3.43-3.30 (m, 6H, 2 H-6b, 2 H-4, 2 H-3), 3.16-3.12 (m, 2H, 2 H-5) ppm; $^{13}\text{C NMR}$

(150 MHz, DMSO-*d*₆, 300 K, TMS): δ = 157.1 (2 C-12), 146.9 (2 C-15), 142.3 (2 C-10), 125.0 (2 C-9), 122.2 (2 C-14, 2 C-16), 114.8 (2 C-13, 2 C-17), 99.9 (2 C-1), 74.2 (2 C-5), 70.8 (2 C-3), 70.1 (2 C-2), 66.8 (2 C-4), 64.9 (2 C-7), 61.3 (2 C-11), 61.2 (2 C-6), 49.4 (2 C-8) ppm; UV/Vis (DMSO) λ_{max} = 448 nm; ϵ = 2466 \pm 782 L x mol⁻¹ x cm⁻¹.

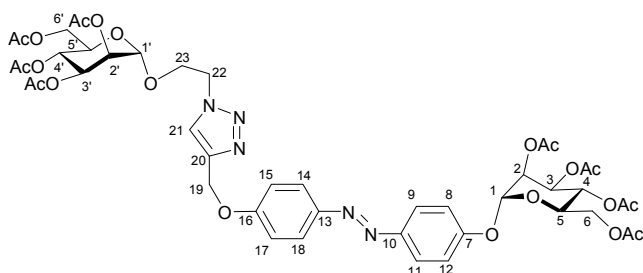
Glycosylation: Acetylated monoglycosylated azobenzene glycoconjugate 10 (a z o-Man [OAc]₄):



A mixture of azobenzene alcohol **2** (100 mg, 0.397 mmol, 1 equiv.) and the glycosyl donor **9**^{3,4} (293 mg, 0.595 mmol, 1.5 equiv.) were dried under vacuum for about 15 minutes, then added of dry CH₂Cl₂ (6 mL) was added and the reaction mixture cooled to 0 °C. The Lewis acid BF₃ x Et₂O (75 μ L, 0.595 mmol, 1.5 equiv.) was added and the reaction mixture stirred at room temperature for overnight. Then, TLC showed complete consumption of **2**. Solid NaHCO₃ was added and CH₂Cl₂ (30 mL). It was washed with water (10 mL) and the organic layer dried over MgSO₄. It was filtered and the filtrate concentrated under reduced pressure. Purification of the crude product by column chromatography on silica gel (cyclohexane/ethyl acetate, 7:3) gave the title compound as a pale yellow low melting solid (203 mg, 0.348 mmol, 88%). *R_f* 0.29 (cyclohexane/ethyl acetate, 7:3); $[\alpha]_D^{22}$ = +72.7 (*c* = 0.81, CH₂Cl₂); m.p.: 54 °C; ¹H NMR (500 MHz, CDCl₃, 300 K, TMS): δ = 7.90 (d, *J* = 9.0 Hz, 2H, H-14, H-18), 7.88 (d, *J* = 8.9 Hz, 2H, H-9, H-11), 7.21 (d, *J* = 9.0 Hz, 2H, H-8, H-12), 7.09 (d, *J* = 9.0 Hz, 2H, H-25, H-17), 5.61 (d, *J* = 1.7 Hz, 1H, H-1), 5.58 (dd, *J* = 10.0, 3.5 Hz, 1H, H-3), 5.48 (dd, *J* = 3.5, 1.9 Hz, 1H, H-2), 5.38 (dd-t, *J* = 10.1 Hz, 1H, H-4), 4.78 (d, *J* = 2.4 Hz, 2H, H-19a, H-19b), 4.29 (dd, *J* = 12.2, 5.5 Hz, 1H, H-6a), 4.12-4.08 (m, 2H, H-5, H-6b), 2.56 (t, *J* = 2.38 Hz, 1H, H-21), 2.22, 2.06, 2.05, 2.03 (each s, each 3H, 4 C(O)CH₃) ppm; ¹³C NMR (150 MHz, CDCl₃, 300 K, TMS): δ = 170.5, 169.9, 169.9, 169.7 (4 C(O)CH₃), 159.7 (C-16), 157.2 (C-7), 148.5 (C-10), 147.5 (C-13), 124.5 (C-14, C-18), 124.3 (C-9, C-11), 116.7 (C-8, C-12), 115.2 (C-15, C-17), 97.1 (C-1), 78.1 (C-20), 75.9 (C-21), 69.4 (C-5), 69.3 (C-2), 68.8 (C-3), 65.8 (C-4), 62.1 (C-6), 56.0 (C-19),

20.8, 20.8, 20.7, 20.7 (4 C(O)CH₃) ppm; ESI MS calcd for C₂₉H₃₀N₂O₁₁: *m/z* 605.184 [M+Na]⁺; found: *m/z* 605.173 [M+Na]⁺; IR (ATR) 3287, 2955, 1743, 1597, 1496, 1209, 1025, 840, 599 cm⁻¹.

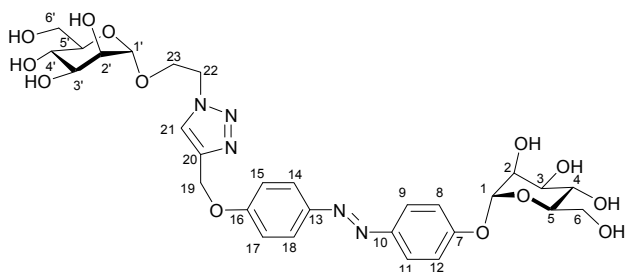
Click reaction: Acetylated bisglycosylated azobenzene glycoconjugate **11 (Man-α z o-Man [OAc]₈):**



To a mixture of the alkyne **10** (100 mg, 0.172 mmol, 1.0 equiv.), the mannoside **4**² (86 mg, 0.206 mmol, 1.2 equiv.), CuSO₄ x 5H₂O (6 mg) and Cu powder (60 mg) a mixture of *tert*-butanol, THF and water (1:1:1, 6 mL) was added. The reaction mixture was heated at 70 °C for 16 h. Then, TLC showed complete consumption of starting material **10**. The reaction mixture was diluted with ethyl acetate (30 mL), Cu was removed by filtration using celite, and the filtrate was dried over MgSO₄. It was filtered and the filtrate concentrated under reduced pressure. Purification of crude product by column chromatography on silica gel using 1% MeOH in CH₂Cl₂ gave the required product **11** as a pale yellow solid (122 mg, 0.122 mmol, 82%). *R_f* 0.33 (cyclohexane/ethyl acetate; 2:3); [α]_D²² = + 66.8 (c = 1.05, CH₂Cl₂); m.p. 72-75 °C; ¹H NMR (500 MHz, CDCl₃, 300 K, TMS): δ = 7.89-7.86 (m, 4H, aryl-H), 7.79 (s, 1H, H-21), 7.20 (d, *J* = 9.0 Hz, 2H, aryl-H), 7.12 (d, *J* = 9.0 Hz, 2H, aryl-H), 5.61 (d, *J* = 1.7 Hz, 1H, H-1), 5.58 (dd, *J* = 10.0, 3.6 Hz, 1H, H-3), 5.48 (dd, *J* = 3.5, 1.8 Hz, 1H, H-2), 5.38 (dd~t, *J* = 10.2 Hz, 1H, H-4), 5.31 (s, 2H, H-11), 5.24-5.23 (m, 2H, H-4', H-3'), 5.21 (m_c, 1H, H-2'), 4.80 (d, *J* = 1.4, 1H, H-1'), 4.63 (t, *J* = 5.1 Hz, 2H, H-8), 4.29 (dd, *J* = 12.3, 5.5 Hz, 1H, H-6'a), 4.20 (dd, *J* = 12.3, 5.4 Hz, 1H, H-6'b), 4.16-4.07 (m, 3H, H-23a, H-5, H-6a), 4.04 (dd, *J* = 12.3, 2.4 Hz, 1H, H-6b), 3.89 (m_c, 2H, H-7), 3.54 (ddd, *J* = 9.5, 5.3, 2.3 Hz, H-5'), 2.22, 2.14, 2.09, 2.06, 2.05, 2.03, 2.00, 1.93 (each s, each 3H, 8 C(O)CH₃) ppm; ¹³C NMR (125 MHz, CDCl₃, 300 K, TMS): δ = 170.5, 170.5, 170.5, 169.9, 169.8, 169.7, 169.7, 169.6 (8 C=O), 160.5 (C-16), 157.2 (C-7),

148.5 (C-10), 147.3 (C-13), 143.9 (C-20), 124.6 (C-14, C-18), 124.3 (C-9, C-11), 124.1 (C-21), 116.7 (C-8, C-12), 115.1 (C-15, C-17), 97.5 (C-1'), 95.7 (C-1), 69.3 (C-5, C-5'), 69.2 (C-2, C-2'), 68.8 (C-3, C-3'), 66.2 (C-23), 65.9 (C-4'), 65.7 (C-4), 62.2 (C-6, C-6'), 62.1 (C-19), 49.8 (C-22), 20.9, 20.8, 20.8, 20.7, 20.7, 20.6, 20.6, 20.6 (8 COCH₃) ppm; ESI MS calcd for C₄₃H₅₃N₅O₂₁: *m/z* 1022.323 [M+Na]⁺; found: *m/z* 1022.290 [M+Na]⁺; IR (ATR) 2932, 1739, 1598, 1367, 1211, 1032, 843, 599 cm⁻¹.

Deprotection: Bisglycosylated azobenzene glycoconjugate **12** (Man-α-z-o-Man):



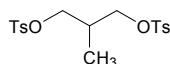
The acetyl-protected biglycosylated azobenzene glycoconjugate **11** (50 mg, 0.05 mmol) was dissolved in anhydrous methanol (2 mL) and a catalytic amount of solid NaOMe was added. The reaction mixture was stirred at room temperature for 5 h. Then, TLC control indicated that the starting material had fully disappeared. It was neutralized with Amberlite IR 120 ion exchange resin and filtered. The filtrate was evaporated to yield **12** as a yellow solid (30.8 mg, 0.047 mmol, 93%). *R_f* 0.31 (CH₂Cl₂ / MeOH, 7:3); [α]_D²² = +31.2 (*c* = 0.91, MeOH); ¹H NMR (600 MHz, DMSO-*d*₆, 300 K, TMS): δ = 8.22 (s, 1H, H-21), 7.85 (d, *J* = 8.9 Hz, 2H, aryl-H), 7.82 (d, *J* = 8.9 Hz, 2H, aryl-H), 7.24 (d, *J* = 9.0 Hz, 2H, aryl-H), 7.22 (d, *J* = 9.1 Hz, 2H, H-15, H-17), 5.50 (d, *J* = 1.6 Hz, 1H, H-1), 5.24 (s, 2H, H-19a, H-19b), 4.63 (d, *J* = 1.5 Hz, 1H, H-1'), 4.59 (dd, *J* = 6.3, 4.2 Hz, 1H, H-22a), 4.56 (dd, *J* = 6.6, 4.0 Hz, 1H, H-22b), 3.96 (ddd, *J* = 10.7, 6.5, 4.1 Hz, 1H, H-23a), 3.86 (dd, *J* = 3.3, 1.9 Hz, 1H, H-2), 3.80 (ddd, *J* = 10.8, 6.5, 4.0 Hz, 1H, H-23b), 3.70 (dd, *J* = 9.2, 3.5 Hz, 1H, H-3), 3.56-3.36 (m, 9H, H-6'a, H-6a, H-2', H-4', H-6'b, H-6b, H-4, H-3', H-5'), 3.14 (dd, *J* = 11.1, 4.6 Hz, 1H, H-5) ppm; ¹³C NMR (150 MHz, DMSO-*d*₆, 300 K, TMS): δ = 160.8 (C-16), 158.8 (C-7), 147.4 (C-10), 146.8 (C-13), 142.7 (C-20), 125.5 (C-21), 124.7 (C-9, C-11), 124.4 (C-14, C-18), 117.5 (C-8, C-12), 115.8 (C-15, C-17), 100.2 (C-1'), 99.0 (C-1), 75.5 (C-5'), 74.4 (C-5), 71.03 (C-3'), 70.84 (C-3), 70.3 (C-2'), 70.2 (C-2), 67.0

(C-4'), 66.9 (C-4), 65.3 (C-23), 61.8 (C-19), 61.4 (C-6'), 61.2 (C-6), 49.9 (C-22) ppm; UV/Vis (DMSO) $\lambda_{\max} = 360$ nm; $\epsilon = 25562 \pm 865$ L x mol⁻¹ x cm⁻¹; MALDI-TOF MS calcd for C₂₉H₃₇N₅O₁₃: m/z 686.283 [M+Na]⁺; found: m/z 686.131 [M+Na]⁺.

After irradiation: Z-12:

¹H NMR (600 MHz, DMSO-*d*₆, 300 K, TMS): $\delta = 8.16$ (s, 1H, H-21), 7.02 (d, $J = 8.6$ Hz, 2H, H-8, H-12), 6.97 (d, $J = 8.8$ Hz, 2H, H-16, H-17), 6.85 (d, $J = 8.8$ Hz, 2H, H-14, H-18), 6.82 (d, $J = 8.7$ Hz, 2H, H-9, H-11), 5.35 (bs, 1H, H-1), 5.09 (2, 2H, H-19a, H-19b), 4.61 (bs, 1H, H-1'), 4.57 (dd, $J = 8.9, 4.1$ Hz, 1H, H-22a), 4.53 (dd, $J = 9.8, 4.2$ Hz, 1H, H-22b), 3.93 (dd, $J = 10.2, 4.4$ Hz, 1H, H-23a), 3.79 (m, 2H, H-2, H-23b), 3.57-3.34 (m, 10H, H-2', H-3, H-4', H-6'a, H-6a, H-4, H-3', H-5', H-6'b, H-6b), 3.12 (m_c, 1H, H-5) ppm; ¹³C NMR (125 MHz, DMSO-*d*₆, 300 K, TMS): $\delta = 157.6$ (C-16), 155.6 (C-7), 148.2 (C-10), 147.2 (C-13), 142.7 (C-20), 125.5 (C-21), 122.8 (C-9, C-11), 122.2 (C-14, C-18), 117.5 (C-8, C-12), 115.3 (C-15, C-17), 100.2 (C-1'), 99.2 (C-1), 75.3 (C-5'), 74.4 (C-5), 71.0 (C-3'), 70.8 (C-3), 70.3 (C-2'), 70.2 (C-2), 67.0 (C-4'), 66.9 (C-4), 65.3 (C-23), 61.6 (C-19), 61.4 (C-6'), 61.2 (C-6), 49.9 (C-22) ppm; UV/Vis (DMSO) $\lambda_{\max} = 448$ nm; nm $\epsilon = 2316 \pm 61$ L x mol⁻¹ x cm⁻¹.

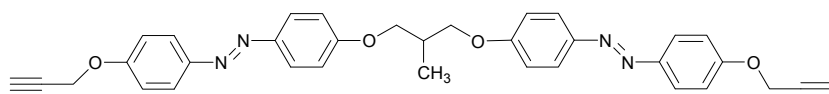
1,3-Dihydroxy-2-methyl-1,3-di-*O*-tosyl-propane **14**⁵



According to the literature, a mixture of the diol **13** (1.0 g, 0.011 mmol, 1.0 equiv.) in pyridine (20 mL) was treated with tosyl chloride (6.30 g, 0.033 mmol, 3 equiv.) and the reaction mixture was stirred at room temperature for 14 h. Then, TLC showed complete consumption of the starting material. Aqueous 6N HCl (100 mL) was added and the aqueous phase extracted with ethyl acetate (2 x 50 mL). The combined organic layers were washed with water and brine and dried over MgSO₄. It was filtered and concentrated under reduced pressure. Purification of the crude product by column chromatography on silica gel (cyclohexane/ethylacetate, 4:1) gave the ditosylate **14** as a white solid (3.67 g, 0.01 mmol, 83%). R_f 0.27 (cyclohexane/ethyl acetate); m.p.: 71 °C; ¹H NMR (200 MHz, CDCl₃, 300 K, TMS): $\delta = 7.74$ (d, $J = 8.4$ Hz, 4H, aryl-H), 7.34 (d, $J = 8.5$ Hz, 4H, aryl-H), 3.90 (dd, $J = 5.7$ Hz, 1.5 Hz, 4H, 2 CH₂-O), 2.45 (s, 6H, Ts-

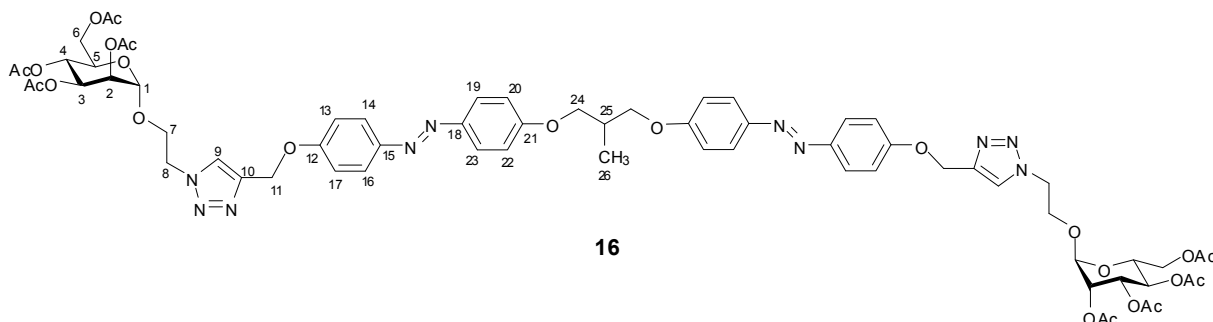
CH₃), 2.14 (tt, *J* = 14.4 Hz, 7.1 Hz, 1H, CH(CH₃)), 0.91 (d, *J* = 6.9 Hz, 3H, CH(CH₃)) ppm; ¹³C NMR (125 MHz, CDCl₃, 300 K, TMS): δ = 145.1 (C_q, aryl-C), 132.6 (C_q, aryl-C), 129.9, 127.8 (aryl-C), 70.3 (2 CH₂), 33.0 (CH), 21.6 (Ts-CH₃), 12.9 (CH-CH₃) ppm; ESI MS calcd for C₁₈H₂₂O₆S₂: *m/z* 421.085 [M+Na]⁺; found: *m/z* 421.077 [M+Na]⁺; IR (ATR) 2973, 1597, 1355, 1174, 1095, 936, 848, 667 cm⁻¹.

Bivalent azobenzene dialkyne **15**:



A solution of the alcohol **2** (82.3 mg, 0.327 mmol, 2.6 equiv.) and K₂CO₃ (52 mg, 0.377 mmol, 3 equiv.) in DMF (2 mL) was stirred at room temperature for ~30 min, then added the ditosylate **14** (50 mg, 0.125 mmol, 1.0 equiv.) was added. the reaction mixture was heated at 100 °C for 16 h until TLC showed complete absence of **14**. After the solvent was evaporated under reduced pressure, the residue was dissolved in ethyl acetate (30 mL) and washed with water (2 x 25 mL). The organic phase was dried over MgSO₄, its was filtered and concentrated under reduced pressure. Purification by column chromatography on silica gel (cyclohexane/ethylacetate, 4:1) gave product **15** as a pale yellow liquid (52 mg, 0.09 mmol, 74%); m.p.: 164-166 °C; ¹H NMR (500 MHz, CDCl₃, 300 K, TMS): δ = 7.89 (d, *J* = 9.0 Hz, 4H), 7.88 (d, *J* = 8.9 Hz, 4H), 7.09 (d, *J* = 9.1 Hz, 4H), 7.03 (d, *J* = 9.0 Hz, 4H), 4.77 (d, *J* = 2.4 Hz, 4H), 4.15 (dd, *J* = 9.2 Hz, 6.2 Hz, 2H), 4.09 (dd, *J* = 9.2 Hz, 5.8 Hz, 2H), 2.56 (t, *J* = 2.4 Hz, 2H), 2.54-2.53 (m, 1H), 1.25 (d, *J* = 6.9 Hz, 3H) ppm; ¹³C NMR (125 MHz, CDCl₃, 300 K, TMS): δ = 161.1 (C_q, aryl-C), 159.4 (C_q, aryl-C), 147.6 (C_q, aryl-C), 147.1 (C_q, aryl-C), 124.5 (aryl-C), 124.3 (aryl-C), 115.1 (aryl-C), 114.7 (aryl-C), 78.2 (H-C≡C-CH₂), 75.9, (H-C≡C-CH₂) 69.9 (2 CH₂), 56.0 (H-C≡C-CH₂), 33.8 (HC-CH₃), 14.1 (HC-CH₃) ppm; ESI MS calcd for C₃₄H₃₀N₄O₄: *m/z* 559.226 [M+Na]⁺; found: *m/z* 559.241 [M+Na]⁺; IR (ATR) 3275, 2916, 1596, 1579, 1495, 1232, 1146, 1013, 841, 666 cm⁻¹.

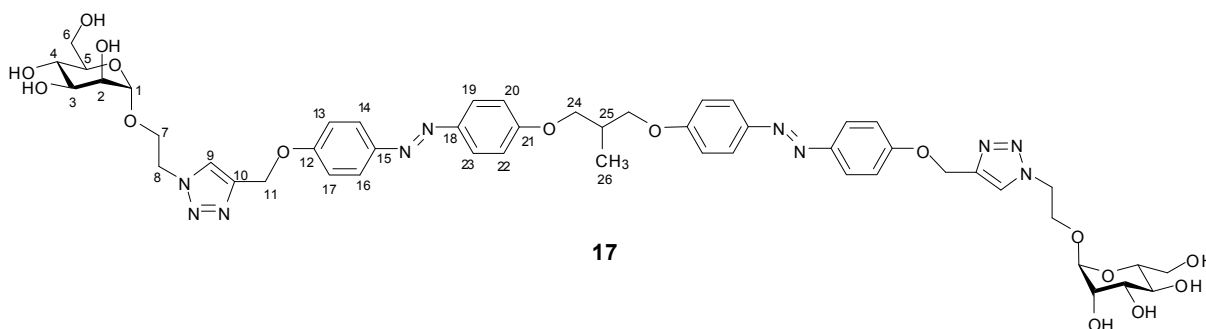
Click reaction: Acetylated bivalent azobenzene glycoconjugate **16 (Man- α z o- α z o-Man [OAc]₈):**



To a mixture of the dialkyne **15** (50 mg, 0.089 mmol, 1.0 equiv.), the mannoside **4** (89.7 mg, 0.215 mmol, 2.4 equiv.). CuSO₄ x 5H₂O (6 mg) and Cu powder (60 mg) was added to a mixture of *tert*-butanol and water (1:1, 5 mL). The reaction mixture was stirred at 70 °C for 48 h. Then, TLC showed complete absence of **15**. The reaction mixture was diluted with ethyl acetate (30 mL), Cu was removed by filtration using celite, and the filtrate was dried over MgSO₄. It was filtered and the filtrate concentrated under reduced pressure. Purification of crude product by column chromatography on silica gel (3% MeOH in CH₂Cl₂) gave the required product **16** as a pale yellow solid (101 mg, 0.01 mmol, 81%); R_f: 0.28 (3% MeOH in Dichloromethane); $[\alpha]_D^{22} = +21.1$ (c = 0.94, CH₂Cl₂); m.p. 85 °C (decompos.); ¹H NMR (600 MHz, CDCl₃, 300 K, TMS): δ = 7.88-7.86 (m, 8H, 2 H-14, 2 H-16, 2 H-19, 2 H-23), 7.79 (s, 2H, 2 H-9), 7.11 (d, *J* = 9.0 Hz, 4H, 2 H-13, 2 H-17), 7.02 (d, *J* = 9.0 Hz, 4H, 2 H-20, 2 H-22), 5.29 (bs, 4H, 2 H-11), 5.24- 5.23 (m, 4H, 2 H-4, 2 H-3), 5.20 (dd, *J* = 2.9, 1.6 Hz, 2H, 2 H-2), 4.79 (d, *J* = 1.4 Hz, 2H, 2 H-1), 4.62 (t, *J* = 5.2 Hz, 4H, 2 H-8), 4.19 (dd, *J* = 12.3, 5.3 Hz, 2H, 2 H-6a), 4.14 (dd, *J* = 9.6, 5.9 Hz, 4H, 2 H-24a, 2 H-7a), 4.07 (dd, *J* = 9.2, 5.6 Hz, 2H, 2 H-24b), 4.04 (dd, *J* = 12.3, 2.3 Hz, 2H, 2 H-6b), 3.90-3.87 (m, 2H, 2 H-7b), 3.53 (ddd, *J* = 9.5, 5.2, 2.2 Hz, 2H, 2 H-5), 2.54 (tt, *J* = 12.5, 6.3 Hz, 1H, H-25), 2.14, 2.09, 2.00, 1.98 (s, 3H, C(O)CH₃ x 2), 1.24 (d, *J* = 6.92 Hz, 3H, H-26) ppm; ¹³C NMR (150 MHz, CDCl₃, 300 K, TMS): δ = 170.6, 169.9, 169.9, 169.6 (2 C=OCH₃), 161.1 (2 C-21), 160.2 (2 C-12), 147.4 (2 C-15), 147.0 (2 C-18), 144.0 (2 C-10), 124.4 (2 C-14, 2 C-16, 2 C-19, 2 C-23), 124.1 (2 C-9), 115.0 (2 C-13, 2 C-17) 114.7 (2 C-20, 2 C-22), 97.4 (2 C-1), 69.8 (2 C-24), 69.4 (2 C-5), 69.2 (2 C-2), 68.8 (2 C-3), 66.2 (2 C-7), 65.6 (2 C-4), 62.2 (2 C-6), 62.1 (2 C-11), 49.8 (2 C-8), 33.7 (C-25), 20.8, 20.7, 20.7, 20.6 (2 COCH₃), 14.1 (C-26) ppm; ESI MS calcd for C₆₆H₇₆N₁₀O₂₄: *m/z* 1393.503

$[M+1]^+$; found: m/z 1393.550 $[M+1]^+$; IR (ATR) 2928, 1742, 1597, 1498, 1367, 1215, 1041, 840, 553 cm^{-1} .

Deprotection: Bivalent azobenzene glycoconjugate 17 (Man- α -z-o-a-z-o-Man):

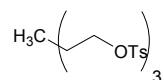


The acetyl-protected divalent azobenzene glycoconjugate **16** (90 mg, 0.06 mmol, 1.0 equiv.) was dissolved in anhydrous methanol (3 mL) and a catalytic amount of solid NaOMe was added. The reaction mixture was stirred at room temperature overnight. TLC control ($\text{CH}_2\text{Cl}_2/\text{MeOH}$, 3:7) indicated that the starting material had fully disappeared. It was neutralized with Amberlite IR 120 ion exchange resin and filtered. The filtrate was evaporated to yield **17** as a yellow solid (62 mg, 0.058 mmol, 91%). R_f 0.24 ($\text{CH}_2\text{Cl}_2 / \text{MeOH}$, 3:7); $[\alpha]_D^{22} = +17.9$ ($c = 0.43$, DMSO); m.p. 148-150 $^\circ\text{C}$; ^1H NMR (600 MHz, $\text{DMSO}-d_6$, 300 K, TMS): $\delta = 8.22$ (s, 2H, 2 H-9), 7.83 (m, 8H, 2 H-14, 2 H-16, 2 H-19, 2 H-23'), 7.21 (d, $J = 8.8$ Hz, 4H, 2 H-13, 2 H-17), 7.14 (d, $J = 8.8$ Hz, 4H, 2 H-20, 2 H-22), 5.23 (s, 4H, 2 H-11), 4.62 (bs, 2H, 2 H-1), 4.60 (dd, $J = 8.9, 4.8$ Hz, 2H, 2 H-8), 4.55 (dd, $J = 9.8, 3.7$ Hz, 2H, 2 H-8a), 4.12 (td, $J = 14.9, 9.3$ Hz, 4H, 2 H-24), 3.91-3.94 (m, 2H, 2 H-7a), 3.82-3.78 (m, 2H, 2 H-7b), 3.64-3.54 (m, 4H, 2 H-6a, 2 H-2), 3.42-3.34 (m, 6H, 2 H-3, 2 H-6b, 2 H-4), 3.15-3.12 (m, 2H, 2 H-5), 2.47-2.44 (m, 1H, H-25), 1.15 (d, $J = 6.7$ Hz, 3H, H-26) ppm; ^{13}C NMR (150 MHz, $\text{DMSO}-d_6$, 300 K, TMS): $\delta = 161.2$ (2 C-21), 160.5 (2 C-12), 146.6 (2 C-15), 146.5 (2 C-18), 142.5 (2 C-10), 125.3 (2 C-9), 124.5 (2 C-13, 2 C-17), 124.4 (2 C-19, 2 C-23), 115.6 (2 C-14, 2 C-16), 115.4 (2 C-20, 2 C-22), 100.0 (2 C-1), 74.2 (2 C-5), 70.1 (2 C-3), 70.2 (2 C-2), 69.9 (2 C-24), 66.8 (2 C-4), 65.2 (2 C-7), 61.7 (2 C-11), 61.2 (2 C-6), 49.7 (2 C-8), 33.3 (C-25), 14.0 (C-26) ppm; MALDI-TOF MS calcd for $\text{C}_{50}\text{H}_{60}\text{N}_{10}\text{O}_{16}$: m/z 1079.418 $[M+\text{Na}]^+$; found: m/z 1079.4622 $[M+\text{Na}]^+$; UV/Vis (DMSO) $\lambda_{\text{max}} = 364$ nm; $\epsilon = 29063 \pm 950 \text{ L x mol}^{-1} \text{ x cm}^{-1}$.

After irradiation: Z-17:

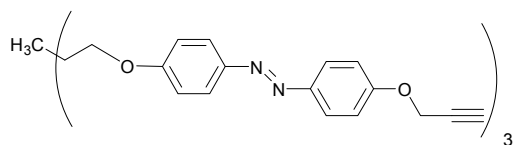
^1H NMR (600 MHz, DMSO- d_6 , 300 K, TMS): δ = 8.16 (s, 2H, 2 H-9), 6.97 (d, J = 8.3 Hz, 4H, 2 H-20, 2 H-22), 6.92-6.83 (m, 12H, 2 H-13, 2 H-17, 2 H-14, 2 H-16, 2 H-19, 2 H-23'), 5.09 (s, 4H, 2 H-11), 4.61 (s, 2H, H-1), 4.58-4.51 (m, 4H, 2 H-8), 3.95-3.90 (m, 6H, 2 H-7a, 2 H-24), 3.79-3.77 (m, 2H, 2 H-7b), 3.59-3.53 (m, 4H, 2 H-6a, 2 H-2'), 3.41-3.35 (m, 6H, 2 H-4, 2 H-6b', 2 H-3), 3.15-3.12 (m, 2H, 2 H-5), 2.31 (dd, J = 12.2, 5.7 Hz, 1H, H-25), 1.05 (d, J = 5.7 Hz, 3H, H-26) ppm; ^{13}C NMR (150 MHz, DMSO- d_6 , 300 K, TMS): δ = 157.9 (2 C-21), 157.3 (2 C-12), 147.2 (2 C-18), 146.9 (2 C-15), 142.5 (2 C-10), 124.4 (2 C-9), 122.6 (2 C-19, 2 C-23'), 122.4 (2 C-14, 2 C-16), 115.1 (2 C-20, 2 C-22), 114.9 (2 C-13, 2 C-17), 100.0 (2 C-1), 74.2 (2 C-5), 70.9 (2 C-3), 70.2 (2 C-2), 69.6 (2 C-24), 66.8 (2 C-4), 65.2 (2 C-7), 61.5 (2 C-11), 61.2 (2 C-6), 49.7 (2 C-8), 33.2 (C-25), 14.1 (C-26) ppm; UV/Vis (DMSO) λ_{max} = 449 nm; ϵ = 2544 ± 77 L x mol $^{-1}$ x cm $^{-1}$.

2,2,2-Tri-[(*O*-tosyl)-2'-hydroxyethyl]ethane **19⁶**



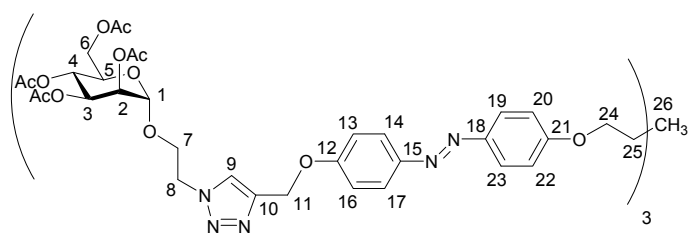
To a solution of the triol **18** (2.0 g, 16.66 mmol, 1.0 equiv.) in pyridine (20 mL) tosyl chloride (12.6 g, 66.66 mmol, 4 equiv.) was added and the reaction mixture stirred at room temperature for 16 h. Then, TLC showed complete absence of **18**. Aqueous HCl (6N, 200 mL) was added and then it was extracted with ethyl acetate (2 x 100 mL). The combined organic layers were washed with water and brine, and dried over MgSO₄. After filtration, the filtrate was concentrated under reduced pressure to give product **19** as a white solid (10.3 g, 17.69 mmol, quant.). R_f : 0.24 (cyclohexane/ethyl acetate, 7:3); m.p. 132-135 °C; ^1H NMR (500 MHz, CDCl₃, 300 K, TMS): δ = 7.70 (d, J = 8.3 Hz, 6H), 7.35 (d, J = 7.9 Hz, 6H), 3.76 (s, 6H), 2.46 (s, 9H), 0.88 (s, 3H) ppm; ^{13}C NMR (125 MHz, CDCl₃, 300 K, TMS): δ = 145.2 (C_q, aryl-C), 131.9 (C_q, aryl-C), 130.1, 127.9 (aryl-C), 69.8 (3 CH₂), 39.4 (CH₃-C), 21.7 (Ts-CH₃), 14.2 (CH₃-C) ppm; ESI MS calcd for C₂₆H₃₀O₉S₃: m/z 605.105 [M+Na] $^+$; found: m/z 605.013 [M+Na] $^+$; IR (ATR) 1598, 1355, 1174, 1096, 960, 835, 666 cm $^{-1}$.

Trivalent azobenzene trialkyne **20**:



A mixture of the alcohol **2** (156 mg, 0.619 mmol, 3.6 equiv.) and K_2CO_3 (42.6 mg, 0.309 mmol, 1.8 equiv.) in DMF (6 mL) was stirred at room temperature for ~30 min, then the tritosylate **19** (100 mg, 0.172 mmol, 1.0 equiv.) was added and the reaction mixture stirred at 100 °C for 16 h. Then, TLC showed complete consumption of **19**. After the solvent was evaporated under reduced pressure, the residue was dissolved in ethyl acetate (30 mL) and washed with water (2 x 25 mL). The combined organic phases were dried over $MgSO_4$, it was filtered and the filtrate concentrated under reduced pressure. Purification by column chromatography on silica gel (cyclohexane/ethylacetate, 3:2) gave product **20** as a pale yellow syrup (86.8 mg, 0.110 mmol, 65%). R_f 0.26 (cyclohexane/ethyl acetate, 3:7); 1H NMR (500 MHz, $CDCl_3$, 300 K, TMS): δ = 7.88 (d, J = 9.1 Hz, 6H), 7.87 (d, J = 9.1 Hz, 6H), 7.08 (d, J = 9.1 Hz, 6H), 7.05 (d, J = 9.0 Hz, 6H), 4.76 (s, 6H), 2.56 (t, J = 2.4 Hz, 3H), 1.48 (s, 3H) ppm; ^{13}C NMR (125 MHz, $CDCl_3$, 300 K, TMS): 159.9, 158.4, 146.6, 146.2, 123.4, 123.3, 114.1, 113.8, 77.1, 74.9, 69.3, 55.0, 39.5, 16.3 ppm; IR (ATR) 3288, 2924, 1595, 1580, 1496, 1214, 1145, 1019, 835, 548 cm^{-1} .

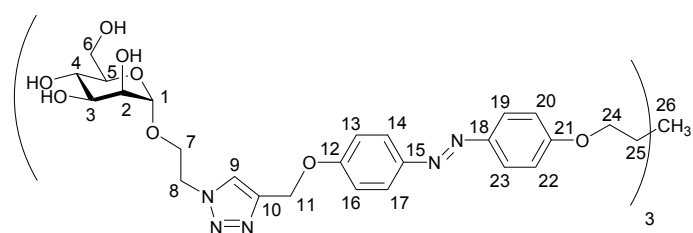
Click reaction: Acetylated trivalent azobenzene glycoconjugate **21** ($[Man-\alpha z o(OAc_{12})]_3$):



To a mixture of the trialkyne **20** (100 mg, 0.128 mmol, 1.0 equiv.), the mannoside **4**² (192 mg, 0.462 mmol, 3.6 equiv.). $CuSO_4 \cdot x H_2O$ (12 mg) and Cu powder (120 mg) was added to a mixture of *tert*-butanol, THF and water (1:1:1, 6 mL). The reaction mixture was refluxed for 16 h until TLC showed absence of starting material **20**. The reaction mixture was diluted with ethyl acetate (30 mL), Cu was removed by filtration using celite, and the filtrate was dried over $MgSO_4$. After filtration it was concentrated under reduced pressure. Purification by column

chromatography on silica gel (2% MeOH in CH₂Cl₂) gave the required product **21** as a pale yellow syrup (209 mg, 0.10 mmol, 79%). *R_f* 0.29 (3% MeOH in CH₂Cl₂); $[\alpha]_D^{22} = +19.7$ (*c* = 1.15, CH₂Cl₂); m.p. 103-106 °C; ¹H NMR (600 MHz, CDCl₃, 300 K, TMS): δ = 7.87 (d, *J* = 8.8 Hz, 12H, 3 H-14, 3 H-16, 3 H-19, 3 H-23), 7.80 (s, 3H, 3 H-9), 7.11 (d, *J* = 9.0 Hz, 6H, 3 H-13, 3 H-17), 7.05 (d, *J* = 9.0 Hz, 6H, 3 H-20, 3 H-22), 5.30 (bs, 6H, 3 H-11a, 3H-11b), 5.25- 5.23 (m, 6H, 3 H-4, 3 H-3), 5.21 (dd, *J* = 2.9, 1.6 Hz, 3H, 3 H-2), 4.80 (d, *J* = 1.4 Hz, 3H, 3 H-1), 4.63 (t, *J* = 5.2 Hz, 6H, 3 H-8a, 3-H-8b), 4.22 (bs, 6H, 3 H-24), 4.21- 4.18 (m, 3H, 3 H-6a), 4.14 (td, *J* = 10.7, 5.4 Hz, 3H, 3 H-7a), 4.04 (dd, *J* = 12.3, 2.3 Hz, 3H, 3 H-6b), 3.89 (td, *J* = 10.7, 10.1, 3H, 3 H-7b), 3.55-3.52 (m, 3H, 3 H-5), 2.14, 2.09, 1.99, 1.98 (each s, each 9H, 12 C(O)CH₃), 1.41 (s, 3H, 3 H-26) ppm; ¹³C NMR (150 MHz, CDCl₃, 300 K, TMS): δ = 170.6, 169.9, 169.9, 169.6 (12 C=O), 160.9 (3 C-21), 160.2 (3 C-12), 147.4 (3 C-15), 147.2 (3 C-18), 144.0 (3 C-10), 124.4 (3 C-14, 3 C-16, 3 C-19, 3 C-23), 124.1 (3 C-9), 115.0 (3 C-13, 3 C-17), 114.8 (3 C-20, 3 C-22), 97.4 (3 C-1), 70.3 (3 C-24), 69.4 (3 C-5), 68.8 (3 C-2), 68.8 (3 C-3), 66.2 (3 C-7), 65.6 (3 C-4), 62.2 (3 C-6), 62.1 (3 C-11), 49.8 (3 C-8), 40.5 (C-25), 20.8, 20.7, 20.7, 20.6 (12 COCH₃), 17.3 (C-26) ppm; MALDI-TOF MS calcd for C₉₈H₁₁₁N₁₅O₃₆: *m/z* 2074.731 [M+1]⁺; found: *m/z* 2074.391 [M+1]⁺; IR (ATR) 2926, 1742, 1596, 1498, 1367, 1215, 1042, 840, 553 cm⁻¹.

Deprotection: Trivalent azobenzene glycoconjugate **22** ([Man-*α*z o]₃):



The acetyl-protected trivalent azobenzene glycoconjugate **21** (100 mg, 0.048 mmol) was dissolved in anhydrous methanol (3 mL) and a catalytic amount of solid NaOMe was added. The reaction mixture was stirred at room temperature for 16 h until TLC control (CH₂Cl₂ / MeOH, 3:7) indicated that the starting material had fully disappeared. It was neutralized with Amberlite IR 120 ion exchange resin and filtered. The filtrate was evaporated to yield **22** as a yellow solid (78 mg, 0.049 mmol, quantitative). *R_f* 0.21 (CH₂Cl₂ / MeOH, 3:7); $[\alpha]_D^{22} = +13.7$ (*c* = 0.92,

DMSO); m.p. 166-167 °C; ¹H NMR (600 MHz, DMSO-*d*₆, 300 K, TMS): δ = 8.21 (s, 3H, 3 H-9), 7.83-7.81 (m, 12H, 3 H-14, 3 H-16, 3 H-19, 3 H-23), 7.20 (d, *J* = 8.6 Hz, 6H, 3 H-13, 3 H-17), 7.17 (d, *J* = 9.0 Hz, 6H, 3 H-20, 3 H-22), 5.22 (s, 6H, 3 H-11a, 3 H-11b), 4.63 (s, 3 H-1), 4.59-4.53 (m, 6H, 3 H-8a, 3 H-8b), 4.22 (bs, 6H, 3 H-24a, 3 H-24b), 3.97-3.94 (m, 3H, 3 H-7a), 3.81-3.79 (m, 3H, 3 H-7b), 3.64-3.54 (m, 6H, 3 H-6a, 3 H-2), 3.42 (dd, *J* = 11.6, 6.2 Hz, 3H, 3 H-6b), 3.39-3.34 (m, 6H, 3 H-3, 3 H-4), 3.14-3.13 (m, 3H, 3 H-5), 1.32 (s, 3H, 3 H-26) ppm; ¹³C NMR (150 MHz, DMSO-*d*₆, 300 K, TMS): δ = 161.2 (3 C-21), 160.6 (3 C-12), 146.6 (3 C-15, 3 C-18), 142.7 (3 C-10), 125.4 (3 C-9), 124.5 (3 C-14, 3 C-16, 3 C-19, 3 C-23), 115.6 (3 C-20, 3 C-22), 115.5 (3 C-13, 3 C-17), 110.0 (3 C-1), 74.2 (3 C-5), 70.9 (3 C-3), 70.2 (3 C-2), 70.1 (3 C-24), 66.9 (3 C-4), 65.2 (3 C-7), 61.7 (3 C-11), 61.3 (3 C-6), 49.8 (3 C-8), 40.4 (C-25), 17.2 (C-26) ppm; MALDI-TOF MS calcd for C₇₄H₈₇N₁₅O₂₄: *m/z* 1592.6048 [M+Na]⁺; found: *m/z* 1592.6006 [M+Na]⁺; UV/Vis (DMSO) λ_{max} = 364 nm; ε = 29426 ± 958 L x mol⁻¹ x cm⁻¹.

After irradiation: Z-22:

¹H NMR (600 MHz, DMSO-*d*₆, 300 K, TMS): δ = 8.15 (s, 3H, 3 H-9), 6.96 (d, *J* = 8.2 Hz, 6H, 3 H-14, 3 H-16), 6.88 (d, *J* = 8.5 Hz, 6H, 3 H-20, 3 H-22), 6.83-6.81 (m, 12H, 3 H-13, 3 H-17, 3 H-19, 3 H-23), 5.08 (s, 6H, 3 H-11a, 3 H-11b), 4.61 (s, 3H, 3 H-1), 4.59-4.53 (m, 6H, 3 H-8a, 3 H-8b), 4.23 (bs, 6H, 3 H-24a, 3 H-24b), 3.95 (dd, *J* = 10.6, 6.0 Hz, 3H, 3 H-7a), 3.80 (dd, *J* = 10.8, 6.5 Hz, 3H, 3 H-7b), 3.69-3.53 (m, 6H, 3 H-6a, 3 H-2), 3.41 (dd, *J* = 11.8, 5.8 Hz, 3H, 3 H-6b), 3.39-3.34 (m, 6H, 3 H-3, 3 H-4), 3.14-3.12 (m, 3H, 3 H-5), 1.16 (s, 3H, H-26) ppm; ¹³C NMR (150 MHz, DMSO-*d*₆, 300 K, TMS): δ = 157.3 (3 C-21, 3 C-12), 147.2 (3 C-15), 147.0 (3 C-18), 142.6 (3 C-10), 125.4 (3 C-9), 122.6 (3 C-13, 3 C-17), 122.4 (3 C-19, 3 C-23), 115.1 (3 C-14, 3 C-16), 115.0 (3 C-20, 3 C-22), 110.0 (3 C-1), 74.2 (3 C-5), 70.9 (3 C-3), 70.2 (3 C-2), 70.0 (3 C-24), 66.9 (3 C-4), 65.2 (3 C-7), 61.7 (3 C-11), 61.3 (3 C-6), 49.8 (3 C-8), 40.4 (C-25), 17.2 (C-26) ppm; UV/Vis (DMSO): λ_{max} = 449 nm; ε = 2749 ± 101 L x mol⁻¹ x cm⁻¹.

3. Photochemistry of azobenzene glycoconjugates

Half life determination: $E \rightarrow Z$ photoisomerisation was effected using a high pressure mercury lamp UV-P 250C from Panacol-Elosol (50 μM solution, 30 min at 365 nm). The bandpass filters were obtained from Laser components. All photoisomerization and relaxation experiments were performed in DMSO. Upon irradiation of azobenzene glycosides in the ground state (GS) at 365 nm, the absorption spectra showed an increase in the absorbance in the $n\text{-}\pi^*$ transition and simultaneous decrease in the $\pi\text{-}\pi^*$ transition, as expected, indicating the generation of the respective Z isomer. The $E:Z$ ratios in the ground state (GS) as well as in the photostationary state (PSS) were determined by integration of the respective signals in the ^1H NMR spectra.

To make sure that in case of the di- and trivalent azobenzene glycoconjugates **17** and **22** PSS was reached after irradiation for 30 min, $E:Z$ ratios were also determined after 60 and 90 min of irradiation, respectively: no significant change was observed in comparison to 30 min irradiation time.

The kinetics of the $Z \rightarrow E$ relaxation process were determined by UV-Vis spectroscopy in the dark employing 50 μM solutions in DMSO at 18 $^\circ\text{C}$. For determination of the rate constants, a graph of $\ln(A_\infty - A_t)$ was plotted as a function of time; where A_∞ is the absorbance of $\pi\pi^*$ transition at infinitive time and A_t is the absorbance at time t after start of the relaxation process. The negative slope k of the linear plot is the rate constant of the $Z \rightarrow E$ relaxation process. The half life $\tau_{1/2}$ was determined as $\tau_{1/2} = \ln 2/k$.

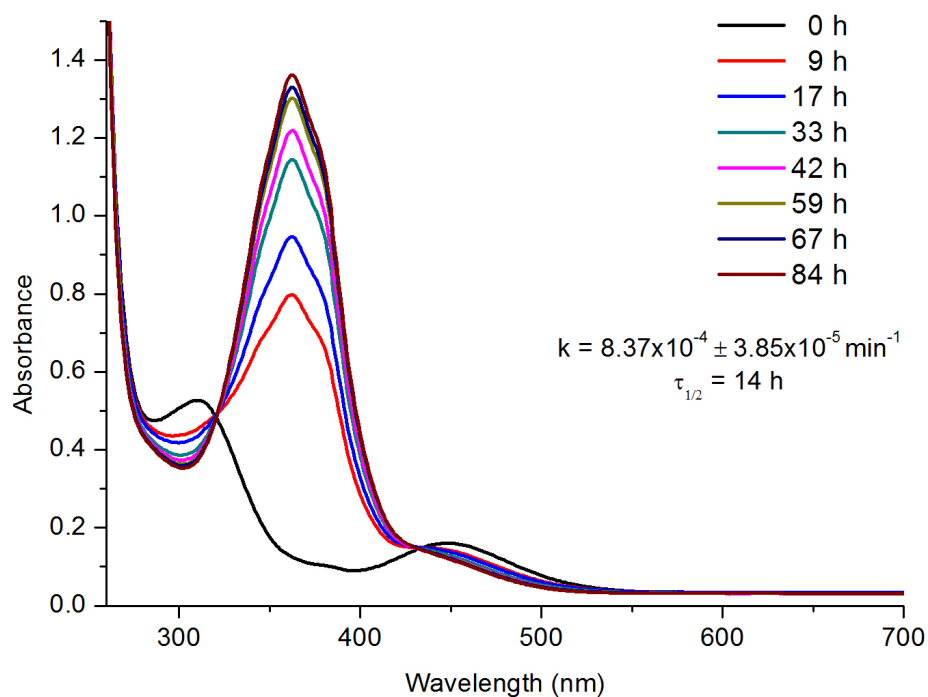


Figure S1. Thermal relaxation of Z-8 to E-8 (Man-a z o-Man) in DMSO; $\tau_{1/2} = 14 \text{ h}$.

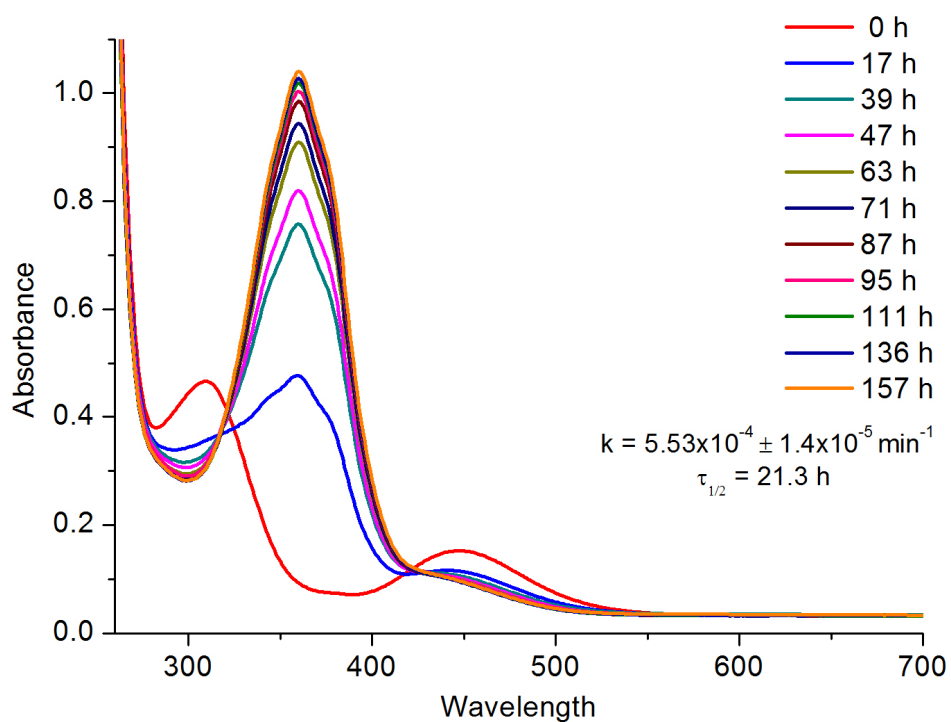


Figure S2. Thermal relaxation of Z-12 to E-12 (Man-a z o-Man) in DMSO; $\tau_{1/2} = 21.3 \text{ h}$.

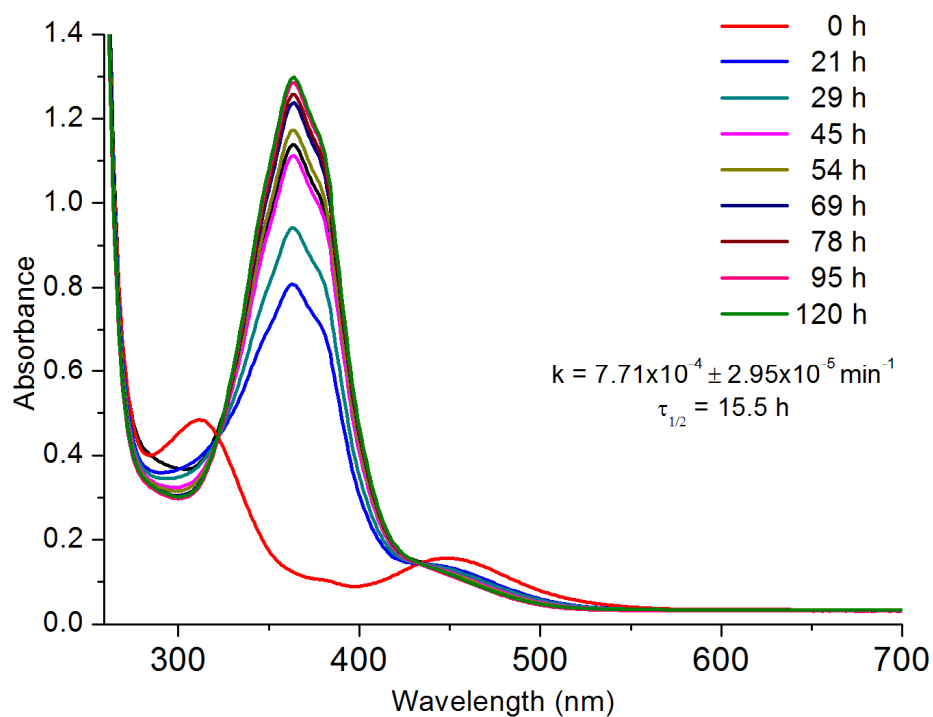


Figure S3. Thermal relaxation of Z-17 to E-17 (Man-a z o-a z o-Man) in DMSO; $\tau_{1/2} = 15.5 \text{ h}$.

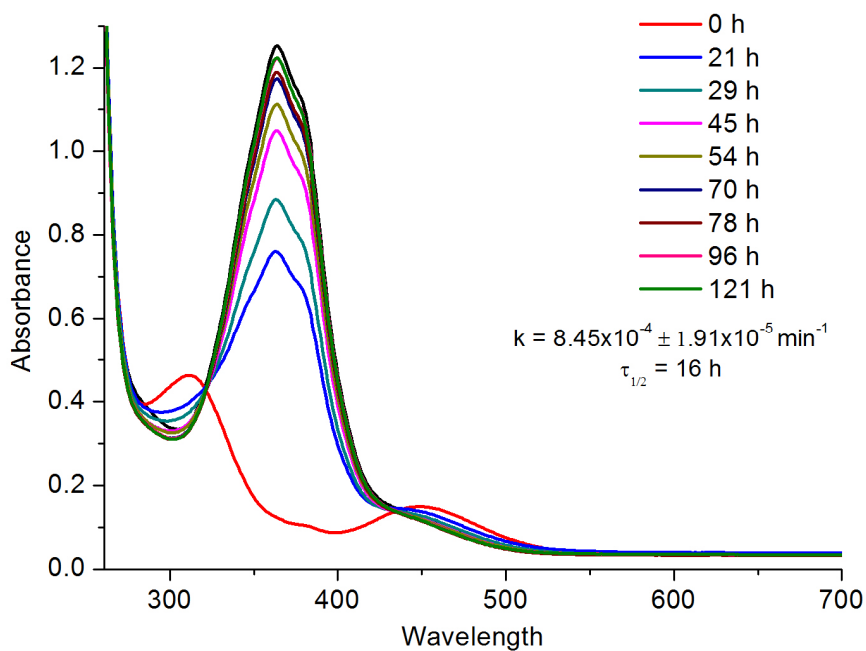


Figure S4. Thermal relaxation of Z-22 to E-22 ([Man-a z o]₃) in DMSO; $\tau_{1/2} = 16 \text{ h}$.

4. NMR Spectra of azobenzene glycoconjugates

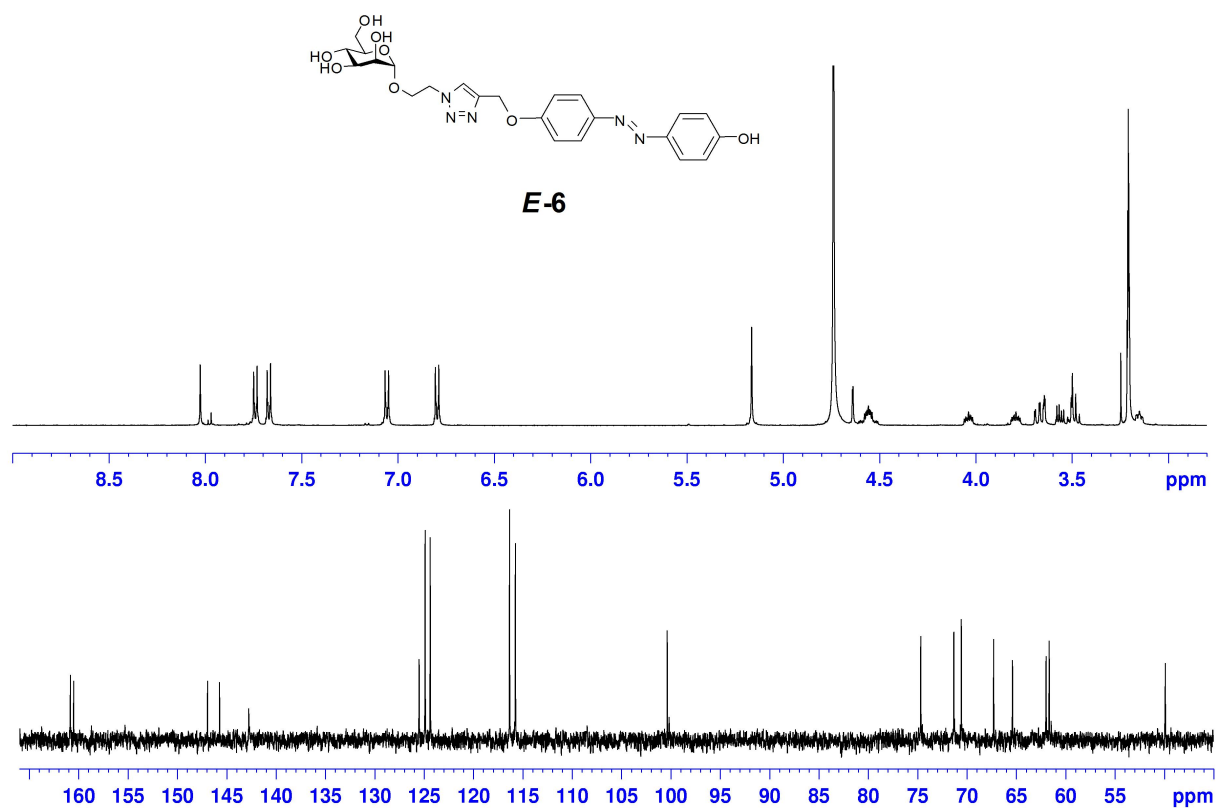


Figure S5. ^1H NMR (500 MHz, CD_3OD) and ^{13}C NMR (125 MHz, CD_3OD) of **E-6** (Man-a z o).

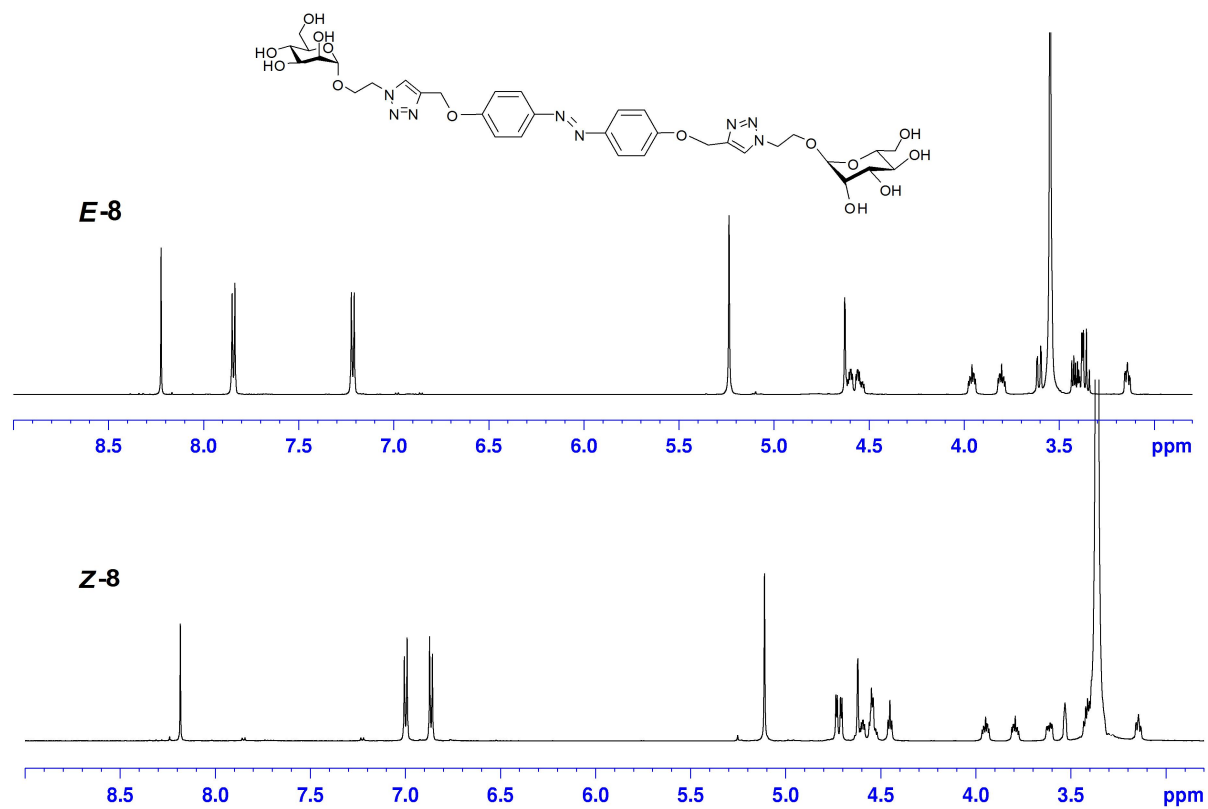


Figure S6. ^1H NMR (600 MHz, DMSO-*d*₆) of *E-8* and *Z-8* (Man- α -z-o-Man).

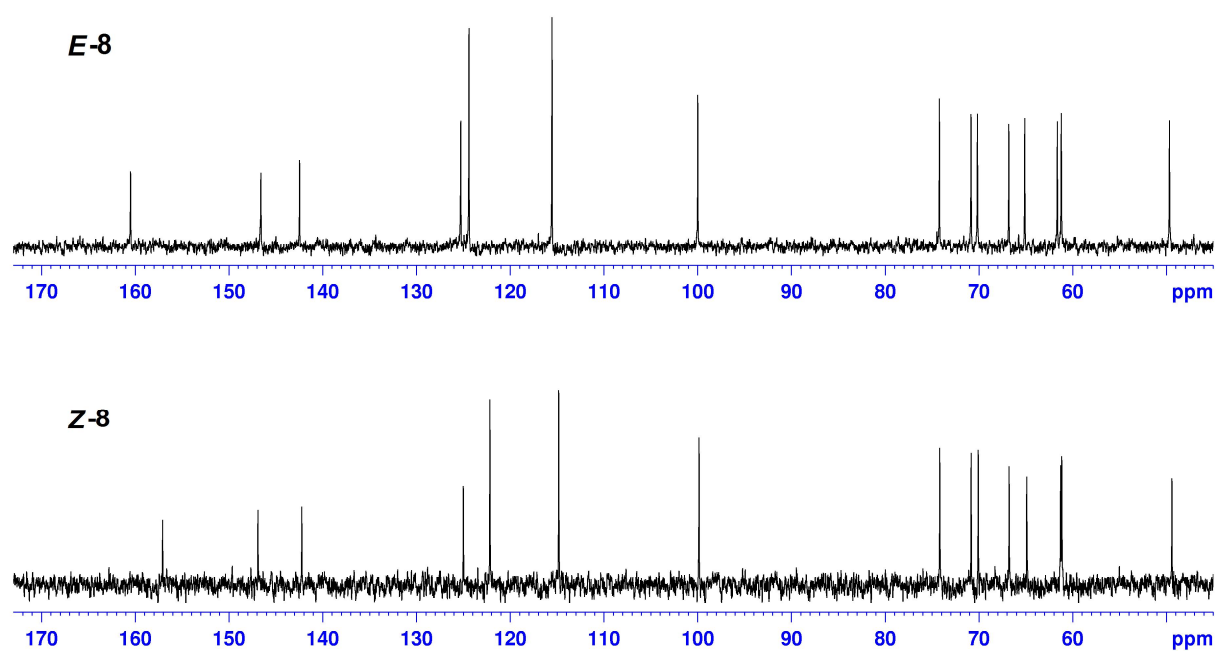


Figure S7. ^{13}C NMR (150 MHz, $\text{DMSO-}d_6$) of *E*-8 and *Z*-8 (Man-a z o-Man).

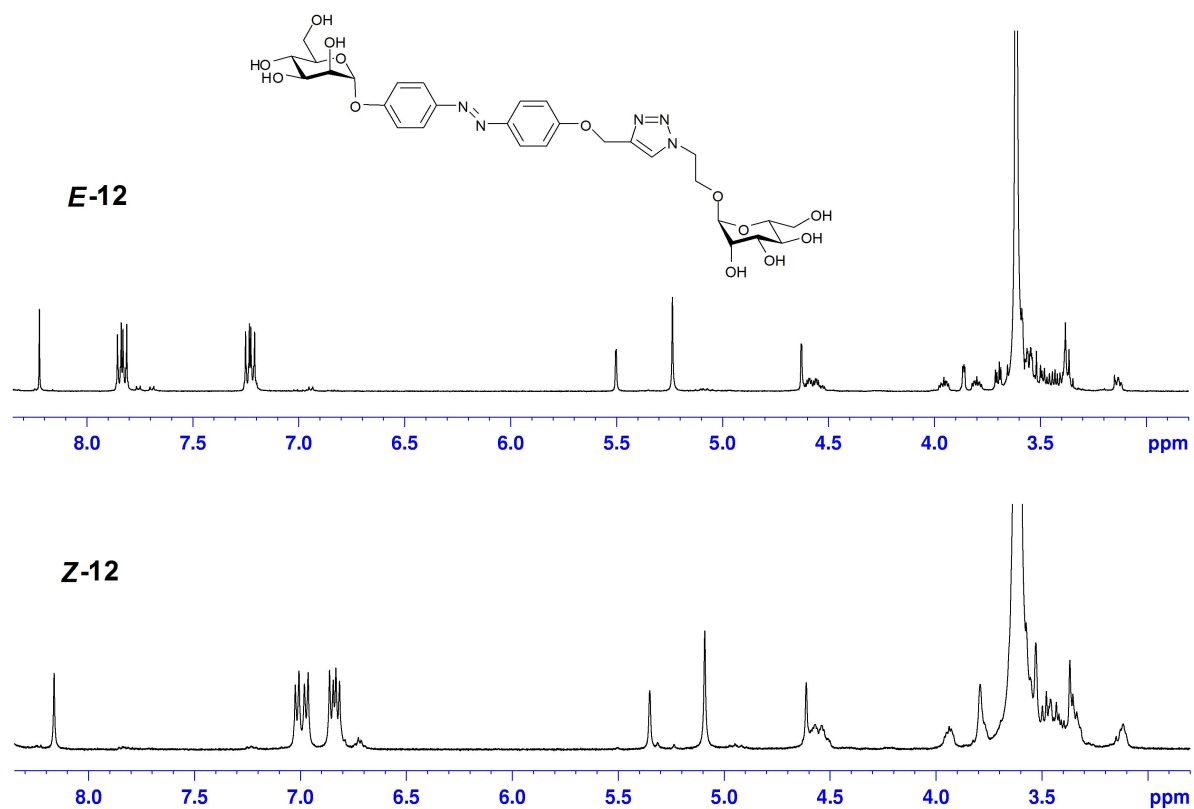


Figure S8. ¹H NMR (600 MHz, DMSO-*d*₆) of *E*-12 and *Z*-12 (Man-a z o-Man).

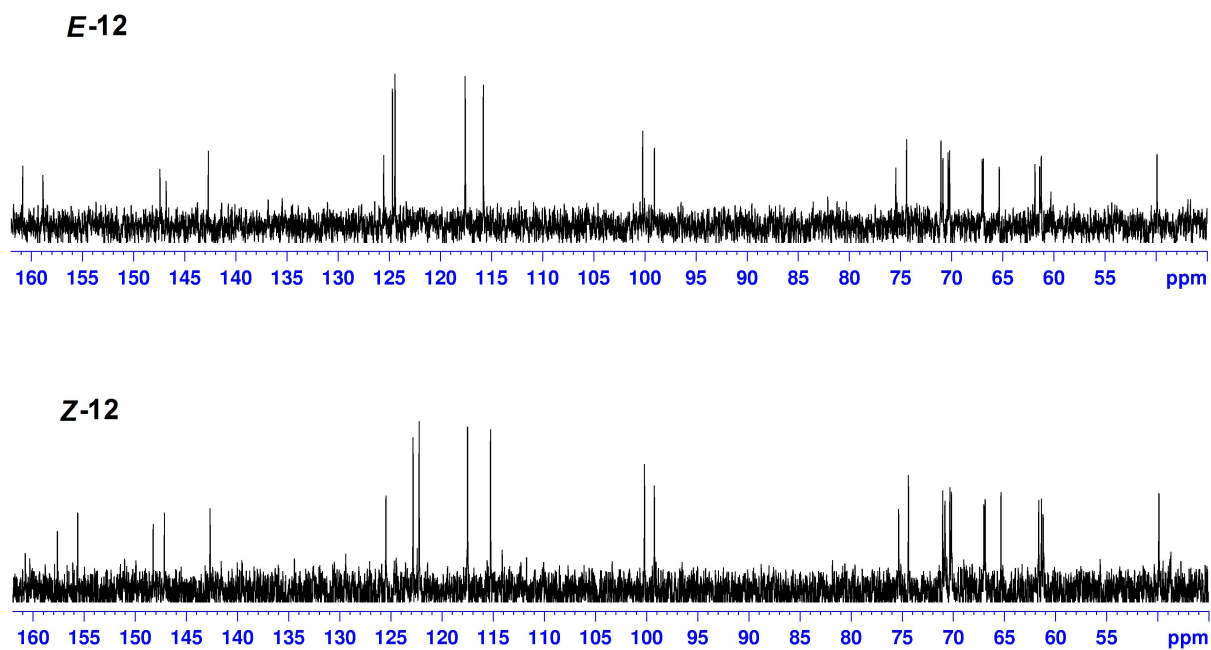


Figure S9. ¹³C NMR (150 MHz, DMSO-*d*₆) of *E*-12 and *Z*-12 (Man-a z o-Man).

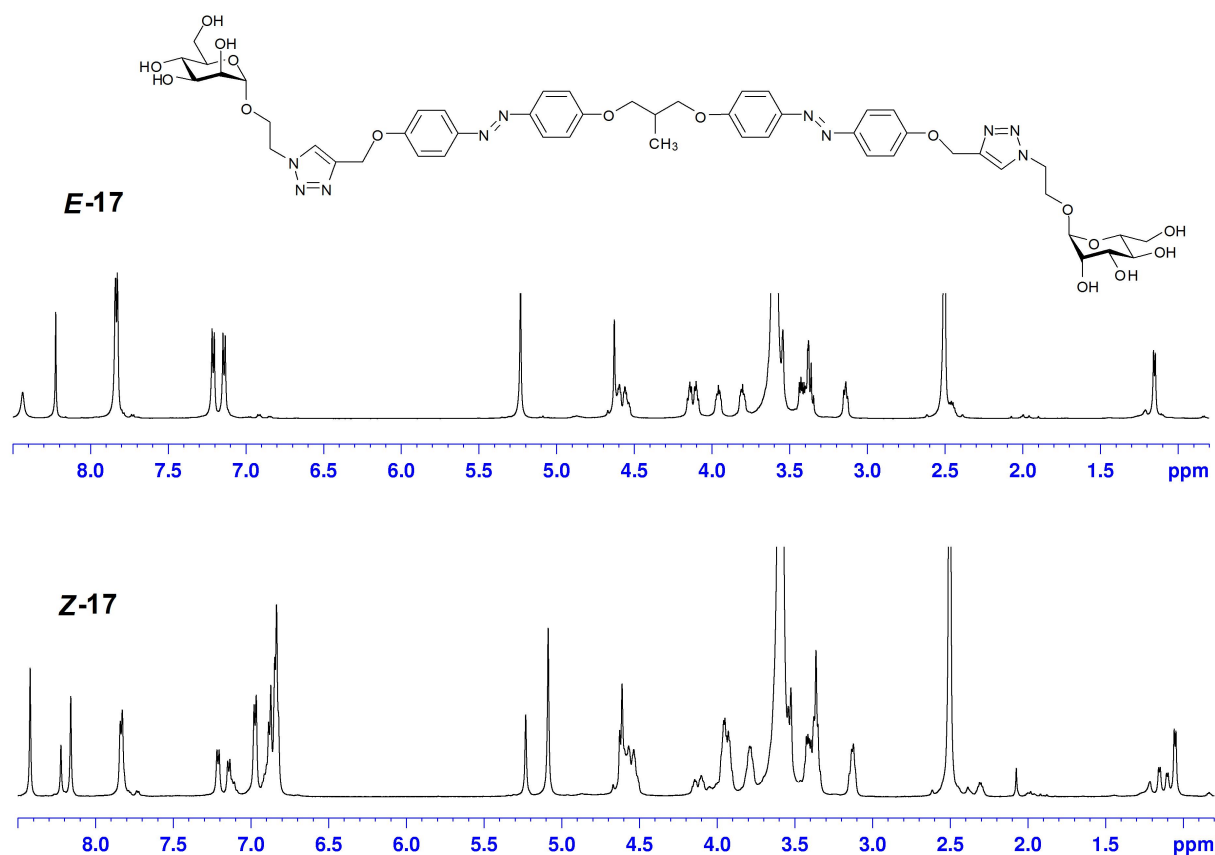


Figure S10. ¹H NMR (600 MHz, DMSO-*d*₆) of *E-17* and *Z-17* (Man-a z o-a z o-Man).

Note, that there is an equilibrium of *EE*, *EZ*, and *ZZ* isoforms after irradiation ('*Z-17*') as can be seen from the three doublets for the protons of the methyl group at the focal point of the molecule at 1.0-1.2 ppm.

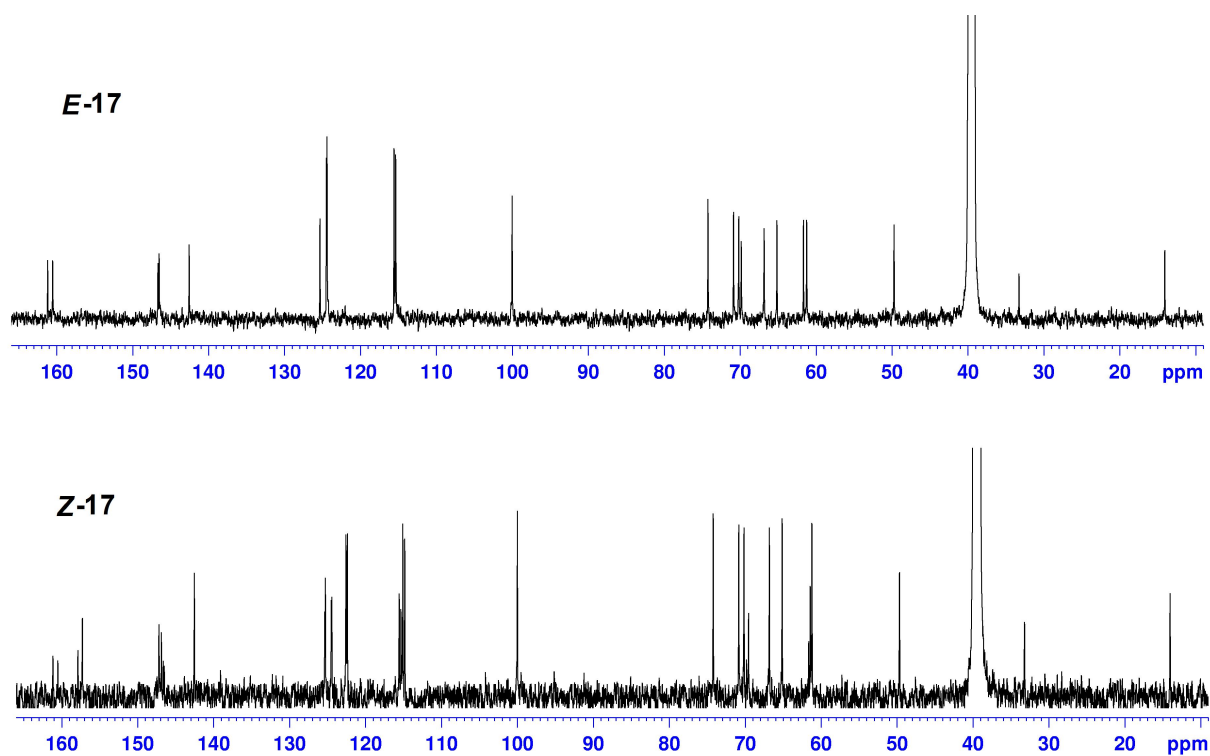


Figure S11. ^{13}C NMR (150 MHz, $\text{DMSO-}d_6$) of *E*-17 and *Z*-17 (Man-a z o-a z o-Man).

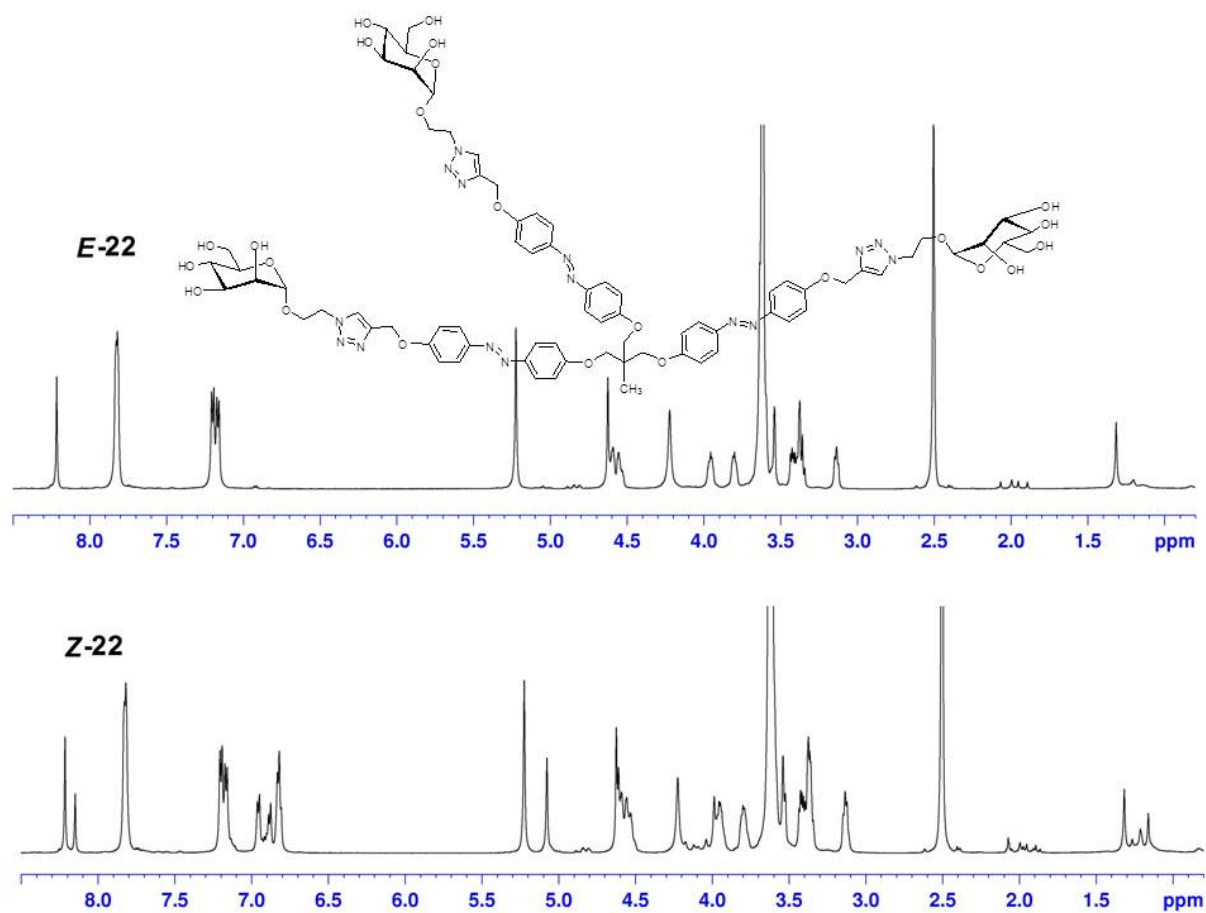


Figure S12. ¹H NMR (600 MHz, DMSO-*d*₆) of *E*-22 and *Z*-22 ([Man-a z o]₃).

Note, that there is an equilibrium of *EEE*, *EEZ*, *EZZ*, and *ZZZ* isoforms after irradiation (*'Z-22'*) as can be seen from the four signals for the protons of the methyl group at the focal point of the molecule. at 1.1-1.4 ppm.

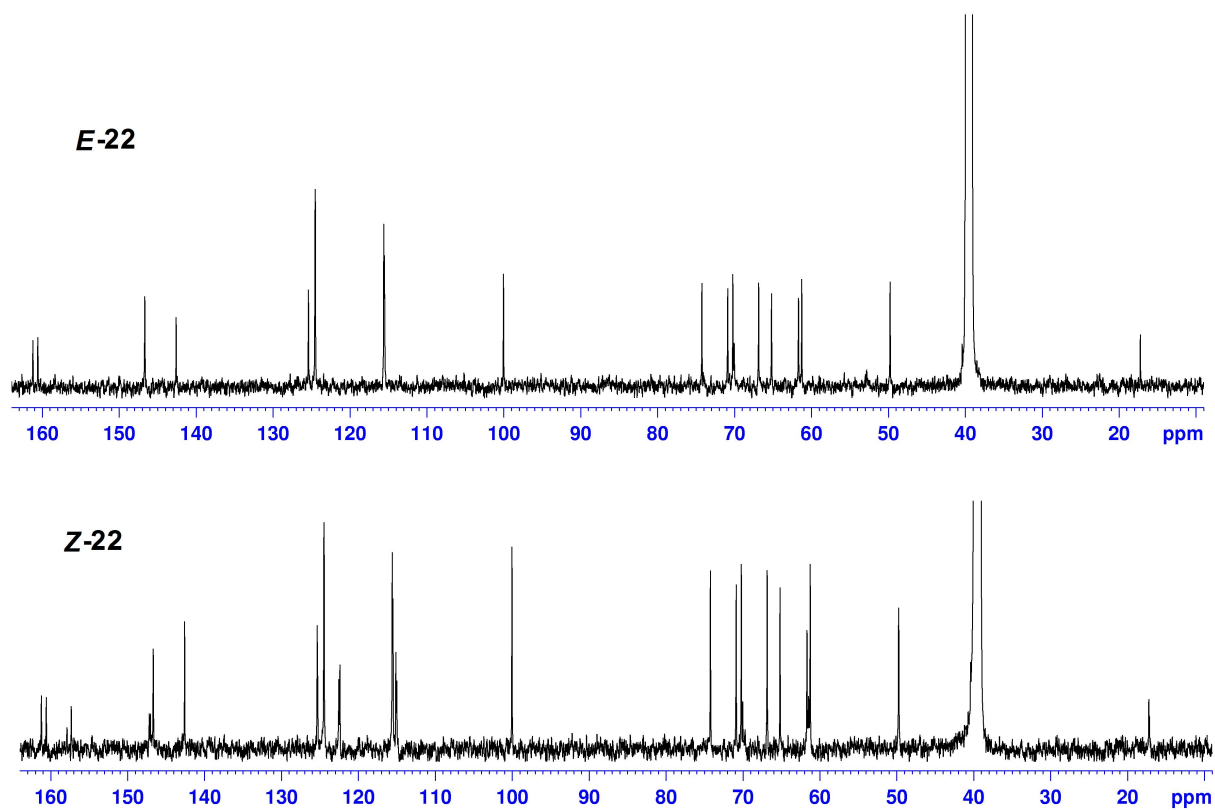


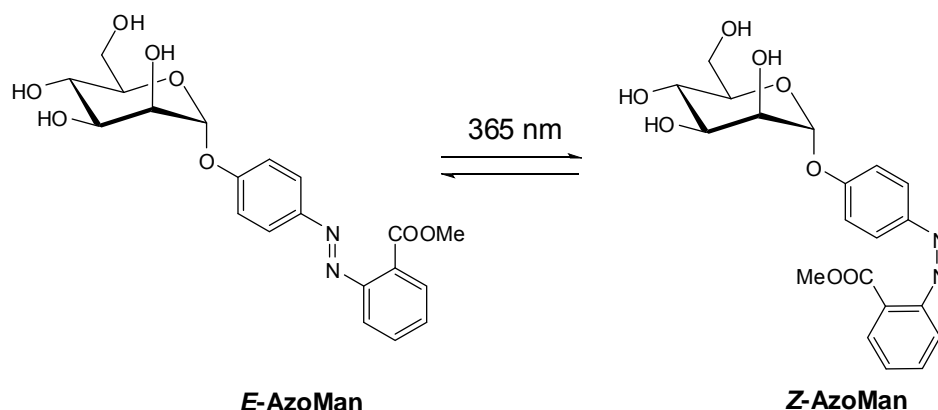
Figure S13. ¹³C NMR (150 MHz, DMSO-*d*₆) of *E*-22 and *Z*-22 ([Man-*a* z o]₃).

5. References

1. J. M. Casas-Solvas, M. C. Martos-Maldonado and A. Vargas-Berenguel, *Tetrahedron*, 2008, **64**, 10919-10923.
2. A. Y. Chernyak, G. V. M. Sharma, L. O. Kononov, P. R. Krishna, A. B. Levinsky, N. K. Kochetkov and A. V. Rama Rao, *Carbohydr. Res.*, 1992, **223**, 303-309.
3. J. Kerékgyártó, J. P. Kamerling, J. B. Bouwstra, J. F. G. Vliegenthart, *Carbohydr. Res.*, 1989, **186**, 51-62.
4. T. K. Lindhorst, S. Kötter, U. Krallmann-Wenzel, S. Ehlers, *J. Chem. Soc., Perkin Trans. I*, **2001**, 823-831.
5. E. R. Nelson, M. Maienthal, L. A. Lane, A. A. Benderly, *J. Am. Chem. Soc.*, 1957, **79**, 3467-3469.
6. L. Beaufort, L. Delaude and A. F. Noels, *Tetrahedron*, 2007, **63**, 7003-7008.

3.4 UV-Vis spectroscopy of azobenzene glycosides in the presence of bacteria.

Bacterial adhesion is the first step for biofilm formation and colonization to the surface of the host cell, which cause serious health problems.^[1, 2] For example, urinary tract infections (UTIs) are initiated by the adhesion of uropathogenic *E. coli* (UPEC) to the carbohydrate receptors on the surface of bladder epithelium. α -D-Mannose-specific binding of UPEC is mediated by a lectin called FimH, which is located at the tips of type 1-fimbriae.^[3] This carbohydrate-protein interactions are influenced by several factors like nature of the ligand, multivalency of carbohydrate epitopes and conformational flexibility.^[4-8] In order to investigate the impact of conformational flexibility, photoswitchable ligand AzoMan (*E*-*para*-(*ortho*-methoxycarbonyl-phenylazo)phenyl- α -D-mannoside) was synthesized (chapter 3.2). Azobenzene was chosen as a photoswitchable unit, because it adopts different structure (*E* and *Z*) upon irradiation at a particular wavelength of light (Scheme 3.4.1).



Scheme 3.4.1: *E:Z* isomerization of AzoMan.

For any kind biological testing, as a prerequisite, the respective compound should show good solubility in water/aqueous buffer. Indeed AzoMan showed an excellent solubility in polar organic solvents as well as in water. Owing to good solubility AzoMan was tested as inhibitor of type 1-fimbriae mediated bacterial adhesion by various biological testing systems. Firstly, adhesion of non-fluorescent *E. coli* bacteria (strain HB101 pPKL4) to both the isomers of AzoMan (*E*- and *Z*-) was monitored by UV-Visible spectroscopy (Fig 3.4.2 & 3.4.3).

secondly, enzymatic activity of bacterial lectin FimH (PKL1162) in isomerization process of *Z*-AzoMan → *E*-AzoMan was studied by saturation transfer difference (STD) NMR experiments and described earlier.^[9] Finally, compound *E*-AzoMan was tested as inhibitor to live human epithelial cells (see 3.4.3).^[10]

Before testing the isomers of azobenzene glycosides to *E. coli* bacteria, their photochromic properties were studied in solution. Due to the good solubility of AzoMan in water and preferred solvent for biological testing, water was used as a solvent for photoisomerization studies. *E*→*Z* photoisomerization and thermal reverse isomerization of *Z*→*E* was measured by UV-Vis spectroscopy, experiments were performed in dark conditions to prevent light induced switching (Fig 3.4.1).

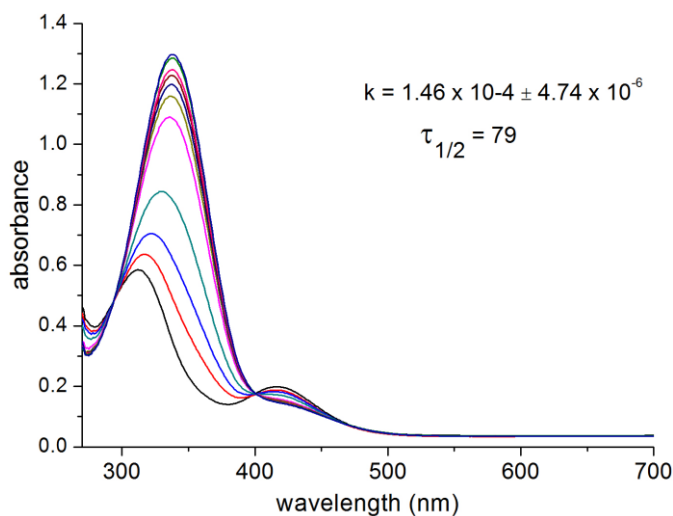


Figure 3.4.1: UV visible spectra showing thermal reversion *E*-1 to *Z*-1 in H₂O (40 μM) at 18±2 °C in the dark (thermal relaxation) as a function of time.

The absorption spectra of *E*-1 exhibits an absorption maximum at 338 nm corresponding to the π - π^* transition of the -N=N- group. Upon irradiation at 365 nm for about 10 min by LED photostationary state (pss) was reached, observed by the increase in absorbance at n - π^* transition for *Z*-1 at 416 nm, and simultaneous decrease in the π - π^* transition, an clear indication of the formation of the *cis*-isomer. Continuous irradiation for another 5 minutes shows no change in the UV-Vis spectroscopy, confirming the pss was reached in 10 min. Thermal relaxation of *Z*→*E* showed a half-life ($\tau_{1/2}$) of 79 h which is sufficient enough to perform the biological testing.^[7]

The *E:Z* ratios of AzoMan before irradiation and after irradiation (i.e) photostationary states (pss) were determined by the integration of the anomeric proton of the mannose in ^1H NMR spectroscopy. Before irradiation ~99% of *E*-AzoMan and in the pss state ~88% of *Z*-AzoMan was observed by ^1H NMR spectroscopy. Greater half-life and higher ratios of isomers is good enough to test the individual isomers for biological testing.

3.4.1 Monitoring the complexation between bacteria-AzoMan by UV-Vis spectroscopy

To understand the role of conformational control in adhesion of bacterial lectin FimH to carbohydrate recognition, two different isomers of AzoMan were tested and monitored by UV-Vis spectroscopy (Fig 3.4.2). To avoid the turbidity problem in measuring UV-Vis spectroscopy, fixing the bacterial concentration was essential and thus following experiments were performed. A known amount of **E-1** (2 mL, 30 μM) was taken in the UV cuvette and added *E. coli* strain HB101 pPKL4 (250 μl , 20 mg/mL) and recorded the UV-Vis spectroscopy. Due to higher concentration of *E. coli* bacteria, turbidity in the solution was observed and UV-Vis spectroscopy was unable to measure. Attempts in reducing the concentration of *E. coli* bacteria from 10 mg/mL, 5 mg/mL showed poor base line in the UV-Vis spectrum. However addition of *E. coli* strain HB101 pPKL4 (250 μL , 2 mg/mL) to the *E*-1 (2 mL, 30 μM) gave good UV spectrum (Fig 3.4.3). Hence further experiments were performed by fixing the bacterial concentration to 2 mg/mL.

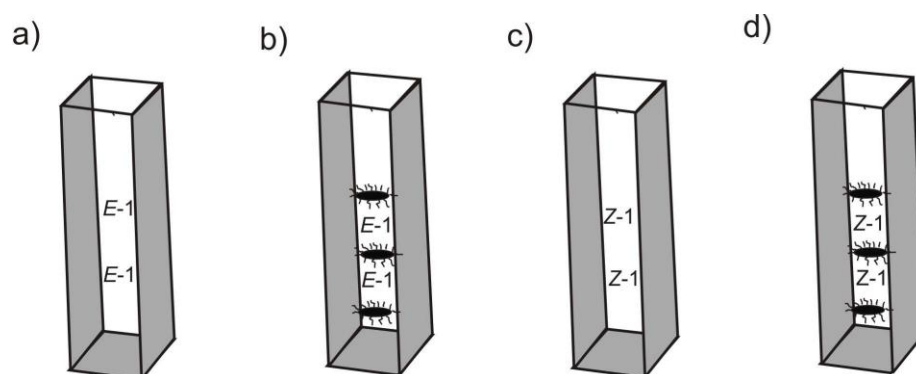


Figure 3.4.2: Monitoring the bacterial adhesion by UV-Visible spectroscopy, a) *E*-AzoMan (2 mL, 30 μM) b) *E*-AzoMan and *E. coli* strain HB101 pPKL4 (250 μL , 2 mg/mL) c) *Z*-AzoMan (2 mL, 30 μM) b) *Z*-AzoMan and *E. coli* strain HB101 pPKL4 (250 μL , 2 mg/mL).

Firstly, to the pure *E*-AzoMan in the UV cuvette, *E. coli* (250 μL , strain HB101 pPKL4) was added (Fig 3.4.2b) and UV-Vis spectroscopy was measured at 0 and 30 minutes. For control

experiment and for direct comparison, pure *E*-AzoMan in the UV cuvette (Fig 3.4.2a) was also measured at same interval of time. The testing results showed that, adhesion of bacteria to the *E*-AzoMan was not observed by UV-Vis spectroscopy. UV-Vis spectrums of only *E*-AzoMan and *E*-AzoMan in the presence of bacteria are nearly the same (Fig 3.4.3a).

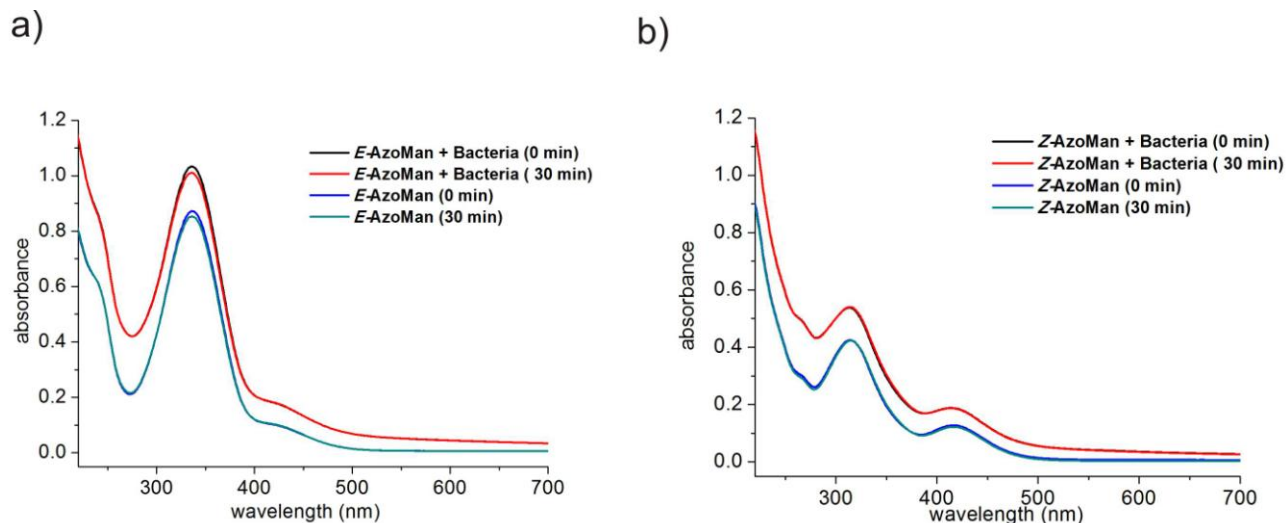


Figure 3.4.3: UV-Vis spectroscopy of a) only *E*-AzoMan at 0 and 30 min; after adding *E. coli* bacteria (250 μ L, strain HB101 pPKL4) to *E*-AzoMan in the UV cuvette at 0 and 30 min. b) *Z*-AzoMan (at pss) at 0 and 30 min, after adding *E. coli* bacteria (250 μ L, strain HB101 pPKL4) to *Z*-AzoMan in the UV cuvette at 0 and 30 min.

In a similar manner, bacterial adhesion to the *Z*-AzoMan isomer was also performed. To get the *Z*-AzoMan, *E*-AzoMan was irradiated at 365 nm using light emitting diode (LED) until it reaches the photostationary state (pss) which was reached between 8-10 minutes. To the obtained *Z*-AzoMan (Fig 3.4.2d), *E. coli* (250 μ L, strain HB101 pPKL4) was added and UV-Vis spectroscopy was measured at 0 and 30 minutes. For control experiment and for direct comparison *Z*-AzoMan (Fig 3.4.2c) was also measured at 0 and 30 minutes. No significant difference between the pure *Z*-AzoMan and *Z*-AzoMan in presence of bacteria was observed by UV-Vis spectroscopy (Fig 3.4.3b).

In conclusion, no difference was observed, whether bacteria were added to *E*-AzoMan or to *Z*-AzoMan, by UV-Vis spectroscopy. May be if the molecules are immobilized on surfaces then there could be an effect in adhesion of bacteria to adhesive surfaces. In another experiment, *E*-AzoMan was performed as a better inhibitor for bacterial adhesion of *E. coli* to live human *HT-29* cells compared to the standard MeMan and *p*NPMan, has been reported (see 3.4.3).

References

- [1] M. Hartmann, T. K. Lindhorst, *Eur. J. Org. Chem.* **2011**, 20, 3583-3609.
- [2] E. K. Mulholland, R. A. Adegbola, *N. Engl. J. Med.* **2005**, 352, 75-77.
- [3] V. Tchesnokova, P. Aprikian, D. Kisiela, S. Gowey, N. Korotkova, W. Thomas, E. Sokurenko, *Infect. Immun.* **2011**, 79, 3895-3904.
- [4] J. J. Lundquist, E. J. Toone, *Chem. Rev.* **2002**, 102, 555-578.
- [5] N. P. Pera, H. M. Branderhorst, R. Kooij, C. Maierhofer, M. van der Kaaden, R. M. J. Liskamp, V. Wittmann, R. Ruijtenbeek, R. J. Pieters, *ChemBioChem* **2010**, 11, 1896-1904.
- [6] N. Jayaraman, *Chem. Soc. Rev.* **2009**, 38, 3463-3483.
- [7] V. Chandrasekaran, K. Kolbe, F. Beiroth, T. K. Lindhorst, *Beilstein J. Org. Chem.* **2013**, 9, 223-233.
- [8] O. Srinivas, N. Mitra, A. Surolia, N. Jayaraman, *Glycobiology* **2005**, 15, 861-873.
- [9] M. Hartmann, *Dissertation CAU Kiel* **2011**.
- [10] M. Hartmann, H. Papavlassopoulos, V. Chandrasekaran, C. Grabosch, F. Beiroth, T. K. Lindhorst, C. Röhl, *FEBS Lett.* **2012**, 586, 1459-1465.

3.4.3 Inhibition of Bacterial Adhesion to Live Human Cells: Activity and cytotoxicity of synthetic mannosides.

Mirja Hartmann, Heike Papavlassopoulos, Vijayanand Chandrasekaran, Carsten Grabosch, Femke Beiroth, Thisbe K. Lindhorst, Claudia Röhl

FEBS Lett. **2012**, 586, 1459-1465.

The inhibitory potency of azobenzene glycoside (*E*-AzoMan) was tested on human colon carcinoma cell monolayers (Fig 3.4.3) and their toxicity on the human cells was evaluated. *E*-AzoMan showed a high inhibitory potency than the standard MeMan and showed low toxicity.

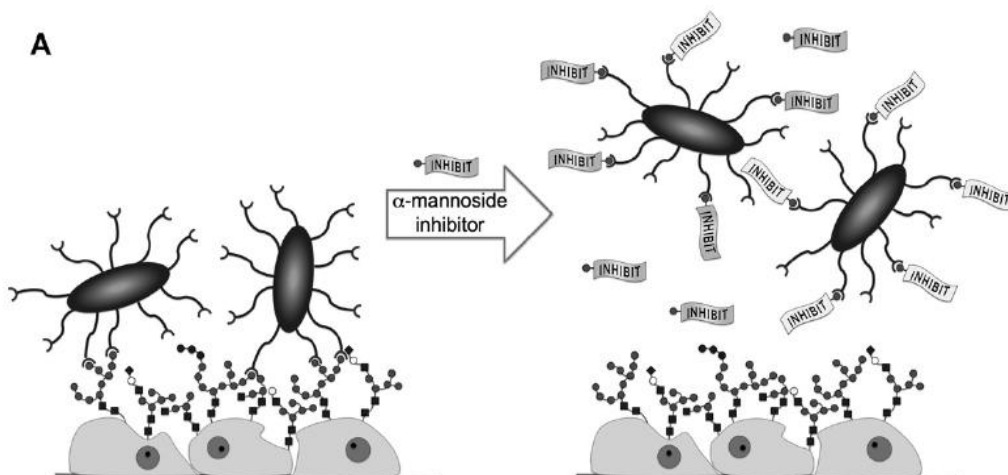


Figure 3.4.3: A cartoon of α -D-mannose-specific inhibition of adhesion of *E. coli* bacteria to a live human epithelial cells.

In this collaborative work, M. Hartmann did the bacteria testing, H. Papavlassopoulos performed the cytotoxicity assays, C. Grabosch synthesized squaric acid mannoside (SAMan), F. Beiroth did the molecular modeling and I synthesized the azobenzene mannoside (AzoMan). T. K. Lindhorst, C. Röhl, H. Papavlassopoulos and M. Hartmann wrote the manuscript.



Inhibition of bacterial adhesion to live human cells: Activity and cytotoxicity of synthetic mannosides

Mirja Hartmann^a, Heike Papavlassopoulos^b, Vijayanand Chandrasekaran^a, Carsten Grabosch^a, Femke Beiroth^a, Thisbe K. Lindhorst^{a,*}, Claudia Röhl^{b,*}

^aOtto Diels Institute of Organic Chemistry, Christiana Albertina University of Kiel, Otto-Hahn-Platz 3-4, D-24098 Kiel, Germany

^bInstitute of Toxicology and Pharmacology for Natural Scientists, Christiana Albertina University of Kiel, Brunswiker Str. 10, D-24105 Kiel, Germany

ARTICLE INFO

Article history:

Received 16 December 2011

Revised 16 March 2012

Accepted 19 March 2012

Available online 10 April 2012

Edited by Renee Tsolis

Keywords:

Bacterial adhesion

α -Mannoside inhibitor

HT-29 cell

Cytotoxicity

Anti-adhesion therapy

Type 1 fimbriated *E. coli*

ABSTRACT

Bacterial adhesion to glycosylated surfaces is a key issue in human health and disease. Inhibition of bacterial adhesion by suitable carbohydrates could lead to an anti-adhesion therapy as a novel approach against bacterial infections. A selection of five α -mannosides has been evaluated as inhibitors of bacterial adhesion to the polysaccharide mannan, as well as to the surface of live human HT-29 cells. Cell toxicity studies were performed to identify the therapeutic window for a potential in vivo-application of the tested carbohydrates. A previously published mannosidic squaric acid diamide was shown to be exceptionally effective as inhibitor of the bacterial lectin FimH.

© 2012 Federation of European Biochemical Societies. Published by Elsevier B.V. All rights reserved.

1. Introduction

Carbohydrates are involved in numerous important biological events such as in cell recognition and cell adhesion [1]. They are found as part of cell surface glycoconjugates, making up a characteristic layer that is surrounding a eukaryotic cell and called its glycocalyx. There is an overwhelming molecular complexity of the glycocalyx which is interrogated by a class of specialized proteins, namely the lectins [2]. To learn more about carbohydrate–lectin

interactions, synthetic glycosides and glycomimetics, respectively, have been utilized as modulators and inhibitors of the occurring molecular recognition processes [3–8]. As also adhesion of microbes to the surface of their target cells is frequently mediated by carbohydrate–protein interactions, its inhibition by suitable glycosides could provide means against, i.e., bacterial colonization and biofilm formation [9–12].

Bacteria use long hairy organelles, called fimbriae or pili, to facilitate adhesion to cell surfaces. One of the best characterized fimbriae are type 1 fimbriae, that comprise an α -D-mannoside-specific lectin at their tips, named FimH [13]. Type 1 fimbriae are critical virulence factors in uropathogenic *Escherichia coli* (UPEC) and widely distributed among Enterobacteriaceae [14]. A large collection of different mannosides and mannose conjugates, respectively, have been made and tested as inhibitors of type 1 fimbriae-mediated bacterial adhesion, primarily in vitro [15]. Only few examples have been published, where mannoside inhibitors of type 1 fimbriae-mediated bacterial adhesion have been tested with cells or in animal models, respectively [16–21]. Here, it has become our goal to examine a selection of most promising inhibitors of mannose-specific bacterial adhesion with live human cells (Fig. 1A) and test their cytotoxicity, in order to assess the therapeutic potential of these compounds.

Abbreviations: AzoMan, *E*-para-(ortho-methoxycarbonyl-phenylazo)phenyl α -D-mannoside; CRD, carbohydrate recognition domain; DMEM, Dubecco's modified eagle medium; EC₅₀, half-maximal effective concentration; *E. coli*, *Escherichia coli*; FBS, fetal bovine serum; HepMan, heptyl α -D-mannoside; IC₅₀, half-maximal inhibitory concentration; IP, inhibitory potency; MEM, minimal essential medium; MeMan, methyl α -D-mannoside; MTT, 3-(4,5-dimethylthiazol-2-yl)-2,5-diphenyl-tetrazolium bromide; pNPMAN, para-nitrophenyl α -D-mannoside; PBS, phosphate buffered saline; PBST, PBS + 0.5% Tween20; RIP, relative inhibitory potency; SAMAN, p-[N-(4-ethylamino-2,3-dioxocyclobut-1-enyl)amino]phenyl α -D-mannoside; SE, standard error; SEM, standard error of the mean

* Corresponding authors. Fax: +49 431 8807410 (T.K. Lindhorst), +49 431 5973558 (C. Röhl).

E-mail addresses: tklind@oc.uni-kiel.de (T.K. Lindhorst), roehl@toxi.uni-kiel.de, claudia.roehl@gmx.net (C. Röhl).

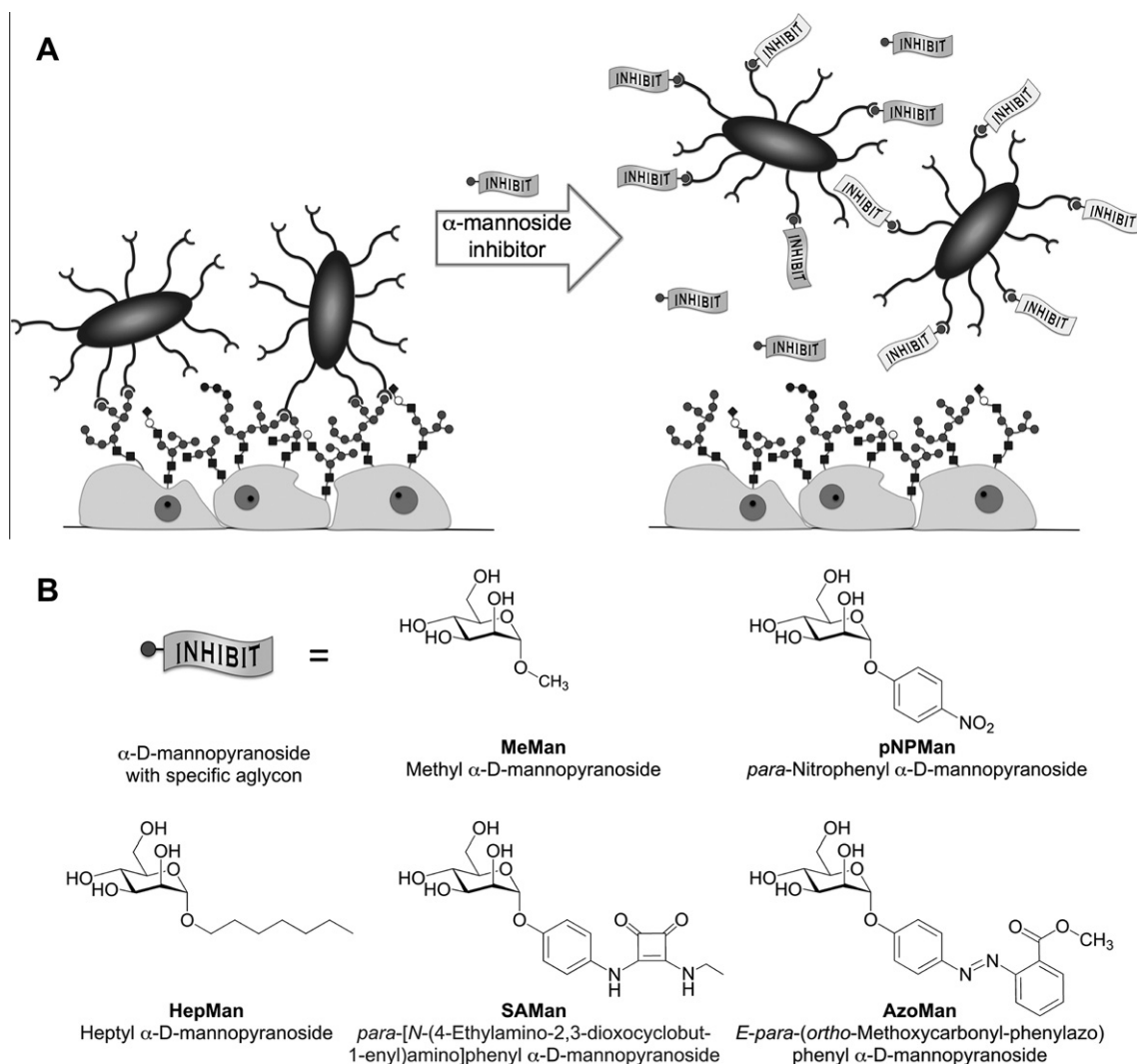


Fig. 1. Five synthetic α -mannoside inhibitors of bacterial adhesion to eukaryotic cells. (A) The cartoon illustrates fimbriae-mediated adhesion of bacteria to the glycocalyx of cells and its prevention by suitable α -mannoside inhibitors and (B) structures and names (abbreviations and IUPAC nomenclature) of tested α -mannoside inhibitors.

In the past, we have typically tested and ranked synthetic mannosides as inhibitors of bacterial adhesion to the polysaccharide mannan [15,22]. Owing to the known structure of the type 1 fimbrial lectin FimH [17,23,24], the affinity of α -D-mannoside ligands can be greatly improved by variation of the aglycone moiety, whereas the mannose glycone part must not be changed. Recently, we have added a very potent low-molecular weight mannoside to the collection (SAMan, Fig. 1B), which has the potential to serve as a lead structure for the development of FimH antagonists [25,26]. Hence, it is important to evaluate its inhibitory potency with human cells as well as to test its cytotoxicity. In addition, a novel azo-benzene mannoside (AzoMan, Fig. 1B) was tested as anti-adhesive and both mannosides, SAMan and AzoMan, were compared to known inhibitors of type 1 fimbriae-mediated bacterial adhesion [27], namely methyl α -D-mannoside (MeMan), *p*-nitrophenyl α -D-mannoside (pNPMa), and heptyl mannoside (HepMan). The latter has recently been described as high-affinity ligand for FimH [17,28,29].

Highly glycosylated HT-29 mammalian colon cells were chosen to study bacterial adhesion, its inhibition, and cytotoxicity of the mannosidic inhibitors. The inhibitory potencies determined using HT-29 cells were compared to the results from a test, where the polysaccharide mannan was used as the adhesive layer.

2. Materials and methods

2.1. Synthetic mannosides (Fig. 1B)

Methyl α -D-mannoside (MeMan) and *para*-nitrophenyl α -D-mannoside (pNPMa) were purchased from Sigma-Aldrich and Senn Chemicals, respectively. For the synthesis of the squaric acid diamide conjugate SAMan, pNPMa was reduced to the corresponding amine and subsequently coupled to squaric acid diethyl-ester to obtain the respective squaric acid monoamide [25]. This was in turn converted into the target squaric acid diamide SAMan by reaction with ethylamine [26]. Mannosides HepMan and AzoMan were synthesized by standard glycosylation of heptanol and *ortho*-(*para*-hydroxyphenylazo)benzoic acid methyl ester, respectively, according to the trichloroacetimidate method [30] followed by final deprotection. Purity of the synthesized mannosides was confirmed by analytical HPLC and/or elemental analysis.

2.2. Cultivation of bacteria

The GFP-tagged type 1 fimbriated *E. coli* strain PKL1162 was grown as published [22]. Details are described in the [Supplementary material](#).

2.3. Mammalian cell culture

HT-29 cells (human colon adenocarcinoma grade II cell line) (DSMZ, Braunschweig, Germany) were kept in culture medium consisting of DMEM/high glucose (PAA) supplemented with 10% heat inactivated FBS (PAA), 2 mM l-glutamine (PAA), and 1 × MEM non-essential amino acids (PAA). For the experiments, HT-29 cells were seeded into 96-well microtiter plates (0.32 cm²/well) at a seeding density of 300000 cells/cm² in 313 μl/cm² medium. For the toxicity assays (Lowry and MTT test) clear flat bottom microtiter plates (Falcon®, Becton Dickinson, Heidelberg, Germany) and for the adhesion-inhibition assay black wall, flat clear-bottom plates (Corning Incorporated Life Sciences, MA, USA) were used. For fluorescence microscopy cells were seeded on medium chamber containing glass slides (Labtec™). Cells were kept at 37 °C and 5% CO₂.

2.4. Treatment of HT-29 cells with α-mannosides

For the adhesion-inhibition assay and the cytotoxicity assays HT-29 cells were seeded into culture plates and after 48 h treated with different concentrations of the respective mannoside inhibitors. Stock solutions and solutions of the final concentrations were made up in HT-29 cell culture medium. Mannoside inhibitors were applied in the following concentration ranges: MeMan (1 μM–1000 mM), pNPMAN (0.1 μM–15 mM), HepMan (0.1 μM–10 mM), SAMan (0.01 μM–1.5 mM), and AzoMan (0.01 μM–2 mM). The concentration of SAMan solutions could not be increased over 10 mM due to its limited solubility in PBS. Fluorescence readout in the adhesion-inhibition assay was performed after 45 min, cytotoxicity measurements were performed after 24 h.

2.5. Inhibition of adhesion of *E. coli* PKL1162 to mannan

Mannosides MeMan, pNPMAN, HepMan, SAMan, and AzoMan were tested as inhibitors of type 1 fimbriae-mediated adhesion of *E. coli* to the polysaccharide mannan as published [22]. Details are described in the [Supplementary material](#).

2.6. Inhibition of adhesion of *E. coli* PKL1162 to HT-29 cells

HT-29 cells were grown in black wall, clear flat bottom plates without change of culture medium for 72 h until a confluent monolayer was formed. Then, cells were washed with 37 °C tempered DMEM and their intact state was checked under the microscope. Then, serial dilutions of the tested mannosides in DMEM at 37 °C (50 μl/well) and bacterial suspension in DMEM at 37 °C (50 μl/well) were added to the wells. For blanks to determine maximal fluorescence values cells were treated only with DMEM (50 μl/well) and bacterial suspension (50 μl/well). The control wells were filled with DMEM and the plate was incubated for 45 min at 37 °C. All wells were washed 3 times with PBS (150 μl/well) and filled with PBS (100 μl/well). Then, fluorescence of the GFP-tagged bacteria was read out (Tecan microplate reader GENios Pro, excitation wavelength, 485 nm, emission wavelength 535 nm).

2.7. Phase contrast and fluorescence microscopy showed binding of PKL1162 to HT-29 cells

See details in the [Supplementary material](#) (Fig. S3).

2.8. Cytotoxicity assays with mannoside inhibitors on HT-29 cells

2.8.1. Cell protein (Lowry assay)

To determine total protein amounts, cells were washed 3 times with PBS and incubated for 45 min with 0.5 N NaOH (60 μl/well).

Cell protein contents were measured by colorimetric determination at 620 nm (photometer 340 ATTC, SLT Labinstruments), according to the method described by Lowry [31]. Bovine serum albumin was used as standard.

2.8.2. Cell viability (MTT test)

Cells were washed once with PBS before it was replaced with 100 μl fresh growth medium per well. Cell viability was determined by means of the MTT assay [32,33]. In brief, 25 μl MTT [3-(4,5-dimethylthiazol-2-yl)-2,5-diphenyltetrazolium bromide] solution (1 mg/ml medium) was added to each well (37 °C, 7.8% CO₂) and 100 μl solubilization solution (20% (w/v) SDS, 2.5% (v/v) 1 N HCl and 2.5% (v/v) acetic acid (80%) in 50% (v/v) DMF, pH 2) was added 15 min later. Production of formazan by viable cells was assessed after 90 min (37 °C, 7.8% CO₂) by measuring the absorbance at a wavelength of 570 nm (photometer 340 ATTC, SLT Labinstruments, Germany).

2.9. Phase contrast microscopy with mannoside inhibitors on HT-29 cells

Morphological changes of HT-29 cell monolayers (in clear-bottom microtiter plates) were examined in parallel to cytotoxicity assays employing an inverted phase contrast microscope (IMT-2, Olympus, Hamburg, Germany) equipped with a digital camera (E-300, Olympus, Hamburg, Germany); cf. [Supplementary material](#) (Fig. S4).

2.10. Statistics

Statistics were calculated as described in the [Supplementary material](#).

3. Results

Five α-D-mannosides were selected (Fig. 1B) and tested as inhibitors of type 1 fimbriae-mediated bacterial adhesion in two different scenarios: (i) employing mannan-coated microtiter wells and (ii) HT-29 cellular surfaces. All tested compounds could reduce binding of *E. coli* to both surfaces.

3.1. Effect of α-mannoside inhibitors on adhesion of *E. coli* to the polysaccharide mannan

Inhibitory potencies were deduced from the results of 4–5 independent assays for each compound. Sigmoidal dose–response curves were derived to determine IC₅₀ values of each tested

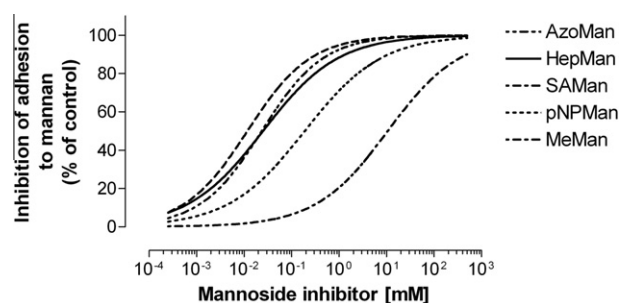


Fig. 2. Bacterial adhesion-inhibition assay on mannan. Type 1 fimbriae-mediated adhesion of *E. coli* bacteria to a mannan-coated surface is prevented by mannosides, which inhibit the respective lectin–carbohydrate interaction. Each line represents the sigmoidal concentration–effect curves fitted by non-linear regression from 2 to 8 independent experiments. Single data points are not shown for better clarity. Complete data are presented in the [Supplementary material](#).

mannoside (Fig. 2). Relative inhibitory potencies (RIP values) were calculated based on the inhibitory potency of MeMan, with $IP_{MeMan} \equiv 1$, to gain better comparability of the testing results. Thus, increasing RIP values were identified in the order MeMan < pNPMMan < HepMan < AzoMan < SAMan (Table 1). The two reference mannosides MeMan and pNPMMan clearly had the lowest inhibitory potency, whereas HepMan and AzoMan performed in the same range. SAMan, however, showed the best value as inhibitor of bacterial adhesion to mannan, surpassing the inhibitory potency of AzoMan by a factor of two.

3.2. Effect of α -mannoside inhibitors on adhesion of *E. coli* to HT-29 cell monolayers

To test bacterial adhesion to eukaryotic cells, type 1 fimbriated bacteria PKL1162 were allowed to adhere to a HT-29 human colon carcinoma cell monolayer, which is highly mannosylated. After incubation of the fluorescent bacterial suspension in DMEM over HT-29, PKL1162 *E. coli* were firmly adhered to the cell monolayer and could not be removed by washing with buffer. This was confirmed by phase contrast and fluorescence microscopy (Supplementary material, Fig. S3). Incubation of human primary fibroblast cell monolayers with bacteria, on the other hand, did not lead to reliable adhesion of bacteria.

In analogy to the results obtained on mannan, MeMan and pNPMMan were the weakest inhibitors of bacterial adhesion to HT-29 cells, followed by HepMan. HepMan, however, performed significantly weaker in this assay than when bacterial adhesion to mannan was inhibited. Furthermore, the performance of AzoMan and SAMan as inhibitors of bacterial adhesion differed with HT-29 cells compared to mannan as adhesive layer. On cells, they showed very similar inhibitory potencies with a slight advance for AzoMan. Thus, ranking of these two mannosides was reversed as compared to bacterial adhesion to mannan. Also, the MeMan-based RIP value of AzoMan is more than twofold as big when bacterial adhesion to cells was tested than in the mannan case. Overall, the inhibitor concentrations, which were required to effect 50% inhibition of bacterial adhesion to HT-29 cells were approximately one order of magnitude lower than in case of bacterial adhesion to mannan (Fig. 3, Table 1).

3.3. Effect of α -mannoside inhibitors on human HT-29 cells

To determine the toxicity of mannoside inhibitors, total cell protein, cell viability and the morphology of confluent cell monolayers were examined. For both parameters, cell protein and viability, a concentration-dependent toxicity could be induced for four of the five tested substances (Fig. 4) with their toxic potencies decreasing in the order AzoMan > HepMan > pNPMMan >> MeMan according to their half-maximal effective concentrations (EC_{50} values) shown in Table 2. Due to the limited solubility of SAMan, which could not be concentrated higher than 1.5 mM in aqueous buffer, no toxic effect could be induced by this mannoside at all. On the other hand, SAMan is one of the most potent known inhib-

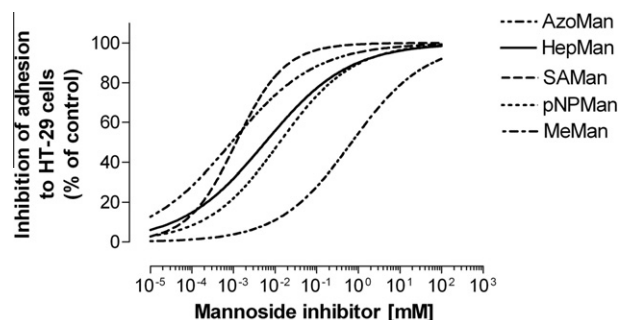


Fig. 3. Bacterial adhesion-inhibition assay on HT-29 cells. Mannose-specific inhibition of type 1 fimbriae-mediated adhesion of *E. coli* bacteria to a HT-29 colon carcinoma cell monolayer. Each line represents the sigmoidal concentration-effect curves fitted by non-linear regression from 3 to 4 independent experiments. Single data points are not shown for better clarity. Complete data are presented in the Supplementary material.

itors of type 1 fimbriae-mediated bacterial adhesion. Taken that together with its obviously non-critical toxicity, SAMan appears to be an ideal lead structure for the design of FimH antagonists.

Morphological changes of the confluent HT-29 monolayer-like formation of round shaped cells and disruption of the cell layer were examined using light microscopy (Supplementary material, Fig. S4). At concentrations around the EC_{50} values, no cytotoxic effects were observed for any of the inhibitors but MeMan. In case of MeMan destructive changes of the cell monolayer became obvious already at a concentration of 500 mM ($EC_{50} = 656$ mM). This finding could well correspond to the particularly steep slopes of the viability curve of MeMan (Fig. 4B).

3.4. Correlation of the anti-adhesive effect of mannoside inhibitors on bacteria with their toxicity on HT-29 cells

To compare the anti-adhesive effect of the tested mannoside inhibitors on bacteria and their toxicity on HT-29 cells, their EC_{50} values were calculated and compared to the IC_{50} values (Table 2). For all five substances the concentration range inducing 50% inhibition of bacterial adhesion is clearly lower than the concentration that induces 50% cell death. The therapeutic ratios of EC_{50}/IC_{50} reveal a narrow range (from 507 to 1133) for all tested substances, with that of SAMan even lying beyond 1250. For comparison reasons EC_{50}/IC_{50} quotients for *E. coli* adhered to mannan are also listed in Table 2.

4. Discussion

The obtained results allow to compare the data about the anti-adhesive potential of synthetic mannosides that were recorded with a 'simulated high-mannose type' carbohydrate surface (namely mannan-coated) with those resulting from tests with live highly mannosylated cells. Type 1 fimbriated *E. coli* bind to terminal α -D-mannosyl units on many cell types, but not on all. For

Table 1
Half-maximal inhibitory concentrations (IC_{50}) and relative inhibitory potencies of α -mannosides as inhibitors of bacterial adhesion to an artificial mannan test surface and to HT-29 human colon carcinoma cells.

α -Man inhibitor	<i>E. coli</i> adhered to mannan		<i>E. coli</i> adhered to HT-29 cells	
	IC_{50} (mM) (mean \pm SEM)	RIP_{MeMan}	IC_{50} (mM) (mean \pm SEM)	RIP_{MeMan}
MeMan	10.67 \pm 1.26	$IP \equiv 1$	0.69 \pm 0.23	$IP \equiv 1$
pNPMMan	0.19 \pm 0.04	57	0.013 \pm 0.006	74
HepMan	0.025 \pm 0.004	427	0.0058 \pm 0.0035	166
AzoMan	0.024 \pm 0.003	445	0.0009 \pm 0.0005	1067
SAMan	0.012 \pm 0.001	889	0.0012 \pm 0.0003	800

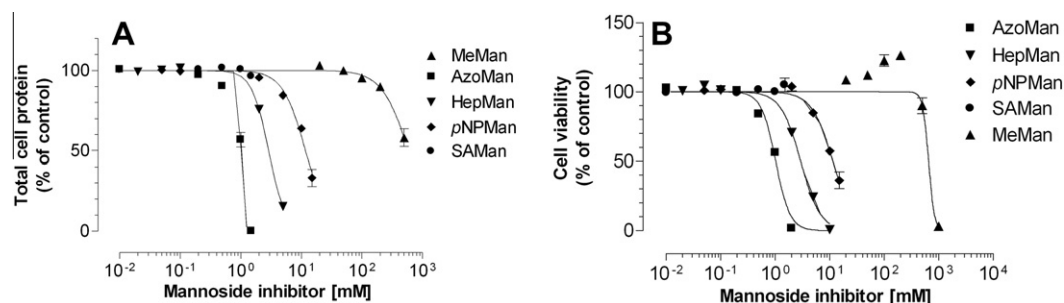


Fig. 4. Total cell protein and cell viability curves of two toxicity assays. Effect of five different mannoside inhibitors on total cell protein (A) and the viability (B) of HT-29 colon carcinoma cells after 24 h of incubation. Each symbol represents the mean \pm SE of 3–4 independent experiments. Sigmoidal concentration–effect curves were fitted by non-linear regression.

Table 2

Effective concentrations of cytotoxicity (EC_{50}) of α -mannoside inhibitors and their half-maximal correlation indices deduced from correlation of their anti-adhesive and their cytotoxic effects (EC_{50}/IC_{50} ratio).

α -Man inhibitor	HT-29 cells (toxicity, MTT) EC_{50} (mM) (mean \pm SEM)	<i>E. coli</i> adhered to HT-29 cells EC_{50}/IC_{50}	<i>E. coli</i> adhered to mannan EC_{50}/IC_{50}
MeMan	656 \pm 101	951	61
pNPMAN	11.49 \pm 0.50	884	60
HepMan	2.94 \pm 0.11	507	118
AzoMan	1.02 \pm 0.03	1133	43
SAMan	>1.5	>1250	>125

example, mannose-specific adhesion of bacteria to human primary fibroblast cells did not occur, since these cells do not have the appropriate glycosylation pattern. On the contrary we have successfully utilized HT-29 human colon carcinoma cells to test inhibition of bacterial adhesion. It particularly valuable to compare these data that were obtained with colon cells with literature data on inhibition of bacterial adhesion to human epithelial bladder cells [17,20,21], as *E. coli* residing in the intestine can cause cystitis once they reach the urogenital tract.

As it is easier and less expensive, many synthetic mannosides have been tested as inhibitors of *E. coli* adhesion to mannan-coated surfaces or to more elaborated glycoarrays [22,34]. These studies have revealed that the molecular details of the carbohydrate decoration of a test surface are critical in bacterial adhesion. Hence, it has been asked to which extent such rather artificial glyco-surfaces can resemble the glycocalyx of a eukaryotic cell in an adhesion assay. From the results depicted in Table 1 it can be seen that the relative inhibitory potencies of the tested mannosides do not differ to a large extent when the physiological surface (HT-29 cells) is compared to mannan. Thus, mannan can be considered as a reasonable model for the glycosylated cell surface in this case. Nevertheless it should be pointed out, that the anti-adhesive potential of a specific mannoside that was found in a mannan-based assay does not necessarily parallel with its potency in a cell-based test. For example, the relative inhibitory potency of HepMan on mannan is \sim 2.5 times higher than on HT-29 cells; on the other hand, in case of AzoMan the situation is nearly reversed. However, strikingly, all IC_{50} values which were determined for bacterial adhesion to HT-29 cells were lower by a factor of \sim 10 when compared to the IC_{50} values deduced on mannan. An obvious interpretation of this result is that bacterial binding to HT-29 cells is weaker than to mannan. This could be explained by comparison of the glycosylation pattern of HT-29 cells and yeast mannan. Whereas mannan from *Saccharomyces cerevisiae* comprises a multitude of α 1,3-linked mannosyl residues, this epitope is diluted by other mannosidic linkages in case of the high-mannose type glycoproteins on HT-29 cells, displaying lower affinity to FimH. The most striking discrepancy in

the inhibition data obtained on mannan versus HT-29 cell adhesive layer is the relative behavior of HepMan and AzoMan. While these two mannosides showed almost the same RIP as inhibitors of adhesion to mannan, AzoMan is approximately 6 times more potent as inhibitor of bacterial adhesion to HT-29 cells than HepMan. To facilitate the interpretation of this finding, computer-aided docking studies were performed to assess complexation of both synthetic mannosides by the bacterial lectin FimH. As described earlier [25,26], two extreme conformations of FimH were taken as starting point for the simulation, one with the tyrosine gate at the entrance of the carbohydrate binding site in a closed conformation [24], and the other with an open-gate conformation [35]. Docking reveals scoring values, more negative values correlating with predicted high affinities, and higher scores reflecting diminished binding potency. The obtained scores for HepMan are -21.5 for the closed-gate structure of FimH and -19.7 for the open-gate structure; AzoMan on the other hand scores much better with the respective values being -35.6 and -33.5 , respectively. The docked mannoside conformations suggest that π -stacking of the azobenzene aglycon with the tyrosine gate at the entrance of the FimH carbohydrate binding site is more favorable to enhance affinity than the interactions that can be established by HepMan (details see Supplementary material, Figs. S5 and S6).

This computer-aided assessment of the affinities of FimH for HepMan and AzoMan parallels nicely with the experimental findings obtained in the HT-29 cell assay, but not with the results obtained on mannan. A possible interpretation could be found in multivalency effects that might dominate inhibition of bacterial adhesion in case of the less sensitive scenario on mannan, whereas in case of the cell-based adhesion assay the individual complexation event between a mannosidic inhibitor and type 1 fimbrial FimH might gain more importance. This hypothesis receives some support by the clear multivalency effects that have been found with multivalent HepMan conjugates [36,37].

HepMan is known as a promising high-affinity FimH antagonist [17,20,24] and has been tested earlier with human epithelial bladder 5637 cells in a flow cytometry-based assay [21]. In this assay, HepMan performed 64 times better than MeMan (based on IC_{50} determination). In another report a 100-fold lower concentration of HepMan (1 mM), in comparison to MeMan, was enough to completely inhibit bacterial binding to bladder cells [17]. In our study with HT-29 human carcinoma cells, the relative performance of HepMan and MeMan was similar: here the inhibitory potency of HepMan surpassed that of MeMan by even 166-fold, suggesting an even better effect of HepMan in the intestine. A 5.8 μ M concentration of HepMan led to 50% inhibition of bacterial adhesion to HT-29 cells and \sim 1 mM HepMan led to 90% reduction of bacterial adhesion (Table 3).

To relate the anti-adhesive potential of the tested mannoside inhibitors to their cytotoxicity, the respective half-maximal

Table 3
Biocompatibility index: EC₁₀/IC₉₀ quotients of α -mannoside inhibitors of bacterial adhesion based on their cytotoxicity determined with HT-29 cells and their inhibitory potencies in adhesion of bacteria to mannan and human cells, respectively.

α -Man inhibitor	HT-29 cells (toxicity, MTT)	<i>E. coli</i> adhered to HT-29 cells			<i>E. coli</i> adhered to mannan		
	EC ₁₀ (mM) (mean \pm SE)	IC ₉₀ (mM) (mean \pm SE)	RIP _{MeMan}	EC ₁₀ /IC ₉₀	IC ₉₀ (mM) (mean \pm SE)	RIP _{MeMan}	EC ₁₀ /IC ₉₀
MeMan	501 \pm 59	61.0 \pm 46.9	IP \equiv 1	8.2	495 \pm 131	IP \equiv 1	1.01
pNPMan	4.26 \pm 0.53	1.11 \pm 1.07	55	3.8	11.2 \pm 5.1	44	0.38
HepMan	1.17 \pm 0.09	0.96 \pm 1.34	64	1.2	1.37 \pm 0.52	361	0.85
AzoMan	0.52 \pm 0.04	0.15 \pm 0.17	407	3.5	0.63 \pm 0.20	786	0.83
SAMan	>1.5	0.022 \pm 0.015	2773	>68.2	0.34 \pm 0.08	1447	>4.41

correlation indices were calculated (EC₅₀/IC₅₀, Table 2). According to these therapeutic ratios, AzoMan and SAMan are leading compounds in the tested library. We have considered that for a reasonable medical application 50% cell death is too high and otherwise 50% inhibition of adhesion not sufficient for an anti-adhesion treatment. Thus, EC₁₀/IC₉₀ ratios were calculated for a more ambitious estimate of a possible therapeutic window (Table 3). As the EC₁₀ reflects those concentrations leading to only 10% cell death and the IC₉₀ value corresponds to 90% inhibition of bacterial adhesion the ratio EC₁₀/IC₉₀ can be taken as a robust biocompatibility index and considered as measure for the therapeutic window of an anti-adhesive compound. The EC₁₀/IC₉₀ ratios follow a different course than EC₅₀/IC₅₀ ratios, resulting from the specific slopes of the fitted dose–response curves at different concentrations. The determined EC₁₀/IC₉₀ ratios indicate increasing cell biocompatibility in the order of HepMan < AzoMan/pNPMan < MeMan << SAMan. According to this analysis SAMan shows by far the best biocompatibility leaving even MeMan far behind.

Surprisingly, HepMan appears less biocompatible according to the herein reported toxicity studies. The EC₅₀ value determined for HepMan is \sim 3 mM, however it has been reported that no acute toxicity of HepMan was assessed when HepMan was administered to mice even at 50 mM concentrations [16,17,24,29]. Possibly, the animal organism can cope with harmful effects, which cannot be compensated by a confluent cell layer applied in vitro.

Interestingly the rather unusual azobenzene mannoside AzoMan shows no extreme toxicity when compared to the less foreign glycoside MeMan, for example. This is in accordance with reports on biocompatibility of azobenzene dyes [38]. Thus this compound becomes a promising candidate for the development of photo-switchable anti-adhesive surfaces [39]. Isomerization of the azobenzene N=N double bond allows to manipulate the orientation of the attached mannose portion for binding, an approach which is currently under investigating in our laboratory.

In conclusion, in this study inhibition of bacterial adhesion to HT-29 human carcinoma cells by five different mannosides was compared to data obtained in a mannan-based assay and to literature-known results obtained with human epithelial bladder cells. In addition, cytotoxicity studies were performed to assess the biocompatibility of the anti-adhesive mannosides. The mannosidic squaric acid derivative SAMan [26] turned out to be a particularly potent inhibitor of type 1 fimbriae-mediated bacterial adhesion with the potential to be developed and employed in in vivo-studies, owing to its advantageous biocompatibility index. This mannoside comes close to a 3000-fold higher potency when compared to MeMan to effect 90% inhibition of bacterial adhesion to human colon cells. Moreover, SAMan did not cause any cytotoxicity effects even when a saturated solution was applied to the cells.

Acknowledgments

We thank Dr. Andrea Kristina Horst for her valuable advice. Support by the DFG (SFB 677) is acknowledged. Cytotoxicity exper-

iments were supported by a grant from the Medical Faculty of Christiana Albertina University of Kiel.

Appendix A. Supplementary data

Supplementary data associated with this article can be found, in the online version, at <http://dx.doi.org/10.1016/j.febslet.2012.03.059>.

References

- Varki, A. (1993) Biological roles of oligosaccharides: all the theories are correct. *Glycobiology* 3, 97–130.
- Lis, H. and Sharon, N. (1998) Lectins: carbohydrate-specific proteins that mediate cellular recognition. *Chem. Rev.* 98, 637–6749.
- Bertozzi, C.R. and Kiessling, L.L. (2001) Chemical glycobiology. *Science* 291, 2357–2364.
- Lindhorst, T.K. (2002) Artificial multivalent sugar ligands to understand and manipulate carbohydrate–protein interactions. *Top. Curr. Chem.* 218, 201–235.
- Lahmann, M. (2009) Architectures of multivalent glycomimetics for probing carbohydrate–lectin interactions. *Top. Curr. Chem.* 288, 17–65.
- Chabre, Y.M. and Roy, R. (2010) Design and creativity in synthesis of multivalent neoglycoconjugates. *Adv. Carbohydr. Chem. Biochem.* 63, 165–393.
- Kiessling, L.L. and Splain, R.A. (2010) Chemical approaches to glycobiology. *Annu. Rev. Biochem.* 79, 619–653.
- Dondoni, A. and Marra, A. (2010) Calixarene and calixresorcarene glycosides: their synthesis and biological applications. *Chem. Rev.* 110, 4949–4977.
- Sharon, N. (2006) Carbohydrates as future anti-adhesion drugs for infectious diseases. *Biochim. Biophys. Acta* 1760, 527–537.
- Pieters, R.J. (2009) Intervention with bacterial adhesion by multivalent carbohydrates. *Med. Res. Rev.* 27, 796–816.
- Ernst, B. and Magnani, J.L. (2009) From carbohydrate leads to drugs. *Nat. Rev. Drug Discov.* 8, 661–677.
- Ghosh, S. and Panaccione, R. (2010) Anti-adhesion molecule therapy for inflammatory bowel disease. *Ther. Adv. Gastroenterol.* 3, 239–258.
- Knight, S.D. and Bouckaert, J. (2009) Structure, function, and assembly of type 1 fimbriae. *Top. Curr. Chem.* 288, 67–107.
- Olsen, K., Oelschlaeger, T.A., Hacker, J. and Khan, A.S. (2009) Carbohydrate receptors of bacterial adhesins: implications and reflections. *Top. Curr. Chem.* 288, 109–120.
- Hartmann, M. and Lindhorst, T.K. (2011) The bacterial LectinFimH, a target for drug discovery – carbohydrate inhibitors of type 1 fimbriae-mediated bacterial adhesion. *Eur. J. Org. Chem.* 3583–3609.
- Han, Z., Pinkner, J.S., Ford, B., Obermann, R., Nolan, W., Wildman, S.A., Hobbs, D., Ellenberger, T., Cusumano, C.K., Hultgren, S.J. and Janetka, J.W. (2010) Structure-based drug design and optimization of mannoside bacterial FimH antagonists. *J. Med. Chem.* 53, 4779–4792.
- Wellens, A., Garofalo, C., Nguyen, H., Van Gerven, N., Slättegård, R., Hernalsteens, J.P., Wyns, L., Oscarson, S., De Greve, H., Hultgren, S.J. and Bouckaert, J. (2008) Intervening with urinary tract infections using anti-adhesive based on the crystal structure of the FimH–oligomannose-3 complex. *PLoS ONE* 3 (4), e2040.
- Svanborg-Edén, C., Freter, R., Hagberg, L., Hull, R., Hull, S., Leffler, H. and Schoolnik, G. (1982) Inhibition of experimental ascending urinary tract infection by an epithelial cell-surface receptor analog. *Nature* 289, 560–562.
- Arce, E., Nieto, P.M., Díaz, V., Castro, R.G., Bernadi, A. and Rojo, J. (2003) Glycodendritic structures based on boltorn hyperbranched polymers and their interactions with *Lens culinaris* lectin. *Bioconj. Chem.* 14, 817–823.
- Klein, T., Abgottspon, D., Wittwer, M., Rabbani, S., Herold, J., Jiang, X., Kleeb, S., Lüthi, C., Scharenberg, M., Bezencon, J., Gubler, E., Pang, L., Smiesko, M., Cutting, B., Schwardt, O. and Ernst, B. (2010) FimH antagonists for the oral treatment of urinary tract infections: from design and synthesis to in vitro and in vivo evaluation. *J. Med. Chem.* 53, 8627–8641.

- [21] Scharenberg, M., Abgottspon, D., Cicek, E., Jiang, X., Schwardt, O., Rabbani, S. and Ernst, B. (2011) A flow cytometry-based assay for screening FimH antagonists. *Assay Drug Dev. Technol.* 9, 455–464.
- [22] Hartmann, M., Horst, A.K., Klemm, P. and Lindhorst, T.K. (2010) A kit for the investigation of live *Escherichia coli* cell adhesion to glycosylated surfaces. *Chem. Commun.* 46, 330–332.
- [23] Choudhury, D., Thompson, A., Stojanoff, V., Langermann, S., Pinkner, J., Hultgren, S.J. and Knight, S.D. (1999) X-ray structure of the FimC–FimH chaperone-adhesin complex from uropathogenic *Escherichia coli*. *Science* 285, 1061–1066.
- [24] Bouckaert, J., Berglund, J., Schembri, M., De Genst, E., Cools, L., Wuhrer, M., Hung, C.-S., Pinkner, J., Slättegård, R., Zavialov, A., Choudhury, D., Langermann, S., Hultgren, S.J., Wyns, L., Klemm, P., Oscarson, S., Knight, S.D. and De Greve, H. (2005) Receptor binding studies disclose a novel class of high-affinity inhibitors of the *Escherichia coli* FimH adhesin. *Mol. Microbiol.* 55, 441–455.
- [25] Sperling, O., Fuchs, A. and Lindhorst, T.K. (2006) Evaluation of the carbohydrate recognition domain of the bacterial adhesin FimH: design, synthesis and binding properties of mannoside ligands. *Org. Biomol. Chem.* 4, 3901–3912.
- [26] Grabosch, C., Hartmann, M., Schmidt-Lassen, J. and Lindhorst, T.K. (2011) Squaric acid monoamide mannosides as ligands for the bacterial lectin FimH: covalent inhibition or not? *ChemBioChem* 12, 1066–1074.
- [27] Lindhorst, T.K. (2011) Ligands for FimH in: *Synthesis and Biological Applications of Glycoconjugates* (Renaudet, O. and Spinelli, N., Eds.), pp. 12–35. Bentham eBooks, eISBN: 978-1-60805-277-6.
- [28] Touaibia, M., Wellens, A., Shiao, T.C., Wang, Q., Sirois, S., Bouckaert, J. and Roy, R. (2007) Mannosylated G(0) dendrimers with nanomolar affinities to *Escherichia coli* FimH. *ChemMedChem* 2, 1190–1201.
- [29] Rabbani, S., Jiang, X., Schwardt, O. and Ernst, B. (2010) Expression of the carbohydrate recognition domain of FimH and development of a competitive binding assay. *Anal. Biochem.* 407, 188–195.
- [30] Schmidt, R.R. and Kinzy, W. (1994) Anomeric-oxygen activation for glycoside synthesis: the trichloroacetimidate method. *Adv. Carbohydr. Chem. Biochem.* 50, 21–123.
- [31] Lowry, O.H., Rosebrough, N.J., Farr, A.L. and Randall, R.J. (1951) Protein measurement with the folin phenol reagent. *J. Biol. Chem.* 193, 265–275.
- [32] Mosmann, T. (1983) Rapid colorimetric assay for cellular growth and survival: application to proliferation and cytotoxicity assays. *J. Immunol. Methods* 65, 55–63.
- [33] Röhl, C., Armbrust, E., Herbst, E., Jess, A., Gülden, M., Maser, E., Rimbach, G. and Bösch-Saadatmandi, C. (2010) Mechanisms involved in the modulation of astroglial resistance to oxidative stress induced by activated microglia: antioxidative systems, peroxide elimination, radical generation, lipid peroxidation. *Neurotox. Res.* 17, 317–331.
- [34] Gómez-García, M., Benito, J.M., Butera, A.P., Ortiz Mellet, C., García Fernández, J.M. and Jiménez Blanco, J.L. (2012) Probing carbohydrate–lectin recognition in heterogeneous environments with monodisperse cyclodextrin-based glycoclusters. *J. Org. Chem.* 77, 1273–1288.
- [35] Hung, C.-S., Bouckaert, J., Hung, D., Pinkner, J., Widberg, C., Defusco, A., Auguste, C.G., Strouse, R., Langermann, S., Waksman, G. and Hultgren, S.J. (2002) Structural basis of tropism of *Escherichia coli* to the bladder during urinary tract infection. *Mol. Microbiol.* 44, 903–915.
- [36] Gouin, S.G., Wellens, A., Bouckaert, J. and Kovensky, J. (2009) Synthetic multimeric heptyl mannosides as potent antiadhesives of uropathogenic *Escherichia coli*. *ChemMedChem* 4, 749–755.
- [37] Almant, M., Moreau, V., Kovensky, J., Bouckaert, J. and Gouin, S.G. (2011) Clustering of *Escherichia coli* type-1 fimbrial adhesins by using multimeric heptyl α -D-mannoside probes with a carbohydrate core. *Chem. Eur. J.* 17, 10029–10038.
- [38] Yoshino, J., Furuta, A., Kambe, T., Itoi, H., Kano, N., Kawashima, T., Ito, Y. and Asashima, M. (2010) Intensely fluorescent azobenzenes: synthesis, crystal structures, effects of substituents, and application to fluorescent vital stain. *Chem. Eur. J.* 16, 5026–5035.
- [39] Russew, M.-M. and Hecht, S. (2010) Photoswitches: from molecules to materials. *Adv. Mater.* 22, 3348–3360.

Research Letter for FEBS Letters

Appendix A – Supplementary Data

S1

Inhibition of bacterial adhesion to live human cells: Activity and cytotoxicity 3 of synthetic mannosides

Mirja Hartmann^a, Heike Papavlassopoulos^b, Vijayanand Chandrasekaran^a, Carsten Grabosch^a, Femke Beiroth^a, Thisbe K. Lindhorst^{a,*}, Claudia Röhl^{b,*}

1. Cultivation of bacteria

2. Inhibition of Adhesion of *E. coli* PKL1162 to mannan and Table S1 and S2 and Figures S1 and S2.

3. Phase contrast and fluorescence microscopy showed binding of PKL1162 to HT-29

4. Supplementary Figure S3. Phase contrast and fluorescence microscopy of the HT-29 cells treated with PKL1162.

5. Phase contrast microscopy with mannoside inhibitors on HT-29 cells and Supplementary Figure S4

6. Computer-aided docking

7. Statistics

1. Cultivation of bacteria [Hartmann, M., Horst, A.K., Klemm, P., and Lindhorst, T.K. (2010). A kit for the investigation of live *Escherichia coli* cell adhesion to glycosylated surfaces. *Chem. Commun.* 46, 330-332]. The GFP-tagged type 1 fimbriated *Escherichia coli* strain PKL1162 was grown in liquid culture using LB media containing ampicilline and chloramphenicol overnight at 37 °C under slight agitation. After harvesting and washing twice with phosphate buffered saline (PBS) and once with antibiotic-free DMEM, PKL1162 were suspended in DMEM to a concentration of 2 mg/ml.

2. Inhibition of adhesion of *E. coli* PKL1162 to mannan [Hartmann, M., Horst, A.K., Klemm, P., and Lindhorst, T.K. (2010). A kit for the investigation of live *Escherichia coli* cell adhesion to glycosylated surfaces. *Chem. Commun.* 46, 330-332]. Mannosides MeMan, pNPMAN, HepMan, SAMAN, and AzOMan were tested as inhibitors of type 1 fimbriae-mediated adhesion of *E. coli* PKL1162 to the polysaccharide mannan. Black 96-well polystyrene microtiter plates (Thermo Fisher Scientific, Nunc, MaxiSorp) were coated with mannan solution (1.2 µg/ml in carbonate buffer pH 9.5, 120 µl/well) by drying overnight at 37 °C. The plates were washed twice with PBST (150 µl/well) and blocked with BSA solution (5 % in PBS, 150 µl/well) for 2 h at 37 °C. The wells were washed three times with PBST (150 µl/well). Serial dilutions of the respective mannoside inhibitors in PBS were prepared and transferred to the mannan-coated and BSA-blocked 96-well plates (50 µl/well). *E. coli* PKL1162 were suspended in PBS (2 mg/ml) and 50 µl was added to each well. The plate was agitated at 37 °C for 45 min to allow binding of the bacteria. Then the wells were washed three times with PBS (150 µl/well) to remove non-adhered bacteria. All wells were filled with PBS (100 µl/well) and the surface-bound bacteria were detected via fluorescence readout (Tecan microplate reader F200, excitation wavelength, 485 nm, emission wavelength 535 nm). Maximal fluorescence values were determined in control (blank) measurements employing *E. coli* suspension, whereas no inhibitor was added. Control measurements with

blocked but uncoated microtiter plates showed, that unspecific bacterial adhesion was negligible.

The inhibitory potency of a mannoside inhibitor at a given concentration was calculated as follows, based on the measured fluorescence:

$$\text{inhibition (\%)} = \frac{\text{fluorescence (blank)} - \text{fluorescence (mannoside inhibitor)}}{\text{fluorescence (blank)}} \cdot 100$$

To determine the half-maximal inhibitory concentration (IC_{50}) of a mannoside inhibitor, the calculated inhibition values were plotted against the employed inhibitor concentrations to obtain a sigmoidal dose-response curve. IC_{50} values were deduced graphically as the concentration at which the half-maximal inhibition was reached. To be able to compare the results obtained from independent assays on different microtiter plates, all IC_{50} values were referenced to the IC_{50} of MeMan, which was tested in parallel on each plate. This led to relative inhibitory potencies (RIP) for all mannosides. All RIP values are thus consistently referenced to the inhibitory potency of MeMan ($IP_{MeMan} \equiv 1$).

exp no.	MeMan				SAMan				PNPMan				HepMan				AzoMan											
	526_3	526_4	602_1	602_2	610_1	610_2	610_3	610_4	526_3	602_1	610_1	610_2	610_3	610_4	526_3	602_1	602_2	610_1	610_2	610_3	610_4	526_4	602_1	602_2	610_1	610_3	610_4	
conojJM																												
5.00E+02	95.45	98.90	99.75	99.97	103.37	102.43	101.14	99.98																				
2.50E+02	85.11	87.87			97.12	91.73	93.83	85.87																				
1.87E+02	82.04	82.27			69.37	69.76	78.26	75.81																				
5.66E+01			56.08	52.87																								
5.00E+01	69.35	72.42	42.38	36.63																								
2.50E+01			41.12	50.76	62.93	65.37																						
1.85E+01																												
1.00E+01																												
6.17E+00			35.62	39.46	38.52	35.05																						
5.00E+00	43.83	45.63			25.81	29.16																						
2.50E+00			28.32	24.96	23.43	21.69																						
2.00E+00																												
1.00E+00	36.12	22.89			97.05	99.85	99.52	101.61	101.25	75.92	94.20	92.53	96.65	99.27	99.05	104.40	100.47	98.70										
6.88E-01																												
5.00E-01			87.63																									
4.00E-01																												
2.50E-01			7.19	10.71	65.45																							
2.29E-01																												
2.00E-01	28.16	7.98			91.65	93.19	94.77	61.53	69.26	61.44	83.06	87.99	85.71															
1.00E-01																												
8.00E-02																												
7.62E-02			6.50	10.67	3.79	-2.53																						
5.00E-02	18.96	17.06			69.88	56.31	66.19	73.58	67.42	37.27	57.90	70.37	75.76	47.11	31.24	64.86	64.89	86.51										
4.00E-02																												
2.54E-02			14.09	-2.67	-2.07	7.54																						
2.50E-02																												
2.00E-02			2.95	3.88																								
60E-02																												
1.00E-02			52.13																									
8.00E-03	12.88	11.98			39.37	45.01	39.05	48.15	10.19	13.75	6.63	26.69	29.79	40.92	53.97	20.33	42.39	42.41										
MeMan					SAMan				PNPMan				HepMan				AzoMan											

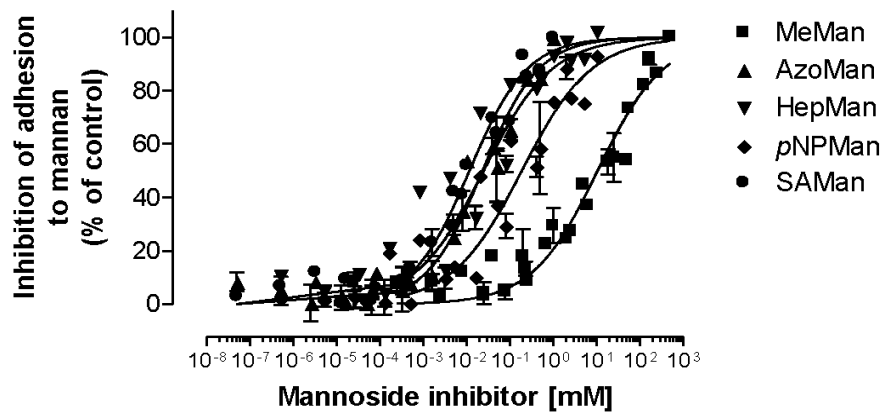


Figure S1. Inhibition of bacterial adhesion to mannan. Type 1 fimbriae-mediated adhesion of *E. coli* bacteria to a mannan-coated surface is prevented by mannosides, that inhibit the respective lectin-carbohydrate interaction. Each symbol represents the mean \pm SE of 2-8 independent experiments (cf. Table S1). Sigmoidal concentration-effect curves were fitted by nonlinear regression.

exp. no.	MeMan				SAMan				pNPMan				HepMan				AzoMan			
	408.1	408.2	413.1	413.2	408.2	413.2	421.2	421.4	408.1	413.1	421.3	421.1	408.1	413.1	421.3	421.1	408.2	413.2	421.2	421.4
conc. / μM																				
1.00E-05					22.28	20.21	44.74	0.00												
1.00E-04					14.02	13.44	14.26	8.02												
1.00E-03	15.82	7.57	21.95	18.99	20.09	52.25	0.00	6.08												
1.00E-02	7.03	24.20	22.43	12.91	19.14	33.01	30.20	24.43												
1.00E-01	-36.98	4.23	22.90	27.45	21.61	47.16	38.78	14.63												
5.00E-01					96.92	97.15	96.18	89.73												
1.00E+00	3.90	43.94	44.62	43.40	57.82	72.51	71.53	70.58												
1.00E+01	73.78	77.21	88.37	88.79	88.38	91.31	92.68	88.63												
1.00E+02	94.70	94.41	91.74	96.64	90.59	93.05	96.36	95.80												

Table S2. Inhibition of bacterial adhesion to HT-29 human colon carcinoma cells. Inhibition values for the inhibitors MeMan, SAMan, pNPMan, HepMan, and AzoMan are given in %. The inhibition curves in the publication (cf. Fig. 3) were deduced as mean of the four to eight independent assays with the respective inhibitors shown in this table. The full data set was used for Figure S2

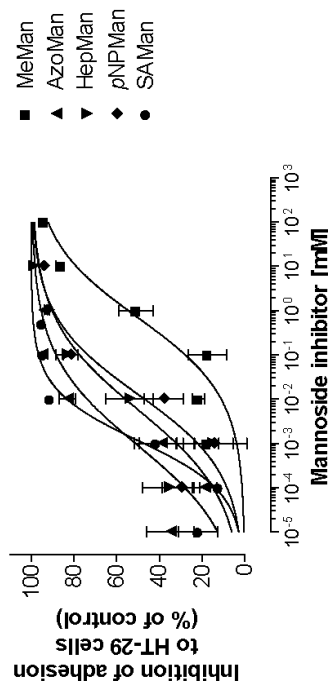


Figure S2. Inhibition of bacterial adhesion to HT-29 human colon carcinoma cells. Mannose-specific inhibition of type 1 fimbriae-mediated adhesion of *E. coli* bacteria to a HT-29 colon carcinoma cell monolayer. Each symbol represents the mean \pm SE of 3-4 independent experiments (cf. Table S2). Sigmoidal concentration-effect curves were fitted by nonlinear regression.

3. Phase contrast and fluorescence microscopy showed binding of PKL1162 to HT-29 cells. A HT-29 cell monolayer was incubated with the *E. coli* suspension in DMEM (2 mg/ml), for 45 min at 37 °C, and washed three times with PBS. The microscope slide was investigated in phase contrast microscopy and fluorescence microscopy (inverted microscope Wilovert AFL with FITC fluorescence filter and EOS 500D camera, Canon) (Supplementary Figure S3).

4. Supplementary Figure S3

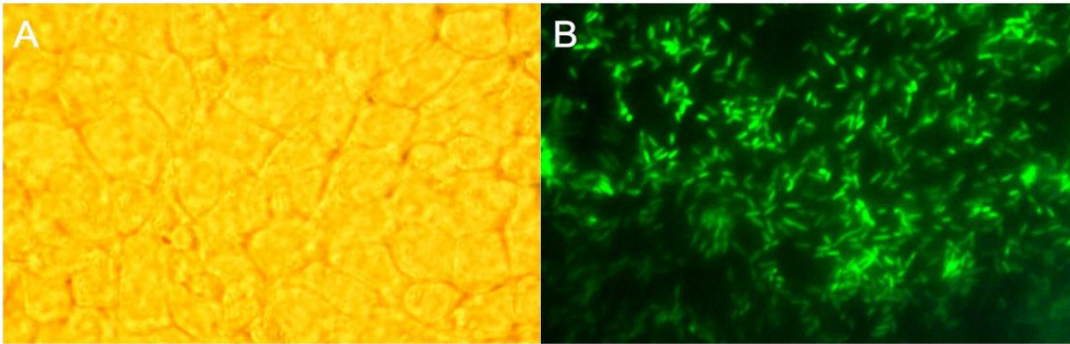


Figure S3. Phase contrast and fluorescence microscopy of the HT-29 cells treated with PKL1162. *E. coli* bacteria grown for 45 min on top of a confluent monolayer of HT-29 colon carcinoma cells after washing three times with PBS. **A:** Phase contrast microscopy of the HT-29 monolayer; **B:** fluorescence microscopy of the same area on the microscope slide reveals GFP-labelled *E. coli* bacteria on the HT-29 cells.

5. Phase contrast microscopy with mannoside inhibitors on HT-29 cells and

Supplementary Figure S4. Phase contrast microscopy was performed to examine morphological changes of HT-29 cell monolayers; cf. Supplementary Figure S4.

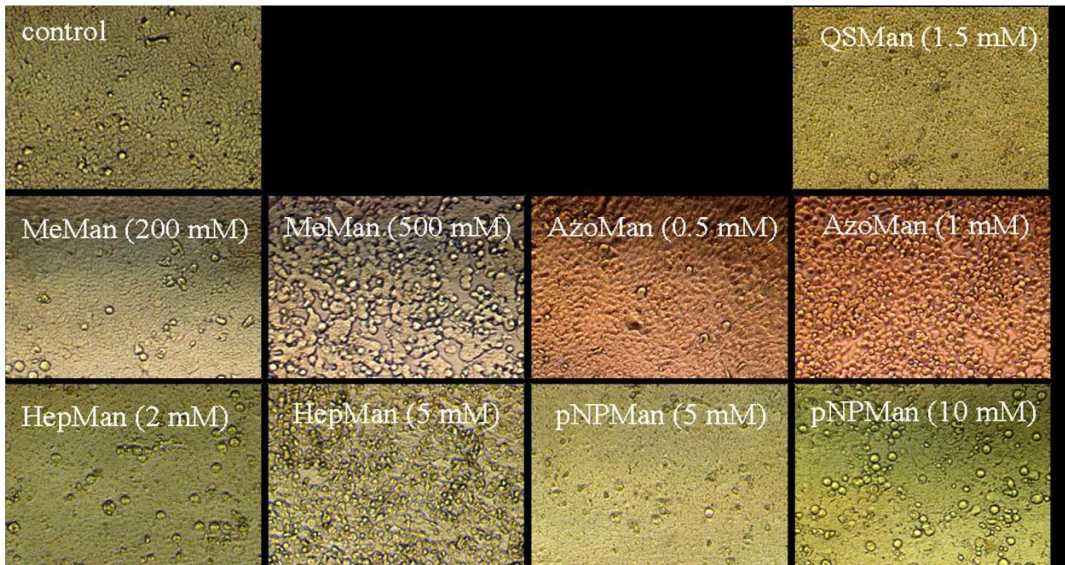


Figure S4. Phase contrast microscopy of the HT-29 cells treated with mannosides. Morphology of HT-29 colon carcinoma cell monolayers treated for 24 h with different α -mannoside inhibitors at concentrations around their EC_{50} values.

6. Computer-aided docking.

Flexible docking studies with the mannosides HepMan and AzoMan were performed using the FlexX algorithm as implemented in Sybyl 6.9. In this process FlexX-Scoring values were calculated for each of the 30 docked conformations (cf. Tables S3-S6). Docking for both molecules was performed employing two different FimH crystal structures, resembling the open- and the closed-gate conformation, respectively, with PDB codes: 1KLF (open-gate) and 1UWF (closed-gate structure). Minimization of the molecules and FlexX calculations were done by using the Tripos Force Field and Gasteiger-Hückel charges. The following scoring values were obtained:

	FlexX score for open-gate structure of FimH	FlexX score for closed-gate structure of FimH
HepMan (cf. Figure S5)	-21.5	-19.7
AzoMan (cf. Figure S6)	-35.6	-33.5

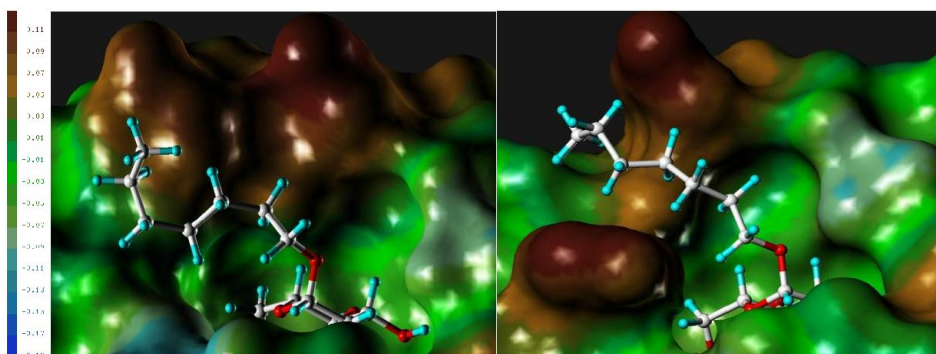


Figure S5. Representative conformations of HepMan as complexed with the closed-gate conformation of FimH (left, hit 1, score -21.5) and the open-gate conformation (right, hit 3, score -19.7). The protein FimH is displayed as Connolly surface, coloured according to the lipophilic potential of the protein surface (brown areas show high lipophilicity, blue areas high hydrophilicity).

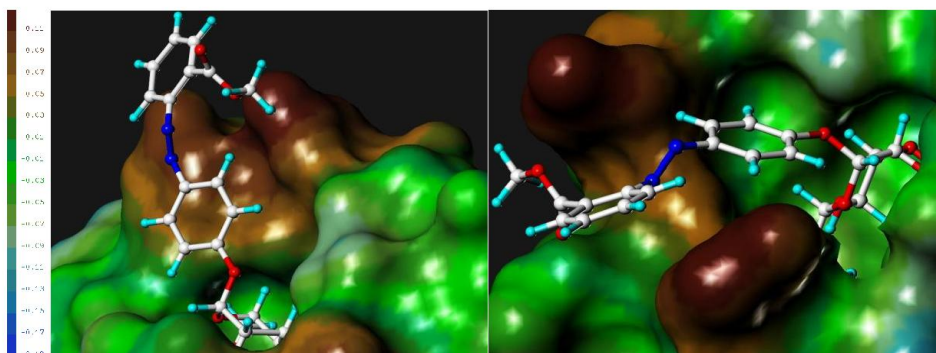


Figure S6. Representative conformations of AzoMan as complexed with the closed-gate conformation of FimH (left, hit 1, score -35.6) and the open-gate conformation (right, hit 1, score -33.5). The protein FimH is displayed as Connolly surface, coloured according to the lipophilic potential of the protein surface (brown areas show high lipophilicity, blue areas high hydrophilicity).

No.	Total Score	Match-Score	Lipo-Score	Ambig-Score	Clash-Score	Rot-Score	RMS-Value	Simil-Index	#Match	Avg. Volume	Max. Volume	Frag.No.
1	-19.866	-27.398	-9.127	-6.969	1.428	16.800	0.000	-1.000	12	0.060	0.574	1
2	-19.816	-27.543	-9.456	-6.934	1.916	16.800	0.787	-1.000	10	0.083	0.496	1
3	-19.719	-27.541	-9.224	-6.810	1.656	16.800	0.789	-1.000	10	0.062	0.404	1
4	-19.568	-27.053	-9.446	-6.991	1.722	16.800	0.730	-1.000	11	0.081	0.702	1
5	-19.305	-27.718	-8.580	-6.787	1.580	16.800	0.545	-1.000	10	0.055	0.284	1
6	-19.260	-26.990	-9.037	-6.944	1.512	16.800	0.683	-1.000	11	0.073	0.776	1
7	-19.254	-27.703	-8.427	-6.640	1.316	16.800	0.720	-1.000	10	0.046	0.280	1
8	-19.241	-27.767	-8.401	-7.125	1.352	16.800	0.997	-1.000	12	0.091	0.591	1
9	-19.165	-28.043	-8.553	-7.210	2.441	16.800	1.001	-1.000	11	0.184	1.760	1
10	-19.135	-27.522	-8.072	-6.873	1.132	16.800	1.094	-1.000	11	0.035	0.177	1
11	-19.131	-27.260	-8.700	-7.076	1.706	16.800	0.824	-1.000	11	0.079	0.587	1
12	-19.097	-27.900	-8.267	-6.998	1.367	16.800	0.663	-1.000	11	0.110	0.975	1
13	-19.092	-27.572	-8.314	-6.604	1.198	16.800	0.760	-1.000	11	0.039	0.192	1
14	-19.015	-27.971	-8.203	-6.917	1.376	16.800	0.612	-1.000	12	0.094	0.675	1
15	-18.986	-27.302	-8.360	-6.893	1.370	16.800	0.180	-1.000	11	0.055	0.501	1
16	-18.980	-27.046	-8.757	-6.825	1.448	16.800	0.645	-1.000	11	0.068	0.694	1
17	-18.966	-27.520	-8.271	-6.698	1.323	16.800	1.248	-1.000	11	0.043	0.275	1
18	-18.929	-27.602	-7.780	-6.864	1.117	16.800	1.463	-1.000	11	0.035	0.176	1
19	-18.889	-27.669	-8.461	-6.917	1.959	16.800	0.925	-1.000	10	0.085	0.411	1
20	-18.881	-27.628	-8.121	-6.443	1.112	16.800	0.994	-1.000	11	0.034	0.152	1
21	-18.800	-27.840	-8.043	-6.982	1.366	16.800	0.675	-1.000	11	0.124	1.183	1
22	-18.776	-27.060	-8.436	-6.875	1.395	16.800	0.524	-1.000	11	0.053	0.441	1
23	-18.768	-27.437	-8.304	-6.958	1.731	16.800	0.593	-1.000	12	0.063	0.359	1
24	-18.762	-27.957	-7.250	-6.939	1.183	16.800	1.774	-1.000	11	0.043	0.234	1
25	-18.756	-27.279	-9.189	-6.921	2.433	16.800	0.653	-1.000	10	0.140	0.817	1
26	-18.755	-27.753	-8.522	-6.972	2.291	16.800	0.479	-1.000	12	0.170	1.811	1
27	-18.751	-27.707	-8.480	-6.892	2.128	16.800	0.690	-1.000	11	0.107	0.660	1
28	-18.751	-27.631	-7.739	-6.970	1.389	16.800	1.389	-1.000	11	0.052	0.295	1
29	-18.743	-27.603	-8.326	-6.845	1.332	16.800	0.856	-1.000	10	0.093	0.793	1
30	-18.704	-27.320	-8.276	-6.679	1.371	16.800	0.688	-1.000	11	0.054	0.479	1

Table S3. Scoring values of HepMan with open-gate structure of FimH.

No.	Total Score	Match-Score	Lipo-Score	Ambig-Score	Clash-Score	Rot-Score	RMS-Value	Simil.-Index	#Match	Avg. Volume	Max. Volume	Frag.No.
1	-21.503	-30.724	-8.579	-5.941	1.542	16.800	0.000	-1.000	10	0.077	0.436	1
2	-21.399	-30.602	-8.706	-6.044	1.752	16.800	0.672	-1.000	10	0.106	0.939	1
3	-21.392	-30.357	-9.094	-5.849	1.708	16.800	0.832	-1.000	10	0.082	0.402	1
4	-21.249	-30.464	-8.438	-6.061	1.514	16.800	0.714	-1.000	10	0.078	0.439	1
5	-21.132	-30.282	-8.504	-5.961	1.414	16.800	0.714	-1.000	10	0.065	0.405	1
6	-21.112	-30.295	-9.097	-6.072	2.152	16.800	0.446	-1.000	10	0.117	0.805	1
7	-20.859	-30.418	-8.071	-5.938	1.369	16.800	0.828	-1.000	10	0.061	0.388	1
8	-20.851	-30.246	-8.445	-6.035	1.675	16.800	0.757	-1.000	10	0.076	0.356	1
9	-20.823	-29.872	-8.772	-6.262	1.883	16.800	0.567	-1.000	10	0.114	1.035	1
10	-20.684	-30.461	-7.874	-5.916	1.366	16.800	0.671	-1.000	10	0.060	0.453	1
11	-20.670	-30.364	-8.418	-5.900	1.812	16.800	0.912	-1.000	10	0.077	0.372	1
12	-20.588	-30.036	-9.263	-6.015	2.526	16.800	0.700	-1.000	10	0.153	1.367	1
13	-20.562	-30.080	-8.600	-5.881	1.800	16.800	0.652	-1.000	10	0.076	0.340	1
14	-20.561	-29.686	-8.467	-5.920	1.312	16.800	0.822	-1.000	10	0.059	0.363	1
15	-20.539	-30.202	-9.253	-6.326	3.043	16.800	0.632	-1.000	10	0.217	1.427	1
16	-20.538	-30.192	-8.174	-5.976	1.604	16.800	0.760	-1.000	10	0.071	0.346	1
17	-20.490	-29.746	-0.020	-5.950	1.029	16.000	0.617	-1.000	10	0.109	0.960	1
18	-20.489	-30.126	-8.136	-5.994	1.568	16.800	0.828	-1.000	10	0.065	0.361	1
19	-20.483	-30.632	-7.943	-5.886	1.778	16.800	0.764	-1.000	10	0.109	0.987	1
20	-20.475	-30.059	-8.142	-5.699	1.225	16.800	0.933	-1.000	10	0.056	0.380	1
21	-20.461	-30.709	-7.772	-5.659	1.479	16.800	1.433	-1.000	10	0.064	0.428	1
22	-20.451	-30.484	-8.082	-5.570	1.485	16.800	1.094	-1.000	10	0.064	0.399	1
23	-20.410	-30.095	-8.301	-6.436	2.223	16.800	0.660	-1.000	10	0.124	0.770	1
24	-20.365	-30.313	-7.825	-5.808	1.381	16.800	1.505	-1.000	10	0.062	0.380	1
25	-20.353	-30.763	-7.645	-5.963	1.819	16.800	0.739	-1.000	10	0.128	1.365	1
26	-20.336	-30.556	-8.021	-5.865	1.905	16.800	1.581	-1.000	10	0.085	0.409	1
27	-20.303	-30.367	-7.889	-6.097	1.850	16.800	0.853	-1.000	10	0.094	0.554	1
28	-20.207	-29.615	-8.095	-6.038	1.341	16.800	0.760	-1.000	11	0.064	0.423	1
29	-20.188	-30.638	-7.612	-5.684	1.547	16.800	1.467	-1.000	10	0.066	0.417	1
30	-20.175	-30.688	-7.410	-5.697	1.419	16.800	0.764	-1.000	10	0.062	0.426	1

Table S4. Scoring values of HepMan with closed-gate structure of FimH.

No.	Total Score	Match-Score	Lipo-Score	Ambig-Score	Clash-Score	Rot-Score	RMS-Value	Simil.-Index	#Match	Avg. Volume	Max. Volume	Frag. No.
1	-33.517	-35.510	-7.691	-8.099	1.183	11.200	0.000	-1.000	22	0.039	0.589	1
2	-32.812	-34.990	-7.526	-8.098	1.202	11.200	0.219	-1.000	21	0.045	0.687	1
3	-31.594	-34.063	-7.826	-8.268	1.963	11.200	0.861	-1.000	20	0.093	1.776	1
4	-31.246	-34.279	-7.442	-7.860	1.735	11.200	2.724	-1.000	20	0.069	0.920	1
5	-31.124	-33.804	-8.312	-7.987	2.379	11.200	0.743	-1.000	19	0.120	1.702	1
6	-30.858	-34.323	-8.306	-7.511	2.682	11.200	0.662	-1.000	21	0.140	1.378	1
7	-30.787	-34.148	-6.394	-7.689	0.844	11.200	2.882	-1.000	20	0.018	0.187	1
8	-30.761	-34.372	-6.626	-7.640	1.278	11.200	2.780	-1.000	20	0.036	0.386	1
9	-30.309	-34.240	-6.578	-7.378	1.288	11.200	2.722	-1.000	19	0.042	0.788	1
10	-30.300	-32.468	-8.418	-7.644	1.630	11.200	0.673	-1.000	22	0.068	1.199	1
11	-30.200	-34.223	-6.469	-7.311	1.203	11.200	2.823	-1.000	19	0.036	0.642	1
12	-30.177	-33.666	-6.220	-7.693	0.802	11.200	2.169	-1.000	21	0.021	0.422	1
13	-29.951	-34.100	-7.415	-7.618	2.582	11.200	2.650	-1.000	20	0.118	1.213	1
14	-29.795	-33.696	-6.442	-7.526	1.270	11.200	2.730	-1.000	19	0.036	0.636	1
15	-29.728	-32.493	-7.916	-7.909	1.990	11.200	4.468	-1.000	13	0.052	0.468	1
16	-29.613	-33.339	-6.004	-7.699	0.829	11.200	2.285	-1.000	21	0.023	0.457	1
17	-29.494	-33.157	-5.970	-7.827	0.860	11.200	2.207	-1.000	21	0.022	0.359	1
18	-29.201	-32.907	-7.556	-7.580	2.242	11.200	4.609	-1.000	14	0.069	0.619	1
19	-28.899	-33.631	-6.603	-7.873	2.608	11.200	2.368	-1.000	20	0.153	1.520	1
20	-28.869	-30.199	-8.397	-8.601	1.727	11.200	1.578	-1.000	19	0.065	1.161	1
21	-28.700	-31.733	-7.574	-7.861	1.868	11.200	5.076	-1.000	13	0.048	0.396	1
22	-28.673	-33.826	-6.694	-7.555	2.802	11.200	4.220	-1.000	15	0.124	1.505	1
23	-28.672	-29.583	-8.505	-8.508	1.325	11.200	1.770	-1.000	19	0.057	1.115	1
24	-28.275	-30.439	-8.661	-8.636	2.861	11.200	3.430	-1.000	17	0.158	1.539	1
25	-28.092	-33.509	-6.659	-7.663	3.139	11.200	4.310	-1.000	16	0.146	1.364	1
26	-28.073	-29.081	-8.872	-8.312	1.592	11.200	0.719	-1.000	19	0.060	0.979	1
27	-28.013	-29.831	-9.341	-8.866	3.425	11.200	2.888	-1.000	17	0.159	2.449	1
28	-27.975	-30.618	-8.524	-8.712	3.279	11.200	1.443	-1.000	20	0.169	1.837	1
29	-27.895	-33.159	-6.830	-7.268	2.762	11.200	2.531	-1.000	20	0.150	1.902	1
30	-27.882	-31.426	-7.214	-7.528	1.686	11.200	1.530	-1.000	20	0.089	2.075	1

Table S5. Scoring values of AzoMan with open-gate structure of FimH.

No.	Total Score	Match- Score	Lipo- Score	Ambig- Score	Clash- Score	Rot- Score	RMS- Value	Siril. Index	#Match	Avg. Volume	Max. Volume	Frag. No.
1	-35.596	-36.921	-7.687	-8.322	0.734	11.200	0.000	-1.000	17	0.014	0.175	1
2	-35.198	-36.890	-7.459	-8.194	0.746	11.200	0.648	-1.000	17	0.015	0.190	1
3	-35.022	-36.829	-7.420	-8.043	0.671	11.200	0.656	-1.000	17	0.012	0.137	1
4	-34.171	-36.045	-9.854	-8.578	3.706	11.200	2.526	-1.000	14	0.163	1.617	1
5	-33.231	-36.827	-7.058	-7.819	1.873	11.200	0.600	-1.000	17	0.069	0.975	1
6	-33.225	-35.902	-7.301	-7.622	1.000	11.200	0.612	-1.000	16	0.018	0.173	1
7	-33.223	-35.924	-7.192	-7.885	1.179	11.200	0.559	-1.000	16	0.026	0.274	1
8	-33.156	-34.946	-7.668	-7.707	0.563	11.200	0.386	-1.000	17	0.009	0.082	1
9	-32.895	-35.565	-6.880	-8.155	1.104	11.200	0.453	-1.000	14	0.027	0.410	1
10	-32.710	-35.784	-7.085	-7.428	0.987	11.200	0.767	-1.000	16	0.019	0.183	1
11	-32.694	-36.403	-6.806	-7.754	1.669	11.200	0.906	-1.000	17	0.058	0.751	1
12	-32.625	-35.580	-7.065	-8.364	1.784	11.200	1.251	-1.000	18	0.058	0.626	1
13	-32.418	-35.204	-6.807	-8.492	1.485	11.200	1.329	-1.000	17	0.046	0.655	1
14	-32.342	-35.175	-7.083	-7.984	1.300	11.200	1.037	-1.000	16	0.034	0.415	1
15	-32.317	-36.016	-6.333	-7.938	1.370	11.200	0.879	-1.000	18	0.041	0.439	1
16	-32.129	-34.666	-7.765	-8.419	2.121	11.200	1.352	-1.000	17	0.059	0.594	1
17	-32.073	-35.122	-6.844	-8.036	1.328	11.200	1.115	-1.000	15	0.036	0.429	1
18	-32.025	-35.478	-6.251	-7.824	0.928	11.200	0.563	-1.000	14	0.023	0.315	1
19	-32.005	-32.759	-8.944	-8.147	1.245	11.200	2.846	-1.000	18	0.033	0.434	1
20	-31.784	-34.843	-6.709	-8.381	1.549	11.200	1.077	-1.000	14	0.050	0.566	1
21	-31.778	-35.595	-5.870	-7.904	0.990	11.200	0.785	-1.000	14	0.028	0.416	1
22	-31.667	-34.300	-8.003	-7.771	1.807	11.200	2.386	-1.000	15	0.066	1.153	1
23	-31.431	-32.554	-8.804	-7.793	1.120	11.200	2.895	-1.000	18	0.032	0.414	1
24	-31.243	-33.475	-9.438	-7.542	2.611	11.200	4.892	-1.000	14	0.125	1.547	1
25	-31.200	-32.194	-8.904	-7.949	1.246	11.200	2.930	-1.000	17	0.037	0.391	1
26	-31.132	-35.273	-5.725	-7.693	0.959	11.200	0.828	-1.000	14	0.026	0.338	1
27	-31.087	-33.734	-7.690	-9.248	2.985	11.200	2.289	-1.000	13	0.108	0.947	1
28	-30.968	-33.571	-9.095	-8.360	3.458	11.200	5.755	-1.000	14	0.186	2.470	1
29	-30.842	-33.479	-9.093	-7.459	2.588	11.200	2.812	-1.000	17	0.097	0.911	1
30	-30.758	-34.932	-5.996	-7.540	1.110	11.200	0.902	-1.000	13	0.027	0.375	1

Table S6. Scoring values of Azoman with closed-gate structure of FimH.

7. Statistics. Seven determinations with two to three wells per test compound concentration for the fluorescence-based inhibition assays and three to eight determinations with three wells per test compound concentration for the cytotoxicity assays were carried out as mentioned above with cultures of different subcultivations. Mean values of determinations from different cultures and the standard errors of the mean (SEM) were calculated and shown in the diagrams (Fig. 2, 4, and 5). Median effective and inhibitory concentrations ($EC_{10,50}$ and $IC_{50,90}$ values) were determined by using the software *GraphPad Prism* version 4.01 for Windows (GraphPad Software, San Diego California USA, www.graphpad.com). Curve fitting was done by nonlinear regression analysis using the Hill equation:

$$Y = \frac{BOTTOM + (TOP - BOTTOM)}{1 + 10^{\log\left(\frac{EC_{50}}{X}\right) \bullet Hillslope}}$$

with X = non-logarithmic concentrations of α -mannoside inhibitors and the constraints BOTTOM = 0 and TOP = 100.

4. Preparation and applications of azobenzene glycosides on surfaces

Investigation of carbohydrate-protein interactions using glycoarrays is of growing interest and has received much attention in the glycosciences.^[45, 104-106] Glycoarrays are carbohydrate-functionalized surfaces, in which carbohydrates are immobilized on different surfaces like gold, glass or polystyrene. Each surface requires a specific type of functional group for immobilization of the respective molecule.

For example, one of the most reliable and flexible constructions of well-ordered glycoarrays are self-assembled monolayers (SAMs) on gold.^[107, 108] For the formation of SAMs, mercapto-functionalized alkanes are used to form ordered layers on the gold surface via the formation of Au-S bonds. SAMs that are functionalized with carbohydrate head groups, are called glyco-SAMs.^[109-110] Glyco-SAMs offer an extensive control over the density and orientation of the carbohydrate ligands on the surface. In addition, glyco-SAMs can be used to study carbohydrate-protein interactions on surfaces.^[111] When SAMs are used that expose photoswitchable glycoazobenzene moieties, even conformational effects of carbohydrate recognition can be studied. Thus, we have designed photoswitchable glyco-SAMs to form carbohydrate-functionalized monolayers on gold-surfaces (chapter 4.1). In addition, glycoazobenzene decorated gold nanoparticles (GNPs) were formed and their photoisomerization and interaction with lectin ConA was studied (chapter 4.2).

4.1 Monitoring of *trans*→*cis* isomerization of azobenzene glyco-SAMs on gold surfaces using IRRAS

The molecules that were required for the formation of such SAMs are prepared by a combination of glycosylation and Mitsunobu reaction (Fig 4.1). To study the success of *E*→*Z* isomerization of azobenzene glyco-SAMs on the gold wafers, this process was monitored by infrared reflection absorption spectroscopy (IRRAS) in collaboration with the group of Prof. F. Tuczek (CAU Kiel). The respective work is presented here in the form of a first manuscript.

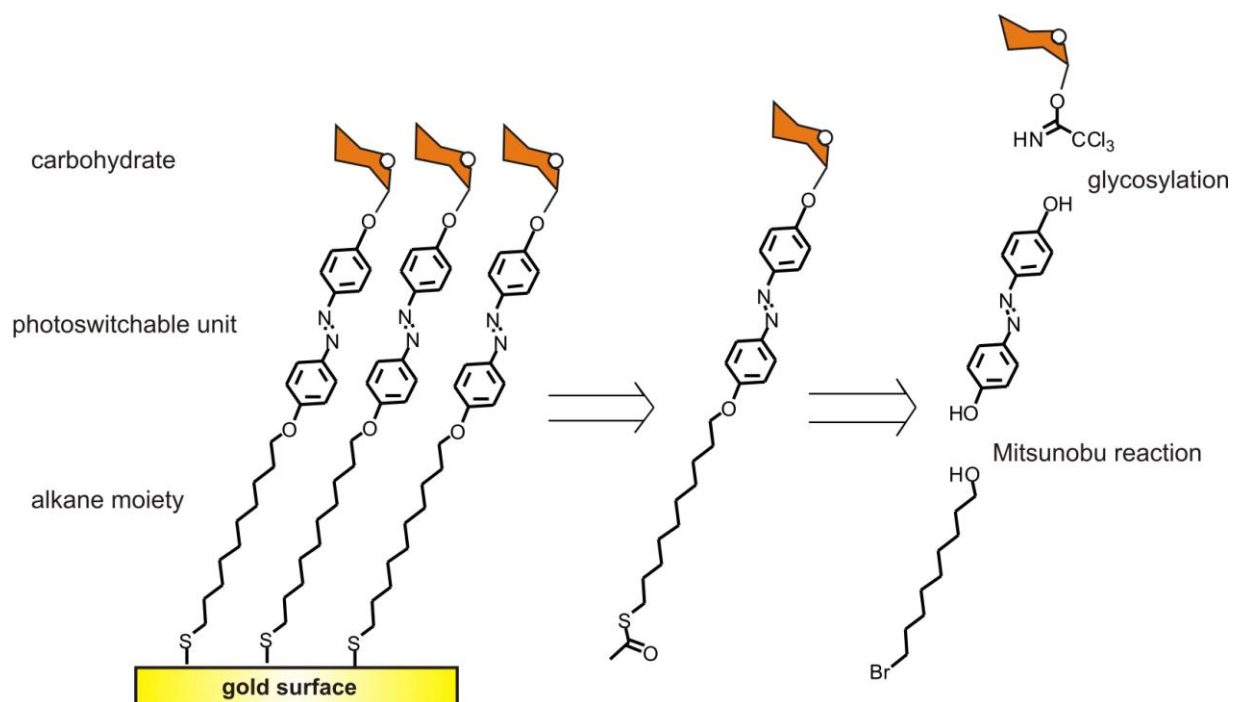


Figure 4.1: Schematic depiction for the construction of photoswitchable azobenzene glyco-SAMs on gold.

In this collaborative work, K. Kathirvel and H. Jacob (Prof. Tuczek research group) did the IRRAS measurements. I did the synthesis and characterization of the substances, studied the photochromic properties in solution, prepared the SAMs and mSAMs. I and T. K. Lindhorst wrote the manuscript.

Monitoring of *trans*→*cis* isomerization of azobenzene glyco-SAMs on gold surfaces using IRRAS

Vijayanand Chandrasekaran ^a, Ketheeswari Kathirvel ^b, Hanne Jacob ^b Felix Tuzek ^b, Thisbe K. Lindhorst ^{a*}

^a *Otto Diels Institute for Organic Chemistry, Christiana Albertina University of Kiel, Otto-Hahn-Platz 3-4, D-24098 Kiel, Germany, tkind@oc.uni-kiel.de*

^b *Institute for Inorganic Chemistry, Christiana Albertina University of Kiel, Olshausenstr. 40, 24098 Kiel, Germany*

4.1.1 Introduction

Besides proteins and nucleic acids, the third class of essential biomolecules, the carbohydrates, serve as molecular key players in cell recognition and cell communication. They are displayed on cell surfaces largely in the form of glycoconjugates, that are partly embedded in the plasma membrane or are attached to the cell surface molecules by adhesive forces forming a sticky, nanodimensioned layer termed “glycocalyx”. Glycocalyx carbohydrates like mannosides and other glycosides are implicated in essential biological events such as cell development and health, cell adhesion, cell signaling and immune response.^[1-3] However, the glycome of a cell comprises an overwhelming molecular complexity and it has been difficult to connect carbohydrate-dependent biological phenomena to distinct carbohydrate structures. To deepen our understanding of the various molecular interactions that occur on glycosylated cell surfaces, carbohydrate-protein and recently also carbohydrate-carbohydrate interactions have been extensively studied.^[4-8] In addition, it has been attempted to vary the presentation of carbohydrate ligands on surfaces and their conformational availability. A well-defined and reliable system for studies of this kind is offered by self-assembled monolayers on gold, in short SAMs^[9-11] which can be functionalized with carbohydrate head groups to obtain “glyco-SAMs”.^[12-17]

In order to obtain switchable monolayers, SAMs have also been fabricated employing photoresponsive functionalized azobenzene derivatives.^[18] In azobenzene SAMs the $E \rightarrow Z$ isomerization of an immobilized azobenzene derivative allows to manipulate the spatial arrangement of functional groups connected to the azobenzene moiety. It has become our goal to utilize a new class of glycosidic azobenzenes to switch the status of a glycosylated monolayer to eventually study the effect of conformational changes within a glycosylated surface on carbohydrate-specific cellular adhesion. This will allow to learn more about the importance of conformational control in carbohydrate recognition, a well-known biological principle, that has not received considerable attention in the glycosciences so far.

For any biological study with switchable surfaces, it is of primary importance to characterize if irradiation of the surface has the desired effect on the immobilized molecular monolayer. Consequently, we have synthesized glycosidic azobenzene derivatives suited for SAM formation on gold (Fig. 4.1.1) and investigated infrared reflection absorption spectroscopy (IRRAS) to monitor isomerization of the monolayer upon irradiation at the appropriate wavelength of 365 nm.

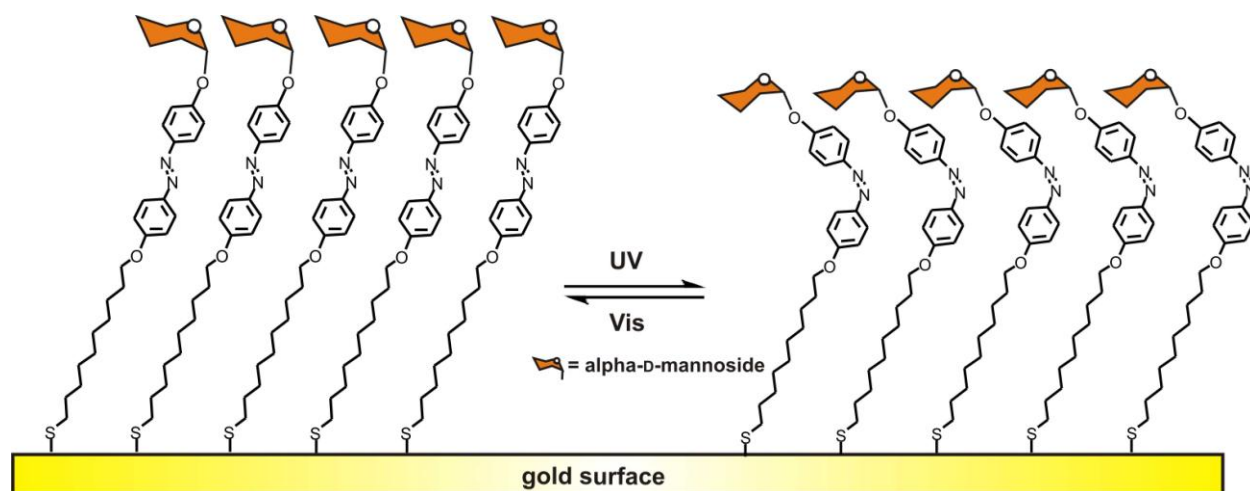
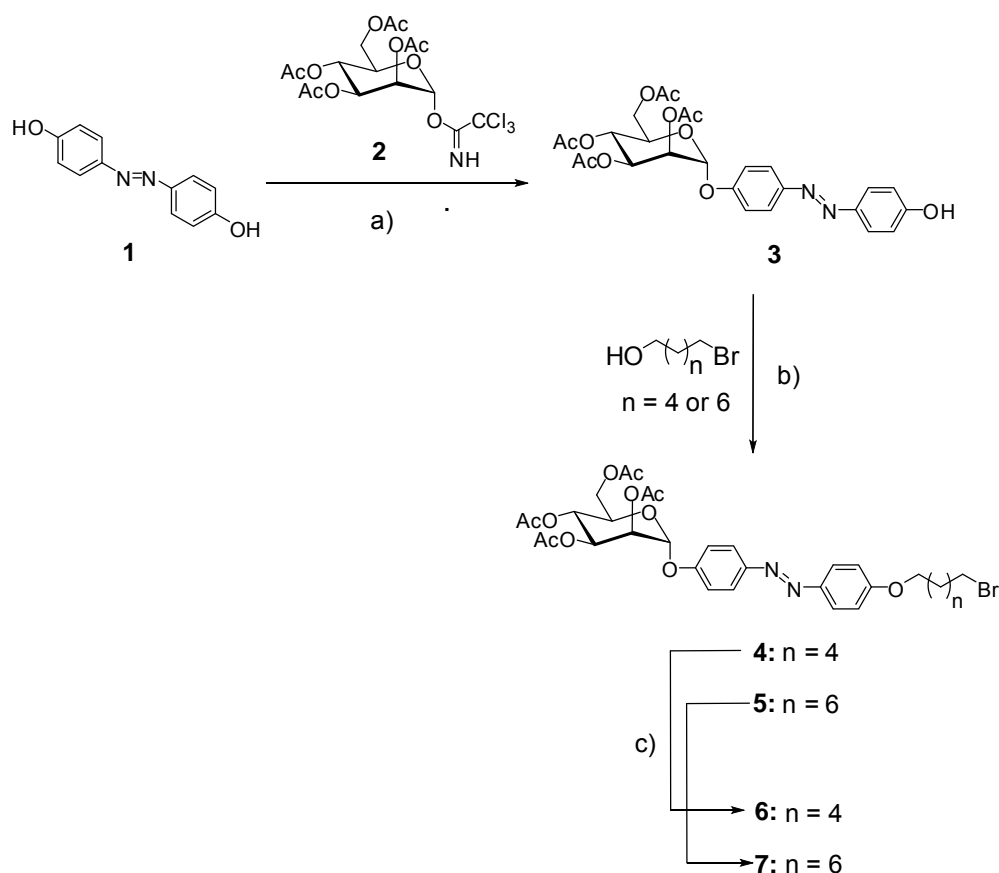


Figure 4.1.1: Schematic representation of switchable glyco-SAMs on a Au(111) surface. Photoinduced $trans \rightarrow cis$ isomerization of azobenzene glycoside head groups is thought to change the presentation of carbohydrate ligands on a surface.

Results and discussion

4.1.2 Synthesis of azobenzene derivatives for SAM formation

To achieve our target molecules for glyco-SAM formation, azobenzene glycoside **3** was prepared first (Scheme 4.1.1). Thus, *p,p'*-dihydroxyazobenzene **1** was synthesised according to a literature procedure.^[19] Glycosylation of **1** with mannosyl donor **2** gave the glycosylated product **3** in 37% yield.^[20] Reaction of **3** with 6-bromohexan-1-ol and 10-bromodecan-1-ol under Mitsunobu conditions gave the required product **4** in 82% and **5** in 79% yield respectively.^[21, 22] At room temperature potassium thioacetate converted the bromo alkanes **4** and **5** into the desired thioacetates **6** and **7** in 88 and 91% yields.^[23] The obtained glycothioacetates were used for the formation of self-assembled monolayers (SAMs) on gold wafers.



Scheme 4.1.1: a) $\text{BF}_3 \cdot \text{Et}_2\text{O}$, dry CH_2Cl_2 , $0\text{ }^\circ\text{C} \rightarrow \text{rt}$, overnight, 37%; b) PPh_3 , DEAD, rt, 5 h, 82% (**4**), 79% (**5**); c) KSac , rt, overnight, 88% (**6**), 91% (**7**).

4.1.3 Fabrication of SAMs and their characterization by IRRAS

First, optimal conditions for SAM formation were investigated. SAM formation on Au(111) depends on the formation of Au-S bonds between the gold surface and an applied thiols. Thioacetates are advantageous over free thiols as they are stable against oxidation to the respective disulfides, which readily occurs at air.^[24, 25] In order to obtain SAMs, thioacetates can be easily deprotected by deacetylation with a base to form the respective thiols.^[26, 27] Some investigations, however, have shown that no cleavage agent is required to form SAMs with thioacetates and direct deprotection to deliver the thiol can occur at the gold surface.^[28] Thus, the formation of SAMs using thioester **6** has been tested by both methods, direct adsorption and base-promoted adsorption. In direct adsorption higher concentrations of the thioester substrate are required to achieve monolayer coverage in a given interval. In addition, slow deprotection of the acetyl group of thioester **6** required longer reaction times to form a well-ordered SAM. When SAM formation was performed base-promoted, using ammonium hydroxide in a solution of **6**, SAMs of higher quality were obtained (Fig 4.1.2). In case of base-promoted adsorption, the vibrational band exhibits stronger intensity when compared to that of the direct adsorption, whereas in direct adsorption some of the bands were broadened.

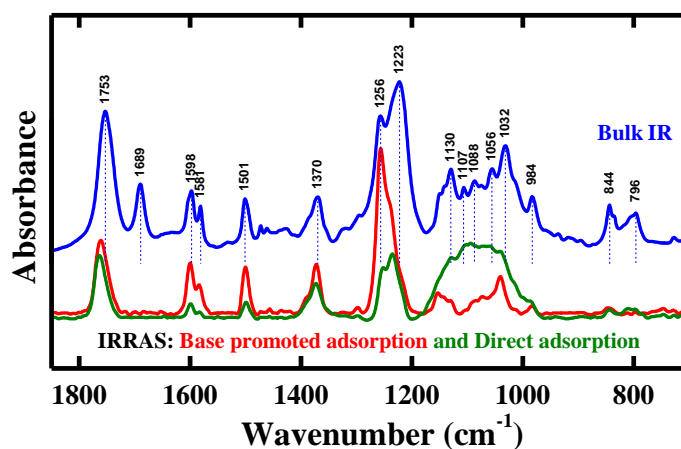


Figure 4.1.2: Mid- to low-frequency regions of IR spectroscopic data of bulk **6** in KBr and SAM of **6** prepared by direct and base-promoted method.

In the bulk spectrum of compound **6**, C=O stretching vibration of the acetyl group originating from the mannoside moiety is observed at 1753 cm^{-1} . The carbonyl band from thioester is observed at a lower frequency at 1689 cm^{-1} . In both, direct and base-promoted adsorption of **6**, the absence of the C=O stretching vibration related to thioester indicates the complete conversion of thioacetate to thiolate, chemisorbed to the gold surface. The intensity of the carbonyl band related to ester groups from the sugar unit remains almost the same in both direct and base-promoted adsorption. The employed weak base (which) selectively deprotects the thioacetate bond without affecting the O-acetyl protecting groups of the mannoside moiety. In addition, the employed basic conditions did not affect or even destroy the monolayer. On the contrary, base results in SAMs of better quality. Consequently, base-promoted adsorption was used to prepare all other monolayers investigated in this study.

It has been shown earlier that thiols and thioacetates, respectively, of longer chain length result in better SAMs than shorter chain molecules.^[29] In order to study the effect of chain lengths on the SAM formation glycosylated azobenzene alkanethioacetates with two different alkane spacer lengths were used (Fig 4.1.3) compound **6** with a hexyl spacer and compound **7** with a decyl spacer.

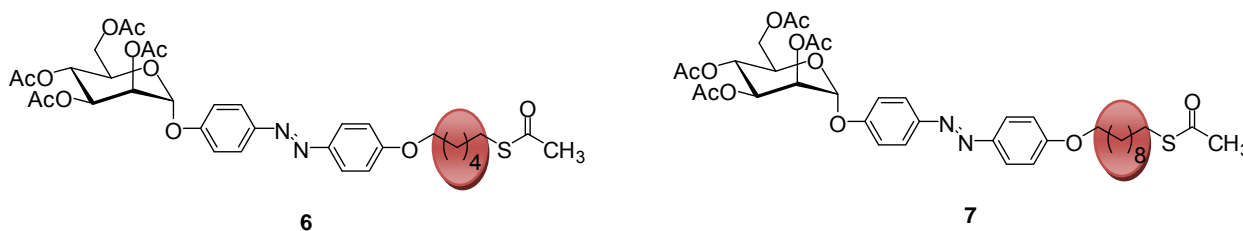


Figure 4.1.3: Glycoazobenzenes with different alkane spacer lengths used for SAM formation.

Indeed, SAM formation with mannoside **7** resulted in a well-ordered monolayer with a higher degree of surface coverage and less defects than those SAMs formed from mannoside **6**. In the mid- to low-frequency regions ($1800\text{-}800\text{ cm}^{-1}$) the IRRAS spectra of compounds **6** and **7** look similar. The CH₂ symmetric and asymmetric stretching vibrations are more pronounced in the case of compound **7** and relatively weak in the case of compound **6**. These results encouraged us to use the longer chain length compound **7** for further experiments and explore the $E\rightarrow Z$ isomerization on the gold surface.

As per the surface selection rule (SSR), only the vibrations with a component of the transition dipole moment (TDM) aligned perpendicular to surface plane can interact with the incident light and can be observed in the infrared spectrum. The presence of less number of bands in the IRRAS when compared to that of the bulk spectrum is a result of the surface selection rule. Vibrational bands with TDMs that are exactly perpendicular to the gold surface are most intense. On the other hand the TDMs which are parallel to the metal surface are absent. Some TDMs are neither parallel nor perpendicular are seen in IRRAS. In compound **7** the highly intense peak originates from the carbonyl group of the mannose sugar. This indicates that the molecules are oriented perpendicular to the surface. The bulk KBr pellet IR measurements and calculated vibrational frequencies were assigned for compound **7** to compare with the IRRAS measurements (Table S1: see supporting information).

4.1.4 *E*→*Z* isomerization of compound **7** in solution

As the mannosyloxy-azobenzene alkane thioester **7** formed glyco-SAMs which could be characterized by IRRAS, their photoisomerization was studied next. Before exploring the *E*→*Z* isomerization of compound **7** on the gold surface, its photochromic properties were determined in solution. Photoirradiation of *trans*-**7** in CDCl₃ was carried out in the dark at room temperature using high pressure Hg lamp. Photostationary states (pss) were reached after 30 min and formation of *cis*-**7** was monitored by UV-Vis and ¹H NMR spectroscopy. Based on the integration of anomeric H-1 protons, the *cis*:*trans* ratio was determined by proton NMR spectroscopy. In the ground state more than >99% of the *trans*-isomer was observed and after irradiation > 99% of the *cis* isomer was observed, in PSS (Fig 4.1.4).

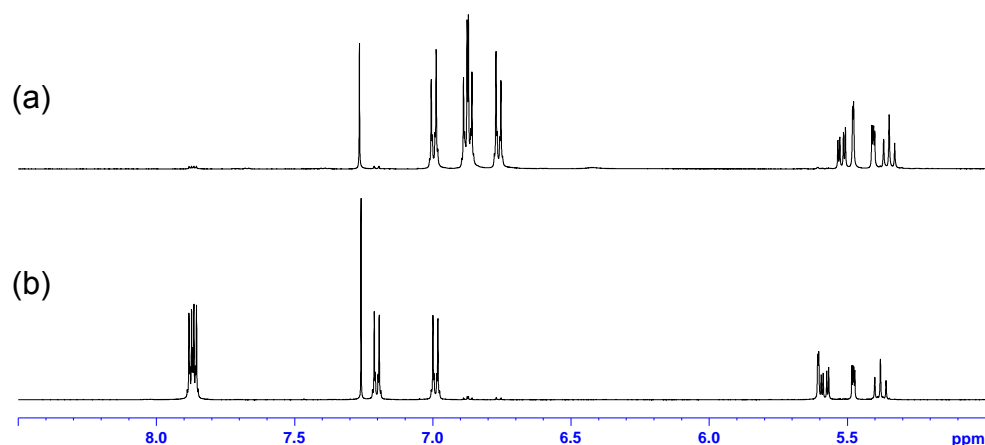


Figure 4.1.4: Partial ¹H NMR spectra (500 MHz, CDCl₃) spectra (a) *cis*-**7**; (b) *trans*-**7**.

In addition, $E \rightarrow Z$ isomerization of compound **7** can be nicely distinguished by UV-VIS spectroscopy, showing the typical absorption maxima of 353 nm for the *trans*-isomer and after reaching PSS an increase in absorption maxima of 444 nm and decrease in absorption at 353 nm for *cis*-isomer was observed (Fig 4.1.5). By using UV-Vis spectroscopy, the rate constant and half life of both *cis*-configured azobenzene mannosides **6** and **7** were obtained (see supporting information).

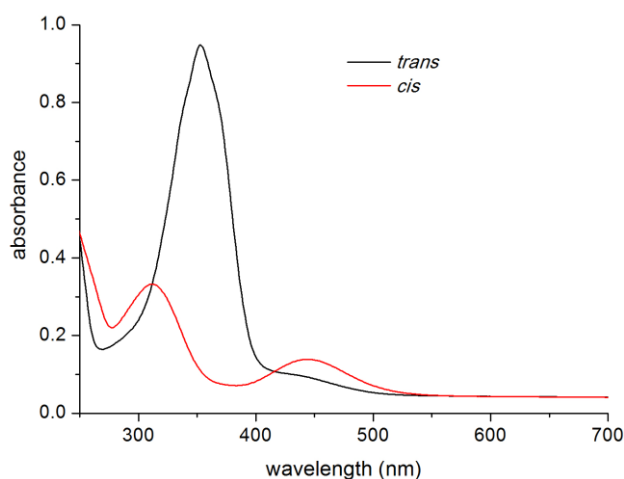


Figure 4.1.5: UV-Visible spectra of *cis*-**7** and *trans*-**7** in ethanol at ± 18 °C

4.1.5 IRRAS study of $E \rightarrow Z$ isomerization of photoswitchable glyco-SAMs

Next, it has to be tested by IRRAS whether $E \rightarrow Z$ isomerization of azobenzenes glyco-SAMs occurs. This was tested applying two different approaches. In the first approach a solution of the *trans*-isomer was irradiated to reach the PSS to obtain the *cis*-isomer and then gold wafers were immersed into the irradiated solution to form a SAM with *cis*- isomer of **7** on the gold surface. By this approach, no difference in the vibrational structures was observed between the *cis*- and *trans*-isomers of compound **7** on the gold surface by IRRAS.

In the second approach, the SAMs were first formed from *trans*-**7** on the gold surface. Then the *trans*-**7**-functionalized gold substrates were irradiated with UV light at 365 nm for about 30-45 min to form the *cis*-**7**. It is noted after irradiation, a peak at 1253 cm^{-1} assigned for C-O stretching, carbon from the aromatic ring attached to the oxygen of anomeric carbon of

mannose, showed a slight decrease in intensity. Mid to low frequency region of compound **7** with *cis*- and *trans*-isomers are shown (Fig 4.1.6a), a decrease in the intensity at 1253 cm⁻¹ for the *cis*-isomer with respect to the *trans*-isomer are observed (Fig 4.1.6b).

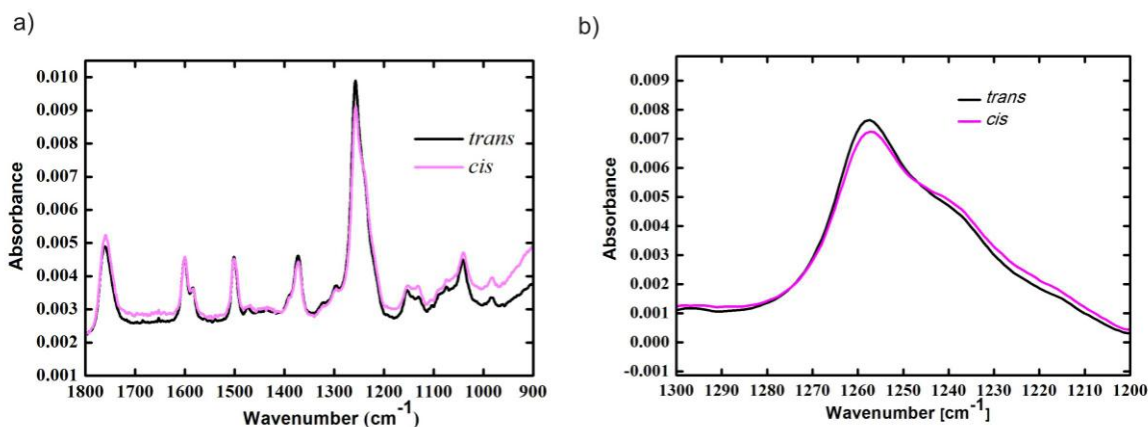


Figure 4.1.6: *cis-trans* isomerization of compound **7** on the gold surface by IRRAS spectra a) Mid to low frequency region of *trans*- and *cis*-isomer; b) C_{aromatic}-O_{mannose} stretching frequency of *trans* and *cis*-isomer.

In solution *E*→*Z* isomerization of compound **7** was clearly differentiated by UV-Vis and ¹H NMR spectroscopy. But, this was not observed on the gold surface. It might be reasoned that, in solution azobenzene molecules are free in motion but on the surface these molecules are closely packed where steric hindrance comes into play. The closely packed arrangements of molecules on SAM can alter the behavior and in addition, the molecules are tilted on the surface which may also cause less degree of freedom required for the *E*→*Z* isomerization process.

4.1.6 Preparation of mixed monolayers and IRRAS study of *E*→*Z* isomerization

From the previous experiment it was observed that the *trans*-**7** forms a well-ordered SAM which is stable at room temperature. But apparently the *E*→*Z* isomerisation of this SAM did not work, most likely due to steric hindrance. To address these concerns, mixed SAMs (*m*SAMs) were prepared, which increase the space between *trans*-**7** molecules and the *E*→*Z* isomerization on the surface should be facilitated. *m*SAMs formation was effected by two different approaches: a co-adsorption method and a two- step deposition method. In the co-

adsorption method, the SAM is formed from a mixture of different substances. Firstly, a solution mixture of diluting molecule **8** or **9**, respectively (Fig 4.1.7) along with the required azobenzene derivative **7** was used for *m*SAMs formation. The second method is a two-step deposition process: first a SAM was formed using either **8** or **9** and later it was allowed to undergo an exchange reaction by addition of *trans*-**7** to form *m*SAMs. As ‘diluter’ molecules, in this study the phenoxy-headed hexylthioacetate **8** and 1-undecanethioacetate **9** were used and prepared according to the literature.^[23, 30, 31]



Figure 4.1.7: ‘Diluter’ molecules for formation mixed SAMs.

Compound **8** was chosen as the bulky phenyl head group might push the azobenzene moieties apart and to facilitate *E*→*Z* isomerization on the *m*SAMs (Fig 4.1.8).

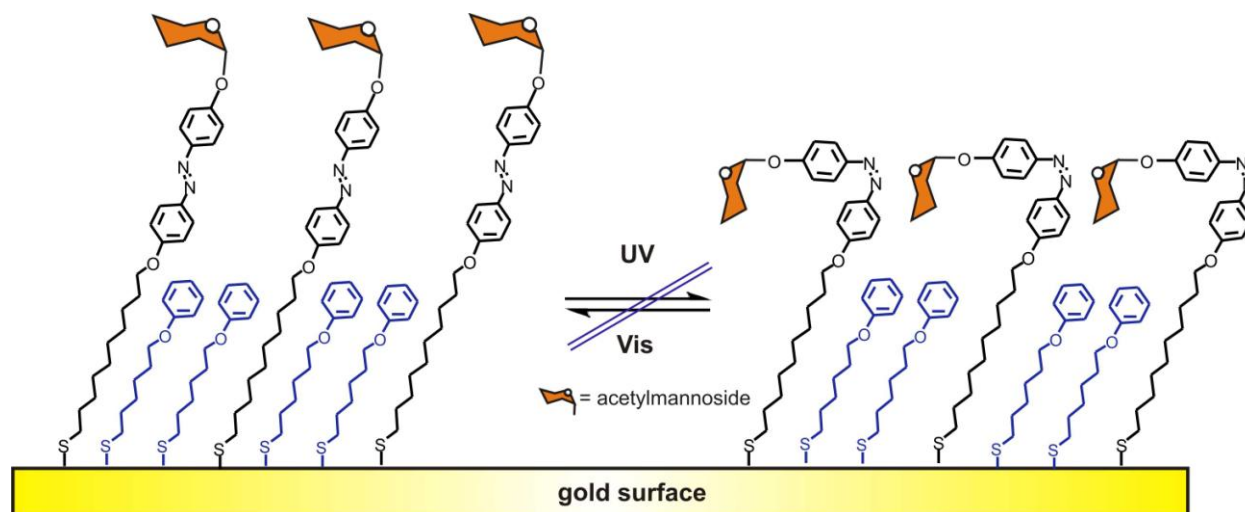


Figure 4.1.8: Schematic representation of *E*→*Z* isomerization of *m*SAMs formed from **7** and **8**.

In the two-step deposition approach, the SAM was formed using **8** in 1 mM ethanol and immersion for 24 h. In the second step, the SAM obtained from diluter molecule **8** was then immersed into a 1 mM solution of *trans*-**7**. The carbonyl band related to the mannosyl moiety was expected in the respective IRRAS spectrum. This particular vibrational band is used as a marker to follow the exchange reaction. Unfortunately even after 2 days no vibrational band

related to C-O was observed, this supports the assumption that exchange reaction was not successful. In the co-adsorption method, *m*SAMs was performed by using different ratios of diluter and azobenzene glycosides (a solution of **7** and **8** at ratios of (a) 3:7, (b) 1:1, (c) 1:10) were tried. In the respective IRRAS spectrum, the vibrational bands related to *trans*-**7** are dominating and no bands related to **8** are pronounced, confirming the formation of *m*SAMs by this approach was also unsuccessful.

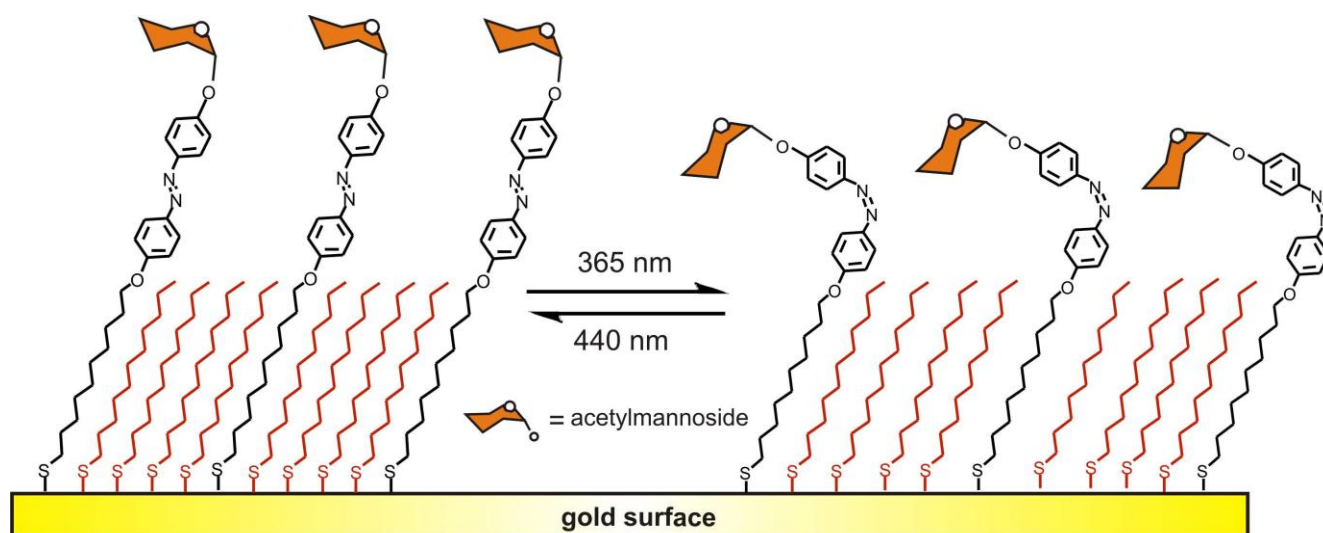


Figure 4.1.9: *E*→*Z* isomerization of *m*SAMs formed from **7** and **9**.

Our next attempt was to prepare the mixed monolayer using **9** as the diluting molecule (Fig 4.1.9). The, formation of mixed SAMs was attempted by using different ratios of *trans*-**7** and **9**. The best result was obtained with a ratio of **7**:**9** of 1:4. Typically, an ethanolic mixture of *trans*-**7** and **9** was co-adsorbed with a total thiol concentration of 1 mM for 24 hours. Finally, with this *m*SAMs photoirradiation at 365 nm for about 30 min was successful, leading to *cis*-isomer of **7** on the gold surface (Fig 4.1.10).

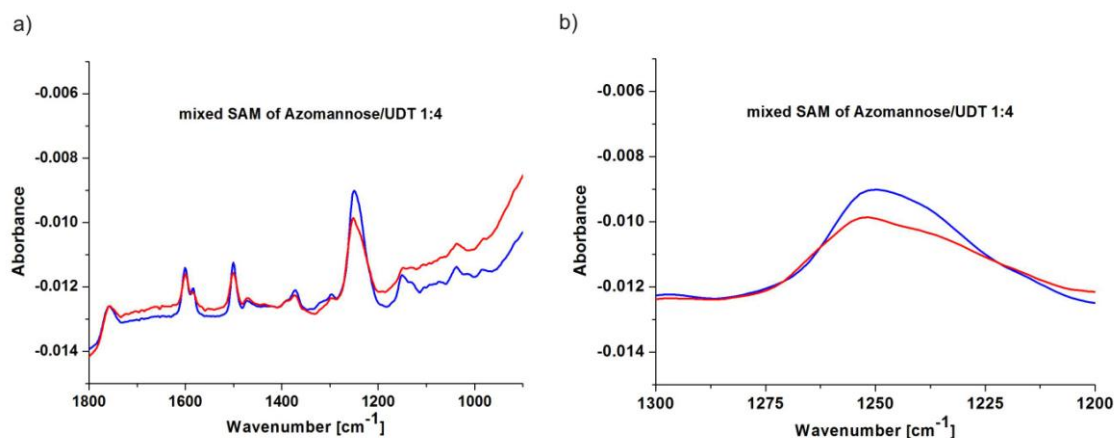


Figure 4.1.10: $E \rightarrow Z$ isomerization of m SAMs formed from $trans$ -**7** and **9** (1:4). (a) Mid to low frequency regions; (b) C-O stretching frequency (1253 cm^{-1}) of $trans$ - and cis - m SAMs.

After photoirradiation, a change in the vibrational frequency at $\sim 1253 \text{ cm}^{-1}$ was observed and rest of the vibrational frequencies did not alter much (Fig 4.1.10a). After irradiation, pronounced difference in the intensity of the C-O stretching band was observed (Fig 4.1.10b). Thus, this m SAM was suited to effect $E \rightarrow Z$ photoisomerization on SAM.

4.1.7 Conclusion

In conclusion, photoswitchable azobenzene glycosides were synthesised in high yields and used for the formation of self-assembled monolayers (SAMs). SAM formation of acetyl protected azobenzene mannosides was monitored by IRRAS. The $E \rightarrow Z$ isomerization process was successful in m SAMs using **7** and **9** with the ratio of 1:4. Our next goal is to reproduce the m SAMs with OH-free mannoside as a photoswitchable adhesive surface and test bacterial adhesion to the different isomers on the surface.

Experimental

Materials and Methods

Thin-layer chromatography was performed on silica gel plates (GF 254, Merck). Detection was effected by UV and subsequent charring with 10% sulphuric acid in EtOH followed by

heat treatment ~ 180 °C. Flash chromatography was performed on silica gel 60 (230-400 mesh, particle size 0.040-0.063 mm, Merck) using distilled solvents. Optical rotations were measured with a Perkin-Elmer 241 polarimeter (sodium D-line: 589 nm, length of cell: 1 dm) in the noted solvent. ¹H and ¹³C NMR spectra were recorded with Bruker DRX-500 and AV-600 spectrometers. Chemical shifts are reported relative to internal tetramethylsilane (δ = 0.00 ppm) or D₂O (δ = 4.76 ppm). Data are reported as follows: chemical shift, multiplicity (s = singlet, d = doublet, t = triplet, q = quadruplet and m = multiplet), coupling constant in Hz, integration and assignment. IR spectra were measured with a Perkin Elmer FT-IR Paragon 1000 (ATR) spectrometer. ESI-MS measurements were recorded at the Esquire-LC from Bruker Daltonics. MALDI-TOF mass spectra were recorded on a Bruker Biflex III instrument with 19 kV acceleration voltage. 2,5-dihydroxybenzoic acid (DHB) was used as a matrices. Air/moisture sensitive reactions were carried out under nitrogen. UV-Vis absorption spectra were performed on Perkin-Elmer Lambda-14 and Varian Cary-5000 with temperature (18 ± 1 °C). Photoirradiation was carried out with a high pressure mercury lamp UV-P 250C from Panacol-Elosol. The bandpass filters were purchased from Laser components. Melting points were determined on Büchi 510 apparatus. Glass substrates with a 50 Å titanium base layer and a 1000 Å evaporated gold film were purchased from EMF Corporation (Ithaca, NY) for IRRAS measurements.

Synthesis of photoswitchable azobenzene glycosides

4-(4'-Hydroxyphenylazo)phenyl α-D-mannopyranoside (3): The azobenzene derivative **1** (200 mg, 0.934 mmol) and the mannosyl donor **2** (1.0 g, 2.03 mmol) were dissolved in dry CH₃CN (15 mL), BF₃-Et₂O (260 μL, 2.01 mmol) was added at 0 °C, under nitrogen atmosphere and maintained at this temperature for about 15 min. The reaction mixture was stirred at room temperature overnight, then added NaHCO₃ (5 mL) and further diluted with ethyl acetate (100 mL) and washed with water (2×20 mL), phase separated, organic layer dried over Na₂SO₄, filtered and the filtrate was concentrated under reduced pressure to get the crude product which after purification by column chromatography (cyclohexane/ethyl acetate, 6:4) gave the desired mannoside **3** as a yellow crystalline solid (190 mg, 0.349 mmol, 37%). Mp 109-110 °C; *R*_f = 0.26 (cyclohexane/ethyl acetate, 1:1); [α]_D²⁰ = + 0.75 (c = 1.0, CH₂Cl₂); ¹H NMR (600 MHz, CDCl₃, 300.1 K): δ = 7.85 (d, *J* = 8.9 Hz, 2H, 14, 18), 7.83 (d, *J* = 8.9 Hz, 2H, 9, 11), 7.19 (d, *J* = 8.9 Hz, 2H, 15, 17), 6.94 (d, *J* = 8.8 Hz, 2H, 8, 12), 5.61 (d,

$J_{1,2} = 1.6$ Hz, 1H, H-1), 5.59 (dd, $J_{3,4} = 10.0$, $J_{3,2} = 3.4$ Hz, 1H, H-3), 5.48 (dd, $J_{2,3} = 3.5$ Hz, $J_{2,1} = 1.8$ Hz, 1H, H-2), 5.39 (t, $J_{4,3} = J_{4,5} = 10.1$ Hz, 1H, H-4), 4.30 (dd, $J_{6a,5} = 12.1$, $J_{6a,6b} = 5.3$ Hz, 1H, H-6a), 4.12-4.08 (m, 2H, H-5, H6b), 2.22, 2.07, 2.06, 2.04 (s, 12H, 4 OAc); ^{13}C -NMR (150 MHz, CD_3OD , 299.9 K): $\delta = 170.7$, 170.3, 170.1, 169.8 (C=O, OAc), 158.3 (C-7), 157.2 (C-16), 148.5 (C-13), 147.1 (C-10), 124.8 (14/18), 124.3 (9/11), 116.8 (15/17), 115.8 (8/12), 95.7 (C-1), 69.4 (C-5), 69.3 (C-2), 68.9 (C-3), 65.9 (C-4), 62.1 (C-6), 20.9, 20.7, 20.7, 20.7 (CH_3COO); IR (ATR): 3407, 1744, 1587, 1498, 1368, 1211 cm^{-1} ; ESI-MS: Calcd for $\text{C}_{26}\text{H}_{28}\text{N}_2\text{O}_{11}$ $[\text{M}+\text{Na}]^+$: $M_{\text{calcd}} = 567.51$, $M_{\text{found}} = 567.16$.

***trans*-4-(4'-Bromohexylphenylazo)phenyl 2,3,4,6-tetra-O-acetyl- α -D-mannopyranoside (4):**

To a mixture of mannoside **3** (300 mg, 0.551 mmol), 1-bromohexanol (150 mg, 0.827 mmol), triphenylphosphine (217 mg, 0.827 mmol) in dry THF (6 mL) at 0 °C DEAD (143.9 mg, 0.827 mmol) was added and the reaction mixture stirred for 5 h. Then it was evaporated to dryness and the crude product purified by column chromatography (cyclohexane/ethyl acetate, 3:2) gave the title compound **4** as a light yellow solid (320 mg, 0.453 mmol, 82%). Mp 99-100 °C; $R_f = 0.41$ (cyclohexane/ethyl acetate, 3:2); $[\alpha]_D^{20} = +0.588$ ($c = 1.0$, CH_2Cl_2); ^1H NMR (500 MHz, CDCl_3 , 300.0 K): $\delta = 7.81$ (d, $J = 8.9$ Hz, 2H, 14, 18), 7.80 (d, $J = 8.9$ Hz, 2H, 9, 11), 7.14 (d, $J = 8.9$ Hz, 2H, 8, 12), 6.92 (d, $J = 8.9$ Hz, 2H, 15, 17), 5.54 (d, $J_{1,2} = 1.4$ Hz, 1H, H-1), 5.51 (dd, $J_{3,4} = 10.0$, $J_{3,2} = 3.5$ Hz, 1H, H-3), 5.41 (dd, $J_{2,3} = 3.4$ Hz, $J_{2,1} = 1.8$ Hz, 1H, H-2), 5.31 (t, $J_{4,3} = J_{4,5} = 10.2$ Hz, 1H, H-4), 4.22 (dd, $J_{6a,6b} = 12.3$, $J_{6a,5} = 5.5$ Hz, 1H, H-6a), 4.03 ($J_{6b,6a} = 12.4$, $J_{5,6a} = 8.3$, $J_{5,6b} = 2.1$ Hz, 2H, H-5, H6b), 3.98 (t, $J = 6.4$ Hz, 2H, H-19), 3.37 (t, $J = 6.8$ Hz, 2H, H-24), 2.14, 1.99, 1.98, 1.96 (s, 12H, 4 OAc), 1.87-1.80 (m, 2H, H-23), 1.79-1.73 (m, 2H, H-20), 1.48-1.46 (m, 4H, H-22, H-21); ^{13}C NMR (125 MHz, CDCl_3 , 300.0 K): $\delta = 170.5$, 169.9, 169.9, 169.7 (C=O, OAc), 161.5 (16), 157.1 (7), 148.6 (10), 146.9 (13), 124.6 (14/18), 124.2 (9/11), 116.7 (8/12), 114.7 (15/17), 95.8 (C-1), 69.4 (C-5), 69.3 (C-2), 68.8 (C-3), 68.1 (C-19), 65.9 (C-4), 62.1 (C-6), 33.8 (C-24), 32.7 (C-23), 29.0 (C-20), 27.9 (C-21), 25.3 (C-22), 20.9, 20.9, 20.7, 20.7 (CH_3COO) ppm. ESI-MS: Calcd for $\text{C}_{32}\text{H}_{39}\text{BrN}_2\text{O}_{11}$ $[\text{M}+1]^+$ $M_{\text{calcd}} = 708.56$, $M_{\text{found}} = 708.19$.

***trans*-4-(4'-Bromodecylphenylazo)phenyl 2,3,4,6-tetra-O-acetyl- α -D-mannopyranoside (5):**

To a mixture of mannoside **3** (250 mg, 0.459 mmol), 1-bromodecanol (163 mg, 0.689 mmol), triphenylphosphine (180.6 mg, 0.689 mmol) in dry THF (5 mL) at 0 °C DEAD (120 mg, 0.689 mmol) was added and the reaction mixture stirred for 5 h. Then, it was evaporated to

dryness, and the crude product was purified by column chromatography (cyclohexane/ethyl acetate, 3:2) gave the title compound **5** as yellow solid (277 mg, 0.363 mmol, 79%). Mp 107-109 °C; $R_f = 0.19$ (cyclohexane/ethyl acetate, 3:7); $[\alpha]_D^{20} = +0.562$ (c= 1.0, CH₂Cl₂); ¹H NMR (500 MHz, CDCl₃, 300.0 K): $\delta = 7.87$ (d, $J = 9.0$ Hz, 2H, 14, 18), 7.86 (d, $J = 9.0$ Hz, 2H, 9, 11), 7.20 (d, $J = 9.0$ Hz, 2H, 8, 12), 6.99 (d, $J = 9.0$ Hz, 2H, 15, 17), 5.61 (d, $J_{1,2} = 1.8$ Hz, 1H, H-1), 5.58 (dd, $J_{3,4} = 10.0$, $J_{3,2} = 3.6$ Hz, 1H, H-3), 5.48 (dd, $J_{2,3} = 3.5$ Hz, $J_{2,1} = 1.8$ Hz, 1H, H-2), 5.38 (t, $J_{4,3} = J_{4,5} = 10.1$ Hz, 1H, H-4), 4.29 (dd, $J_{6a,6b} = 12.2$, $J_{6a,5} = 5.5$ Hz, 1H, H-6a), 4.12-4.09 (m, 1H, H-5, H6b), 4.04 (t, $J = 6.6$ Hz, 2H, H-19), 3.41 (t, $J = 6.9$ Hz, 2H, H-28), 2.21, 2.06, 2.05, 2.03 (s, 12H, 4 OAc), 1.89-1.79 (m, 4H, H-20, H-27), 1.51-1.45 (m, 2H, H-21), 1.38-1.27 (m, 10H, H-22, H-23, H-24, H-25, H-26); ¹³C NMR (125 MHz, CDCl₃, 300.0 K): $\delta = 170.5$, 169.9, 169.9, 169.7 (C=O, OAc), 161.6 (16), 157.1 (7), 148.6 (10), 146.9 (13), 124.6 (14/18), 124.2 (9/11), 116.7 (8/12), 114.7 (15/17), 95.8 (C-1), 69.4 (C-5), 69.3 (C-2), 68.8 (C-3), 68.3 (C-19), 65.9 (C-4), 62.1 (C-6), 34.0 (C-28), 32.8 (C-20), 29.4 (C-27), 29.4 (C-22), 29.3 (C-23), 29.2 (C-24), 28.7 (C-25), 28.2 (C-26), 20.9, 20.9, 20.7, 20.7 (CH₃COO) ppm; ESI-MS: Calcd for C₃₆H₄₇BrN₂O₁₁ [M+1]⁺ $M_{calcd} = 764.67$, $M_{found} = 764.09$.

4-(4'-Acetylthiohexylphenylazo)phenyl 2,3,4,6-tetra-O-acetyl- α -D-mannopyranoside

(trans-6): To a stirred solution of KSAc (53.0 mg, 0.467 mmol) in DMF (5 mL) the bromide **4** (300 mg, 0.424) was added and the reaction mixture stirred at room temperature overnight. Then, it was diluted with diethylether (100 mL) and the combined organic layer washed with water (25 mL x 2), dried over Na₂SO₄, filtered and the filtrate was evaporated to dryness, and the crude product was purified by column chromatography (cyclohexane/ethyl acetate, 3:2) gave compound **6** as a yellow solid (262 mg, 0.373 mmol, 88%). Mp 102-103 °C; $[\alpha]_D^{20} = +0.39$ (c=0.81, CH₂Cl₂); $R_f = 0.38$ (cyclohexane/ethyl acetate, 3:2); $\epsilon = 48842 \pm 1000$ L.mol⁻¹.cm⁻¹; ¹H NMR (500 MHz, CDCl₃, 300.1 K): $\delta = 7.88$ (d, $J = 9.0$ Hz, 2H, 14, 18), 7.87 (d, $J = 9.0$ Hz, 2H, 9, 11), 7.20 (d, $J = 9.1$ Hz, 2H, 8, 12), 6.99 (d, $J = 9.1$ Hz, 2H, 15, 17), 5.61 (d, $J_{1,2} = 1.8$ Hz, 1H, H-1), 5.58 (dd, $J_{3,4} = 10.0$, $J_{3,2} = 3.6$ Hz, 1H, H-3), 5.48 (dd, $J_{2,3} = 3.5$ Hz, $J_{2,1} = 1.8$ Hz, 1H, H-2), 5.38 (t, $J_{4,3} = J_{4,5} = 10.1$ Hz, 1H, H-4), 4.30 (dd, $J_{6a,6b} = 12.5$, $J_{6a,5} = 5.7$ Hz, 1H, H-6a), 4.12-4.07 (m, 2H, H-5, H6b), 4.03 (t, $J = 6.5$ Hz, 2H, H-19), 2.89 (t, $J = 7.0$ Hz, 2H, H-24), 2.33 (s, 3H, SAc), 2.22, 2.06, 2.05, 2.03 (s, 12H, 4 OAc), 1.85-1.79 (m, 2H, H-23), 1.65-1.59 (m, 2H, H-20), 1.52-1.43 (m, 4H, H-22, H-21); ¹³C NMR (125 MHz, CDCl₃, 300.0 K): $\delta = 195.9$ (C-25, C=O, SAc), 170.5, 169.9, 169.9, 169.7 (C=O, OAc), 161.5 (16), 157.1 (7), 148.6 (10), 146.8 (13), 124.6 (14/18), 124.2 (9/11), 116.7 (8/12), 114.7 (15/17), 95.7 (C-

1), 69.4 (C-5), 69.3 (C-2), 68.8 (C-3), 68.1 (C-19), 65.9 (C-4), 62.1 (C-6), 30.7 (C-26), 29.5 (C-20), 29.1 (C-23), 29.0 (C-24), 28.5 (C-21), 25.6 (C-22), 20.9, 20.9, 20.7, 20.7 ($\underline{\text{C}}\text{H}_3\text{COO}$) ppm; ESI-MS: Calcd for $\text{C}_{34}\text{H}_{42}\text{N}_2\text{O}_{12}\text{S}$ $[\text{M}+\text{Na}]^+$ $M_{\text{calcd}} = 725.25$, $M_{\text{found}} = 725.24$.

4-(4'-Acetylthiododecylphenylazo)phenyl 2,3,4,6-tetra-O-acetyl- α -D-mannopyranoside (*trans*-7): To a stirred solution of KSAc (41 mg, 0.360 mmol) in DMF (5 mL) the bromide **5** (250 mg, 0.328) was added and the reaction mixture stirred at room temperature overnight. Then, it was diluted with diethylether (100 mL), the combined organic layers were washed with water (25 ml x 2), dried over Na_2SO_4 , filtered and the filtrate was evaporated to dryness, and the crude product was purified by column chromatography (cyclohexane/ethyl acetate, 3:2) gave the title compound **7** as a yellow solid (226 mg, 0.298 mmol, 91%). Mp 113-114 °C; $R_f = 0.17$ (cyclohexane/ethyl acetate, 7:3); $[\alpha]_D^{20} = +0.32$ ($c = 0.67$, CH_2Cl_2); $\epsilon = 18715 \pm 498 \text{ L}\cdot\text{mol}^{-1}\cdot\text{cm}^{-1}$; ^1H NMR (500 MHz, CDCl_3 , 300.1 K): $\delta = 7.87$ (d, $J = 9.0$ Hz, 2H, 14, 18), 7.86 (d, $J = 9.0$ Hz, 2H, 9, 11), 7.20 (d, $J = 9.0$ Hz, 2H, 8, 12), 6.99 (d, $J = 9.0$ Hz, 2H, 15, 17), 5.61 (d, $J_{1,2} = 1.7$ Hz, 1H, H-1), 5.58 (dd, $J_{3,4} = 10.0$, $J_{3,2} = 3.6$ Hz, 1H, H-3), 5.48 (dd, $J_{2,3} = 3.5$ Hz, $J_{2,1} = 1.8$ Hz, 1H, H-2), 5.38 (t, $J_{4,3} = J_{4,5} = 10.2$ Hz, 1H, H-4), 4.30 (dd, $J_{6a,6b} = 12.6$, $J_{6a,5} = 5.9$ Hz, 1H, H-6a), 4.13-4.07 (m, 2H, H-5, H6b), 4.03 (t, $J = 6.4$ Hz, 2H, H-19), 2.87 (t, $J = 6.9$ Hz, 2H, H-28), 2.32 (s, 3H, SAc), 2.22, 2.06, 2.05, 2.03 (s, 12H, 4 OAc), 1.84-1.79 (m, 2H, H-20), 1.59-1.54 (m, 2H, H-27), 1.50-1.44 (m, 2H, H-21), 1.37-1.26 (m, 10H); ^{13}C NMR (125 MHz, CDCl_3 , 300.0 K): $\delta = 196.1$ (C-30, C=O, SAc), 170.5, 169.9, 169.9, 169.7 (C=O, OAc), 161.6 (16), 157.1 (7), 148.6 (10), 146.8 (13), 124.6 (14/18), 124.2 (9/11), 116.7 (8/12), 114.7 (15/17), 95.7 (C-1), 69.4 (C-5), 69.3 (C-2), 68.8 (C-3), 68.4 (C-19), 65.9 (C-4), 62.1 (C-6), 30.6 (C-30), 29.5 (C-27), 29.4-26.9 (C-20, C22-C28), 26.0 (C-21), 20.9, 20.9, 20.7, 20.7 ($\underline{\text{C}}\text{H}_3\text{COO}$); ESI-MS: Calcd for $\text{C}_{38}\text{H}_{50}\text{N}_2\text{O}_{12}\text{S}$ $[\text{M}+\text{Na}]^+$ $M_{\text{calcd}} = 781.308$, $M_{\text{found}} = 781.292$.

4-(4'-Acetylthiohexylphenylazo)phenyl 2,3,4,6-tetra-O-acetyl- α -D-mannopyranoside (*cis*-6):

$\epsilon = 4579 \pm 192 \text{ L} \times \text{mol}^{-1} \times \text{cm}^{-1}$

^1H NMR (500 MHz, CDCl_3 , 300.1 K): $\delta = 7.00$ (d, $J = 8.9$ Hz, 2H, 8, 12), 6.88 (d, $J = 8.9$ Hz, 2H, 14, 18), 6.87 (d, $J = 8.9$ Hz, 2H, 9, 11), 6.76 (d, $J = 8.9$ Hz, 2H, 15, 17), 5.52 (dd, $J_{3,4} = 10.0$, $J_{3,2} = 3.5$ Hz, 1H, H-3), 5.48 (d, $J_{1,2} = 1.8$ Hz, 1H, H-1), 5.41 (dd, $J_{2,3} = 3.5$ Hz, $J_{2,1} = 1.8$ Hz, 1H, H-2), 5.35 (t, $J_{4,3} = J_{4,5} = 10.1$ Hz, 1H, H-4), 4.27 (dd, $J_{6a,6b} = 12.6$, $J_{6a,5} = 5.9$ Hz, 1H,

H-6a), 4.09-4.06 (m, 2H, H-5, H6b), 3.92 (t, $J = 6.5$ Hz, 2H, H-19), 2.87 (t, $J = 7.0$ Hz, 2H, H-24), 2.32 (s, 3H, SAc), 2.19, 2.05, 2.03, 2.01 (s, 12H, 4 OAc), 1.79-1.73 (m, 2H, H-23), 1.63-1.57 (m, 2H, H-20), 1.48-1.42 (m, 4H, H-22, H-21); ^{13}C NMR (125 MHz, CDCl_3 , 300.0 K): $\delta = 195.9$ (C-25, C=O, SAc), 170.5, 170.0, 169.9, 169.7 (C=O, OAc), 158.6 (16), 154.4 (7), 148.9 (10), 146.1 (13), 123.2 (14/18), 122.1 (9/11), 116.7 (8/12), 114.3 (15/17), 95.9 (C-1), 69.3 (C-5), 68.7 (C-2), 68.0 (C-3), 68.0 (C-19), 65.9 (C-4), 62.1 (C-6), 30.6 (C-26), 29.4 (C-20), 29.0 (C-23), 28.9 (C-24), 28.5 (C-21), 25.6 (C-22), 20.9, 20.9, 20.7, 20.7 (CH_3COO) ppm.

4-(4'-Acetylthiododecylphenylazo)phenyl 2,3,4,6-tetra-O-acetyl- α -D-mannopyranoside (*cis*-7):

$$\varepsilon = 1780 \pm 69 \text{ L x mol}^{-1} \text{ x cm}^{-1}$$

^1H NMR (500 MHz, CDCl_3 , 300.1 K): $\delta = 7.00$ (d, $J = 8.9$ Hz, 2H, 8, 12), 6.88 (d, $J = 8.9$ Hz, 2H, 14, 18), 6.87 (d, $J = 8.9$ Hz, 2H, 9, 11), 6.76 (d, $J = 8.9$ Hz, 2H, 15, 17), 5.52 (dd, $J_{3,4} = 10.0$, $J_{3,2} = 3.5$ Hz, 1H, H-3), 5.48 (d, $J_{1,2} = 1.7$ Hz, 1H, H-1), 5.41 (dd, $J_{2,3} = 3.5$ Hz, $J_{2,1} = 1.8$ Hz, 1H, H-2), 5.35 (t, $J_{4,3} = J_{4,5} = 9.9$ Hz, 1H, H-4), 4.27 (dd, $J_{6a,6b} = 12.6$, $J_{6a,5} = 6.0$ Hz, 1H, H-6a), 4.09-4.06 (m, 2H, H-5, H6b), 3.92 (t, $J = 6.6$ Hz, 2H, H-19), 2.86 (t, $J = 7.4$ Hz, 2H, H-28), 2.32 (s, 3H, SAc), 2.19, 2.05, 2.03, 2.01 (s, 12H, 4 OAc), 1.78-1.72 (m, 2H, H-20), 1.58-1.53 (m, 2H, H-27), 1.44-1.39 (m, 2H, H-21), 1.34-1.26 (m, 10H); ^{13}C NMR (125 MHz, CDCl_3 , 300.0 K): $\delta = 196.0$ (C-30, C=O, SAc), 170.5, 170.0, 169.9, 169.7 (C=O, OAc), 158.7 (16), 154.4 (7), 148.9 (10), 146.1 (13), 123.2 (14/18), 122.1 (9/11), 116.7 (8/12), 114.3 (15/17), 95.9 (C-1), 69.3 (C-5), 69.3 (C-2), 68.7 (C-3), 68.3 (C-19), 65.9 (C-4), 62.1 (C-6), 30.6 (C-30), 29.5 (C-27), 29.4-26.9 (C-20, C22-C28), 26.0 (C-21), 20.9, 20.9, 20.7, 20.7 (CH_3COO) ppm.

Preparation of SAMs

Self-assembled monolayers (SAMs) were prepared on Au(111) by two different methods. Thioacetates were prepared as 1 mM ethanolic solutions in which the gold wafers were immersed for direct adsorption. According a second method, SAM was formed by the in situ ammonium hydroxide (~63 mM) promoted deprotection of acetyl protected thiols in ethanol solution. In both cases, the sample was removed from the solution after 24 hours of

immersion at room temperature, thoroughly rinsed with ethanol and finally dried in a stream of nitrogen gas.

Instrumentation

Bulk IR: IR for all the compounds was recorded on Bruker VERTEX 70 FT-IR spectrometer in transmission mode using a DTGS detector.

IRRAS: IRRAS was performed using a Bruker VERTEX 70 FT-IR spectrometer equipped with a liquid nitrogen cooled MCT detector and a horizontal reflection unit for grazing incidence (Bruker A518). A p-polarized beam at an incident angle of 80° to the surface normal was used for measurements. The resolution was set to 4 cm^{-1} . The sample chamber was purged with dry nitrogen before and during measurements. A deuterated hexadecane-thiol SAM on Au(111) was used as a reference for the background spectrum. The IRRAS data were processed using the OPUS program (Bruker, Germany).

Calculation details: The vibrational frequencies were calculated using a commercial program package, Gaussian 03, B3LYP (Becke-3-Parameter-Lee-Yang-Parr) functional together with a 6-31++G(d,p) basis set. After geometry optimizations, theoretical frequencies were calculated. No negative frequencies were observed. The vibrational modes were assigned by using the GaussView program.

References

- [1] N. M. Varki, A. Varki, *Lab. Invest.* **2007**, *87*, 851-857.
- [2] P. R. Crocker, J. C. Paulson, A. Varki, *Nat. Rev. Immunol.* **2007**, *7*, 255-266.
- [3] D. B. Werz, R. Ranzinger, S. Herget, A. Adibekian, C.-W. von der Lieth, P. H. Seeberger, *ACS Chem. Biol.* **2007**, *2*, 685-691.
- [4] C. R. Bertozzi, L. L. Kiessling, *science* **2001**, *291*, 2357-2364.
- [5] P.-H. Liang, S.-K. Wang, Chi-Huey Wong, *J. Am. Chem. Soc.* **2007**, *129*, 11177-11184.
- [6] J. F. Popplewell, M. J. Swann, Y. Ahmed, J. E. Turnbull, D. G. Fernig, *ChemBioChem* **2009**, *10*, 1218-1226.
- [7] J. M. d. I. Fuente, S. Penadés, *Glycoconjugate J.* **2004**, *21*, 149-163.
- [8] J. I. Santos, A. C. de Souza, F. J. Cañada, S. Martín-Santamaría, J. P. Kamerling J. Jiménez-Barbero, *ChemBioChem* **2009**, *10*, 511-519.
- [9] R. G. Nuzzo, D. L. Allara, *J. Am. Chem. Soc.* **1983**, *105*, 4481-4483.
- [10] J. C. Love, L. A. Estroff, J. K. Kriebel, R. G. Nuzzo, G. M. Whitesides, *Chem. Rev.* **2005**, *105*, 1103-1170.
- [11] F. Schreiber, *J. Phys. Condens. Matter* **2004**, *16*, R881.
- [12] S. Svedhem, L. Öhberg, S. Borrelli, R. N. Valiokas, M. Andersson, S. Oscarson, S. C. T. Svensson, B. Liedberg, P. Konradsson, *Langmuir* **2002**, *18*, 2848-2858.
- [13] M. Kleinert, N. Röckendorf, T. K. Lindhorst, *Eur. J. Org. Chem.* **2004**, 3931-3940.
- [14] M. Kleinert, T. Winkler, A. Terfort, T. K. Lindhorst, *Org. Biomol. Chem.* **2008**, *6*, 2118-2132.
- [15] C. Grabosch, M. Kleinert, T. K. Lindhorst, *Synthesis* **2010**, *5*, 828-836.

- [16] L. Ban, M. Mrksich, *Angew. Chem.* **2008**, *120*, 3444-3447; *Angew. Chem. Int. Ed.* **2008**, *47*, 3396-3399.
- [17] C. Grabosch, M. Kind, Y. Gies, F. Schweighöfer, A. Terfort, T. K. Lindhorst, *Org. Biomol. Chem.* **2013**, *11*, 4006-4015.
- [18] R. Klajn, *Pure Appl. Chem.* **2010**, *82*, 2247-2279.
- [19] W.-H. Wei, T. Tomohiro, M. Kodaka, H. Okuno, *J. Org. Chem.* **2000**, *65*, 8979-8987.
- [20] T. K. Lindhorst, S. Kotter, U. Krallmann-Wenzel, S. Ehlers, *J. Chem. Soc., Perkin Trans. 1* **2001**, 823-831.
- [21] O. Mitsunobu, M. Yamada, *Bull. Chem. Soc. Jpn.* **1967**, *40*, 2380-2382.
- [22] K. C. K. Swamy, N. N. B. Kumar, E. Balaraman, K. V. P. P. Kumar, *Chem. Rev.* **2009**, *109*, 2551-2651.
- [23] T.-C. Zheng, M. Burkart and D. E. Richardson, *Tetrahedron Lett.* **1999**, *40*, 603-606.
- [24] J. M. Tour, L. Jones, D. L. Pearson, J. J. S. Lamba, T. P. Burgin, G. M. Whitesides, D. L. Allara, A. N. Parikh, S. Atre, *J. Am. Chem. Soc.* **1995**, *117*, 9529-9534.
- [25] R. Klajn, P. J. Wesson, K. J. M. Bishop, B. A. Grzybowski, *Angew. Chem.* **2009**, *121*, 7169-7173; *Angew. Chem. Int. Ed.* **2009**, *48*, 7035-7039.
- [26] L. Cai, Y. Yao, J. Yang, D. W. Price, J. M. Tour, *Chem. Mater.* **2002**, *14*, 2905-2909.
- [27] M. G. Badin, A. Bashir, S. Krakert, T. Strunskus, A. Terfort, C. Wöll, *Angew. Chem.* **2007**, *119*, 3837-3829; *Angew. Chem. Int. Ed.* **2007**, *46*, 3762-3764.
- [28] A. Singh, D. H. Dahanayaka, A. Biswas, L. A. Bumm, R. L. Halterman, *Langmuir* **2010**, *26*, 13221-13226.
- [29] M. Min, G. S. Bang, H. Lee, B.-C. Yu, *Chem. Commun.* **2010**, *46*, 5232-5234.
- [30] T. L. Hutchison, W. J. Brouillette, *Bioorg. Med. Chem.* **1998**, *6*, 2133-2138.
- [31] W. H. McFadden, R. M. Seifert, J. Wasserman, *Anal. Chem.* **1965**, *37*, 560-566.

Supporting Information

Monitoring of *trans*→*cis* isomerization of azobenzene glyco-SAMs on gold surfaces using IRRAS

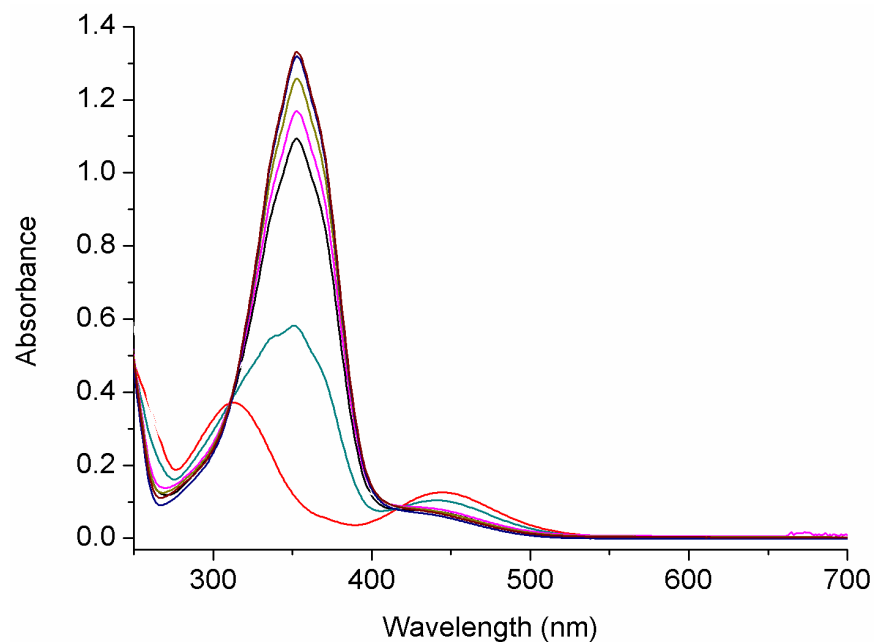


Figure S1: UV visible spectra showing thermal reversion of *cis*-6 to *trans*-6 in ethanol (50 μ M) at 18 $^{\circ}$ C in the dark as a function of time.

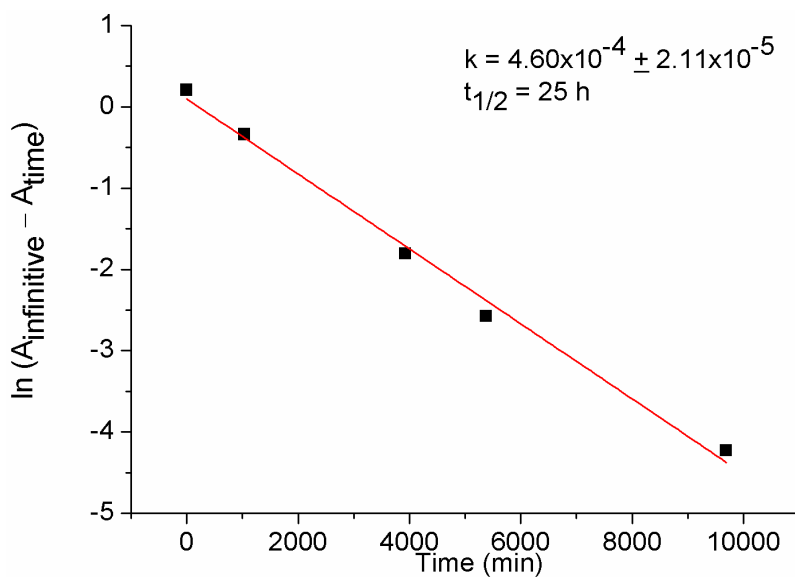


Figure S2: First order kinetics plot for the thermal *cis*-6 to *trans*-6 in ethanol.

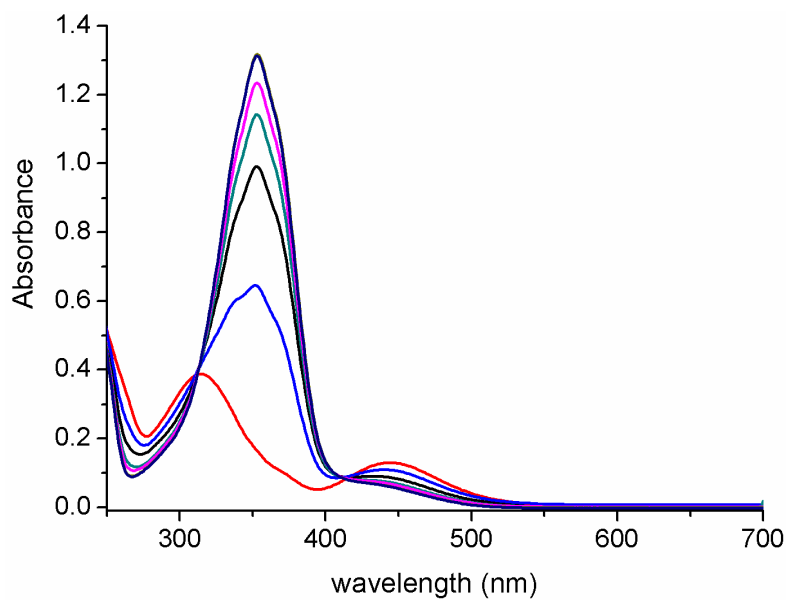


Figure S3: UV visible spectra showing thermal reversion of *cis-7* to *trans-7* in ethanol (50 μM) at 18 $^{\circ}\text{C}$ in the dark as a function of time.

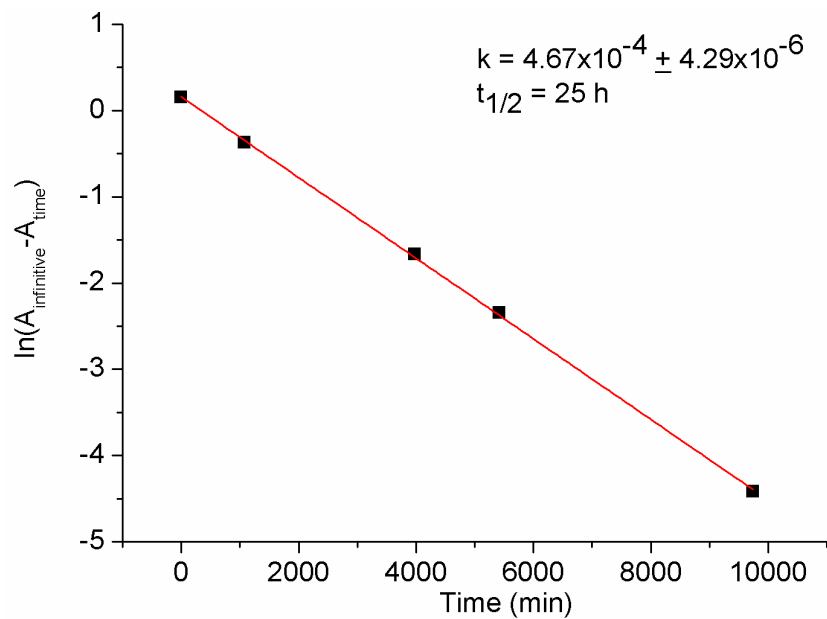


Figure S4: First order kinetics plot for the thermal *cis-7* to *trans-7* in ethanol.

Table S1: The vibrational frequencies (wavenumber, cm^{-1}) for compound **7** obtained from the calculation, transition dipole moment (TDM) with respect to the surface (perpendicular: \perp , parallel: \parallel , and neither parallel nor perpendicular: $//$) and assignment of the bands are given.

Peak Number	Calculated wavenumber (cm^{-1})	Transition Dipole Moment (TDM)	Assignment
1	210,83	//	CH_3 (C-3mann)
2	212,15	//	Molecule deformation
3	221.43	//	CH_3 (C-3 mann)
4	226,79	//	CH_3 (C-3 mann)
5	236,11	//	Molecule deformation
6	240.48	//	Molecule deformation
7	241,77	//	Molecule deformation
8	248,41	\parallel	CH_2 (CH_2SAC)
9	251,35	//	C-6 (mann)
10	259,16	//	Mann deformation
11	278,14	\perp & //	Molecule deformation
12	284,35	//	Mann deformation
13	310,67	//	Mann deformation
14	318,59	//	Mann deformation
15	322,63	//	Mann deformation
16	339,82	// & \parallel	Mann deformation
17	356,25	//	Aromatic & aliphatic deformation

18	380,06	//	Molecule deformation
19	392,31	//	Molecule deformation
20	398,22	//	Molecule deformation
21	415,09	// & ⊥	Mann deformation
22	421,80	//	Aromatic deformation
23	434,60	//	Mann deformation
24	438,51		Aromatic ring deformation
25	444,39	// &	Molecule deformation
26	448,22	//	Molecule deformation
27	458,71	// &	Molecule deformation
28	459,70	//	Molecule deformation
29	488,01	//	Molecule deformation,.
30	491,37	⊥ & //	CH ₃ (OAc Mann)
31	505,57	⊥ & //	CH ₃ (OAc Mann)
32	514,99	// & ⊥	Molecule deformation
33	518,33	// & ⊥	Mann deformation
34	528,44	// & ⊥	Mannose deformation
35	540,64	//	-N=N- & Aromatic ring deformation
36	542,02	//	Mannose ring rocking,
37	556,95	//	CH ₃ (S Ac), rocking,
38	558,91	//	Molecule deformation
39	574,56	//	Molecule deformation
40	595,43	//	Molecule deformation
41	597,07	//	CH ₂ (C-3 Mannose) rocking

42	598,01	//	CH ₂ (C-6 Mannose), rocking
43	599,10	//	CH ₂ (C-4 Mannose), rocking
44	601,45	//	C-O (SC=OCH ₃) deformation
45	615,45	//	C-O & Molecule deformation,
46	621,90	//	C-O & Molecule deformation
47	624,54	//	C-O & Molecule deformation
48	633,89	//	Aromatic and Mannose deformation
49	640,50	//	Aromatic ring deformation
50	646,47	//	CH ₂ (CH ₂ -SAc) deformation
51	649,79	//	Ring 2 deformation
52	666,54	& //	C-C (C-2 mannose) and ring deformation
53	690,21	//	Mannose and Aromatic deformation
54	718,85	// & ⊥.	Mannose and Aromatic deformation
55	728,88	& //	Mannose and Aromatic deformation
56	739,48	//	CH ₂ aliphatic, rocking
57	744,65	& //	Aromatic ring deformation
58	756,09	//	CH ₂ aliphatic, rocking
59	782,25	// & ⊥.	Mannose and Aromatic deformation
60	787,79	// & ⊥.	Mannose and Aromatic deformation
61	799,05	& //	Aromatic ring deformation

62	802,30	//	Mannose and Aromatic deformation
63	813,55	//	Mannose and Aromatic deformation
64	825	//	C-H aromatic wagging
65	831,82	//	CH ₂ (mannose) rocking
66	840,12		Aromatic Ring with liner (R1), C-H twisting
67	848,32	⊥	C-H aromatic(R1)
68	852,36	//	C=C, symmetric stretching
69	864,92	//	C-H asymmetric. Stretching
70	872,97		Aromatic Ring 1, C-H wagging
71	882,61	//	Aromatic Ring 1, C-H twisting
72	883,64	//	Aliphatic CH ₂ rocking
73	926,13	//	O-C asymmetric stretching
74	940,96		N=N asymmetric stretching
75	951,15		C-C asymmetric stretching
76	965,25		C-O wagging
77	967,53		C-H aliphatic, symmetric stretching, (SAcCH ₃)
78	968,84		C-H aromatic, rocking,
79	971,25	//	O-C aromatic (R1), symmetric stretching,
80	979,86	//	C-H aromatic (R2), rocking
81	982,24	//	C-H(CH ₃ of acetyl mann), scissoring
82	986,64	⊥	C-H(CH ₃ of acetyl mann), scissoring

83	993,29	⊥	C-H (CH ₃ of acetyl mann) scissoring
84	995,00		C-H aliphatic, rocking, II
85	1003,98	//	C-C aliphatic, asymmetric stretching
86	1011,81		C-H (CH ₃ of acetyl mann),rocking, II
87	1012,48	//	C-C aliphatic, asymmetric stretching
88	1015,96	⊥	C-O (man- O -COCH ₃), asymmetric stretching
89	1023,09	//	C=C (aromatic ring 1), symm stretching
90	1030,21		C-O (C-3 man C-O -OAc), symm
91	1045,97	//	CH ₂ (C-6 mann) rocking
92	1049,52	⊥	C-C aliphatic, rocking
93	1058,08	⊥	C-C aliphatic symm
94	1064,66	//	CH ₃ (mann) rocking
95	1069,84	//	CH ₃ (mann) rocking
96	1070,77	//	CH ₃ (mann) rocking
97	1073,28	//	CH ₃ (mann) rocking
98	1077,22	//	Mannose deformation
99	1100,98	//	CH ₂ aliphatic, rocking
100	1104,31	//	CH ₂ (mannose) rocking
101	1106,38	//	C-C aliphatic (mannose) symm
102	1117,40	⊥	C-H aromatic (R1), scissoring
103	1123,08	⊥	C-H aromatic (R2), scissoring

103	1125,66	⊥	C ₄ -C ₅ (mannose), symm
104	1129,99	//	CH ₃ (SCOCH ₃), scissoring
105	1140,66	//	C-H (mannose), rocking
106	1151	⊥	C-H aromatic (R2), scissoring
107	1160,25	//	C-H, scissoring
108	1165,02	//	C-H (mannose), deformation
109	1183,01	⊥ & //	O-C & C-H, scissoring
110	1187,43	//	C-H aliphatic, rocking
111	1190,07	⊥	CH ₃ (Acetyl mannose), rocking
112	1200,51	//	Mannose deformation
113	1204,78	//	C-H (Aromatic Ring 1), scissoring
114	1215,19	⊥	C-H (CH ₃ mannose) rocking
115	1225,78	//	Mannose deformation
116	1226,74	//	C-H aliphatic, scissoring
117	1229,48	⊥	C-O aromatic (R2), stretching
118	1233,33	//	C-H (mannose), rocking
119	1252,74	⊥	Aromatic-C-N=N- and C-H (ring) rocking
120	1256,76	//	C-H aliphatic, scissoring
121	1257,16	//	CH ₂ of mannose, rocking,
122	1272,89	⊥	CH ₂ aliphatic, scissoring,
123	1285,96	//	C-H aliphatic, scissoring
124	1300,49	⊥	CH ₂ aliphatic, rocking
125	1318,78	//	C-H, Aromatic R-2, rocking

126	1321,71	⊥	CH ₂ aliphatic, rocking
127	1323,21	//	C-H (mannose), scissoring
128	1330,96	⊥	CH ₂ aliphatic, scissoring
129	1339,02	⊥	CH ₂ aliphatic, scissoring
130	1341,64	⊥	C-H aliphatic, rocking
131	1343,73	//	C-H (mannose), scissoring
132	1346,82	//	C-H (mannose), scissoring
133	1350,23	//	Aromatic ring deformation
134	1359,34	//	Aromatic ring deformation
135	1375,16	//	CH ₂ (mannose), wagging
136	1383,26	⊥	C-H aliphatic, wagging
137	1384,61	//	C-H (mannose), scissoring
138	1386,56	//	C-H (mannose), scissoring
139	1400,56	//	C-H (mannose), scissoring
140	1402,22		CH ₃ (SOAc), scissoring
141	1408,17	//	CH ₃ (mannose), scissoring
142	1409,29	⊥	CH ₂ aliphatic, scissoring
143	1409,46	//	CH ₃ (mannose), wagging
144	1410,97	//	CH ₃ (mannose), wagging
145	1415,39	//	CH ₃ (mannose), wagging
146	1417,07	⊥ & //	Aromatic ring deformation
147	1424,65	⊥	CH ₂ aliphatic, wagging
148	1435,73	//	CH ₂ (mannose), scissoring
149	1453,55	//	C=C aromatic, asymmetric

150	1468,51	//	CH ₂ of (CH ₂ SAC), scissoring
151	1475,48	//	Aromatic ring deformation
152	1475,51		CH ₃ (SOAc), scissoring
153	1477,87	//	CH ₃ (mannose), scissoring
154	1480,27	//	CH ₃ (mannose), scissoring
155	1488,43		CH ₃ (SOAc), scissoring
156	1488,87	//	CH ₃ (mannose), scissoring
157	1489,27	// & ⊥	CH ₃ (mannose), scissoring
158	1491,25	// & ⊥	CH ₃ (mannose), scissoring
159	1498,57		CH ₃ (mannose), scissoring
160	1501,46	⊥	CH ₃ (mannose), scissoring
161	1501,51	⊥	CH ₃ (mannose), scissoring
162	1502,74		CH ₂ aliphatic, scissoring
163	1503,65	⊥	CH ₂ (mannose), scissoring
164	1503,91		CH ₂ (mannose), scissoring
165	1511,88	//	C-H aliphatic, scissoring
165	1518,93	⊥	C-H aliphatic, scissoring
166	1521,33	//	Aromatic deformation
167	1525,95	⊥	CH ₂ aliphatic, scissoring
168	1535,35	⊥	C-H aliphatic, scissoring
169	1615,45	//	Ring deformation (R2)
170	1620,87	//	Ring deformation (R1)
171	1639,69	//	Ring deformation (R2)
172	1640,67	//	Aromatic ring deformation

173	1676,49	//	C=O (SAc), symmetric
174	1710,27	//	C=O (mann-C2), symmetric
175	1736,37	⊥	C=O (mann-C6), symmetric
176	1739,49	⊥	C=O (mann-C3), symmetric
177	3002,50		CH ₂ aliphatic, wagging
178	3009,61		CH ₂ aliphatic, wagging
179	3014,11		CH ₂ aliphatic, wagging
180	3048,16	⊥	CH ₃ (mannose), wagging
181	3051,87		C-H asymmetric stretching
182	3054,24	//	CH ₂ mannose, wagging

4.2 Photosensitive glyconanoparticles: A new tool to switch carbohydrate-protein interactions

In another approach, carbohydrate-protein interactions were studied using gold glyconanoparticles (GNPs). In GNPs, multiple copies of carbohydrates are covalently linked to the surface of gold nanoparticles. GNPs holds some advantages over other multivalent systems like control over the size of the nanoparticle metal core, quantification of the bound ligands on the surface, detection of binding events by surface plasmon resonance and high solubility in aqueous media which is ideal for all the biological testing under physiological conditions.^[112-115]

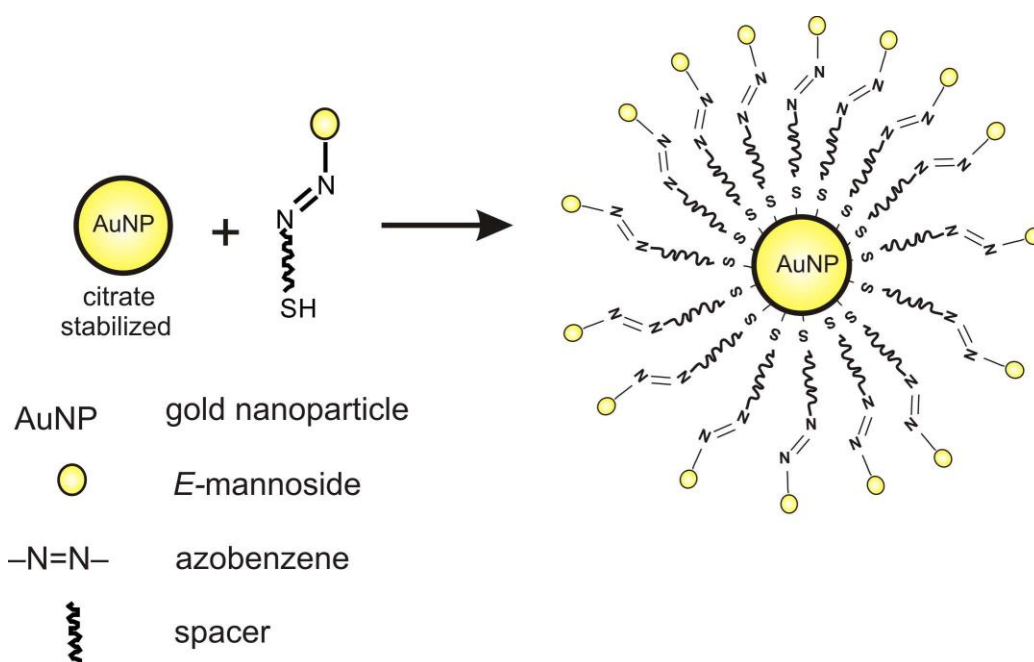


Figure 4.2: Strategy for the synthesis of GNPs functionalized with photoswitchable azobenzene glycosides.

In view of this we have recently developed methods for preparation of photosensitive gold glyconanoparticles (GNPs) (Fig 4.2). Upon irradiation with UV light of appropriate wavelength, photosensitive GNPs undergo *E*→*Z* isomerization of the multivalently presented azobenzene glycosides moieties, resulting in an altered ligand orientation to its binding partners. Multivalent interactions with the two different isomers of GNPs with the lectin Concanavalin A were studied by UV-Vis spectroscopy. The study was performed in collaboration with the group of Prof. Knud J. Jensen (University of Copenhagen, Denmark). A first manuscript is presented in the following.

This collaborative work was financed by a short term scientific mission (STSM) within european cooperation in science and technology (COST). I did the synthesis of all the photoswitchable glycosides at CAU Kiel. Under the supervision of Mikkel B. Thygesen, I prepared the photosensitive gold glyconanoparticles (GNPs) and studied their interactions with Concanavalin A (ConA) in Prof. Knud J. Jensen's research group at University of Copenhagen, Denmark.

Photosensitive glyconanoparticles: A new tool to switch carbohydrate-protein interactions

Vijayanand Chandrasekaran ^a, Mikkel B. Thygesen ^b, Knud J. Jensen ^{b*}, Thisbe K. Lindhorst ^{a*}

^a *Otto Diels Institute for Organic Chemistry, Christiana Albertina University of Kiel, Otto-Hahn-Platz 3-4, D-24098 Kiel, Germany. tkhind@oc.uni-kiel.de*

^b *Faculty of Life Sciences, Centre for Carbohydrate Recognition and Signalling, University of Copenhagen, Thorvaldsensvej 40, 1871 Frederiksberg, Denmark. kjj@life.ku.dk*

4.2.1 Introduction

Carbohydrates are functionalized with gold nanoparticles of sizes between 1 to 100 nanometer, are called Glyconanoparticles (GNPs). Normally, GNPs consists of three important building blocks namely, a gold metal core, carbohydrate ligand and a linker connecting the gold core and the ligand. GNPs are emerging tools in the field of glycobiology due to their enormous potential in biology with applications such as biomedical imaging, in vitro and in vivo imaging, investigation of carbohydrate-protein interactions, glyconanotechnology, etc. ^[1-6] GNPs are highly soluble in water and in aqueous buffer, a prerequisite for biological experiments.^[7] In addition, GNPs can be prepared in various particle size, quantification of the bound ligand on each nanoparticles and furthermore their interactions with proteins can be determined using spectroscopic techniques like UV-Vis spectroscopy, electron microscopy or Dynamic light scattering (DLS).

In GNPs, multiple carbohydrate ligands are attached to the gold core through thiol group. Multivalent presentation of these ligands on the gold nanoparticle increases binding affinity to lectins in many cases. In addition to multivalency effects, carbohydrate-protein interactions

are also influenced by the spatial distribution and orientation of carbohydrate ligands. In order to understand this principle, we are interested in making GNP which can change the orientation or presentation of the ligands, triggered by external stimuli such as light. Incorporation of azobenzene moieties into the GNPs will eventually allow us to follow the effect of conformational change in carbohydrate-protein interactions. Azobenzenes are well established photoswitchable molecules which undergo $E \rightarrow Z$ isomerization at appropriate wavelength. Moreover, azobenzenes are well studied photoswitchable molecule with various biological applications.^[8-13]

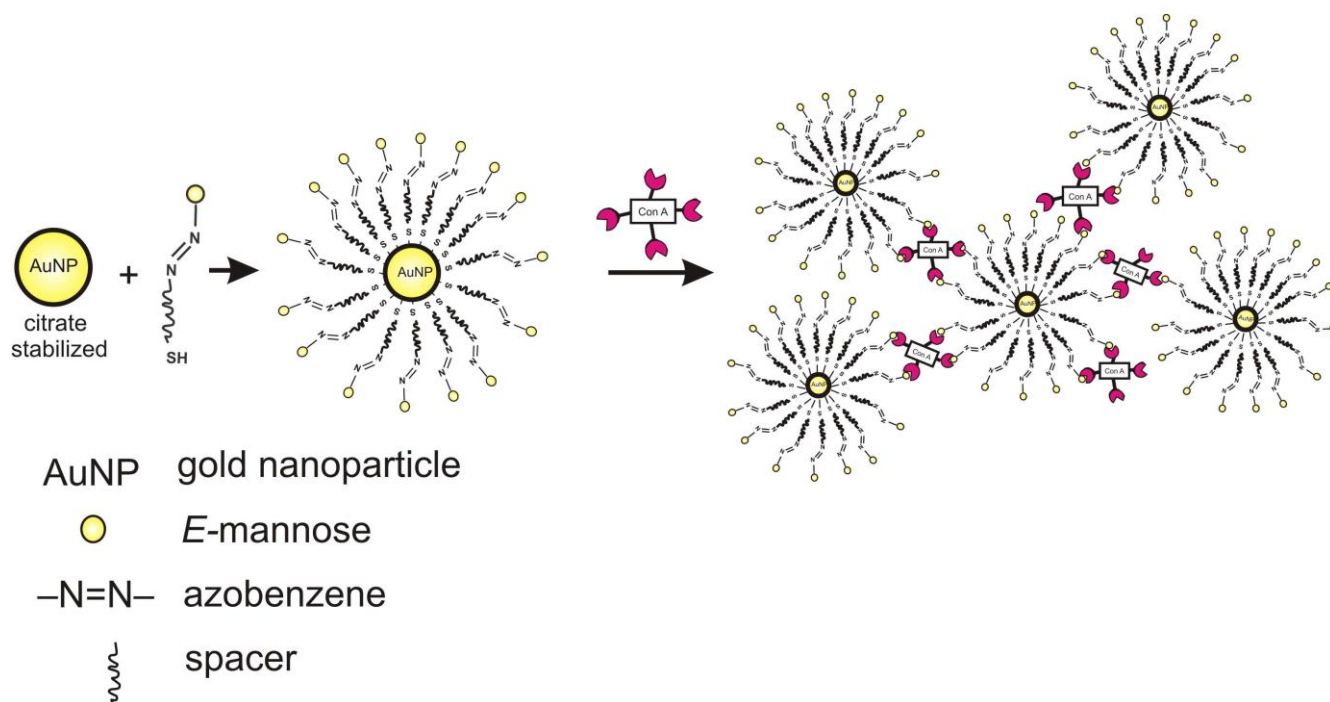


Figure 4.2.1: schematic representation of photosensitive glyconanoparticles and its interaction with ConA.

Here the synthesis of photoswitchable ligands, photoswitchable GNPs and their photochromic properties in solution and on nanoparticle surface were studied and explained. Unlike GNPs, photoswitchable GNPs have an additional photoswitchable unit, namely azobenzene. Photosensitive GNPs and their interaction with the lectin Concanavalin (ConA) from *Concanavalia ensiformis* were studied and reported here (Figure 4.2.1).

Results and Discussion

4.2.2 Synthesis of photoswitchable ligands: The aim was to synthesis three different types of photoswitchable ligands, each are different in their spacer units. Each ligand has three important functional moieties (Figure 4.2.2), mannose as a terminal group and as the specific ligand for the lectin ConA, an azobenzene portion as a switchable unit for the *E*→*Z* photoisomerization and a spacer unit between the anchoring thiol group and the azobenzene chromophore. The structures of mannosides 1, 2 and 3 differ only in their spacer units. Ligand 1 contains only alkyl spacers for dense packing on the Au nanoparticle core shell, ligand 2 contains oligo ethylene glycol (OEG) spacer increases the hydrophilicity of the molecule to dissolve in water and buffer medium and in top of that it avoids unspecific binding of proteins. Finally, a combination of OEG- and alkyl-spacered ligand 3 was prepared. Here, the spacer plays a dual role of providing a dense packing and biocompatibility.

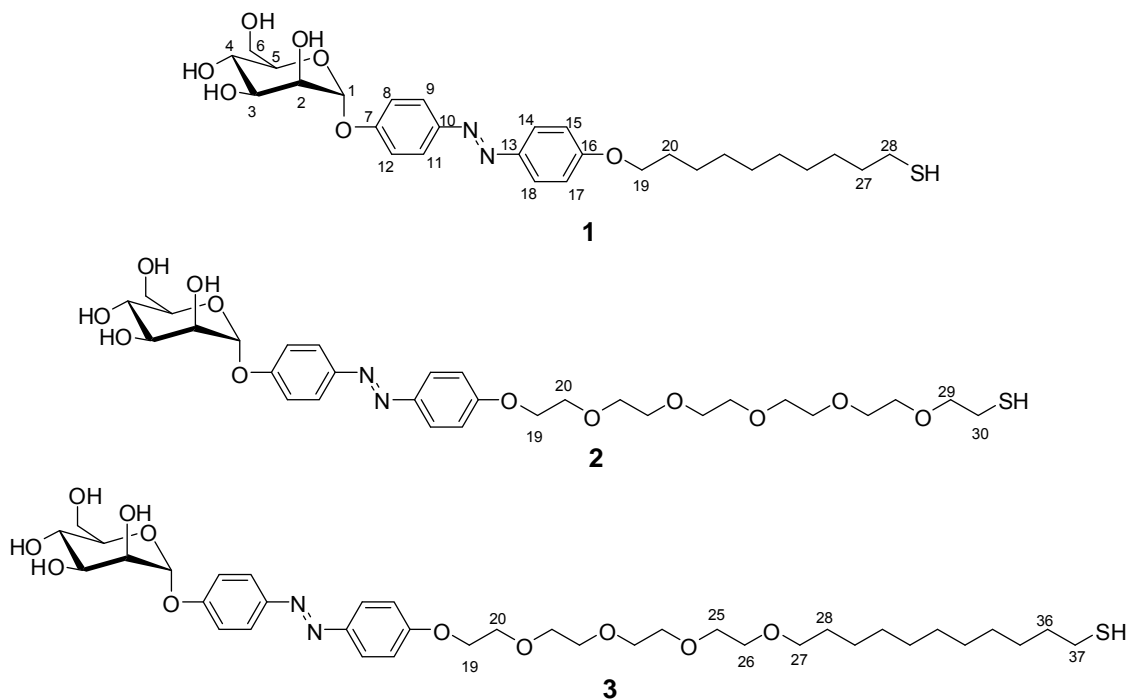
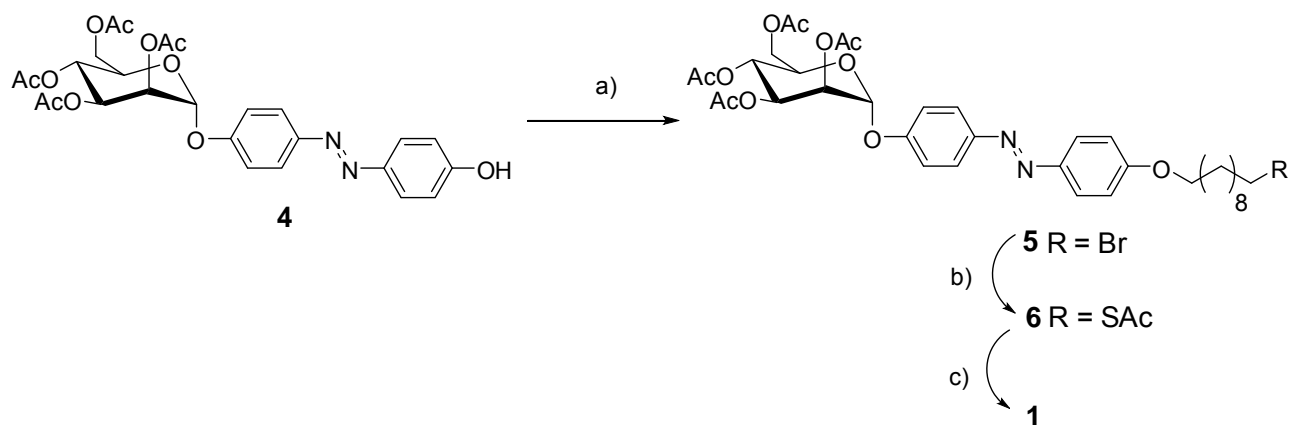


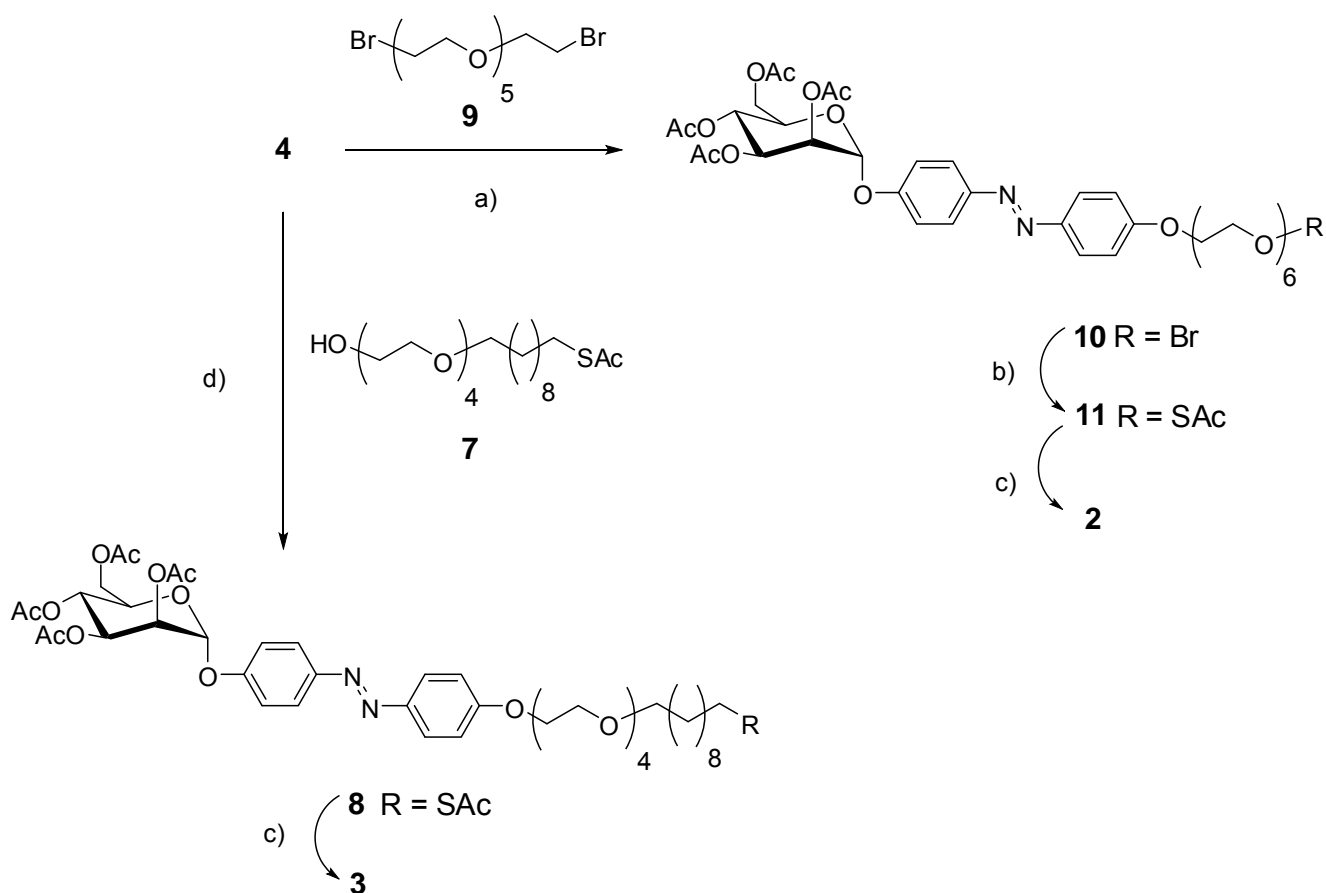
Figure 4.2.2: Structure of compounds used for the synthesis of photosensitive gold glyconanoparticles.

The photoswitchable ligands **1**, **2** and **3** were synthesized from the common intermediate **4**. Compound **4** was prepared by standard glycosylation of *p,p'*-dihydroxy azobenzene as previously described from our lab.^[14, 15] To achieve our first target molecule **1**, Mitsunobu reaction was employed (scheme 4.2.1). Thus, reaction of **4** with 10-bromodecan-1-ol in the presence of triphenylphosphine and diethyl azodicarboxylate (DEAD) gave the required product **5** in 79% yield.^[16] At room temperature potassium thioacetate converted the alkylbromide **5** into the desired thioacetate **6** in 91% yield.^[17] Deprotection of acetyl groups in **6** under Zemplén conditions gave the target compound **1** in 98% yield.^[17]



Scheme 4.2.1: Reaction conditions: (a) Bromodecanol (1.5 equiv.), PPh₃ (1.5 equiv.), DEAD (1.5 equiv.), dry THF, rt, 79%; (b) KSAc (1.1 equiv.), DMF, rt, 91%; (c) NaOMe, MeOH, rt, 98%.

For the synthesis of **2** commercially available hexaethylene glycol was used and converted into the respective dibromide **9** according to the literature.^[18] Reaction of mannoside **4** with **9** under base treatment with K₂CO₃ in DMF gave the bromo- substituted compound **10** in 74% yield. Then, the bromo group was substituted by thioacetate to get required product **11** in good yield. Treatment of **11** under Zemplén conditions gave the target molecule **2** in good yield (Scheme 4.2.2).



Scheme 4.2.2: Reaction conditions: (a) dibromohexaethyleneglycol **9** (2.0 equiv.), K_2CO_3 (2.0 equiv.), DMF, 40 °C, 74%; (b) KSAc (1.1 equiv.), DMF, rt, 86%; (c) NaOMe, MeOH, rt, 97% (**2**), 93% (**3**); (d) PS- PPh_3 (1.5 equiv.), DEAD (1.5 equiv.), acetylthioundecyl-tetraethylene glycol **7** (2.0 equiv.), dry. THF, rt, 71%.

Finally, synthesis of the advanced ligand **3** was carried out in two synthetic steps using Mitsunobu reaction and Zemplén reaction conditions (scheme 4.2.2). Our initial attempt to prepare **3** under Mitsunobu conditions using triphenylphosphine, lead to difficulties in removing the by-product PPh_3O , even after several purification steps. However, this problem was overcome by using the polymer-supported triphenylphosphine (PS- PPh_3). Thus, reaction of **4** with commercially available **7**, in the presence of PS- triphenylphosphine and diethylazodicarboxylate (DEAD) yielded **8** in 71%. Deprotection of O- and S- acetyl protecting groups was achieved in a single step under Zemplén conditions, which gave the final compound **3** in 93% yield.^[17]

4.2.3 Synthesis and characterization of photoswitchable glyco-AuNPs: Citrate-stabilized gold nanoparticles (AuNPs) were prepared according to a modified method of Turkevich *et al.*

to provide AuNPs with an average diameter of 13.2 nm.^[19, 20] The size of the prepared AuNPs was determined by UV-Vis spectroscopy using equation (1), in which A_{spr} is the absorbance at the surface plasma resonance band and A_{450} is the absorbance at 450 nm.^[7, 21, 22] These particles were washed with 1 mM NaOH as described by Whitesides *et al.* in order to facilitate self-assembly with alkanethiols.^[23]

$$d_{\text{AuNPs}} = 0.112 \cdot e^{3A_{\text{spr}}/A_{450}} \quad \text{eq (1)}$$

To the synthesized 13.2 nm AuNPs, photoswitchable ligands **1-3** were attached by stirring in aqueous solution for 14 h at room temperature to get **E-AuNP1**, **E-AuNP2** and **E-AuNP3**. To our surprise ligand-**1** showed poor solubility in organic solvents, water and aqueous buffer. It might be due to the hydrophobic interaction of the alkyl spacers. Due to its poor solubility, preparation of **E-AuNP1** was unsuccessful. Our next attempt was to prepare **E-AuNP2** using ligand **2**. However, during the functionalization of AuNP with ligand **2**, immediate aggregation of the nanoparticles was observed within 5 min. After addition of ligand **2** to the nanoparticle solution, colour of the reaction mixture turned from light red wine to dark brown (see Supporting Information). However, anchoring of ligand **3** onto AuNP was successful and proceeded nicely to afford the photoswitchable glyconanoparticle **E-AuNP3**. By retaining the red wine colour in the reaction mixture solution, an indication for proper functionalization of AuNP. Thus, **E-AuNP3** was chosen as the best candidate for further experiments (see Supporting Information).

The photoswitchable glyconanoparticle **3** (**E-AuNP3**) were prepared as follows. A 5 mM solution of ligand **3** in methanol (1 mL) was added to a stirring solution of AuNP (in 10 mL water) and this mixture was stirred for about 18 h at room temperature. Functionalized **E-AuNP3** were washed with phosphate buffer (0.1 mM) at pH 7.0 (10 mL x 5) by washing in a centrifugal filtration using 50 kDa cut-off. UV-Vis spectroscopy of **E-AuNP3** showed a characteristic peak at 339 nm due to the azobenzene chromophore and at 530 nm arising from surface plasmon resonance band (SPR band). After irradiation at 365 nm for 8-10 min, the **Z-AuNP3** isomer was observed by a decrease in the π - π^* transition of azobenzene chromophore at 339 nm. But, the formation of band at 419 nm region due to the n - π^* transition was weak due to the overlap of SPR absorption band, which was also slightly blue-

shifted from 530 nm to 528 nm due to the influence of switching and isomerization (Figure 4.2.3).

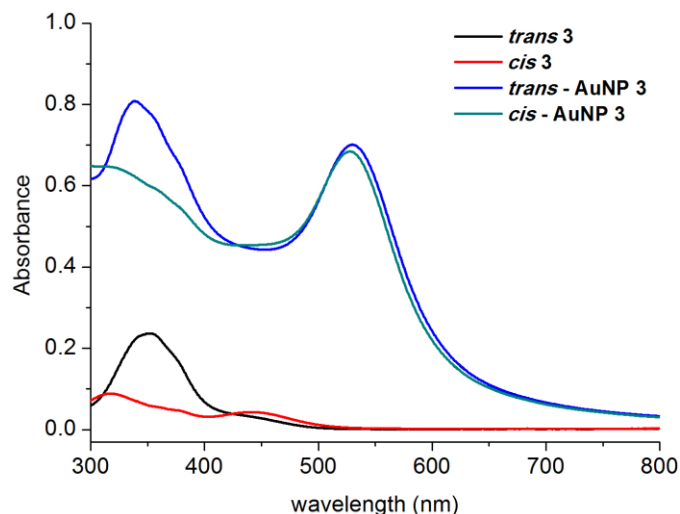


Figure 4.2.3: Monitoring $E \rightarrow Z$ isomerization in solution and on the surface by UV-Vis spectroscopy in 0.1 mM phosphate buffer (pH 7). Isomerization of free ligands, **E-3** (6 μM) and **Z-3** (5 μM). Isomerization of ligand functionalized gold nanoparticles, **E-AuNP-3** (6 nM) and, **Z-AuNP-3** (6 nM).

Formation of two different isomers, **E-AuNP3** and **Z-AuNP3**, was also observed by dynamic light scattering (DLS) measurements, which gave the hydrodynamic diameter $d(H)$ from the core of Au to the head group mannose. The results showed that **E-AuNP3** gave a diameter of 29.5 nm whereas **Z-AuNP3** gave only 16.4 nm. As expected, the difference between these two **E-AuNP3** and **Z-AuNP3** is another clear evidence for the formation of the two different isomers on the AuNP surface.

4.2.4 Photochromic properties of free ligand and photoswitchable glyconanoparticles:

$E \rightarrow Z$ isomerization ratios of the free ligands **1-3** were determined by ^1H NMR spectroscopy by integrating the H-1 proton of mannose (Table 4.2.1). In the ground state (G.S) all the compounds exhibited >98% of E -isomer, after irradiation at 365 nm using light emitting diode (LED) for 8-10 min photostationary state (PSS) was reached. This was clearly observed by the drastic chemical shift in the aromatic protons and H-1 proton of the mannose. But, $E:Z$ ratio of **E-AuNP3** was not determined as ^1H NMR spectra of functionalized glyconanoparticles often gives broad signals and obtaining the $E:Z$ ratio exactly is difficult.

Kinetics and half-life of azobenzene glycosides were studied in the dark at room temperature. Due to the poor solubility of **1** in organic solvent like methanol and ethanol, kinetic measurement of **1** was performed in DMSO, but **2** and **3** were measured in methanol. Before irradiation, the *E*-isomer of all the compounds exhibited an absorption band (λ_{\max}) at 362 nm for **1** and ~353 nm for **2** and **3** due to the π - π^* transition of the azobenzene moiety. Photoirradiation of the *E*-isomer at 365 nm for about 8-10 min leads to photostationary state (PSS) which was observed by a decrease in π - π^* and increase in λ_{\max} of n - π^* region at 449 nm for **1** and ~445 nm for **2** and **3**, a clear indication for the formation of *Z* isomer. Kinetics of back isomerization from *Z*→*E* and corresponding half-life ($\tau_{1/2}$) are given in Table 5.2.1. Azobenzene glycoside **2** showed a greater $\tau_{1/2}$ of 7 h 45 min compared to **1** and **3**.

Table 4.2.1: Photochromic properties of **1**, **2**, **3** and **E-AuNP3**

Compounds	Solvent	Rate Constant (k) min ⁻¹ [a]	<i>E</i> - isomer [b]	<i>Z</i> - isomer [c]
Ligand 1	DMSO	2.01 x 10 ⁻³	> 98	> 98
Ligand 2	MeOH	1.55 x 10 ⁻³	> 97	> 98
Ligand 3	MeOH	2.32 x 10 ⁻³	> 99	> 97
Ligand 3	Phosphate buffer	2.27 x 10 ⁻²	--	--
AuNP-3	Phosphate buffer	1.90 x 10 ⁻²	--	--

Percentage of *E* and *Z* isomers were determined by ¹H NMR spectroscopy based on the integrals of the respective anomeric protons (H-1) [a] rate constants were determined by UV-Vis spectroscopy, [b] before irradiation, [c] after irradiation, photostationary state (pss)

Rate constant (k) and half-life ($\tau_{1/2}$) determination of **E-AuNP3** → **Z-AuNP3** was performed in phosphate buffer. Before irradiation, **E-AuNP3** showed a characteristic peak at 339 nm due to the azobenzene chromophore and a peak at 530 nm arising due surface plasmon resonance (SPR) band of AuNPs. After irradiation with LED at 365 nm for 8-10 min photostationary state (PSS) was reached, indicating the formation of **Z-AuNP3** with a decrease in the π - π^* at 339 nm. However, observation of the n - π^* transition at the 419 nm

region was weak due to the overlap with the broad SPR absorption band. Notably, a slight shift in the SPR band from 530 nm to 528 nm was observed which might be due to the influence of $E \rightarrow Z$ isomerization (Figure 3). It was observed that the rate of back isomerization, $Z \rightarrow E$ on the AuNP surface has a greater half-life compare to the free ligand **3** in phosphate buffer solution.^[24]

4.2.5 Recognition by the lectin ConA: ConA exists as a tetramer at pH 7.0 and each monomeric unit binds to α -D-mannoside. Individual isomers of photoswitchable glyconanoparticles, **E-AuNP3** and **Z-AuNP3** were taken and their interactions with the lectin ConA were tested. Lectin-mediated aggregation was monitored by UV-Vis spectroscopy by the shift in the SPR band. Though the interaction of ConA with glyconanoparticles is known in the literature, the impact of how the conformational control of the photoswitchable AuNP would influence the binding to proteins and lectins has not been explored.^[1, 6, 25, 26]

In light of this, binding affinity of two individual isomers **E-AuNP3** and **Z-AuNP3** with different orientation of ligand to the lectin ConA were tested and the effect of conformational change to binding event was evaluated. Firstly, to a 900 μ L of **E-AuNP3** (5.6 nM in phosphate buffer), 100 μ L of 5 μ M ConA in 0.1 mM phosphate buffer pH 7 was added. To get the **Z-AuNP3**, 900 μ L of **E-AuNP3** (5.6 nM in phosphate buffer) was irradiated for \sim 8-10 min at 365 nm to reach the photo-stationary state (pss), which was confirmed by UV-Vis spectroscopy. To the obtained **Z-AuNP3** was added 100 μ L of 5 μ M of ConA in 0.1 mM of phosphate buffer pH 7. ConA-mediated aggregation of **E-AuNP3** and **Z-AuNP3** was monitored by the shift in the SPR band by UV-Vis spectroscopy. As a control experiment only ConA was also measured by UV-Vis spectroscopy which showed no absorption band. As a negative control bovine serum albumin (BSA), 100 μ L of 5 μ M, was added to **E-AuNP3** (900 μ L in 0.1 mM phosphate buffer) which showed no shift in the UV-Vis spectrum, (i.e). no SPR band shift was observed which indicated that the ligand is specific to ConA only.

We found that the λ_{\max} of the SPR band of **E-AuNP3** after adding ConA moved from 529 nm to 544 nm which clearly showed the selective aggregation between ConA and **E-AuNP3**. In the case of **Z-AuNP-3**, the λ_{\max} of the SPR band before ConA additon was 528 nm; after the addition of ConA the λ_{\max} of the SPR band moved to 540 nm over the period of time. Overall

a red-shift of 14.5 nm was observed for **E-AuNP3** and 12 nm for **Z-AuNP3**. To deduce the kinetics of the binding of lectin ConA with the individual isomers **E-AuNP-3** and **Z-AuNP-3** was obtained by plotting a graph of SPR band shift (nm) as a function of time (Figure 4.2.4). This allowed us to determine the rate of individual isomer binding with ConA, both followed first order kinetics according to using equation (2).^[23]

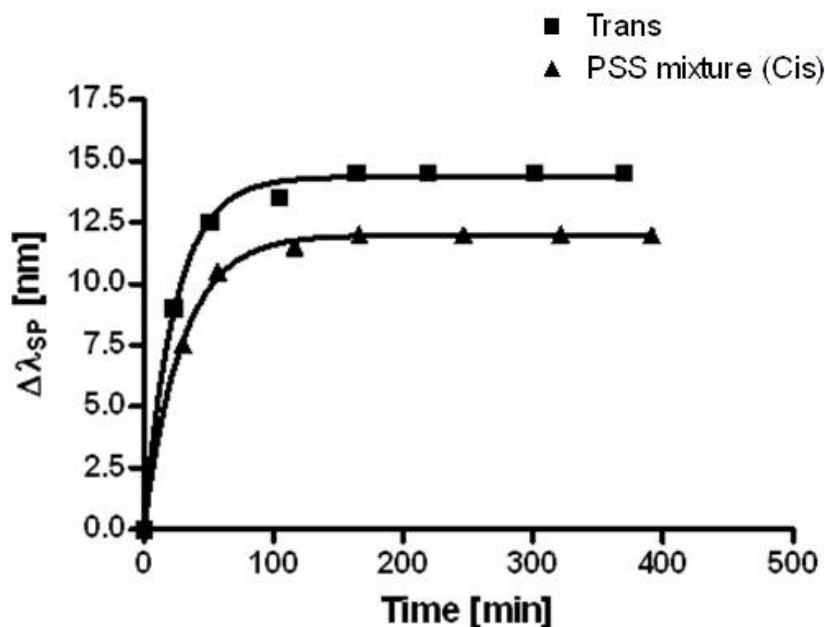


Figure 4.2.4: A plot of λ_{max} of SPR band shifts due to the ConA-mediated aggregation with **E-AuNP3** and **Z-AuNP3** as a function of time.

$$\Delta\lambda_{SP} = \Delta\lambda_{SP,max} [1 - e^{-k_{obs} \cdot t}] \quad \text{eq (2)}$$

where $\Delta\lambda_{SP}$ is the SP band shift over the period of time, $\Delta\lambda_{SP,max}$ is the maximal SP band shift and k_{obs} is the rate constant for the binding event. This preliminary analysis showed that **E-AuNP3** had a greater shift in the SPR band and faster kinetics of aggregation than its **Z-AuNP3** (Figure 4). We speculate that these results indicate that the mannosyl ligands in **E-AuNP3** are more easily available to the lectin relative compare to **Z-AuNP3**. Also, during the interaction between the **Z-AuNP3** and the lectin ConA, there could be a substantial back isomerization of **Z-AuNP3** \rightarrow **E-AuNP3** takes place. This results in a possible mixture of both **E-AuNP3** and **Z-AuNP3** in the system which makes it more complex for the binding event with the lectin ConA, hence slower binding constant for **Z-AuNP3** was observed.

4.2.6 Conclusion

In conclusion, synthetic route to different azobenzene glycosides with varied spacer units has been accomplished. Photochromic properties of free ligands **1- 3** in solution and functionalized ligand **3** on the AuNP surface (**E-AuNP3**→**Z-AuNP3**) were studied. Back isomerization of **Z**→**E** is faster in solution than on the AuNP surface. Investigation of the individual isomers, **E-AuNP3** and **Z-AuNP3**, and its interaction with the lectin ConA was performed. **E-AuNP3** had greater binding with the lectin ConA than the **Z-AuNP3**. The faster binding kinetics of **E-AuNP3** might be due to the spatial orientation and easy availability of the ligand to interact with the lectin compared to the **Z-AuNP3**.

Experimental Section

HAuCl₄ and *Concanavalia ensiformis* (ConA) were purchased from Sigma Aldrich. Air/moisture sensitive reactions were carried out under nitrogen in dry glassware. Thin layer chromatography was performed on silica gel plates (GF 254, Merck). Detection was effected by UV and subsequent charring with 10% sulphuric acid in EtOH followed by heat treatment at ~180 °C. Flash chromatography was performed on silica gel 60 (Merck, 230-400 mesh, particle size 0.040-0.063 mm) using distilled solvents. Optical rotations were measured with a Perkin-Elmer 241 polarimeter (sodium D-line: 589 nm, length of cell: 1 dm) in the solvents indicated. ¹H and ¹³C NMR spectra were recorded on Bruker DRX-500 and AV-600 spectrometers at 300 K. Chemical shifts are reported relative to internal tetramethylsilane (δ = 0.00 ppm) or D₂O (δ = 4.76 ppm). Full assignment of the peaks was achieved with the aid of 2D NMR techniques (¹H-¹H COSY and ¹H-¹³C HSQC). IR spectra were measured with a Perkin Elmer FT-IR Paragon 1000 (ATR) spectrometer. ESI mass spectra were recorded on an Esquire-LC instrument from Bruker Daltonics. MALDI-TOF mass spectra were recorded on a Bruker Biflex III instrument with 19 kV acceleration voltage. 2,5-Dihydroxybenzoic acid (DHB) was used as a matrix. For glyconanoparticle analysis and Lectin mediated aggregation UV-Vis spectroscopy Jasco V-650 spectrometer was used, and for other measurements Perkin-Elmer Lambda-241 was used at a temperature of 18 ± 1 °C. Dynamic light scattering measurements were performed on a BI-200SM instrument from Brookhaven Instruments

Corporation. Photoirradiation was carried out with LED lights from Nichia Corporation (NJSE107) power dissipation: 1.4 W, luminous flux: 44 [lm]

E-p-(p'-Bromodecylphenylazo)phenyl 2,3,4,6-tetra-O-acetyl- α -D-mannopyranoside (5):

To a mixture of **4** (250 mg, 0.459 mmol), 1-Bromodecanol (163 mg, 0.689 mmol), Triphenylphosphine (181 mg, 0.689 mmol) in dry THF (5 mL) at 0 °C was added Diethylazodicarboxylate (120 mg, 0.689 mmol). The reaction mixture was stirred at room temperature for 5 h, then, it was evaporated to dryness to get the crude product. The crude product was purified by column chromatography (cyclohexane: ethyl acetate 3:1) which provided **5** (277 mg, 0.364 mmol, 79%) as yellow crystalline solid. $R_f = 0.19$ (cyclohexane: ethyl acetate 7:3); $[\alpha]_D^{20} = +0.562$ (c= 1.0, CH₂Cl₂); ¹H-NMR (500 MHz, CDCl₃, 300.0 K): $\delta = 7.87$ (d, $J = 9.0$ Hz, 2H; H-14, H-18), 7.86 (d, $J = 9.0$ Hz, 2H; H-9, H-11), 7.20 (d, $J = 9.0$ Hz, 2H; H-8, H-12), 6.99 (d, $J = 9.0$ Hz, 2H; H-15, H-17), 5.61 (d, $J_{1,2} = 1.8$ Hz, 1H; H-1), 5.58 (dd, $J_{2,3} = 3.6$, $J_{3,4} = 10.0$ Hz, 1H; H-3), 5.48 (dd, $J_{1,2} = 1.8$ Hz, $J_{2,3} = 3.8$ Hz, 1H; H-2), 5.38 (t, $J_{3,4} = J_{4,5} = 10.1$ Hz, 1H; H-4), 4.29 (dd, $J_{5,6a} = 5.5$ Hz, $J_{6a,6b} = 12.2$, 1H; H-6a), 4.12-4.09 (m, 2H; H-5, H6b), 4.04 (t, $J = 6.6$ Hz, 2H; H-19), 3.41 (t, $J = 6.9$ Hz, 2H; H-28), 2.21, 2.06, 2.05, 2.03 (s, 12H, 4 OAc), 1.89-1.79 (m, 4H, H-20, H-27), 1.51-1.45 (m, 2H, H-21), 1.38-1.27 ppm (m, 10H, H-22, H-23, H-24, H-25, H-26); ¹³C-NMR (125 MHz, CDCl₃, 300.0 K): $\delta = 170.5$, 169.9, 169.9, 169.7 (C=O, OAc), 161.6 (C-16), 157.1 (C-7), 148.6 (C-10), 146.9 (C-13), 124.6 (C-14/C-18), 124.2 (C-9/C-11), 116.7 (C-8/C-12), 114.7 (C-15/C-17), 95.8 (C-1), 69.4 (C-5), 69.3 (C-2), 68.8 (C-3), 68.3 (C-19), 65.9 (C-4), 62.1 (C-6), 34.0 (C-28), 32.8 (C-20), 29.4 (C-27), 29.4 (C-22), 29.3 (C-23), 29.2 (C-24), 28.7 (C-25), 28.2 (C-26), 20.9, 20.9, 20.7, 20.7 ppm (CH₃COO); ESI-MS calcd for C₃₆H₄₇BrN₂O₁₁ [M+Na]⁺: 785.24; M_{found} = 785.09 .

E-p-(p'-Acetylthio-decyl-phenylazo)phenyl 2,3,4,6-tetra-O-acetyl- α -D-mannopyranoside (6):

A solution of potassium thioacetate (41 mg, 0.361 mmol) and bromo derivative **5** (250 mg, 0.328 mmol) in DMF (5 mL) was stirred at room temperature overnight (15 hr), then it was concentration under reduced pressure. Purification of the crude product by column chromatography (cyclohexane:ethyl acetate, 3:1) gave the title compound **6** as a pale yellow solid (226 mg, 0.298 mmol, 91%). Mp 113-114 °C; $R_f = 0.17$ (cyclohexane:ethyl acetate, 7:3); $[\alpha]_D^{20} = +0.317$ (c= 0.67, CH₂Cl₂); ¹H-NMR (500 MHz, CDCl₃, 300.1 K): $\delta = 7.87$ (d, $J = 9.0$ Hz, 2H; H-14, H-18), 7.86 (d, $J = 9.0$ Hz, 2H; H-9, H-11), 7.20 (d, $J = 9.0$ Hz, 2H; H-8, H-12), 6.99 (d, $J = 9.0$ Hz, 2H; H-15, H-17), 5.61 (d, $J_{1,2} = 1.7$ Hz, 1H; H-1), 5.58 (dd, $J_{2,3} = 3.6$ Hz,

$J_{3,4} = 10.0$, 1H; H-3), 5.48 (dd, $J_{1,2} = 1.8$ Hz, $J_{2,3} = 3.5$ Hz, 1H; H-2), 5.38 (t, $J_{3,4} = J_{4,5} = 10.2$ Hz, 1H; H-4), 4.30 (dd, $J_{5,6a} = 5.9$ Hz, $J_{6a,6b} = 12.6$, 1H; H-6a), 4.13-4.07 (m, 2H; H-5, H6b), 4.03 (t, $J = 6.4$ Hz, 2H; H-19), 2.87 (t, $J = 6.9$ Hz, 2H; H-28), 2.32 (s, 3H; H-30, SCOCH₃), 2.22, 2.06, 2.05, 2.03 (s, 12H; 4 OCOCH₃), 1.84-1.79 (m, 2H; H-20), 1.59-1.54 (m, 2H; H-27), 1.50-1.44 (m, 2H; H-21), 1.37-1.26 ppm (m, 10H; H-22, H-23, H-24, H-25, H-26); ¹³C-NMR (125 MHz, CDCl₃, 300.0 K): $\delta = 196.1$ (C-29, SCOCH₃), 170.5, 169.9, 169.9, 169.7 (4 OCOCH₃), 161.6 (C-16), 157.1 (C-7), 148.6 (C-10), 146.8 (C-13), 124.6 (C-14/C-18), 124.2 (C-9/C-11), 116.7 (C-8/C-12), 114.7 (C-15/C-17), 95.7 (C-1), 69.4 (C-5), 69.3 (C-2), 68.8 (C-3), 68.4 (C-19), 65.9 (C-4), 62.1 (C-6), 30.6 (C-30), 29.5 (C-28), 29.4-26.9 (C-20, C-22, C-23, C-24, C-25, C-26, C-27), 26.0 (C-21), 20.9, 20.9, 20.7, 20.7 ppm (CH₃COO); ESI-MS calcd for C₃₈H₅₀N₂O₁₂S [M+Na]⁺: 781.30; M_{found} = 781.09 .

E-*p*-(*p*'-Mercaptodecyl-phenylazo)phenyl α -D-mannopyranoside (E-1): To a solution of the acetyl-protected glycoside **6** (100 mg, 0.132 mmol) in dry MeOH (6 mL), a catalytic amount of solid NaOMe was added under N₂ atmosphere. The reaction mixture was stirred for 5 h at room temperature, then it was neutralization with Amberlite IR 120 ion-exchange resin and filtered. The filtrate was evaporated under reduced pressure to yield the deprotected mannoside **1** as a yellow solid (71 mg, 1.09 mmol, 98%). Mp 240°C (decomposition); ¹H-NMR (600 MHz, DMSO-d₆, 300.1 K): $\delta = 7.82$ -7.79 (m, 4H; H-9, H-11, H-15, H-17), 7.23 (dd, $J = 8.9$ Hz, $J = 8.9$ Hz, 2H; H-8, H-12), 7.08 (dd, $J = 8.9$ Hz, $J = 8.9$ Hz, 2H; H-15, H-17), 5.49 (s, 1H; H-1), 4.05-4.01 (m, 2H; H-19), 3.85 (dd, $J_{1,2} = 1.9$ Hz, $J_{2,3} = 3.1$ Hz, 1H; H-2), 3.69 (dd, $J_{2,3} = 3.6$ Hz, $J_{3,4} = 9.2$, 1H; H-3), 3.52-3.45 (m, 3H; H-4, H-6a, H-5), 3.37 (dd, $J_{5,6a} = 5.6$ Hz, $J_{6a,6b} = 10.0$, 1H; H-6b), 2.65 (t, $J = 7.2$ Hz, 2H; H-28), 1.73-1.69 (m, 2H; H-20), 1.42-1.21 ppm (m, 14H; H-21, H-22, H-23, H-24, H-25, H-26, H-27); ¹³C-NMR (150 MHz, DMSO-d₆, 300.0 K): $\delta = 161.6$ (C-16), 159.1 (C-7), 148.6 (C-10), 146.1 (C-13), 124.6 (C-14/C-18), 124.1 (C-9/C-11), 117.3 (C-8/C-12), 115.2 (C-15/C-17), 98.9 (C-1), 75.1 (C-5), 69.2 (C-2), 68.6 (C-3), 68.2 (C-19), 66.6 (C-4), 61.2 (C-6), 38.2 (C-28), 29.1-26.5 ppm (C-20, C-21, C-22, C-23, C-24, C-25, C-26, C-27).

Z-*p*-(*p*'-Mercaptodecyl-phenylazo)phenyl α -D-mannopyranoside (Z-1): ¹H-NMR (600 MHz, DMSO-d₆, 300.1 K): $\delta = 7.07$ (dd, $J = 8.8$ Hz, $J = 8.9$ Hz, 2H; H-8, H-12), 6.90-6.87 (m, 6H; H-9, H-11, H-14, H-15, H-17, H-18), 5.41 (s, 1H; H-1), 3.99-3.95 (m, 2H; H-19), 3.85 (m_c, 1H; H-2), 3.71-3.59 (m, 2 H; H-3, H-6a), 3.55-3.49 (m, 2H; H-4, H-6b), 3.39 (ddd, $J_{4,5} = 3.3$

Hz, $J_{5,6a} = 5.9$ Hz, $J_{6a,6b} = 11.4$, 1H; H-5), 2.72 (t, $J = 7.2$ Hz, 2H; H-28), 1.71 (dd, $J = 7.2$ Hz, $J = 14.0$ Hz, 2H; H-20), 1.39-1.28 ppm (m, 14H; H-21, H-22, H-23, H-24, H-25, H-26, H-27); ^{13}C -NMR (150 MHz, DMSO- d_6 , 300.0 K): $\delta = 161.6$ (C-16), 155.5 (C-7), 148.6 (C-10), 146.6 (C-13), 122.8 (C-14/C-18), 122.3 (C-9/C-11), 117.5 (C-8/C-12), 114.8 (C-15/C-17), 99.1 (C-1), 75.4 (C-5), 70.8 (C-3), 70.2 (C-2), 68.2 (C-19), 66.9 (C-4), 61.3 (C-6), 38.2 (C-28), 29.3-25.8 ppm (C-20, C-21, C-22, C-23, C-24, C-25, C-26, C-27).

1,17-Dibromohexaethylene glycol (9): To a solution of hexaethylene glycol (200 mg, 0.709 mmol) in THF (2 mL) was added triphenyl phosphine (372 mg, 1.42 mmol) and CBr_4 (469 mg, 1.42 mmol) at 0°C . The reaction mixture was stirred for 16 h at room temperature. The white residue was filtered and the filtrate was evaporated, the resulting pasty colourless residue was extracted several times with hexane (20 ml x 5). The combined extract was evaporated to get the dibromohexaethylene **9** as colourless oil (237 mg, 0.581 mmol, 82%). $R_f = 0.23$ (ethyl acetate:cyclohexane 4:1); ^1H -NMR (200 MHz, CDCl_3 , 300.0 K): 3.81 (t, $J = 6.3$ Hz, 4H; O- CH_2 - CH_2 -Br), 3.67-3.65 (m, 16H, 4 x O- CH_2 - CH_2 -O), 3.47 ppm (t, $J = 6.3$ Hz, 4H; O- CH_2 - CH_2 -Br), ^{13}C -NMR (75 MHz, CDCl_3 , 300.0 K): $\delta = 71.2$ (O- CH_2 - CH_2 -Br), 70.6-70.4 (O- CH_2 - CH_2 -O), 30.3 ppm (O- CH_2 - CH_2 -Br); ESI-MS Calcd for $\text{C}_{12}\text{H}_{24}\text{Br}_2\text{O}_5$ $[\text{M}+\text{Na}]^+$: 430.99; $M_{\text{found}} = 430.92$.

***E-p*-(*p'*-Bromohexaethyleneglycol-phenylazo)phenyl 2,3,4,6-tetra-O-acetyl-**

α -D-mannopyranoside (10): A mixture of **4** (100 mg, 0.184 mmol), di-bromohexaethylene glycol **9** (149 mg, 0.367 mmol), potassium carbonate (50.7 mg, 0.367 mmol) in dry DMF (3 mL) was stirred at 40°C for overnight, 16 h. The reaction mixture was diluted with ethyl acetate (20 mL), washed with water (10 mL) and dried over Na_2SO_4 . This was filtered and the filtrate was concentrated under reduced pressure. Purification of the crude product by column chromatography (ethyl acetate:cyclohexane 7:3) gave the title compound **10** as reddish brown syrup (118 mg, 0.136 mmol, 74%). $R_f = 0.23$ (ethyl acetate:cyclohexane 7:3); ^1H -NMR (500 MHz, CDCl_3 , 300.0 K): $\delta = 7.88$ (d, $J = 9.0$ Hz, 2H; H-14, H-18), 7.87 (d, $J = 9.0$ Hz, 2H; H-9, H-11), 7.20 (d, $J = 9.0$ Hz, 2H; H-8, H-12), 7.02 (d, $J = 9.0$ Hz, 2H; H-15, H-17), 5.60 (d, $J_{1,2} = 1.8$ Hz, 1H; H-1), 5.57 (dd, $J_{2,3} = 3.6$ Hz, $J_{3,4} = 10.0$, 1H; H-3), 5.47 (dd, $J_{1,2} = 1.8$ Hz, $J_{2,3} = 3.5$ Hz, 1H; H-2), 5.38 (t, $J_{3,4} = J_{4,5} = 10.0$ Hz, 1H; H-4), 4.29 (dd, $J_{5,6a} = 5.6$ Hz, $J_{6a,6b} = 12.4$, 1H; H-6a), 4.22-4.20 (m, 2H; H-19), 4.12-4.07 (m, 2H; H-5, H-6b), 3.90-3.88 (m, 2H; H-20), 3.71 (t, $J = 6.3$ Hz, 2H; H-30), 3.75-3.64 (m, 16H; H-21, H-22, H-23, H-24, H-25, H-26, H-

27, H-28), 3.46 (*t*, *J* = 6.3 Hz, 2H; H-30), 2.21, 2.06, 2.04, 2.03 ppm (each *s*, each 3 H, 4 COCH_3); $^{13}\text{C-NMR}$ (125 MHz, CDCl_3 , 299.9 K): δ = 170.5, 169.9, 169.9, 169.7 (4 COCH_3), 161.2 (C-16), 157.2 (C-7), 148.5 (C-10), 146.9 (C-13), 124.6 (C-14/C-18), 124.2 (C-9/C-11), 116.7 (C-8/C-12), 114.9 (C-15/C-17), 95.7 (C-1), 70.9-70.5 (C-21, C-22, C-23, C-24, C-25, C-26, C-27, C-28) 69.6 (C-29), 69.4 (C-20), 69.3 (C-5), 69.1 (C-2), 68.8 (C-3), 67.6 (C-19), 65.9 (C-4), 62.1 (C-6), 30.3 (C-30), 20.9, 20.7, 20.7, 20.7 ppm (COCH_3); MALDI-TOF Calcd for $\text{C}_{38}\text{H}_{51}\text{BrN}_2\text{O}_{16}$ $[\text{M}+\text{Na}]^+$: 893.24; $M_{\text{found}} = 893.54$.

***E-p*-(*p'*-Acetylthio-hexaethyleneglycol-phenylazo)phenyl 2,3,4,6-tetra-*O*-acetyl- α -*D*-mannopyranoside (11):**

A mixture of bromo derivative **10** (100 mg, 0.115 mmol), and potassium thioacetate (14.4 mg, 0.127 mmol) in DMF (3 mL) was stirred at room temperature overnight (15 hr). The reaction mixture was concentrated under reduced pressure, purification of the crude product by column chromatography (ethyl acetate:cyclohexane 7:3) gave the title compound **11** as brown syrup. (86 mg, 99.3 μmol , 86%) $R_f = 0.23$ (ethyl acetate:cyclohexane 4:1); $[\alpha]_D^{20} = +92.4$ (*c* = 0.8, CH_2Cl_2); $^1\text{H-NMR}$ (500 MHz, CDCl_3 , 300.2 K): δ = 7.81 (*d*, *J* = 8.9 Hz, 2H; H-14, H-18), 7.80 (*d*, *J* = 8.9 Hz, 2H; H-9, H-11), 7.14 (*d*, *J* = 8.9 Hz, 2H; H-8, H-12), 6.95 (*d*, *J* = 8.9 Hz, 2H; H-15, H-17), 5.54 (*d*, $J_{1,2} = 1.7$ Hz; 1H, H-1), 5.51 (*dd*, $J_{2,3} = 3.5$ Hz, $J_{3,4} = 10.0$ Hz, 1H; H-3), 5.41 (*dd*, $J_{1,2} = 1.8$ Hz, $J_{2,3} = 3.5$ Hz, 1H; H-2), 5.31 (*t*, $J_{3,4} = J_{4,5} = 10.2$ Hz, 1H; H-4), 4.22 (*dd*, $J_{5,6a} = 5.6$ Hz, $J_{6a,6b} = 12.3$ Hz, 1H; H-6a), 4.16-4.14 (*m*, 2H; H-19), 4.03 (*m_c*, 2H; H-5, h-6_b), 3.84-3.82 (*m*, 2H; H-20), 3.68-3.66 (*m*, 16H, H-21, H-22, H-23, H-24, H-25, H-26, H-27, H-28), 3.01 (*t*, *J* = 6.5 Hz, 2H, H-30), 2.26 (*s*, 3H; H-32), 2.14, 1.99, 1.98, 1.96 ppm (each *s*, each 3 H, 4 COCH_3); $^{13}\text{C-NMR}$ (125 MHz, CDCl_3 , 300.1 K): δ = 195.5 (C-31), 170.5, 169.9, 169.9, 169.7 (4 COCH_3), 161.2 (C-16), 157.2 (C-7), 148.5 (C-10), 146.9 (C-13), 124.6 (C-14/C-18), 124.2 (C-9/C-11), 116.7 (C-8/C-12), 114.9 (C-15/C-17), 95.7 (C-1), 70.9-69.7 (C-21, C-22, C-23, C-24, C-25, C-26, C-27, C-28), 69.6 (C-29), 69.4 (C-20), 69.3 (C-5), 69.1 (C-2), 68.8 (C-3), 67.8 (C-19), 65.9 (C-4), 62.1 (C-6), 30.5 (C-32), 28.8 (C-30), 20.9, 20.7, 20.7, 20.7 ppm (COCH_3); MALDI-TOF Calcd for $\text{C}_{40}\text{H}_{54}\text{N}_2\text{O}_{17}\text{S}$ $[\text{M}+\text{Na}]^+$: 889.31 ($\text{M}+\text{Na}$) $^+$; $M_{\text{found}} = 889.39$.

***E-p*-(*p'*-Mercaptohexaethyleneglycol-phenylazo)phenyl α -*D*-mannopyranoside (*E*-2):**

Acetyl-protected glycoside **11** (80 mg, 92.4 μmol) was dissolved in dry MeOH (2 mL) and a catalytic amount of solid NaOMe was added under N_2 atmosphere. The reaction mixture was stirred for 4 h at room temperature, then it was neutralization with Amberlite IR 120 ion-

exchange resin and filtered. The filtrate was evaporated under reduced pressure to yield the title mannoside **2** as a orange syrup (59 mg, 88.4 μmol , 97%). $[\alpha]_{\text{D}}^{20} = + 82.3$ ($c = 0.8$, DMSO); $^1\text{H-NMR}$ (500 MHz, CD_3OD , 299.9 K): $\delta = 7.75$ (d, $J = 9.1$ Hz, 2H; H-14, H18), 7.74 (d, $J = 9.0$ Hz, 2H; H-9, H-11), 7.16 (d, $J = 9.1$ Hz, 2H; H-8, H-12), 6.97 (d, $J = 9.1$ Hz, 2H; H-15, H-17), 5.49 (d, $J_{1,2} = 1.6$ Hz, 1H; H-1), 4.12-4.10 (m, 2H; H-19), 3.94 (dd, $J_{1,2} = 1.8$ Hz, $J_{2,3} = 3.4$ Hz, 1H; H-2), 3.82 (dd, $J_{2,3} = 3.5$ Hz, $J_{3,4} = 9.5$ Hz, 1H; H-3), 3.78-3.76 (m, 2H; H-20), 3.69-3.47 (m, 22H; H-4, H-5, H-6a, H-6b, H-21, H-22, H-23, H-24, H-25, H-26, H-27, H-28, H-29), 2.75 (t, $J = 6.4$ Hz, 2H, H-30); $^{13}\text{C-NMR}$ (125 MHz, CD_3OD , 299.9 K): $\delta = 162.6$ (C-16), 160.1 (C-7), 148.7 (C-10), 148.3 (C-13), 125.5 (C-14/C-18), 125.2 (C-9/C-11), 118.0 (C-8/C-12), 116.0 (C-15/C-17), 100.1 (C-1), 75.7 (C-5), 72.4 (C-3), 71.9 (C-2), 71.6-71.5 (C-21, C-22, C-23, C-24, C-25, C-26, C-27, C-28), 71.4 (C-29), 70.8 (C-20), 69.0 (C-19), 68.2 (C-4), 62.7 (C-6), 39.6 ppm (C-30). ESI-MS calcd for $\text{C}_{30}\text{H}_{44}\text{N}_2\text{O}_{12}\text{S}$ $[\text{M}+\text{Na}]^+$: 679.26; $M_{\text{found}} = 679.25$.

Z-p-(p'-Mercaptohexaethyleneglycol-phenylazo)phenyl α -D-mannopyranoside (Z-2): $^1\text{H-NMR}$ (500 MHz, CD_3OD , 300.4 K): $\delta = 7.07$ (d, $J = 9.0$ Hz, 2H; H-8, H12), 6.89-6.87 (m, 6H; H-9, H-11, H-12, H-14, H-15, H-17, H-18), 5.47 (d, $J_{1,2} = 1.7$ Hz, 1H; H-1), 4.12-4.10 (m, 2H; H-19), 3.98 (dd, $J_{1,2} = 1.8$ Hz, $J_{2,3} = 3.4$ Hz, 1H; H-2), 3.86 (dd, $J_{2,3} = 3.5$ Hz, $J_{3,4} = 9.4$ Hz, 1H; H-3), 3.82-3.81 (m, 2H; H-20), 3.74-3.67 (m, 4H; H-4, H-5, H-6a, H-6b), 3.65-3.61 (m, 18H; H-21, H-22, H-23, H-24, H-25, H-26, H-27, H-28, H-29), 2.88 ppm (t, $J = 6.4$ Hz, 2H, H-30); $^{13}\text{C-NMR}$ (125 MHz, CD_3OD , 300.1 K): $\delta = 160.0$ (C-16), 157.1 (C-7), 148.7 (C-10), 148.3 (C-13), 124.1 (C-14/C-18), 123.4 (C-9/C-11), 118.0 (C-8/C-12), 115.8 (C-15/C-17), 100.2 (C-1), 75.6 (C-5), 72.4 (C-3), 71.9 (C-2), 71.7-71.4 (C-4, C-21, C-22, C-23, C-24, C-25, C-26, C-27, C-28), 70.7 (C-20), 70.5 (C-29), 68.9 (C-19), 68.3 (C-4), 62.7 (C-6), 39.6 ppm (C-30).

E-p-(p'-Acetylthioundecyl-tetraethyleneglycol-phenylazo)phenyl 2,3,4,6-tetra-O-acetyl- α -D-mannopyranoside (8): To a suspension of **4** (150 mg, 0.275 mmol) and polymer supported Triphenylphosphine (180 mg, 0.275 mmol, 1.6 mmol g^{-1}) in dry THF (3 mL) diethylazodicarboxylate (86 μL , 0.551 mmol) was added at 0 $^{\circ}\text{C}$. To this cooled solution a predissolved solution of **7** (250 mg, 0.592 mmol) in dry THF (1 mL) was added. The reaction mixture was stirred at room temperature over night (14 h), the resin containing reaction mixture was filtered, thoroughly washed with THF (20 mL), filtrate concentrated under reduced pressure. Purification of the crude product by column chromatography (ethyl

acetate:cyclohexane 4:1) gave compound **8** as yellowish syrup (185 mg, 0.196 mmol, 71%). $R_f = 0.29$ (ethyl acetate:cyclohexane 4:1); $^1\text{H-NMR}$ (500 MHz, CDCl_3 , 300.0 K): $\delta = 7.88$ (d, $J = 9.0$ Hz, 2H; H-14, H-18), 7.87 (d, $J = 9.0$ Hz, 2H; H-9, H-11), 7.21 (d, $J = 9.1$ Hz, 2H; H-8, H-12), 7.02 (d, $J = 9.1$ Hz, 2H; H-15, H-17), 5.61 (s, $J_{1,2} = 1.8$ Hz, 1H; H-1), 5.58 (dd, $J_{2,3} = 3.6$ Hz, $J_{3,4} = 10.0$, 1H; H-3), 5.48 (dd, $J_{1,2} = 1.8$ Hz, $J_{2,3} = 3.5$ Hz; 1H, H-2), 5.38 (t, $J = 10.1$ Hz; H-4), 4.30 (dd, $J_{5,6a} = 5.5$ Hz, $J_{6a,6b} = 12.3$ Hz, 1H, H-6a), 4.22-4.20 (m, 2H; H-19), 4.12-4.07 (m, 2H, H-5, H-6b), 3.90 (dd, $J = 5.3$ Hz, $J = 4.4$ Hz, 2H, H-20), 3.75-3.63 (m, 10 H; H-21, H-22, H-23, H-24, H-25), 3.57 (dd, $J = 3.4$ Hz, $J = 6.1$ Hz, 2H; H-26), 3.44 (t, $J = 6.8$ Hz, 2H; H-27), 2.85 (m, 2H; H-37), 2.32 (s, 3H; H-39, SCOCH_3), 2.22, 2.06, 2.05, 2.03 (each s, each 3 H, 4 COCH_3), 1.55 (m, 4H, H-28, H-36), 1.37-1.21 ppm (m, 14 H; H-29, H-30, H-31, H-32, H-33, H-34, H-35); $^{13}\text{C-NMR}$ (125 MHz, CDCl_3 , 299.9 K): $\delta = 196.0$ (C-38), 170.5, 169.9, 169.8, 169.7 (4 COCH_3), 161.1 (C-16), 157.1 (C-7), 148.5 (C-10), 147.0 (C-13), 124.5 (C-14/C-18), 124.2 (C-9/C-11), 116.7 (C-8/C-12), 114.9 (C-15/C-17), 95.7 (C-1), 70.9-70.5 (C-21, C-22, C-23, C-24, C-25, C-26), 69.6 (C-27), 69.4 (C-5), 69.3 (C-2), 68.8 (C-3), 67.7 (C-20), 65.6 (C-19), 65.9 (C-4), 62.1 (C-6), 30.6 (C-39), 29.6-29.4 (C-28, C-29, C-30, C-31, C-32, C-33, C-34, C-35, C-36), 29.1 (C-37), 20.8, 20.7, 20.7 20.6 ppm (4 x COCH_3); MALDI-TOF Calcd for $\text{C}_{47}\text{H}_{68}\text{N}_2\text{O}_{16}\text{S}$ [$\text{M}+\text{Na}$] $^+$; 971.42; $M_{\text{found}} = 971.72$.

E-p-(p'-Mercaptoundecyl-tetraethyleneglycol-phenylazo)phenyl- α -D-mannopyranoside (E-3): Acetyl-protected glycoside **8** (100 mg, 0.105 mmol) was dissolved in dry MeOH (2 mL) and a catalytic amount of solid NaOMe was added under N_2 atmosphere. The reaction mixture was stirred for 6 h at room temperature, then it was neutralization with Amberlite IR 120 ion-exchange resin and filtered. The filtrate was concentrated under reduced pressure to yield the title mannoside **3** as a pale yellow syrup (72 mg, 97.6 μmol , 93%) $^1\text{H-NMR}$ (600 MHz, CD_3OD , 298.0 K): $\delta = 7.86$ (d, $J = 8.9$ Hz, 2H; H-14, H-18), 7.85 (d, $J = 8.9$ Hz, 2H; H-9, H-11), 7.26 (d, $J = 8.9$ Hz, 2H; H-8, H-12), 7.08 (d, $J = 9.0$ Hz, 2H; H-15, H-17), 5.59 (s, $J_{1,2} = 1.2$ Hz, 1H; H-1), 4.23-4.22 (m, 2H; H-19), 4.04 (dd, $J_{1,2} = 1.8$ Hz, $J_{2,3} = 3.4$ Hz; 1H, H-2), 3.93 (dd, $J_{2,3} = 3.5$ Hz, $J_{3,4} = 9.5$, 1H; H-3), 3.89-3.87 (m, 2H; H-20), 3.75-3.72 (m, 4H; H-4, H-5, H-6a, H-6b), 3.68-3.54 (m, 12H; H-21, H-22, H-23, H-24, H-25, H-26), 3.54 (m, 2H; H-27), 3.43 (t, $J = 6.6$ Hz, 2H; H-27), 2.46 (t, $J = 7.2$ Hz, 2H; H-37), 1.58-1.51 (m, 4H; H-28, H-36); 1.37-1.23 (m, 14 H, H-29, H-30, H-31, H-32, H-33, H-34, H-35); $^{13}\text{C-NMR}$ (150 MHz, CD_3OD , 298.0 K): $\delta = 162.7$ (C-16), 159.9 (C-7), 149.3 (C-10), 148.4 (C-13), 125.5 (C-14/C-18), 125.2 (C-9/C-11), 117.9 (C-8/C-12), 115.9 (C-15/C-17), 100.1 (C-1), 75.7 (C-5), 72.4 (C-27), 71.9 (C-3), 71.8

(C-2), 71.6-71.2 (H-21, H-22, H-23, H-24, H-25, H-26), 70.8 (C-20), 69.0 (C-19), 68.3 (C-4), 62.7 (C-6), 30.7-27.2 (C-28, H- 29, H-30, H-31, H-32, H-33, H-34, H-35, H-36), 24.9 (C-37). MALDI-TOF: Calcd for C₃₇H₅₈N₂O₁₁S [M+Na]⁺; 761.38, M_{found} = 761.72

Z-p-(p'-(4'-Mercaptoundecyl-tetraethyleneglycol-phenylazo)phenyl- α -D-mannopyranoside

(Z-3): ¹H-NMR (600 MHz, CD₃OD, 298.0 K): δ = 7.07 (d, J = 8.7 Hz, 2H; H-8, H-12), 6.91-6.87 (m, 6H; H-9, H-11, H-12, H-14, H-15, H-17, H-18), 5.47 (s, 1H; H-1), 4.12-4.10 (m, 2H; H-19), 3.97 (m_c, 1H, H-2), 3.86 (dd, $J_{2,3}$ = 3.3 Hz, $J_{3,4}$ = 9.4, 1H; H-3), 3.83-3.81 (m, 2H; H-20), 3.76-3.52 (m, 16H; H-4, H-5, H-6_a, H-6_b, H-21, H-22, H-23, H-24, H-25, H-26), 3.45 (t, J = 6.6 Hz, 2H; H-27), 2.67 (t = 7.3 Hz, 2H; H-37), 1.56 -1.53 (m, 4H; H-28, H-36); 1.36-1.24 (m, 14 H; H- 29, H-30, H-31, H-32, H-33, H-34, H-35); ¹³C-NMR (150 MHz, CD₃OD, 298.0 K): δ = 160.1 (C-16), 157.2 (C-7), 149.3 (C-10), 147.8 (C-13), 124.1 (C-14/C-18), 123.4 (C-9/C-11), 118.0 (C-8/C-12), 115.8 (C-15/C-17), 100.2 (C-1), 75.6 (C-5), 72.4 (C-27), 71.8 (C-3), 71.6 (C-2), 71.5-71.2 (C-4, H-21, H-22, H-23, H-24, H-25, H-26), 70.7 (C-20), 68.9 (C-19), 68.3 (C-4), 62.6 (C-6), 30.7-27.2 (C-28, H- 29, H-30, H-31, H-32, H-33, H-34, H-35, H-36), 24.9 ppm (C-37).

Preparation of citrate stabilized gold nanoparticles. HAuCl₄ (80 mg) was added to degassed MilliQ water (100 mL), stirred vigorously and heated to 60 °C for 10 min. To this hot yellow mixture, a solution of sodium citrate (228 mg) in degassed MilliQ water was added quickly between 50-60 °C. The reaction mixture turned to colourless and then became red wine colour. Reflux was continued for another 30 min, then the mixture was brought to room temperature and then it was filtered using suction funnel and the filtrate was stored at refrigerator.

Acknowledgements

Author would like to thank COST office for this STSM project and for the travel grant. Prof. Anne Staubitz for the generous gift of *p-p'*-dihydroxy azobenzene.

References

- [1] J. Rojo, V. Díaz, J. M. de la Fuente, I. Segura, A. G. Barrientos, H. H. Riese, A. Bernad, S. Penadés, *ChemBioChem*. **2004**, *5*, 291-297.
- [2] J. M. de la Fuente, A. G. Barrientos, T. C. Rojas, J. Rojo, J. Cañada, A. Fernández, S. Penadés, *Angew. Chem.* **2001**, *113*, 2317-2321; *Angew. Chem. Intl. Ed.* **2001**, *40*, 2257-2261.
- [3] C.-C. Lin, Y.-C. Yeh, C.-Y. Yang, G.-F. Chen, Y.-C. Chen, Y.-C. Wu, C.-C. Chen, *Chem. Commun.* **2003**, 2920-2921
- [4] J. M. de la Fuente, S. Penadés, *Biochim. Biophys. Acta Gen. Subj.* **2006**, *1760*, 636-651.
- [5] K. Larsen, M. B. Thygesen, F. Guillaumie, W. G. T. Willats, K. J. Jensen, *Carbohydr. Res.* **2006**, *341*, 1209-1234.
- [6] K. M. Halkes, A. Carvalho de Souza, C. E. P. Maljaars, G. J. Gerwig, J. P. Kamerling, *Eur. J. Org. Chem.* **2005**, *2005*, 3650-3659
- [7] M. B. Thygesen, J. Sauer, K. J. Jensen, *Chem. Eur. J.* **2009**, *15*, 1649-1660.
- [8] Y. Wei, S. Han, J. Kim, S. Soh, B. A. Grzybowski, *J. Am. Chem. Soc.* **2010**, *132*, 11018-11020.
- [9] A. A. Beharry, G. A. Woolley, *chem. Soc. Rev.* **2011**, *40*, 4422-4437.
- [10] M. Hartmann, H. Papavlassopoulos, V. Chandrasekaran, C. Grabosch, F. Beiroth, T. K. Lindhorst, C. Roehl, *FEBS Lett.* **2012**, *586*, 1459-1465.
- [11] O. Srinivas, N. Mitra, A. Surolia, N. Jayaraman, *Glycobiology* **2005**, *15*, 861-873.
- [12] V. Chandrasekaran, K. Kolbe, F. Beiroth, T. K. Lindhorst, *Beilstein J. Org. Chem.* **2013**, *9*, 223-233.
- [13] P. K. Jha, V. Kuzovkov, B. A. Grzybowski, M. O. d. I. Cruz, *Soft Matter* **2012**, *8*, 227-234.

- [14] V. Chandrasekaran, T. K. Lindhorst, *Chem. Commun.* **2012**, *48*, 7519-7521.
- [15] T. K. Lindhorst, S. Kötter, U. Krallmann-Wenzel, S. Ehlers, *J. Chem. Soc., Perkin Trans. 1*, **2001**, 823-831.
- [16] T.-C. Zheng, M. Burkart, D. E. Richardson, *Tetrahedron Lett.* **1999**, *40*, 603-606.
- [17] G. Zemplén, E. Pacsu, *Ber. Dtsch. Chem. Ges.* **1929**, *62*, 1613-1614.
- [18] G. Bérubé, D. Rabouin, V. Perron, B. NZemba, R.-C. Gaudreault, S. Parent, È. Asselin, *Steroids* **2006**, *71*, 911-921.
- [19] R. Lévy, N. T. K. Thanh, R. C. Doty, I. Hussain, R. J. Nichols, D. J. Schiffrin, M. Brust, D. G. Fernig, *J. Am. Chem. Soc.* **2004**, *126*, 10076-10084.
- [20] J. Turkevich, P. C. Stevenson, J. Hillier, *J. Phys. Chem.* **1953**, *57*, 670-673
- [21] W. Haiss, N. T. K. Thanh, J. Aveyard, D. G. Fernig, *Anal. Chem.* **2007**, *79*, 4215-4221.
- [22] M. B. Thygesen, K. K. Sorensen, E. Cló, K. J. Jensen, *Chem. Commun.* **2009**, 6367-6369
- [23] C. S. Weisbecker, M. V. Merritt, G. M. Whitesides, *Langmuir* **1996**, *12*, 3763-3772.
- [24] G. Pace, V. Ferri, C. Grave, M. Elbing, C. von Hänisch, M. Zharnikov, M. Mayor, M. A. Rampi, P. Samorí, *PNAS* **2007**, *104*, 9937-9942.
- [25] D. C. Hone, A. H. Haines, D. A. Russell, *Langmuir* **2003**, *19*, 7141-7144.
- [26] N. C. Reichardt, M. Martín-Lomas, S. Penadés, *Chem. Soc. Rev.* **2013**. *in press*

Supporting Information

for

Photosensitive glyconanoparticles: A new tool to switch carbohydrate-protein interaction

Vijayanand Chandrasekaran, Mikkel B. Thygesen, Knud J. Jensen, and
Thisbe K. Lindhorst*

E-mail: tkhind@oc.uni-kiel.de

Table of contents

1. Photoisomerisation

1H-NMR spectra of <i>E-1</i> and <i>Z-1</i>	S3
1H- NMR spectra of <i>E-2</i> and <i>Z-2</i>	S4
13C-NMR spectra of <i>E-2</i> and <i>Z-2</i>	S5
1H -NMR spectra of <i>E-3</i> and <i>Z-3</i>	S6
13C-NMR spectra of <i>E-3</i> and <i>Z-3</i>	S7

UV-Vis spectra of thermal Z-1 → E-1 relaxation	S8
UV-Vis spectra of thermal Z-2 → E-2 relaxation	S9
UV-Vis spectra of thermal Z-3 → E-3 relaxation in methanol	S10
UV-Vis spectra of thermal Z-2 → E-2 relaxation in buffer	S11
UV-Vis spectra of thermal Z-AuNP3 → E-AuNP3 relaxation in buffer	S12
UV-Vis spectra of Con-A induced aggregation with E-AuNP3	S13
UV-Vis spectra of Con-A induced aggregation with Z-AuNP3	S14
2. Dynamic light Scatter (DLS)	
DLS data for E-AuNP3	S15
DLS data for Z-AuNP3	S18
3. Synthesis of Photosensitive glyconanoparticles	S21

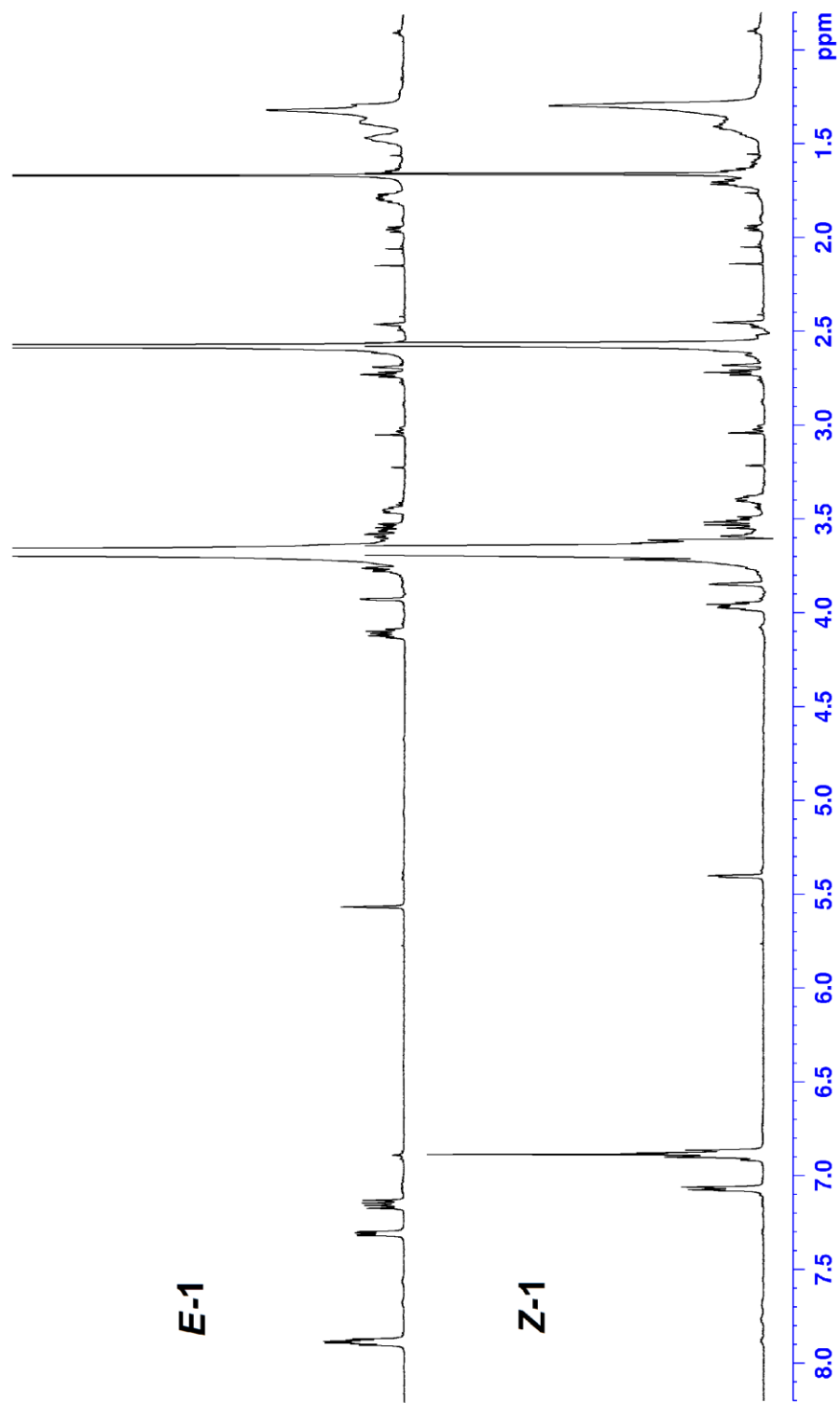


Figure S1: ¹H NMR spectra of **(E)-1** and **(Z)-1** in DMSO-*d*₆ (600 MHz).

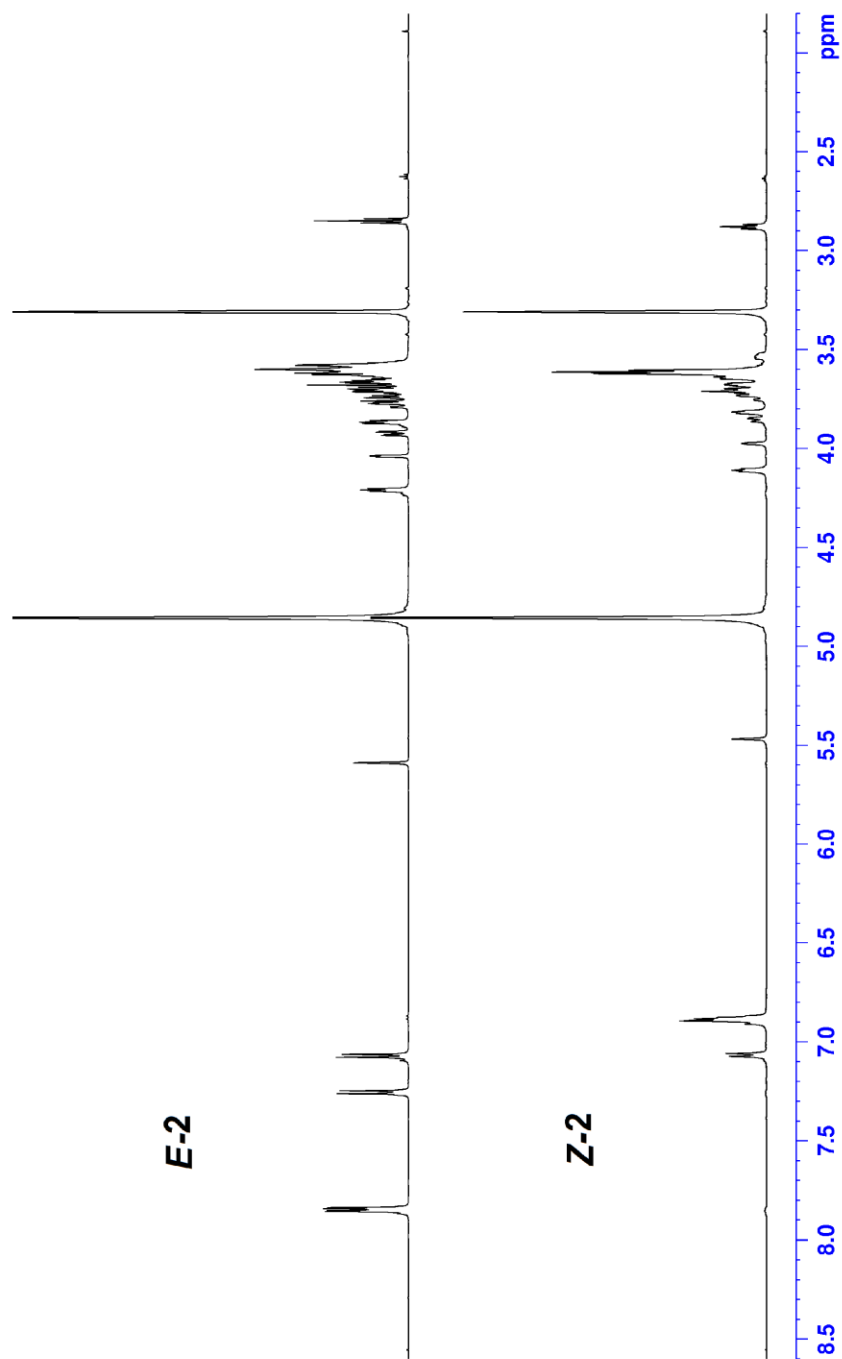


Figure S2: ¹H NMR spectra of (*E*)-2 and (*Z*)-2 in CD₃OD (600 MHz).

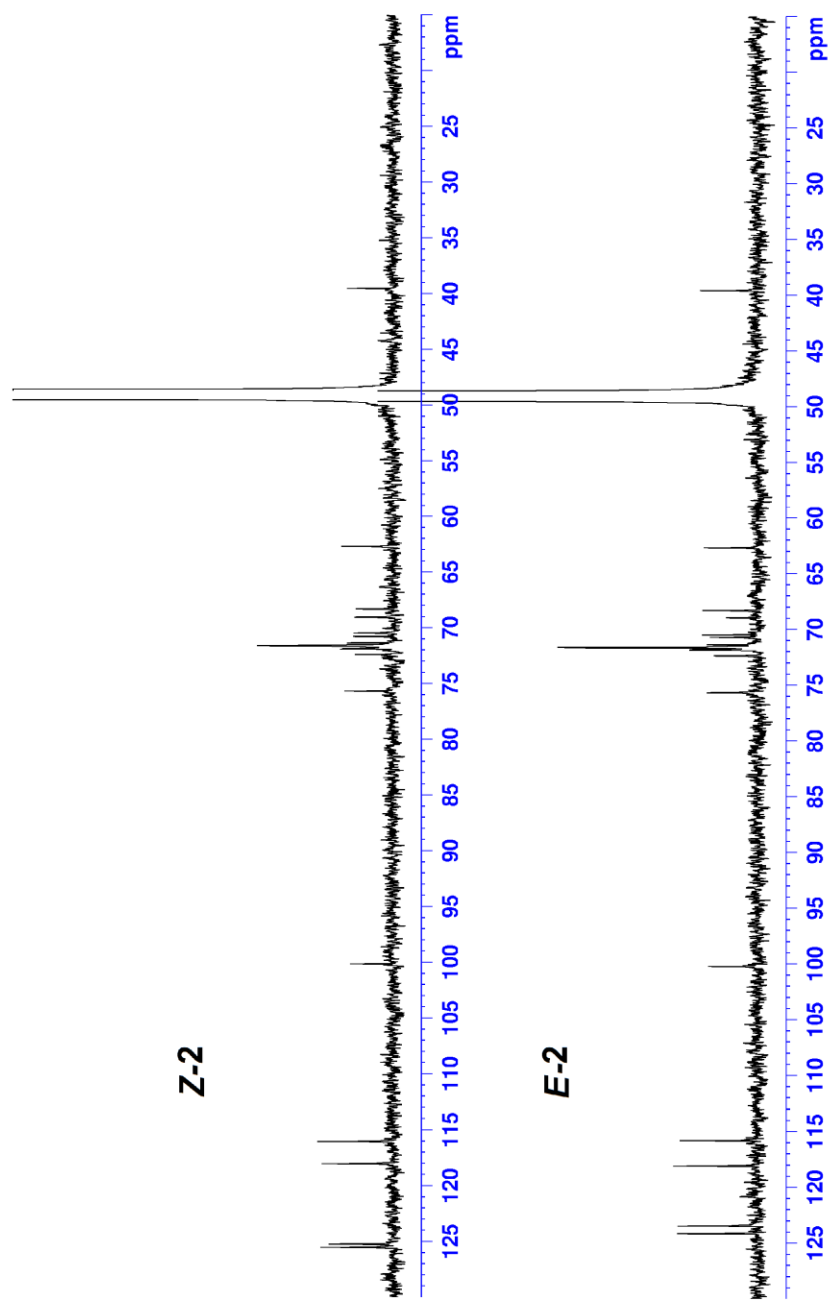


Figure S3: ¹³C NMR spectra of (*E*)-2 and (*Z*)-2 in CD₃OD (150 MHz).

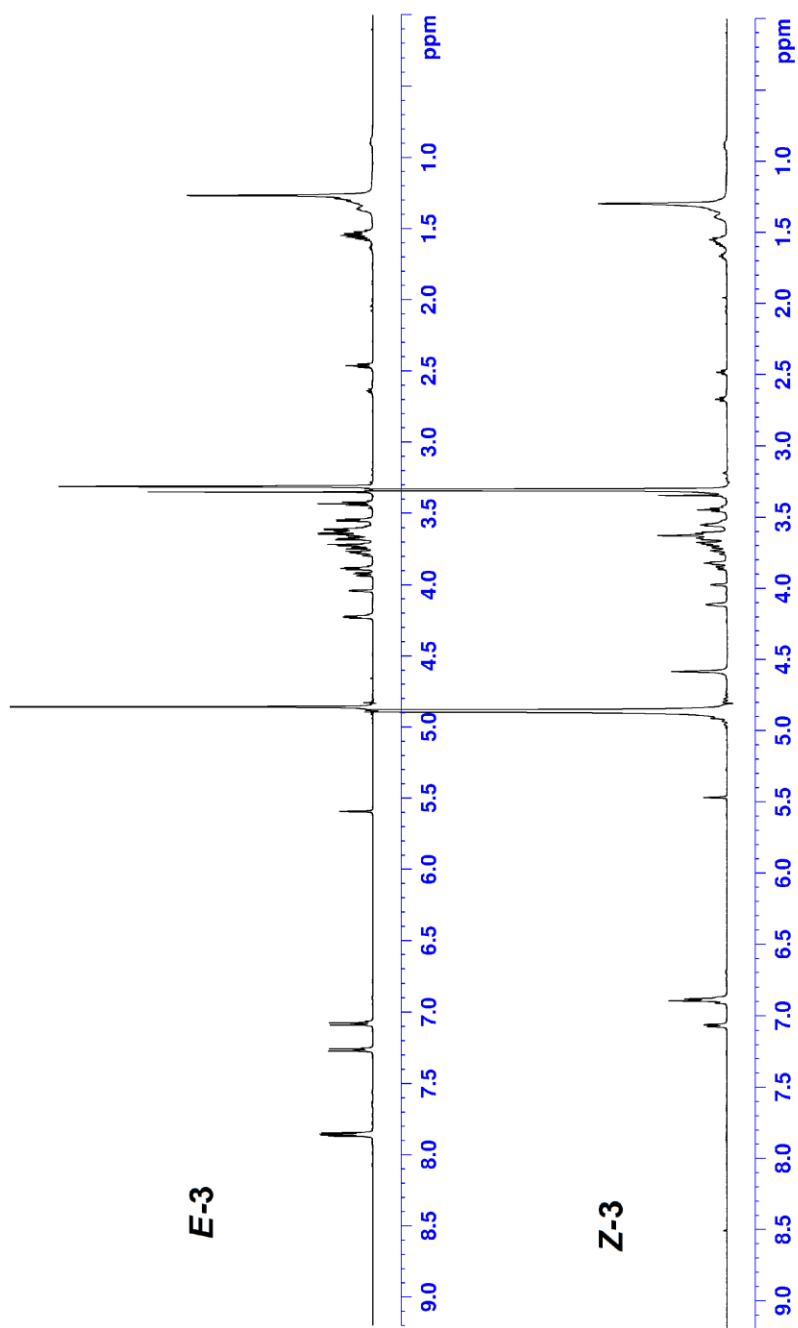


Figure S-4: ¹H NMR spectra of (*E*)-**3** and (*Z*)-**3** in CD₃OD (600 MHz).

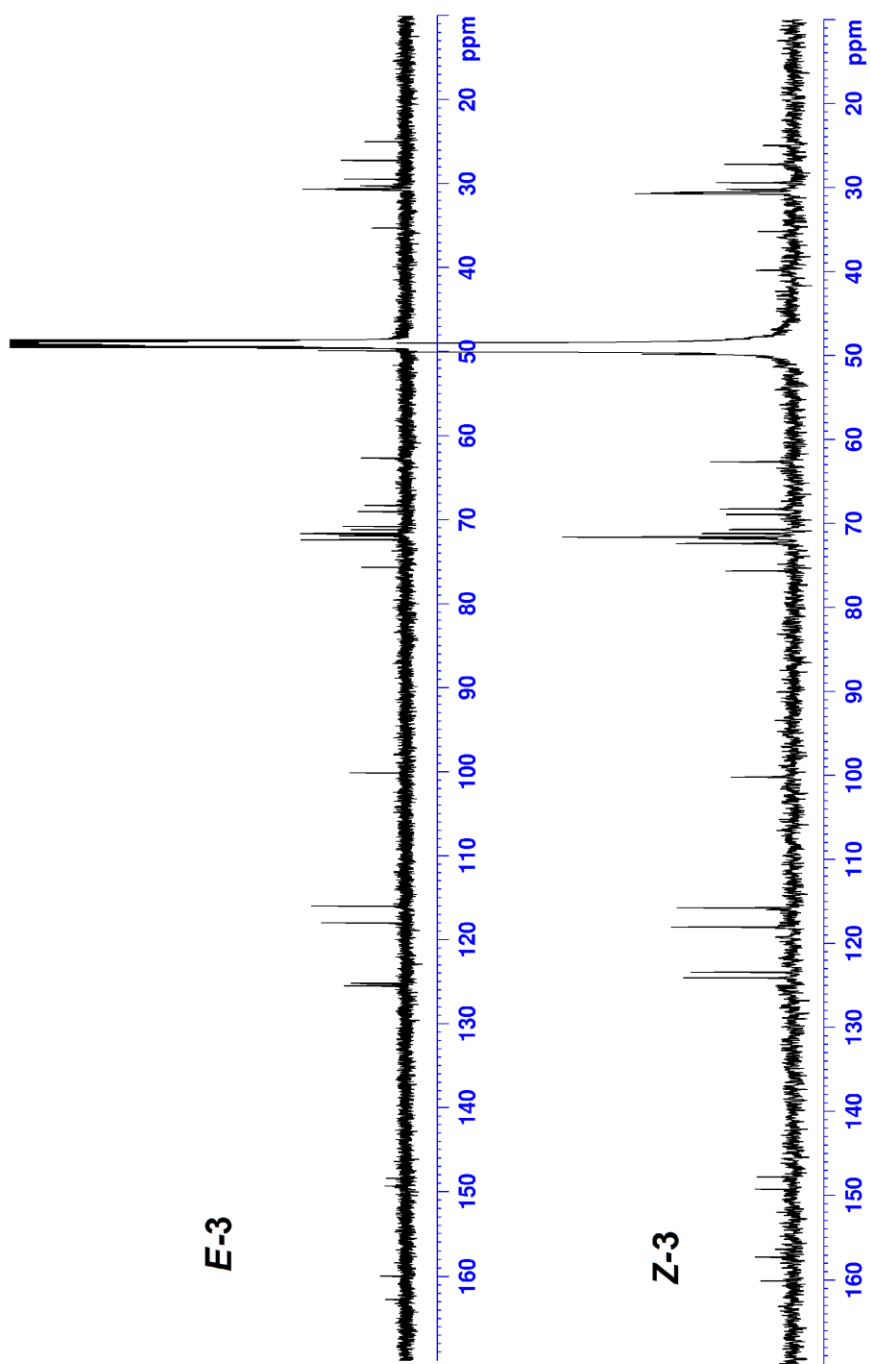


Figure S5: ¹³C NMR spectra of (E)-3 and (Z)-3 in CD₃OD (150 MHz).

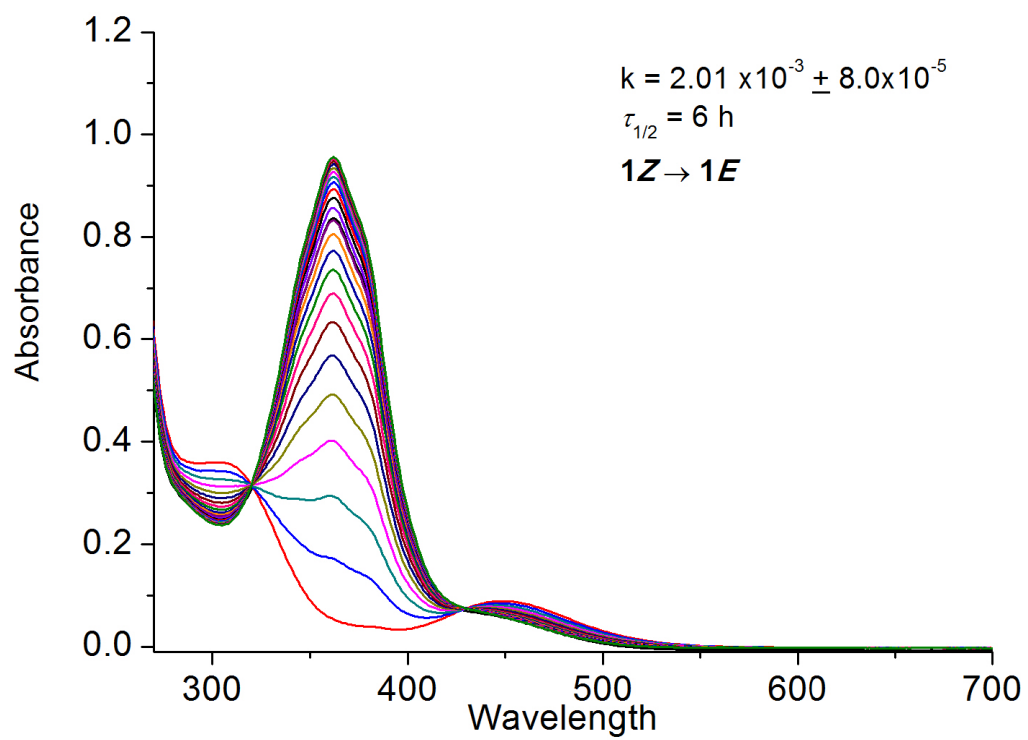


Figure S6: UV-Vis spectra of thermal Z → E relaxation of 1 in DMSO (45 μM) at 18 ± 1 °C.

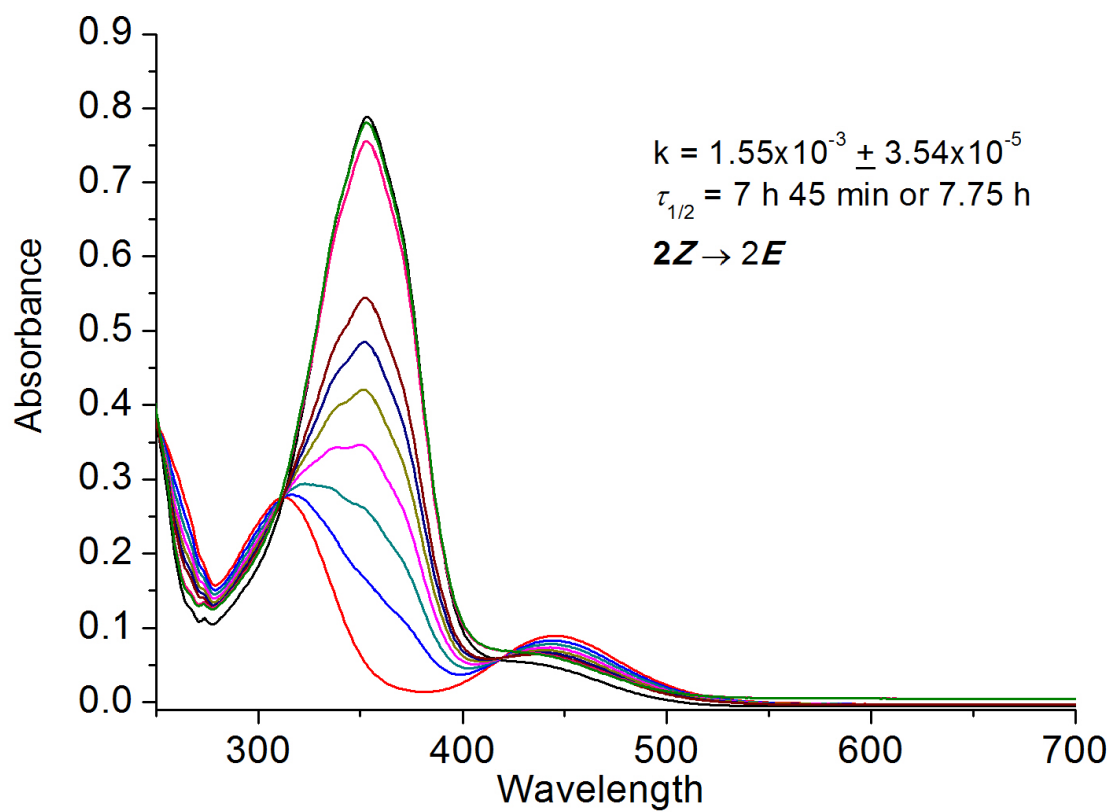


Figure S7: UV-Vis spectra of thermal $Z \rightarrow E$ relaxation of **2** in methanol (30 μM) at 18 ± 1 $^{\circ}\text{C}$.

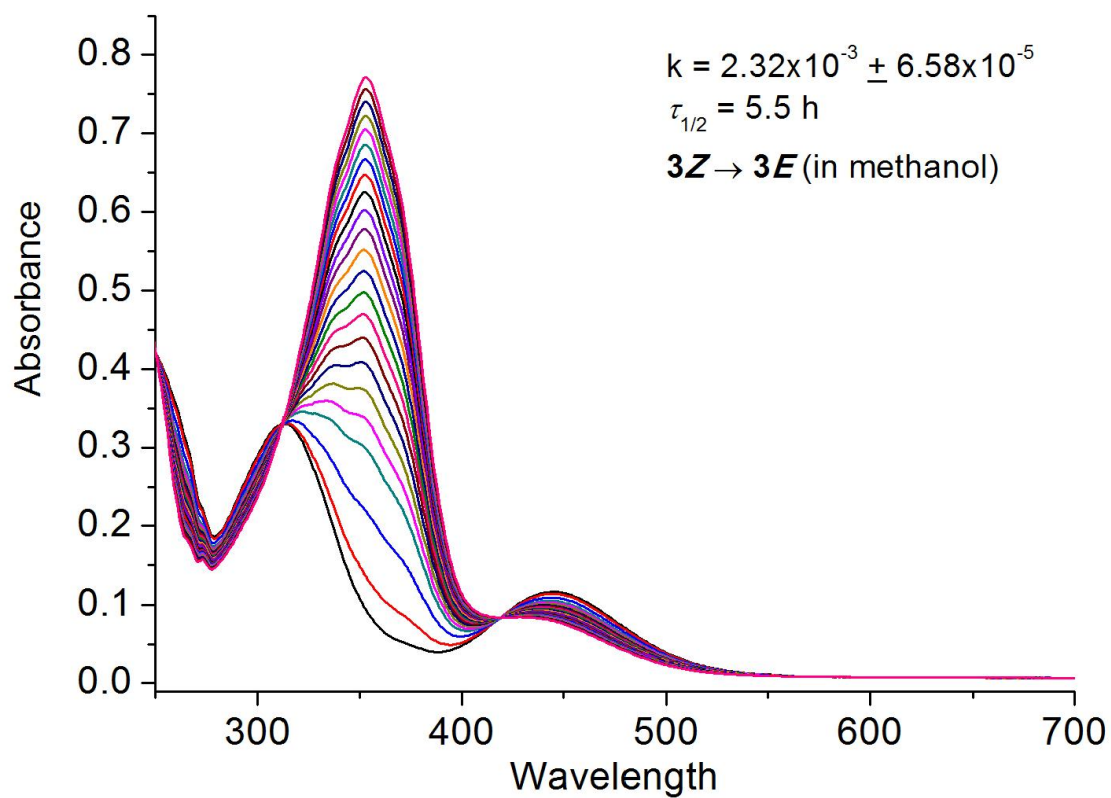


Figure S8: UV-Vis spectra of thermal Z \rightarrow E relaxation of **3** in methanol (25 μM) at 18 ± 1 $^{\circ}\text{C}$.

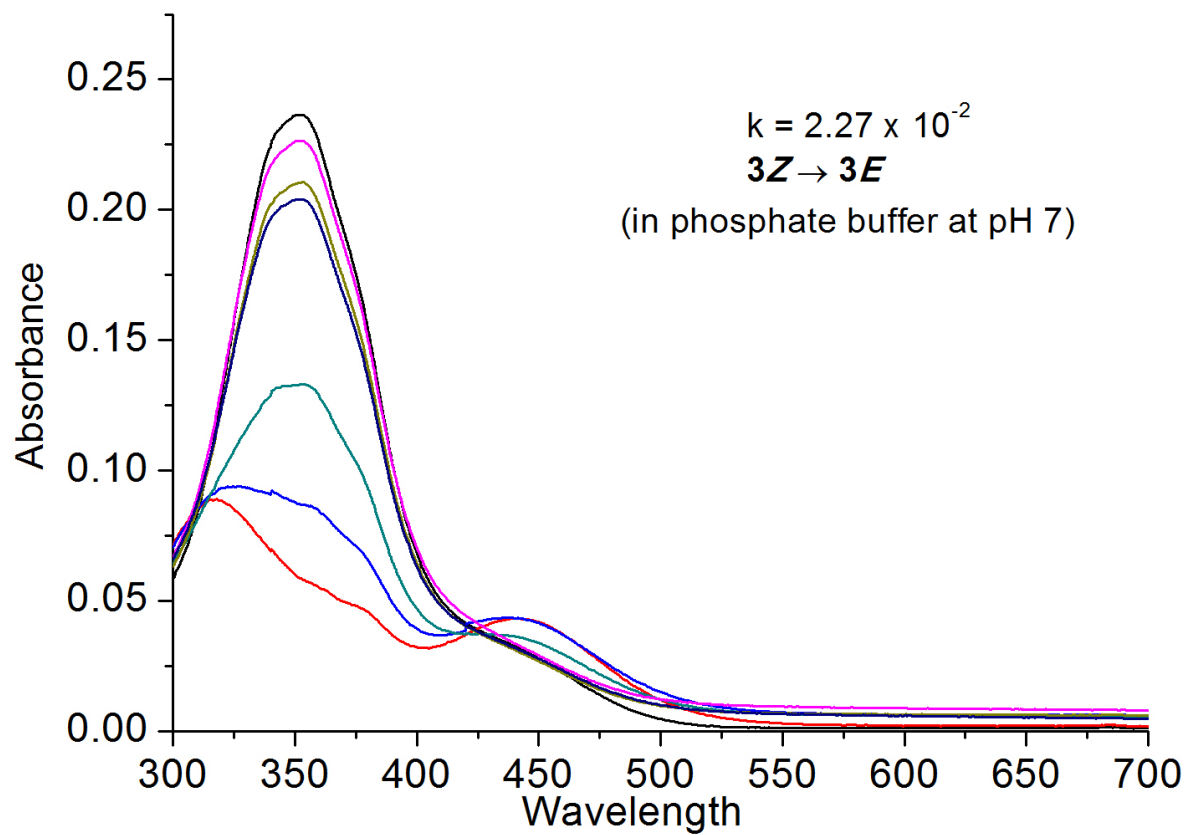


Figure S9: UV-Vis spectra of thermal Z→E relaxation of 3 in 0.1 mM phosphate buffer (~5 nM) at 22 ± 2 °C.

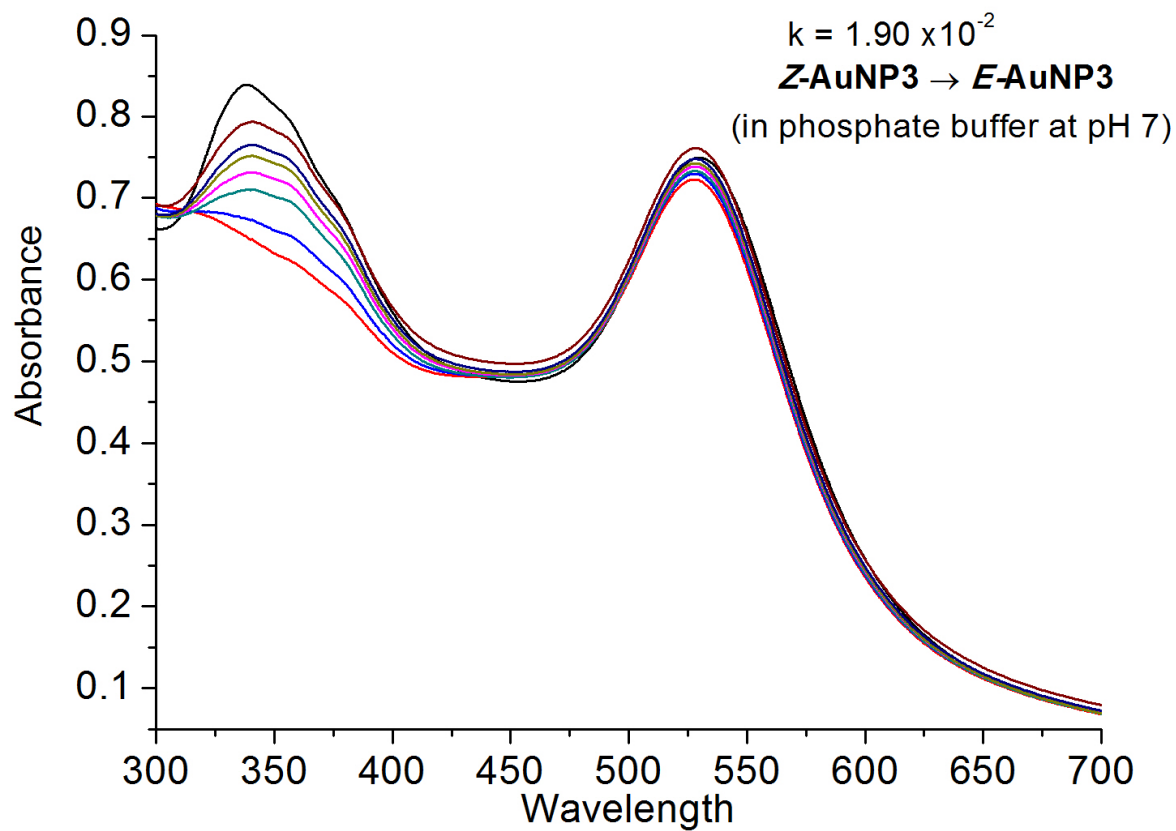


Figure S10: UV-Vis spectra of thermal $Z \rightarrow E$ relaxation of 3 on the goldnanoparticle (AuNP) surface in 0.1 mM phosphate buffer (~ 6 nM) at 22 ± 2 °C.

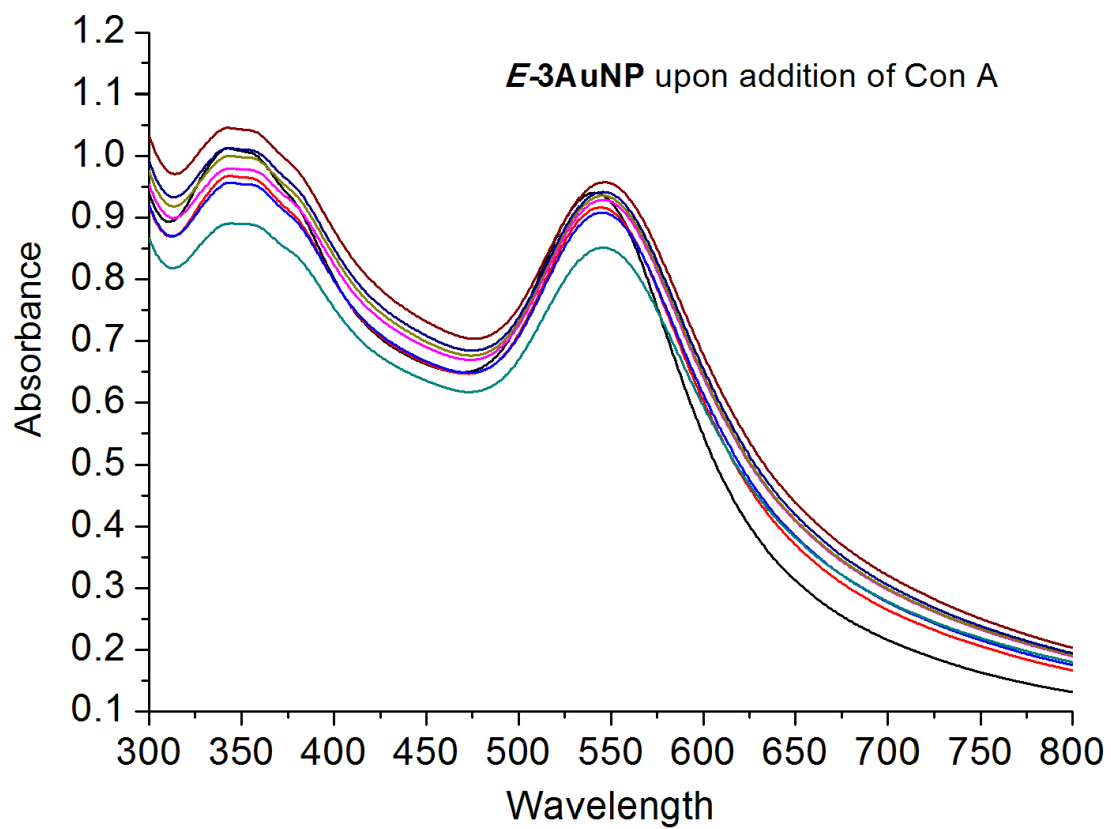


Figure S11: UV-vis spectra of ConA induced aggregation with *E*-AuNP-3 (900 μ l of 5.6 nM) + ConA (100 μ l of 5 μ M) in 0.1 mM phosphate buffer at 22 \pm 2 $^{\circ}$ C

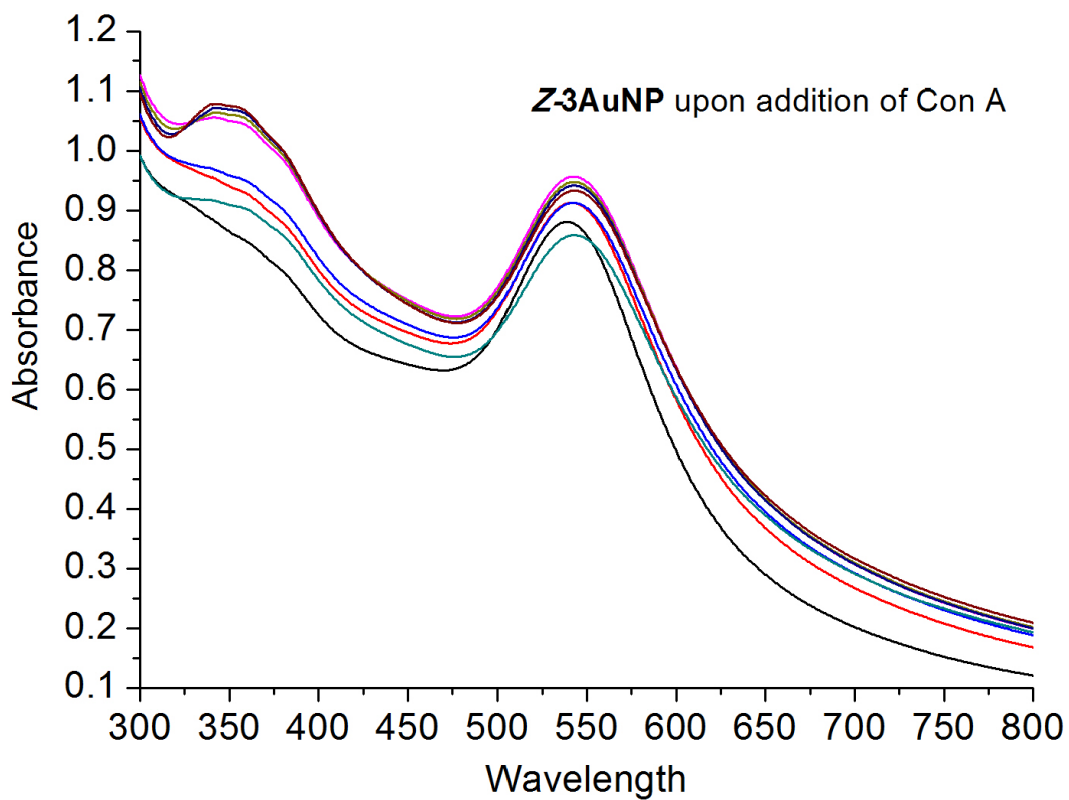
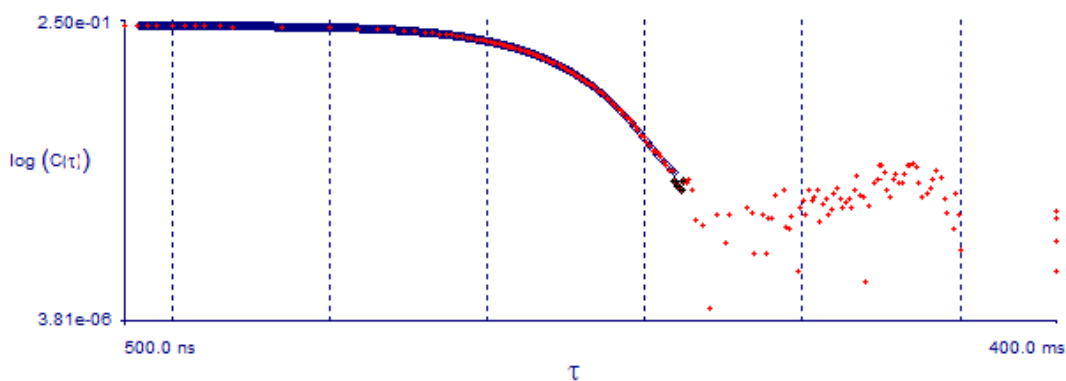


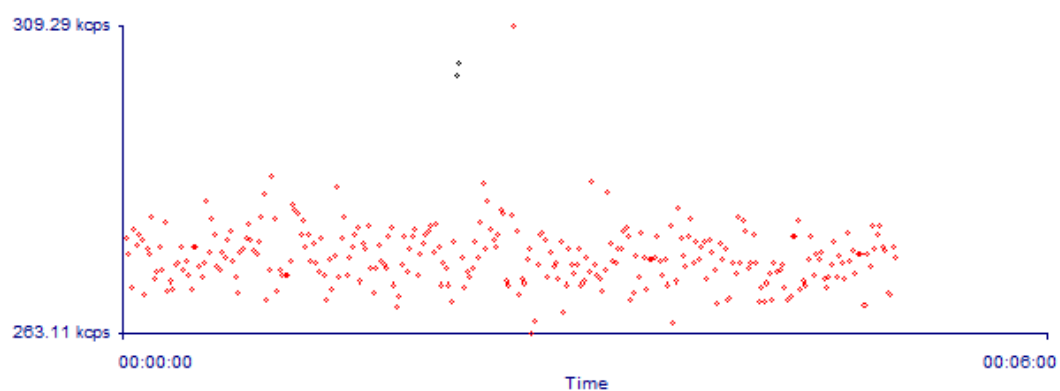
Figure S12: UV-vis spectra of ConA induced aggregation with Z-AuNP-3 (900 μ l of 5.6 nM) + ConA (100 μ l of 5 μ M) in 0.1 mM phosphate buffer at 22 \pm 2 $^{\circ}$ C

2. Dynamic Light Scattering measurements:

DLS data for E-AuNP3: 1 ml of E-AuNP3 (5.5 nM) was dissolved in 5 ml of 0.1 mM phosphate buffer and measured the hydrodynamic diameters, $d(H)$, of E-AuNP3.

STOPPED		M. Base:	1.0204e+08
First Delay:	500.0 nsec	C. Base:	1.0198e+08
Last Delay:	100.0 msec	Base diff:	0.059%
Elapsed Time:	00:05:00	Dust Cutoff:	50.00
Samples:	5.4166e+07	Data Ret:	99.34%
Atot:	7.4321e+07	Eff Dia:	61.0 nm
A CR (avg.):	274.4 kcps	Poly:	0.231
B CR (avg.):	274.4 kcps		



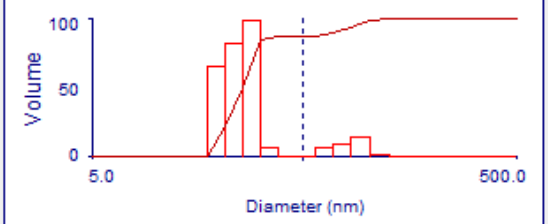


Dbl. exponential fit:

<p>Sample ID 20120731.6.2 Operator ID Unknown Operator Elapsed Time 00:05:00 Mean Diam. 29.5 (nm) Rel. Var. 0.365 Skew 3.042 RmsError 7.0392e-04</p>																												
<table border="1" style="width: 100%; border-collapse: collapse;"> <thead> <tr> <th>d</th> <th>G(d)</th> <th>C(d)</th> <th>d</th> <th>G(d)</th> <th>C(d)</th> <th>d</th> <th>G(d)</th> <th>C(d)</th> </tr> </thead> <tbody> <tr> <td>24.18</td> <td>100</td> <td>92</td> <td></td> <td></td> <td></td> <td></td> <td></td> <td></td> </tr> <tr> <td>89.13</td> <td>9</td> <td>100</td> <td></td> <td></td> <td></td> <td></td> <td></td> <td></td> </tr> </tbody> </table>		d	G(d)	C(d)	d	G(d)	C(d)	d	G(d)	C(d)	24.18	100	92							89.13	9	100						
d	G(d)	C(d)	d	G(d)	C(d)	d	G(d)	C(d)																				
24.18	100	92																										
89.13	9	100																										
<p>Print Window Copy For Spreadsheet Copy to Clipboard Close</p>																												

Contin fit:

Sample ID 20120731.6.2
 Operator ID Unknown Operator
 Elapsed Time 00:05:00
 Mean Diam. 31.4 (nm)
 Rel. Var. 0.395
 Skew 2.450
 RmsError 7.0179e-04

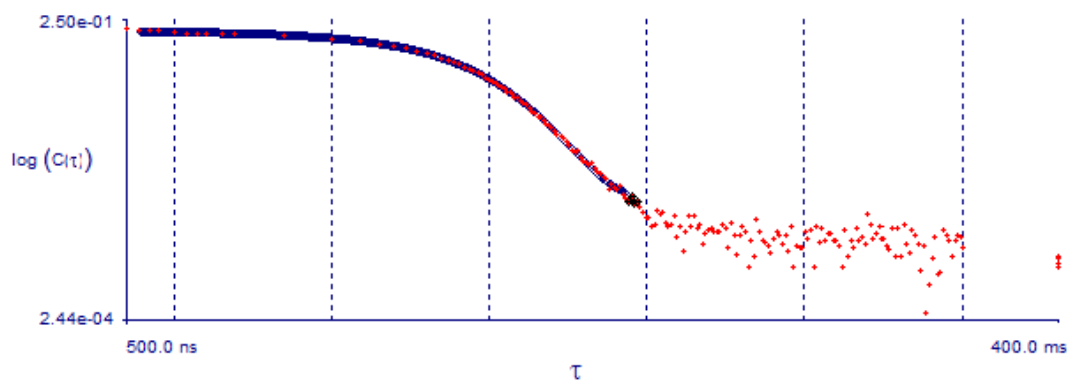


d	G(d)	C(d)	d	G(d)	C(d)	d	G(d)	C(d)
10.63	0	0	91.66	15	99			
12.93	0	0	111.49	2	100			
15.73	0	0	135.61	0	100			
19.13	66	23	164.94	0	100			
23.27	83	51	200.62	0	100			
28.31	100	86	244.02	0	100			
34.43	7	88						
41.88	0	88						
50.94	0	88						
61.96	7	91						
75.36	10	94						

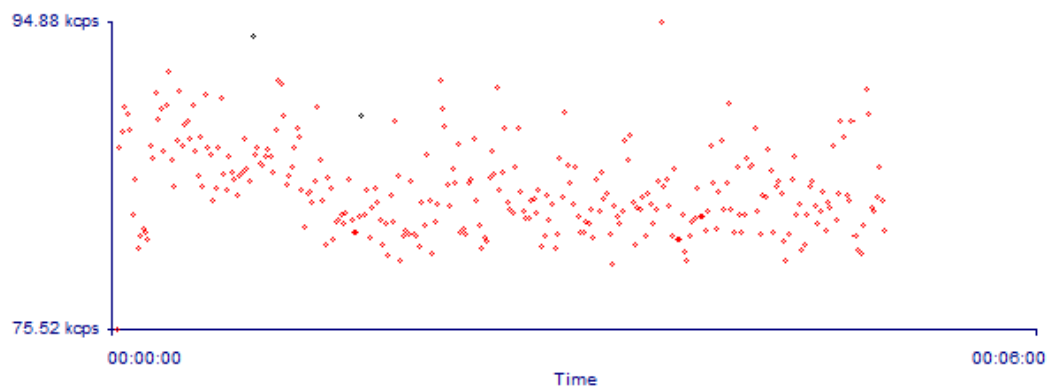
- Print Window
- Copy For Spreadsheet
- Copy to Clipboard
- Close

DLS data for Z-AuNP3: 1 ml of *E*-AuNP3 (5.5 nM) was dissolved in 5 ml of 0.1 mM phosphate buffer and irradiated with 365 nm LED for 10 min, this solution was immediately measured at dark to get the hydrodynamic diameters, $d(H)$, of Z-AuNP3.

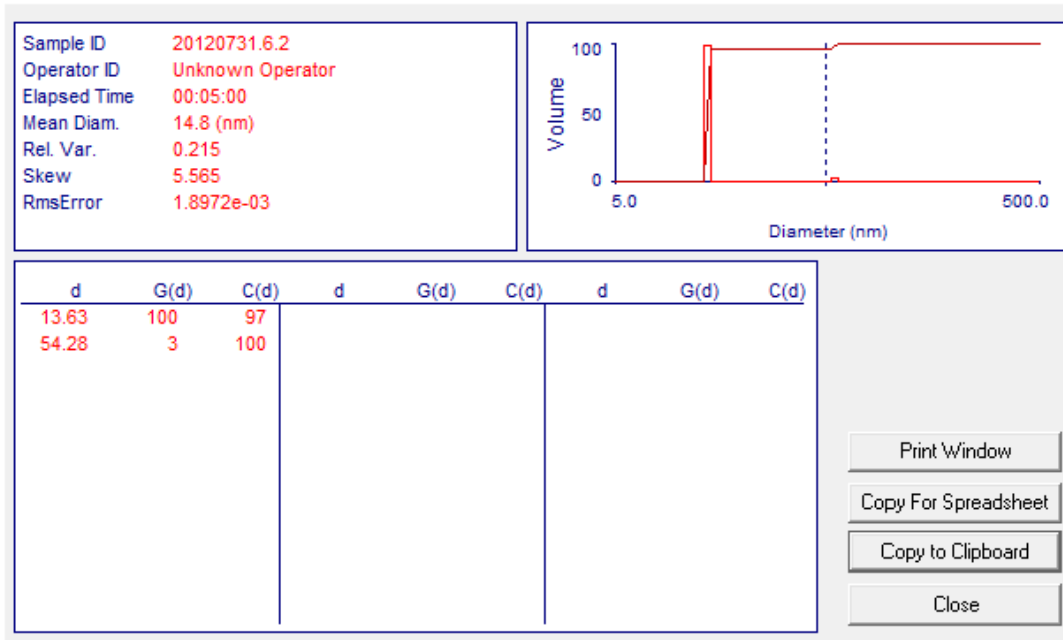
STOPPED		M. Base:	1.0005e+07
First Delay:	500.0 nsec	C. Base:	9.9664e+06
Last Delay:	100.0 msec	Base diff:	0.383%
Elapsed Time:	00:05:00	Dust Cutoff:	50.00
Samples:	5.6164e+07	Data Ret:	99.30%
Atot:	2.3659e+07	Eff Dia:	28.2 nm
A CR (avg.):	84.2 kcps	Poly:	0.276
B CR (avg.):	84.2 kcps		



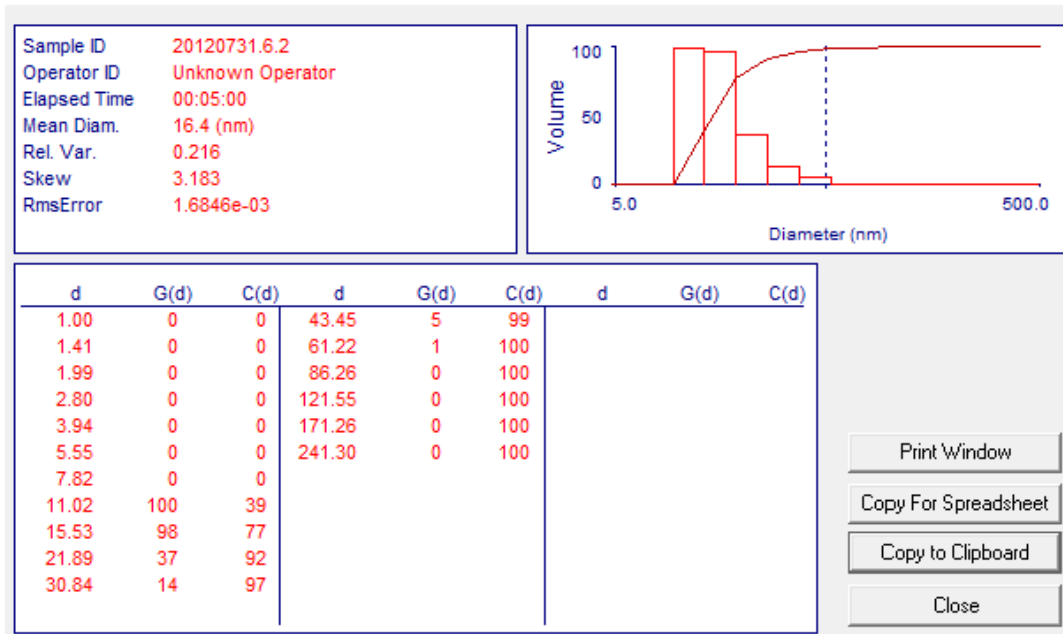
S18



Dbl exponential fit:



Contn fit:



520

3. Synthesis of photoswitchable glyconanoparticles

To stirred solutions of citrate-stabilized gold nanoparticles (9.8 mL), 5 mM of ligand **2** in methanol (1.4mL) was added. In few minutes the reaction mixture turned completely from light red wine to dark brown (**Figure 13a**). However, successful functionalization of ligand **3** on the gold nanoparticle was observed for the preparation of **E-AuNP3**. To stirred solutions of citrate-stabilized gold nanoparticles (9.8 mL), 5 mM of ligand **3** in methanol (1.4mL) was added. A very mild colour change in red wine colour was observed. (**Figure 13b**). The solutions were stirred at room temperature for 16 h and the obtained functionalized gold glyconanoparticle was subjected to centrifugal filtration (Millipore Amicon Centriplus30 kDa). The photoswitchable glyconanoparticles were redissolved in 10 mL of phosphate buffer (100 μ M, pH 7.0) and used for lectin interaction studies.

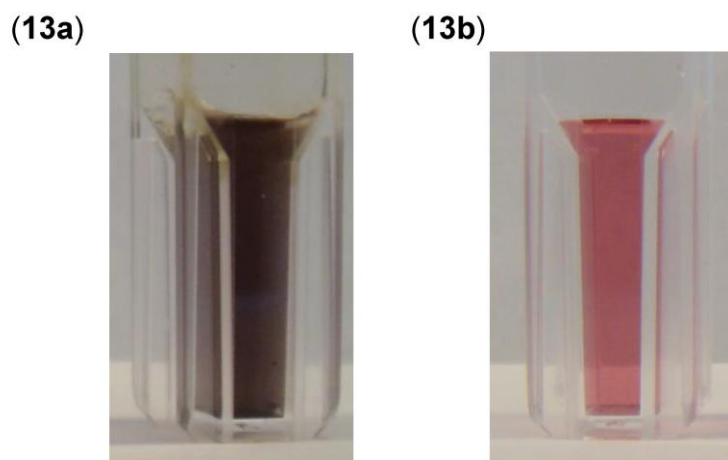


Figure S13: Preparation of photoswitchable glyconanoparticles. (13a) unsuccessful functionalization of ligand **2** on the gold nanoparticles. Due to the nanoparticles mediated aggregation change in the reaction mixture colour from light red wine to dark brown was observed; (13b) successful functionalization of ligand **3** on the gold nanoparticles was observed by the retention of light red wine colour of the reaction mixture, an indication that there is no nanoparticles mediated aggregation.

5 Azobenzene glycoconjugates for conjugation with antifreeze proteins

5.1 Introduction

Some species like plants, fish, insects, fungi, etc. possess the ability to survive in cold regions (polar and alpine) at really low temperature (subzero). One of the mechanisms underlying their survival at subzero temperature is based on the expression of a very special kind of proteins called “antifreeze proteins (AFPs)”. These AFPs have the tendency to bind to ice crystals and prevent them from growing, thus protecting the organism from freezing.^[1, 2] Antifreeze protein (AFP) activity is called "thermal hysteresis". There are two different types of proteins of the same family, one is called antifreeze glycoproteins (AFGPs) and the other is antifreeze protein (AFPs).^[3, 4] In principle, both AFGPs and AFPs exhibit nearly the same functions and properties, in particular to prevent ice growth and prevent organisms from freezing to survive at subzero temperatures.^[2]

AFPs were first discovered in fish, later studies showed the presence of AFPs in other organism like spiders, fungi, bacteria and in plants.^[5] These AFPs are classified into four types, namely type I, type II, type III and type IV. Although all the AFPs, type I to IV, have similar function in preventing death by freezing, their structures differ from organism to organism.^[6-9] For example, cysteine-rich AFPs are found in insects and glycine-rich AFPs are found in plants. Among all the different AFPs, type I are of particular interest because of its simple structure.^[10] Type I AFPs are found in winter flounder. These type I AFPs have applications in the preservation of frozen food, storing cells and for other biomedical purposes.^[5, 11, 12]

We became curious about the applications of AFPs and interested to turn type I APFs into derivatives with a photoswitchable activity. For this purpose, azobenzene crosslinkers were required and thus, bifunctionalized azobenzene glycosides were targeted. $E \rightarrow Z$ isomerization of azobenzene glycosides will alter the protein structure (active in helical conformation, inactive in random coil peptide) and allows us to study the protein activity in a photocontrolled manner. In the depicted example, the E -configured crosslinker retains protein structure and

active in biological function, namely, preventing ice growth. $E \rightarrow Z$ photoisomerization of the crosslinker distorts the protein structure resulting in activity loss (Fig 5.1). This leads to deactivation of its biological function.

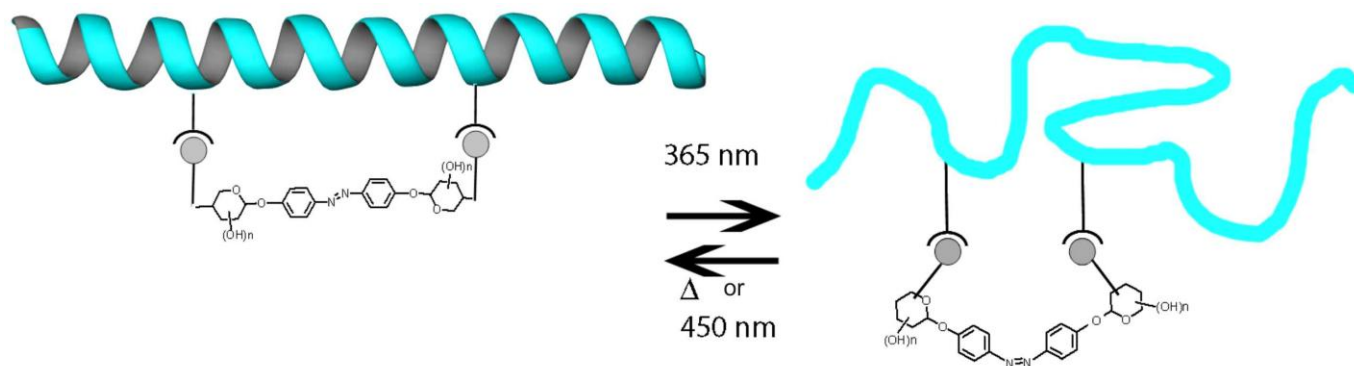


Figure 5.1: Proposed mode of action for the investigation of type I AFPs activity in a photocontrolled manner. The *E*-configured crosslinker retains the protein in its active helical form. After photoirradiation, the *Z*-form of the crosslinker leads to a distorted protein structure and deactivation of its function.

For this project, I synthesized the first prototype crosslinker molecule and rest of the work is currently advanced in collaboration with Prof. Sönnichsen's research group. Synthesis of first crosslinker is described in the following.

5.2 Synthesis of photoswitchable crosslinkers

For the synthesis of our first target compound **9**, two building blocks were needed (Fig 6.2). Glycosylation of diol **7** using **6** should give the symmetrical azobenzene derivative which has to be further reacted with chloroacetic acid under modified Staudinger reaction conditions to yield the target compound **9**. Later, the chloride group in compound **9** will be crosslinked with two cysteine side chains of type I AFPs.

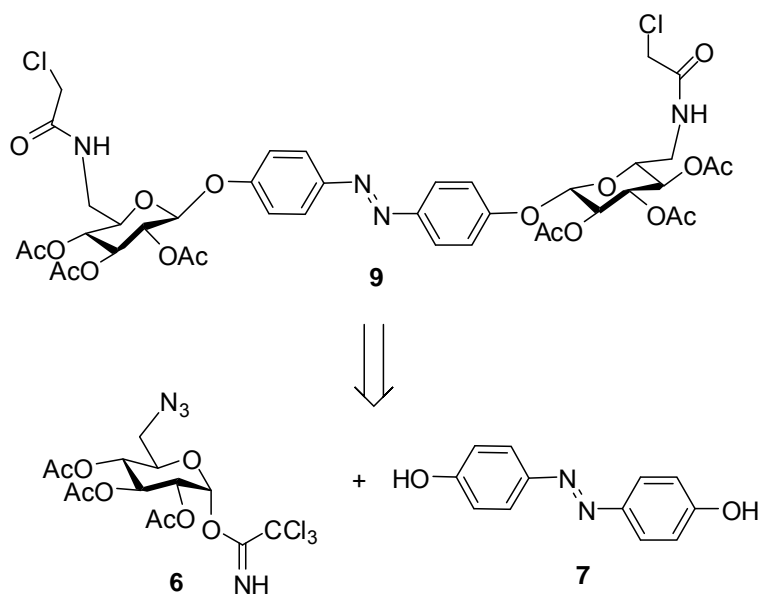
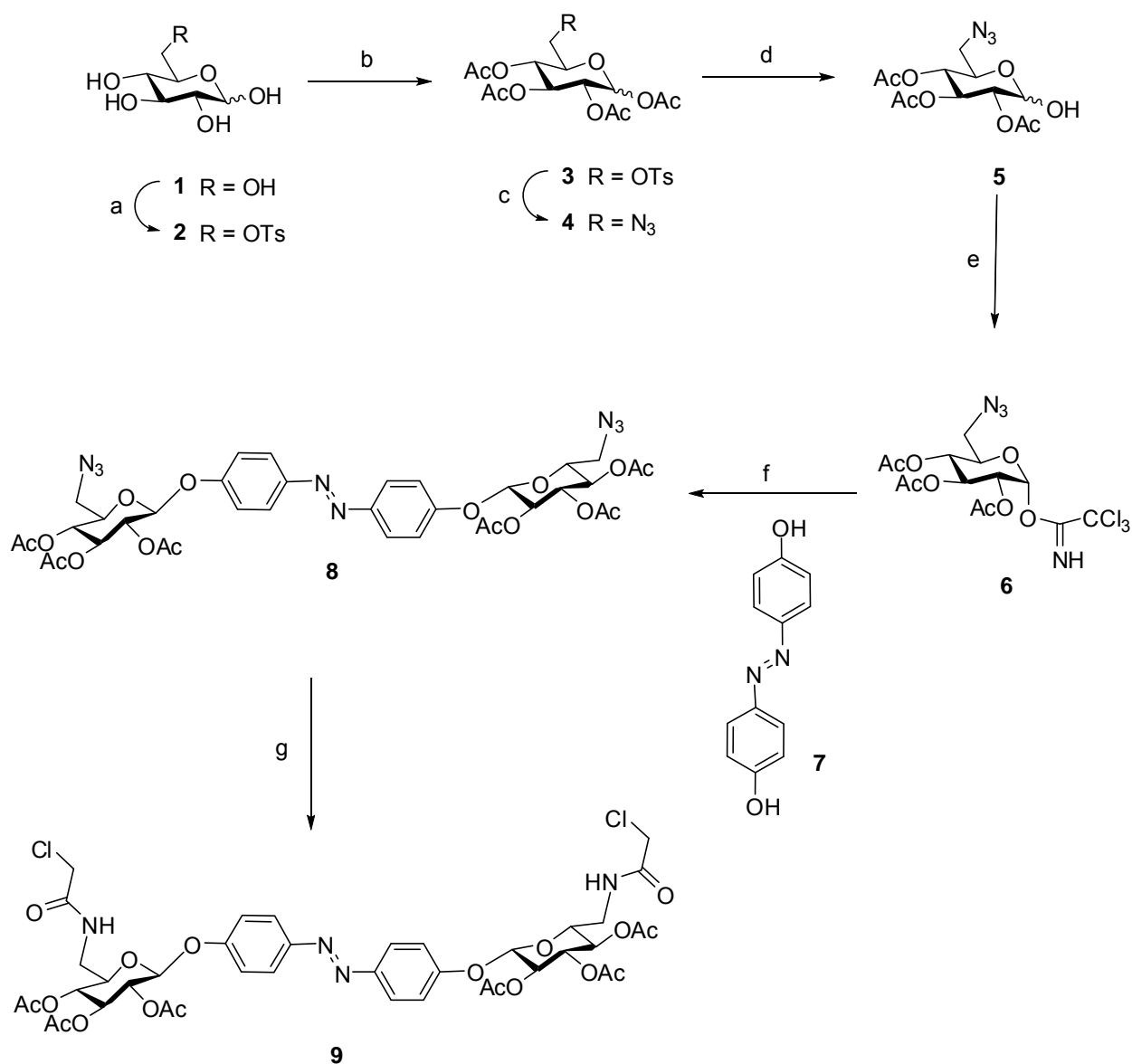


Figure 5.2: Retrosynthesis of photoswitchable crosslinker **9**.

Synthesis of building block **9** was started with glucose **1**. First, the primary hydroxyl group of free sugar **1** was tosylated using *p*-toluene sulphonic acid to provide **2** in moderate yield, after column chromatography (scheme 5.1).^[13] Compound **2** was then protected with acetyl groups using acetic anhydride and pyridine to give **3** in good yield. Later, compound **3** underwent a nucleophilic substitution reaction at C-6 employing NaN_3 providing the glycosyl azide **4** in moderate yield.^[14, 15] Treatment of compound **4** with ethylenediamine and acetic acid at room temperature resulted in the reducing sugar **5**, with the anomeric hydroxyl group unprotected. Reaction of **5** with trichloroacetonitrile and DBU as a base yielded the glucosyl trichloroacetimidate **6** in good yield.^[16]

The next building block **7** was synthesized from *p*-nitrophenol in a single step according to the literature procedure.^[17,18] Glycosylation of **6** with *p,p'*-di-hydroxy azobenzene employing BF_3 -etherate as a promoter provided the symmetrical azobenzene glycoconjugate **8** in low yield. The reaction needs to be optimized to increase the yield substantially. Finally, the desired target compound **9** was prepared by Staudinger ligation of compound **8**.^[19] Thus coupling of **8** and chloroacetic acid in the presence of HATU and tributyl phosphine gave the required symmetrical disaccharide **9** in moderate yield.



Scheme 5.1: a) tosyl chloride, *p*-TsOH, pyridine, rt, overnight, 41%; b) acetic anhydride, pyridine, rt, overnight, 85%; c) NaN₃, TBAB, DMF, 80 °C, 4.5 h and rt overnight, 56%; d) ethylenediamine, acetic anhydride, THF, rt, overnight, 70%; e) trichloroacetonitrile, DBU, CH₂Cl₂, rt, 30 min, 82%; f) BF₃·Et₂O, CH₂Cl₂, rt, overnight, 31%; g) chloroacetic acid, DIC, HATU, Bu₃P, THF, rt, overnight, 69%.

The chloroacetamide groups in compound **9** will eventually serve as short linkers between the carbohydrate and the cysteine side chains of the peptide.^[20, 21] Later, effective switching of the symmetrically crosslinked glycopeptide has to be investigated.

In conclusion, to allow photoswitching of type I AFP activity, a photoswitchable crosslinker **9** was synthesized. Covalent attachment of the crosslinker to the side chain of the protein and investigation of AFPs activity in a photocontrol manner will be studied in collaboration with Prof. Sönnichsen's research group. As the project is currently in progress, the so-far elaborated experimental details are collected in the following.

6-O-Toluolsulfonyl- α,β -D-glucopyranose (2):^[13] D-glucose (10.0 g, 55.5 mmol) was dissolved in pyridine (250 mL) and the mixture was cooled to - 20 °C. To this cooled solution, TsCl (10.6 g, 55.6 mmol) in pyridine (100 mL) was added dropwise and then the reaction mixture was stirred at room temperature overnight. The reaction mixture was evaporated and co-distilled with toluene to get the crude product, which was purified by flash chromatography (ethyl acetate/methanol, 6:1) to give compound **2** as a colorless solid. (7.52 g, 22.5 mmol, 41%). $R_f = 0.5$ (ethyl acetate/methanol, 6:1); $^1\text{H NMR}$ (500 MHz, CD_3OD , 300 K): $\delta = 7.78$ (m, 2H, H_{arom}), 7.45 (m, 2H, H_{arom}), 5.04 (d, $J = 3.7$ Hz, 1H, H-1 α), 4.46 (d, $J = 7.8$ Hz, 1H, H-1 β), 4.35 (dd, $J = 1.9$ Hz, $J = 10.6$ Hz, 1H, H-6 β), 4.29 (dd, $J = 1.9$ Hz, $J = 10.6$ Hz, 1H, H-6 α), 4.20 (dd, $J = 5.5$ Hz, $J = 10.6$ Hz, 1H, H-6' α), 4.15 (dd, $J = 6.1$, $J = 10.6$ Hz, 1H, H-6' β), 3.94 (ddd, $J = 10.0$, $J = 1.9$, 5.5 Hz, 1H, H-5 α), 3.65 (t, $J = 9.5$ Hz, $J = 9.2$ Hz, 1H, H-3 α), 3.47 (ddd, $J = 1.9$ Hz, $J = 6.1$ Hz, $J = 12.0$ Hz, 1H, H-5 β), 3.35 (dd, $J = 9.0$ Hz, $J = 9.4$ Hz, 1H, H-3 β), 3.31 (dd, $J = 3.7$ Hz, $J = 9.5$ Hz, 1H, H-2 α), 3.25 (dd, $J = 9.4$ Hz, $J = 12.0$ Hz, 1H, H-4 β), 3.23 (dd, $J = 9.2$ Hz, $J = 10.0$ Hz, 1H, H-4 α), 3.13 (dd, $J = 7.8$ Hz, $J = 9.0$ Hz, 1H, H-2 β), 2.5 (s, 3H, Ph- CH_3) ppm; $^{13}\text{C NMR}$ (150 MHz, CD_3OD , 300 K): $\delta = 134.3$, 134.2 (C_{arom}), 131.0, 130.9, 130.8, 129.1 (C_{arom}), 98.1 (C-1 β), 93.9 (C-1 α), 77.8 (C-3 β), 75.9 (C-2 β), 75.1 (C-5 β), 74.7 (C-3 α), 73.5 (C-2 α), 71.4 (C-4 α), 71.2 (C-4 β), 71.1 (C-6 α), 70.8 (C-6 β), 70.5 (C-5 α), 21.6 ppm (CH_3).

1,2,3,4-Tetra-O-acetyl-6-O-toluolsulfonyl- α,β -D-glucopyranose (3):^[14] To a solution of **2** (7.50 g, 22.4 mmol) in pyridine (100 mL) was added acetic anhydride (16.9 mL, 165.7 mmol) and the reaction mixture stirred at room temperature for overnight. The reaction mixture was distilled to half the volume, after that dichloromethane (100 mL) was added followed by water (50 mL). Phase separated, compound in aq. phase was extracted twice with dichloromethane (100 mL x 2). The combined organic phase was washed with sat. NaHCO_3 solution (50 mL) and water (50 mL). Organic layer dried over Na_2SO_4 , filtered, filtrate evaporated to dryness to

get the crude product, which was purified by flash column chromatography (ethyl acetate/cyclohexane, 3:1) provided compound **3** as colorless solid (9.54 g, 19.0 mmol, 85%). $R_f = 0.58$ (ethyl acetate/cyclohexane, 3:1); $^1\text{H-NMR}$ (500 MHz, CDCl_3 , 300 K, TMS): $\delta = 7.77$ (d, 2H, H_{arom}), 7.35 (d, 2H, H_{arom}), 6.21 (d, $J = 3.6$ Hz, 1H, H-1 α), 5.65 (d, $J = 8.2$ Hz, 1H, H-1 β), 5.42 (t, $J = 9.8$ Hz, 1H, H-3 α), 5.20 (t, $J = 9.4$, 1H, H-3 β), 5.05 (dd, $J = 8.2$, $J = 9.4$ Hz, 1H, H-2 β), 5.04 (dd, $J = 9.4$, $J = 10.0$ Hz, 1H, H-4 β), 5.02-4.92 (m, 2H, H-2 α , H-4 α), 4.16 (dd, $J = 2.8$, $J = 14.4$ Hz, 1H, H-6 α), 4.15-4.11 (dd, H-6 β , H-6' β , H-5 α , H-6' α), 3.85 (ddd, $J = 10.1$, $J = 2.7$, $J = 4.6$ Hz, 1H, H-5 β), 2.45 (s, 3H, CH_3), 2.15, 2.09, 2.01, 1.99 (s, 12H, 4 OCOCH_3) ppm; $^{13}\text{C-NMR}$ (150 MHz, CDCl_3 , 300 K): $\delta = 170.1$, 170.0, 169.5, 169.2, 169.1, 169.2, 168.2, 168.6 (OCOCH_3), 145.2 ($\text{SO}_3\text{-C}_{\text{arom}}$), 145.1 ($\text{SO}_3\text{-C}_{\text{arom}}$), 132.4 ($\text{C}_{\text{arom-CH}_3}$), 129.8 (C_{arom}), 128.1 (C_{arom}), 128.1 (C_{arom}), 91.2 (C-1 β), 88.7 (C-1 α), 72.4 (C-3 β), 72.4 (C-5 β), 70.0 (C-2 β), 69.6 (C-3 α), 69.7 (C-5 α), 68.8 (C-2 α), 68.9 (C-4 α), 67.2 (C-4 β), 67.2 (C-6 α), 66.8 (C-6 β), 21.6 ($\text{C}_{\text{arom-CH}_3}$), 20.8, 20.7, 20.8, 20.5, 20.5, 20.4, 20.4, 20.3 (OCOCH_3) ppm; ESI-MS: m/z calcd for $\text{C}_{21}\text{H}_{26}\text{O}_{12}\text{S}$: 525.103 ($\text{M} + \text{Na}$) $^+$; $\text{M}_{\text{found}} = 525.104$

1,2,3,4-Tetra-O-acetyl-6-azido-6-deoxy- α,β -D-glucopyranose (4):^[22] A mixture of **3** (13.1 g, 26.1 mmol) and sodium azide (3.60 g, 55.4 mmol) in DMSO (110 mL) was heated to 80 °C for 4.5 h followed by stirring at room temperature for overnight. To the reaction mixture ice water (10 mL) was added followed by ethyl acetate (100 mL). Phase were separated, organic layer washed with water (20 mL), dried over Na_2SO_4 , filtered, filtrate evaporated to dryness. The obtained crude showed a mixture of $\alpha : \beta = 3:1$ by $^1\text{H-NMR}$, which was purified by flash chromatography (ethyl acetate/cyclohexane, 1:1) gave the title compound **4** as colorless solid (7.12 g, 19.1 mmol, 73%). $R_f = 0.27$; $^1\text{H-NMR}$ of α anomer (500 MHz, CDCl_3 , 300 K, TMS): $\delta = 6.36$ (d, $J = 3.7$ Hz, 1H, H-1 α), 5.47 (t, $J = 10.0$ Hz, 1H, H-3 α), 5.15-5.05 (m, 2H, H-2, H-4), 4.08 (ddd, $J = 3.0$ Hz, $J = 5.3$ Hz, $J = 10.2$ Hz, 1H, H-5), 3.34-3.14 (m, 2H, H-6a, H-6b), 2.19, 2.06, 2.03, 2.02 (each s, each 3 H, 4 COCH_3) ppm; $\delta = 170.1$, 169.4, 169.2, 168.9 (OCOCH_3), 88.7 (C-1), 70.9 (C-5), 70.1 (C-4), 69.2 (C-3), 69.0 (C-2), 50.7 (C-6), 20.7, 20.6, 20.6, 20.6 (OCOCH_3) ppm.

O-(2,3,4-Tri-O-acetyl-6-azido-6-deoxy- α -D-glucopyranosyl)-trichloroacetimidate(6):^[16]

Under N_2 atmosphere, to a solution of **5** (250 mg, 0.755 mmol) in dry CH_2Cl_2 (5 mL) were added trichloroacetonitrile (908 μL , 9.06 mmol) and DBU (33 μL , 0.23 mmol) at 0 °C. The

reaction mixture was stirred at room temperature for about 30 min and the reaction mixture was immediately subjected to flash column chromatography (cyclohexane/ethyl acetate, 7:3) gave the mannosyl donor **6** as a colourless solid (293 mg, 0.618 mmol, 82%). $R_f = 0.31$ (cyclohexane/ethyl acetate, 4:1); $^1\text{H-NMR}$ (500 MHz, CDCl_3 , 300 K): $\delta = 8.70$ (s, 1H, $\text{C}(\text{NH})\text{CCl}_3$), 6.59 (d, $J = 3.7$ Hz, 1H, H-1), 5.56 (m_c , H-3), 5.14-5.11 (m, 2H, H-2, H-4), 4.19 (ddd, $J = 10.2$ Hz, $J = 5.5$ Hz, $J = 2.7$ Hz, 1H, H-5), 3.39 (dd, $J = 13.5$ Hz, $J = 2.7$ Hz, 1H, H-6a), 3.34 (dd, $J = 13.6$ Hz, $J = 5.6$ Hz, 1H, H-6b), 2.06, 2.04, 2.02 ppm (each s, each 3 H, 3 COCH_3); $^{13}\text{C-NMR}$ (125 MHz, CDCl_3) $\delta = 170.0$, 169.8, 169.5 (3 COCH_3), 160.7 (s, $\text{C}=\text{NH}-\text{CCl}_3$), 92.7 (C-1), 71.2 (C-5), 70.6 (C-3), 69.7 (C-2), 68.9 (C-4), 50.6 (C-6), 20.7, 20.6, 20.4 ppm (3 COCH_3); ESI-MS m/z Calcd for $\text{C}_{14}\text{H}_{17}\text{Cl}_3\text{N}_4\text{O}_8$: 497.02 (M+Na) $^+$; $M_{\text{found}} = 497.00$.

E-p-[p'-(2,3,4-Tri-O-acetyl-6-azido-6-deoxy- β -D-glucopyranosyl)]phenylazophenyl

2,3,4-tri-O-acetyl-6-azido-6-deoxy- β -D-glucopyranoside (8): To a solution of the mannosyl donor **6** (244 mg, 514 μmol) and *p,p'*-dihydroxyazobenzene **7**^[18] (50.0 mg, 234 μmol) in dry CH_2Cl_2 (5 mL), $\text{BF}_3\cdot\text{Et}_2\text{O}$ (44 μL , 350 μmol) was added at 0 °C under N_2 atmosphere. The reaction mixture was stirred at room temperature overnight and then aq. NaHCO_3 (5 mL) was added to quench the reaction. It was diluted with ethyl acetate (100 mL), the phases were separated and the organic phase was washed with water (2 \times 15 mL). It was dried over Na_2SO_4 , filtered and the filtrate was concentrated under reduced pressure. Purification by flash column chromatography (cyclohexane/ethyl acetate, 8:2) gave the divalent glycoside **8** as pale yellow solids (62.1 mg, 73.8 μmol , 32%). $R_f = 0.18$ (cyclohexane/ethyl acetate, 4:2); $^1\text{H-NMR}$ (500 MHz, CDCl_3): $\delta = 7.89$ (dd, $J = 8.9$ Hz, 4H, H-9, H-11, H-14, H-18), 7.12 (d, $J = 8.9$ Hz, 4H, H-8, H-12, H-15, H-17), 5.32-5.30 (m, 4H, 2 H-2, 2 H-3), 5.20 (m_c , 2H, 2 H-1), 5.01 (m_c , 2H, 2 H-4), 3.83 (ddd, $J = 9.9$ Hz, $J = 7.3$ Hz, $J = 2.7$ Hz, 2H, 2 H-5), 3.45 (dd, $J = 13.4$ Hz, $J = 7.3$ Hz, 2H, 2 H-6a), 3.35 (dd, $J = 13.4$ Hz, $J = 2.7$ Hz, 2H, 2 H-6b), 2.08, 2.07, 2.05 ppm (each s, each 6 H, COCH_3); $^{13}\text{C-NMR}$ (125 MHz, CDCl_3) $\delta = 170.0$, 169.5, 169.3 (3 COCH_3), 158.5, 148.7, 124.5, 117.3, 98.8 (C-1), 73.7 (C-5), 72.5 (C-3), 71.2 (C-2), 69.4 (C-4), 51.3 (C-6), 20.6, 20.6, 20.6 (OCOCH_3); ESI-MS m/z Calcd for $\text{C}_{36}\text{H}_{40}\text{N}_8\text{O}_{16}$: 863.26 (M+Na) $^+$; $M_{\text{found}} = 863.25$.

E-p-[p'-(2,3,4-Tri-O-acetyl-6-[2-chloroacetyl]amido-6-deoxy- β -D-glucopyranosyl)]

phenylazophenyl-2,3,4-tri-O-acetyl-6-[2-chloroacetyl]amino-6-deoxy- β -D-

glucopyranoside (9): A mixture of **8** (50.0 mg, 59.5 μmol) and HATU (67.9 mg, 179 μmol)

was taken and dried under vacuum for about 30 min. Then to the above mixture, chloroacetic acid (16.9 mg, 179 μmol) in dry THF (7 mL) was added under inert atmosphere. The reaction mixture was cooled to 0 °C and added DIC (27.9 μL , 179 μmol) followed by Bu_3P (36 mg, 179 μmol). The reaction mixture was stirred at room temperature for overnight (~16 h) and then added water (10 mL). Product extracted with ethyl acetate (10 mL x 3), combined organic layer dried over Na_2SO_4 , filtered and the filtrate was concentrated under reduced pressure to get the crude, which was purified by flash column chromatography (dichloromethane/ethyl acetate, 6:4) provided **9** as pale yellow solid (38.6 mg, 41.1 μmol , 69%). $R_f = 0.18$ (cyclohexane/ethyl acetate, 4:2); ^1H NMR (500 MHz, CDCl_3): $\delta = 7.88$ (dd, $J = 8.9$ Hz, 4H, H-9, H-11, H-14, H-18), 7.08 (d, $J = 8.9$ Hz, 4H, H-8, H-12, H-15, H-17), 6.97 (t, $J = 6.1$ Hz, 2H, -NH), 5.34-5.27 (m, 4H, 2 H-2, 2 H-3), 5.20 (m_c, 2H, 2 H-1), 5.04 (m_c, 2H, 2 H-4), 4.06 (d, $J = 1.8$ Hz, 4H, - CH_2Cl), 3.85-3.75 (m, 4H, 2 H-5, 2 H-6a), 3.42 (dd, $J = 12.6$ Hz, $J = 6.0$ Hz, 2H, 2 H-6b), 2.09, 2.08, 2.05 ppm (each s, each 6 H, COCH_3); ^{13}C NMR (125 MHz, CDCl_3) $\delta = 170.2$, 169.8, 169.3 (3 COCH_3), 166.2 (COCH_2Cl) 158.4, 148.6, 124.6, 116.9, 98.6 (C-1), 72.8 (C-5), 72.4 (C-3), 71.2 (C-2), 69.0 (C-4), 42.6 (COCH_2Cl), 39.7 (C-6), 20.6, 20.6, 20.6 (OCOCH_3); ESI-MS m/z Calcd for $\text{C}_{36}\text{H}_{40}\text{N}_8\text{O}_{16}$: 863.26 ($\text{M}+\text{Na}$)⁺; $\text{M}_{\text{found}} = 863.25$.

References:

- [1] P. L. Davies, B. D. Sykes, *Curr. Opin. Struct. Biol.* **1997**, 7, 828-834.
- [2] Y. Yeh, R. E. Feeney, *Chem. Rev.* **1996**, 96, 601-618.
- [3] A. L. DeVries, D. E. Wohlschlag, *Science* **1969**, 163, 1073-1075.
- [4] A. L. DeVries, J. Vandenheede, R. E. Feeney, *J. Biol. Chem.* **1971**, 246, 305-308.
- [5] S. Venketesh, C. Dayananda, *Crit. Rev. Biotechnol.* **2008**, 28, 57-82.
- [6] F. D. Sönnichsen, B. Sykes, H. Chao, P. Davies, *Science* **1993**, 259, 1154-1157.
- [7] S. P. Graether, C. M. Slupsky, P. L. Davies, B. D. Sykes, *Biophys. J.* **2001**, 81, 1677-1683.
- [8] F. D. Sönnichsen, C. I. DeLuca, P. L. Davies, B. D. Sykes, *Structure* **1996**, 4, 1325-1337.
- [9] W. Gronwald, M. C. Loewen, B. Lix, A. J. Daugulis, F. D. Sönnichsen, P. L. Davies, B. D. Sykes, *Biochemistry* **1998**, 37, 4712-4721.
- [10] P. L. Davies, C. L. Hew, *The FASEB J.* **1990**, 4, 2460-2468.
- [11] P. Mazur, *Science* **1970**, 168, 939-949.
- [12] K. Muldrew, J. Rewcastle, B. J. Donnelly, J. C. Saliken, S. Liang, S. Goldie, M. Olson, R. Baissalov, G. Sandison, *Cryobiology* **2001**, 42, 182-189.
- [13] J. Compton, *J. Am. Chem. Soc.* **1938**, 60, 395-399.
- [14] E. Hardegger, R. M. Montavon, *Helv. Chim. Acta* **1946**, 29, 1199-1203.
- [15] Z. Györgydeák, L. Szilágyi, *Liebigs Ann. Chem.* **1987**, 1987, 235-241.
- [16] C.-W. T. Chang, Y. Hui, B. Elchert, J. Wang, J. Li, R. Rai, *Org. Lett.* **2002**, 4, 4603-4606.
- [17] R. Willstätter, M. Benz, *Ber. Dtsch. Chem. Ges.* **1906**, 39, 3492-3503.
- [18] W.-h. Wei, T. Tomohiro, M. Kodaka, H. Okuno, *J. Org. Chem.* **2000**, 65, 8979-8987.
- [19] N. Röckendorf, T. K. Lindhorst, *J. Org. Chem* **2004**, 69, 4441-4445.
- [20] G. A. Woolley, *Acc. Chem. Res.* **2005**, 38, 486-493.
- [21] A. A. Beharry, G. A. Woolley, *Chem. Soc. Rev.* **2011**, 40, 4422-4437.
- [22] V. Maunier, P. Boullanger, D. Lafont, Y. Chevalier, *Carbohydr. Res.* **1997**, 299, 49-57.

6. Resume

To investigate the importance of conformational control in carbohydrate-protein interactions such as in the context of glycocalyx biology, we got interested in photoswitchable glycomimetics. Thus, azobenzene glycosides became principal target molecules for our research and a series of different azobenzene glycoconjugates were synthesized, their photochromic properties were studied and their biological properties investigated. The photoswitchable (*E*)-*p*-(Phenylazo)phenyl 3-*O*-(α -D-mannopyranosyl)- α -D-mannopyranoside mannobioside was synthesized as ligand for the bacterial lectin FimH and tested as inhibitor for type 1 fimbriae-mediated adhesion of *E. coli* bacteria in solution (Fig 6.1). Both isomers (*Z* and *E*) showed the same, but a high inhibitory potency than the standard methyl α -D-mannoside in solution (chapter 3.1). This result can be rationalized by computer docking studies which showed that the terminal mannoside is complexed in the carbohydrate binding site for bacterial adhesion, the first mannoside moiety acts as a bulky space, does not involve in the binding event and the azobenzene part is involved in favourable π - π^* interactions with the tyrosine gate at the entrance of the CRD. As the azobenzene is little far away from the binding pocket *E*→*Z* isomerization does not have influence in binding with the bacterial lectin FimH.

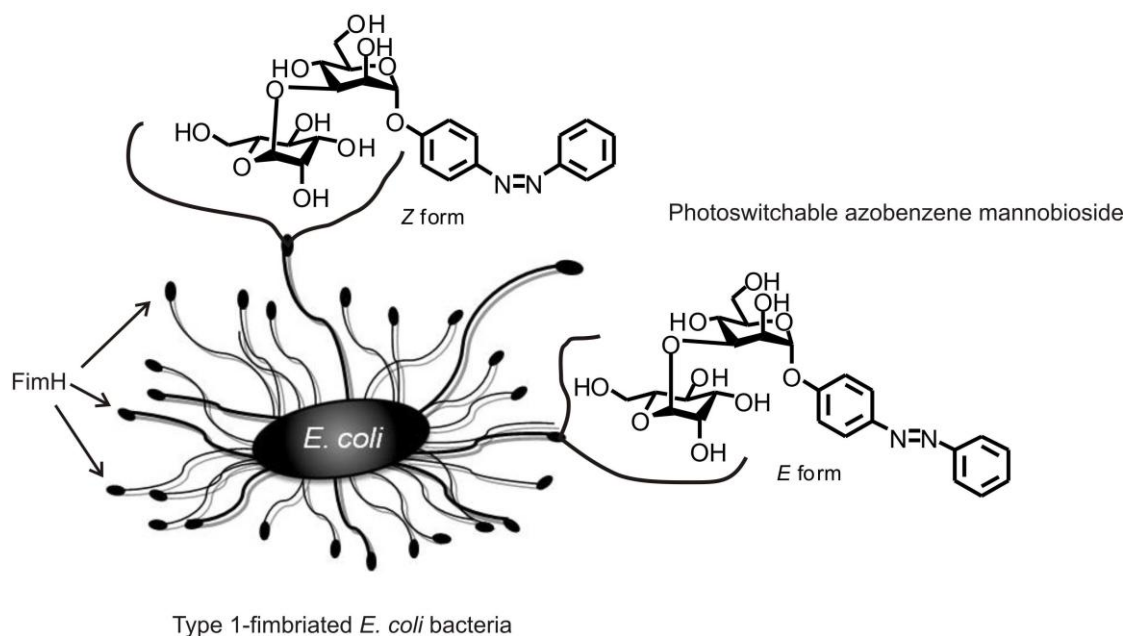


Figure 6.1: Inhibition of type 1 fimbriated *E. coli* bacteria by *E*- and *Z*-configured, respectively, photoswitchable azobenzene mannobioside.

For any advanced biological application of azobenzene glycosides, detailed knowledge about their photochromic properties is essential. Thus, a series of different azobenzene glycosides with varying anomeric configuration and different substituents on the azobenzene moiety were synthesized and their photochromic properties determined (chapter 3.2). Unsubstituted azobenzene glycosides varied with regard to the glycosidic linkage (α or β , mannose or glucose respectively) photoisomerized from $E \rightarrow Z$ completely and showed half lives upto 89 h. However, carboxy- and methoxycarbonyl-substituted azobenzene glycosides showed poor photoisomerization with the half lives ≤ 5 h. This might be due to substitution effects as well as the structure of the carbohydrate glycone. Theoretical studies might help to eventually understand how the photochromic properties of azobenzene glycosides and their kinetics are tuned.

Next, mono-, di- and trivalent azobenzene glycoconjugates were synthesized to investigate multivalent photoswitchable glycomimetics (chapter 3.3). Interestingly, the divalent compound with two azobenzene branches showed a mixture of EE , EZ and ZZ isomers in the PSS. The trivalent analogue having three azobenzene branches showed a mixture of EEE , EEZ , EZZ and ZZZ isomers in the PSS, according to ^1H NMR spectroscopy. The kinetic details of the isomerization process will be further investigated by advanced NMR techniques.

Another interesting photoswitchable ligand of FimH, E - p -(o -Methoxycarbonyl-phenylazo)phenyl α -D-mannoside (AzoMan in Figure 6.2) was synthesized and investigated (chapter 3.4). Type 1 fimbriae-mediated adhesion of *E. coli* bacteria to the isomers of photoswitchable ligand was studied in solution medium and monitored by UV-Vis spectroscopy (Fig 6.2). No significant difference was observed in the adhesion process by UV-Vis spectroscopy. In another experiment, the inhibitory potency of AzoMan was tested with live human cells. AzoMan showed a high inhibitory potency and low toxicity at the same time. Thus, this compound is a prime candidate for potent FimH antagonists.

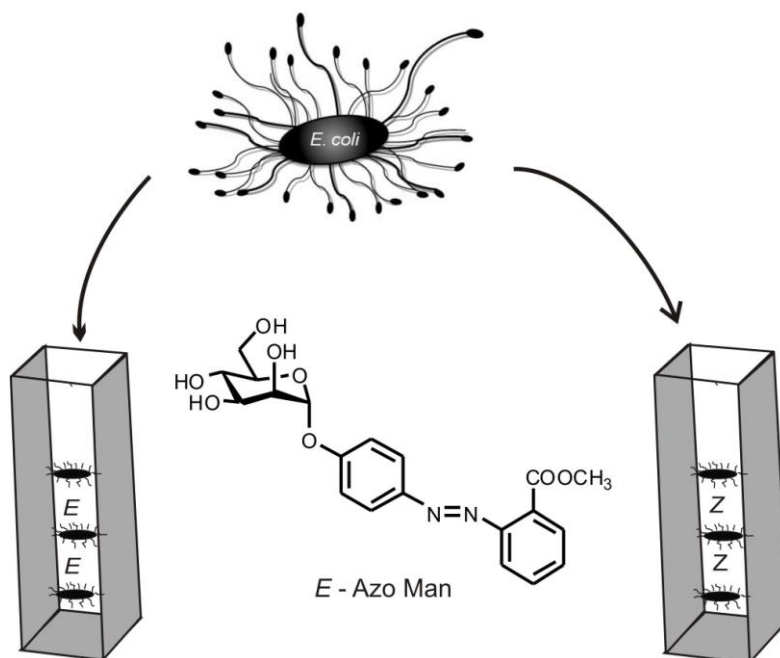


Figure 6.2: Addition of *E. coli* (strain HB101 pPKL4) bacteria to the *E*- and *Z*- isomers of azobenzene mannoside (Azo Man) in the UV-Cuvette. Bacterial adhesion was monitored by UV-Vis spectroscopy.

In all the above methods, molecules were made and tested in solution and this might be one of the reasons why conformation-induced changes of their activity were not observed. We speculated that the scenario will be different once photoswitchable molecules are immobilized on surfaces to form “glycoarrays”. Thus, photoswitchable azobenzene glycosides were immobilized on gold surface to form photoswitchable glyco-SAMs (chapter 4). Switching experiments were performed on the planar gold surface/wafers and *E*→*Z* isomerization was successfully monitored (Fig 6.3) by infrared reflection absorptions Spectroscopy (IRRAS) (chapter 4.1).

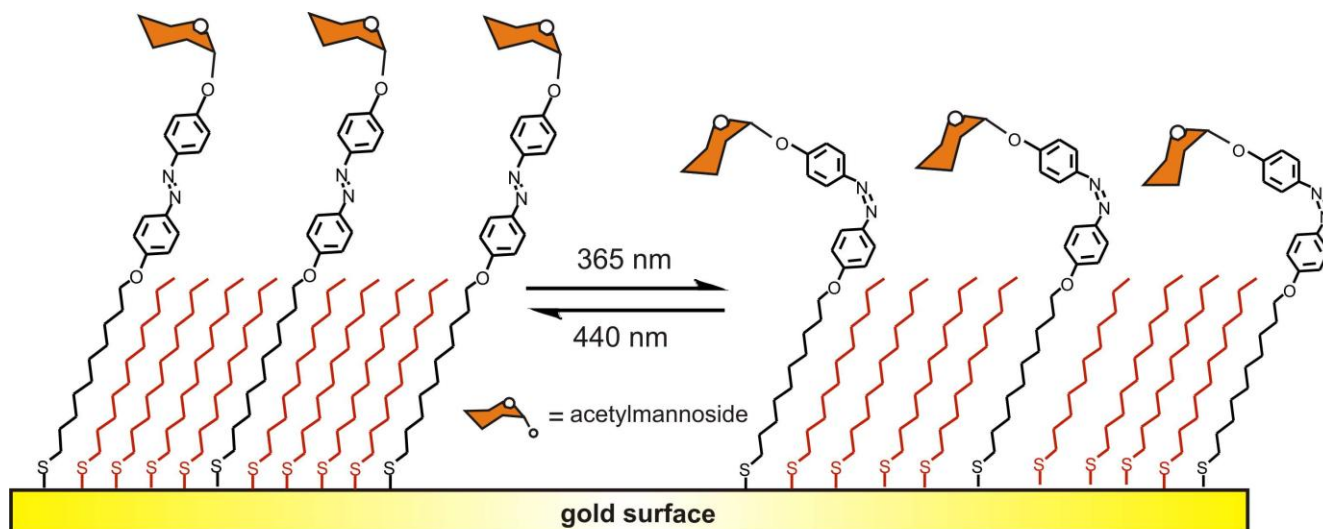


Figure 6.3: mixed SAM formation of azobenzene glycosides with undecane thioacetates (ratio 1:4). $E \rightarrow Z$ isomerisation of mixed SAM on the gold surface was observed by IRRAS.

To understand the conformational control in carbohydrate-protein interactions in multivalent context, photosensitive gold glyconanoparticles (GNPs) were prepared (chapters 4.2). $E \rightarrow Z$ isomerization on the GNPs surface was successfully observed by UV-Vis spectroscopy and dynamic light scattering (DLS) measurements. DLS gave the hydrodynamic diameter $d(H)$ of 29.5 nm for the E -configured GNPs and 16.8 nm for Z -isomer. Interactions of E - and Z -GNPs, respectively, were tested with the lectin ConA and monitored by UV-Vis spectroscopy (Fig 6.4). The results showed that the E -isomer binds ConA more strongly than the Z -isomer. This may be due to the spatial freedom, the E -form of the azobenzene mannoside interacts with the carbohydrate binding sites of ConA effectively. In case of the Z -isomer the terminal mannose is bend downwards, which is critical for lectin binding.

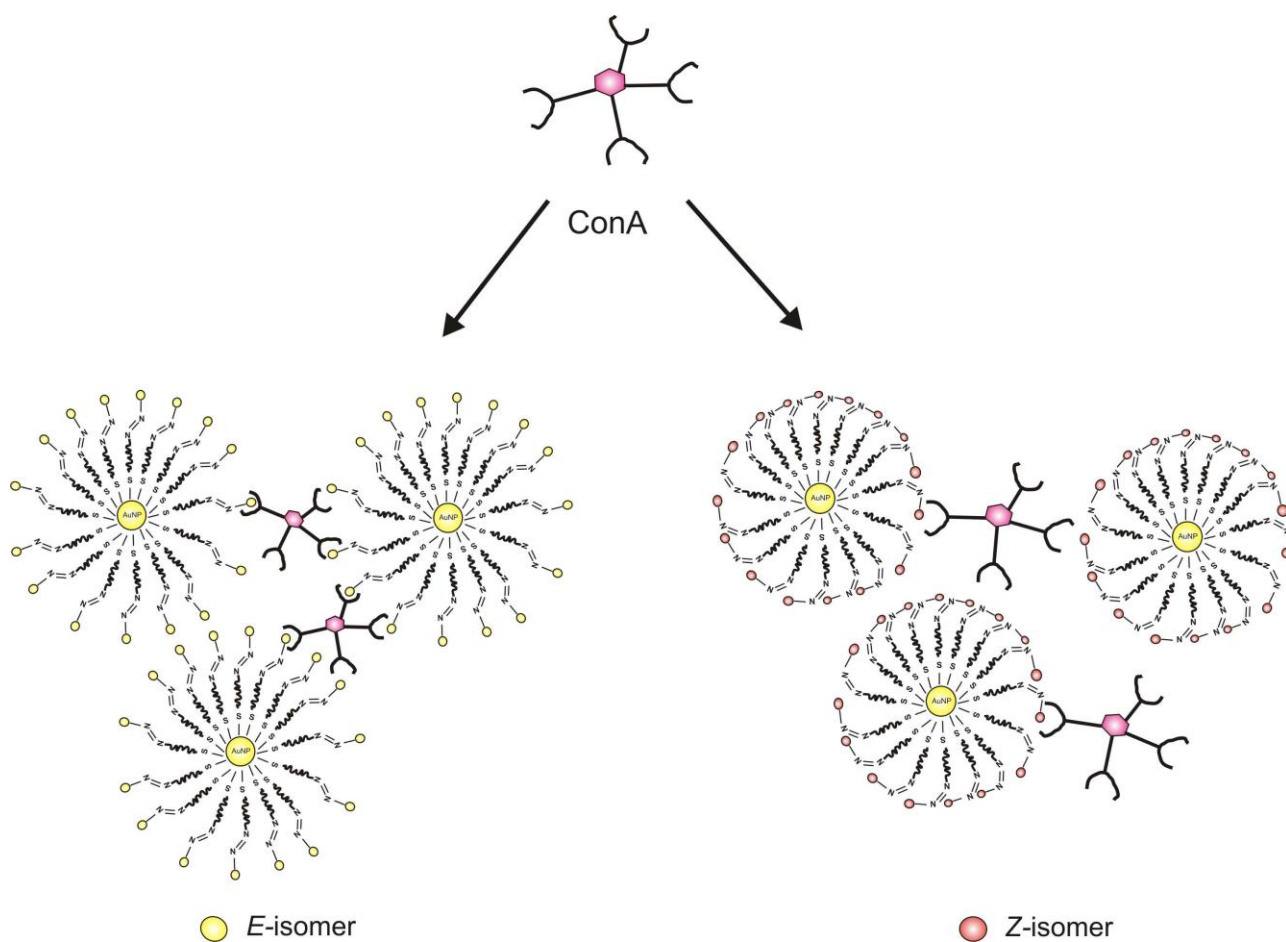


Figure 6.4: Interaction of Con A with *E* and *Z* isomers of photosensitive glyco goldnanoparticles (GNPs). In *E*-isomer ligands are freely available for lectin interactions, whereas in *Z*-isomer ligands are bend downwards making them difficult to interact with lectins.

The above results showed that the conformational changes within azobenzene glycoconjugates lead to clearly pronounced differences in lectin binding once the molecules are immobilized on a surface than when tested in solution. This finding supports that conformational changes of carbohydrate ligands have an effect on cellular adhesion. We strongly believe that the results reported here will shed some light on the importance of conformational control in carbohydrate-receptor functions and will lead to a considerable attention and deeper interest in glycobiology.

Appendix

References

- [1] A. Varki, *Glycobiology* **1993**, *3*, 97-130.
- [2] T. K. Lindhorst, *Essentials of Carbohydrate Chemistry and Biochemistry*, 3rd ed., Wiley-VCH, Weinheim **2007**.
- [3] F. Dang, E. Maeda, T. Osafune, K. Nakajima, K. Kakehi, M. Ishikawa, Y. Baba, *Anal. Chem.* **2009**, *81*, 10055-10060.
- [4] R. B. Dodd, K. Drickamer, *Glycobiology* **2001**, *11*, 71R-79R.
- [5] H. Lis, N. Sharon, *Chem. Rev.* **1998**, *98*, 637-674.
- [6] J. M. Rini, *Annu. Rev. Biophys. Biomol. Struct.* **1995**, *24*, 551-577.
- [7] X. Zeng, C. A. S. Andrade, M. D. L. Oliveira, X.-L. Sun, *Anal. Bioanal. Chem.* **2012**, *402*, 3161-3176.
- [8] R. U. Lemieux, *Chem. Soc. Rev.* **1989**, *18*, 347-374.
- [9] T. K. Lindhorst, *Oligosaccharides and Glycoconjugates in Recognition*, In: *Carbohydrate-Modifying Biocatalysts*, P. Grunwald (Ed.), Pan Stanford Publishing Pte. Ltd., New Jersey, London, Singapore, **2011**, 119-182.
- [10] Y. M. Chabre, R. Roy, *Chem. Soc. Rev.* **2013**, doi: 10.1039/c3cs35483k, *in press*.
- [11] M. Mammen, S-K. Choi, G. M. Whitesides, *Angew. Chem.* **1998**, *110*, 2908-2953; *Angew. Chem. Int. Ed.* **1998**, *37*, 2754-2794.
- [12] L. L. Kiessling, N. L. Pohl, *Chem. Biol.* **1996**, *3*, 71-77.
- [13] Y. C. Lee, R. T. Lee, *Acc. Chem. Res.* **1995**, *28*, 321-327.
- [14] C. L. Yuan, *Carbohydr. Res.* **1978**, *67*, 509-514.
- [15] C. Fasting, C. A. Schalley, M. Weber, O. Seitz, S. Hecht, B. Kokschi, J. Dervedde, C. Graf, E.-W. Knapp, R. Haag, *Angew. Chem.* **2012**, *124*, 10622-10650; *Angew. Chem. Int. Ed.* **2012**, *51*, 10472-10498.
- [16] W. J. Lees, A. Spaltenstein, J. E. Kingery-Wood, G. M. Whitesides, *J. Med. Chem.* **1994**, *37*, 3419-3433.
- [17] R. A. Dwek, *Chem. Rev.* **1996**, *96*, 683-720.
- [18] S. D. Burke, Q. Zhao, M. C. Schuster, L. L. Kiessling, *J. Am. Chem. Soc.* **2000**, *122*, 4518-4519.
- [19] C. R. Bertozzi, L. L. Kiessling, *Science* **2001**, *291*, 2357-2364.

- [20] D. Osrin, S. Vergnano, A. Costello, *Curr. Opin. Infect. Dis.* **2004**, *17*, 217-224.
- [21] C. S. Hung, J. Bouckaert, D. Hung, J. Pinkner, C. Widberg, A. DeFusco, C. G. Auguste, R. Strouse, S. Langermann, G. Waksman, S. J. Hultgren, *Mol. Microbiol.* **2002**, *44*, 903-915.
- [22] M. Hartmann, T. K. Lindhorst, *Eur. J. Org. Chem.* **2011**, *20*, 3583-3609.
- [23] H. Remaut, C. Tang, N. S. Henderson, J. S. Pinkner, T. Wang, S. J. Hultgren, D. G. Thanassi, G. Waksman, H. Li, *Cell* **2008**, *133*, 640-652.
- [24] S. D. Knight, J. Bouckaert, *Top. Curr. Chem.* **2009**, *288*, 67-107.
- [25] I. Le Trong, P. Aprikian, B. A. Kidd, M. Forero-Shelton, V. Tchesnokova, P. Rajagopal, V. Rodriguez, G. Interlandi, R. Klevit, V. Vogel, R. E. Stenkamp, E. V. Sokurenko, W. E. Thomas, *Cell* **2010**, *141*, 645-655.
- [26] M. Dubber, O. Sperling, T. K. Lindhorst, *Org. Biomol. Chem.* **2006**, *4*, 3901-3912.
- [27] M. Kleinert, T. Winkler, A. Terfort, T. K. Lindhorst, *Org. Biomol. Chem.* **2008**, *6*, 2118-2132.
- [28] Grabosch, M. Hartmann, J. Schmidt-Lassen, T. K. Lindhorst, *ChemBioChem* **2011**, *12*, 1066-1074.
- [29] J. Bouckaert, J. Berglund, M. Schembri, E. De Genst, L. Cools, M. Wuhrer, C.-S. Hung, J. Pinkner, R. Slättegård, A. Zavialov, D. Choudhury, S. Langermann, S. J. Hultgren, L. Wyns, P. Klemm, S. Oscarson, S. D. Knight, H. De Greve, *Mol. Microbiol.* **2005**, *55*, 441-455.
- [30] D. Choudhury, A. Thompson, V. Stojanoff, S. Langermann, J. Pinkner, S. J. Hultgren, S. D. Knight, *Science* **1999**, *285*, 1061-1066.
- [31] A. Wellens, C. Garofalo, H. Nguyen, N. Van Gerven, R. Slaettedgard, J. P. Hernalsteens, L. Wyns, S. Oscarson, H. De Greve, S. Hultgren and J. Bouckaert, *PLoS One* **2008**, *3*, 1-13.
- [32] Z. Han, J. S. Pinkner, B. Ford, R. Obermann, W. Nolan, S. A. Wildman, D. Hobbs, T. Ellenberger, C. K. Cusumano, S. J. Hultgren, J. W. Janetka, *J. Med. Chem.* **2010**, *53*, 4779-4792.
- [33] O. Sperling, A. Fuchs, T. K. Lindhorst, *Org. Biomol. Chem.* **2006**, *4*, 3913-3922.
- [34] M. Scharenberg, O. Schwardt, S. Rabbani, B. Ernst, *J. Med. Chem.* **2012**, *55*, 9810-9816.
- [35] R. J. Pieters, *Med. Res. Rev.* **2007**, *27*, 796-816.

- [36] H. Herzner, T. Reipen, M. Schultz, H. Kunz, *Chem. Rev.* **2000**, *100*, 4495-4538.
- [37] D. P. Gamblin, E. M. Scanlan, B. G. Davis, *Chem. Rev.* **2008**, *109*, 131-163.
- [38] X. Zhu, R. R. Schmidt, *Angew. Chem.* **2009**, *121*, 1932-1967; *Angew. Chem. Int. Ed.* **2009**, *48*, 1900-1934.
- [39] L. L. Kiessling, J. E. Gestwicki, L. E. Strong, *Angew. Chem.* **2006**, *118*, 2408-2429; *Angew. Chem. Int. Ed.* **2006**, *45*, 2348-2368.
- [40] N. Jayaraman, *Chem. Soc. Rev.* **2009**, *38*, 3463-3483.
- [41] T. K. Lindhorst, *Top. Curr. Chem.* **2002**, *218*, 201-235.
- [42] M. Lahmann, *Top. Curr. Chem.* **2009**, *288*, 17-65.
- [43] V. Chandrasekaran, K. Kolbe, F. Beiroth, T. K. Lindhorst, *Beilstein J. Org. Chem.* **2013**, *9*, 223-233.
- [44] V. Chandrasekaran, T. K. Lindhorst, *Chem. Commun.* **2012**, *48*, 7519-7521.
- [45] C. Grabosch, K. Kolbe, T. K. Lindhorst, *ChemBioChem* **2012**, *13*, 1874-1879.
- [46] Y. M. Chabre, R. Roy, *Adv. Carbohydr. ChemBioChem.* **2010**, *63*, 165-393.
- [47] R. Roy, D. Zanini, S. J. Meunier, A. Romanowska, *J. Chem. Soc., Chem. Commun.* **1993**, 1869-1872.
- [48] N. Röckendorf, T. K. Lindhorst, *Top. Curr. Chem.* **2001**, *217*, 201-238.
- [49] B. T. Houseman, M. Mrksich, *Chem. Biol.* **2002**, *9*, 443-454.
- [50] K. Palczewski, T. Kumasaka, T. Hori, C. A. Behnke, H. Motoshima, B. A. Fox, I. L. Trong, D. C. Teller, T. Okada, R. E. Stenkamp, M. Yamamoto, M. Miyano, *Science* **2000**, *289*, 739-745.
- [51] X. Tang, I. J. Dmochowski, *Mol. BioSyst.* **2007**, *3*, 100-110.
- [52] I. Ahmed, L. Fruk, *Mol. BioSyst.* **2012**, *9*, 565-570.
- [53] F. Erdmann, Y. Zhang, *Mol. BioSyst.* **2012**, *6*, 2103-2109.
- [54] F. M. Raymo, M. Tomasulo, *Chem. Soc. Rev.* **2005**, *34*, 327-336.
- [55] S. V. Paramonov, V. Lokshin, O. A. Fedorova, *J. Photochem. Photobiol. C., Photochem. Rev.* **2012**, *12*, 209-236.
- [56] Y.-H. Chan, M. E. Gallina, X. Zhang, I. C. Wu, Y. Jin, W. Sun, D. T. Chiu, *Anal. Chem.* **2012**, *84*, 9431-9438.
- [57] J. Cusido, E. Deniz, F. M. Raymo, *Eur. J. Org. Chem.* **2009**, *2009*, 2031-2045.
- [58] T. Koshido, T. Kawai, K. Yoshino, *J. Phys. Chem.* **1995**, *99*, 6110-6114.
- [59] S. Zhiyuan, R. S. Hosmane, M. Tadros, *Tetrahedron Lett.* **1995**, *36*, 3453-3456.

- [60] P. J. Darcy, H. G. Heller, P. J. Strydom, J. Whittall, *J. Chem. Soc., Perkin Trans. 1* **1981**, 202-205.
- [61] M. Jang, L. Cai, G. O. Udeani, K. V. Slowing, C. F. Thomas, C. W. W. Beecher, H. H. S. Fong, N. R. Farnsworth, A. D. Kinghorn, R. G. Mehta, R. C. Moon, J. M. Pezzuto, *Science* **1997**, *275*, 218-220.
- [62] S. Karki, S. Bhutle, S. Sahoo, R. Reddy, J. Balzarini, E. Clercq, S. Darji, *Med. Chem. Res.* **2011**, *20*, 1349-1356.
- [63] M. Frombaum, S. L. Clanche, D. B. Rousselot, D. Borderie, *Biochimie* **2011**, *94*, 269-276.
- [64] F. Krollpfeiffer, C. Mühlhausen, G. Wolf, *Justus Liebigs Ann. Chem.* **1934**, *508*, 39-51.
- [65] M.-M. Russew, S. Hecht, *Adv. Mater.* **2010**, *22*, 3348-3360.
- [66] A. Noble, *Justus Liebigs Ann. Chem.* **1856**, *98*, 253-256.
- [67] C. U. Bang, A. Shishido, T. Ikeda, *Macromol. Rapid Commun.* **2007**, *28*, 1040-1044.
- [68] L. Li, *Mol. Cryst. Liq. Cryst.* **2013**, *518*, 172-172.
- [69] F. Puntoriero, P. Ceroni, V. Balzani, G. Bergamini, F. Vögtle, *J. Am. Chem. Soc.* **2007**, *129*, 10714-10719.
- [70] B. L. Feringa, R. A. van Delden, N. Koumura, E. M. Geertsema, *Chem. Rev.* **2000**, *100*, 1789-1816.
- [71] M. R. Banghart, A. Mourrot, D. L. Fortin, J. Z. Yao, R. H. Kramer, D. Trauner, *Angew. Chem.* **2009**, *121*, 9261-9265; *Angew. Chem. Int. Ed.* **2009**, *48*, 9097-9101.
- [72] A. A. Beharry, G. A. Woolley, *Chem. Soc. Rev.* **2011**, *40*, 4422-4437.
- [73] A. Jain, Y. Gupta, S. K. Jain, *Crit. Rev. Ther. Drug Carrier Syst.* **2006**, *23*, 349-400
- [74] S. Venkataramani, U. Jana, M. Dommaschk, F. D. Sönnichsen, F. Tucek, R. Herges, *Science* **2011**, *331*, 445-448.
- [75] F. Hamon, F. Djedaini-Pilard, F. Barbot, C. Len, *Tetrahedron* **2009**, *65*, 10105-10123.
- [76] E. Merino, *Chem. Soc. Rev.* **2011**, *40*, 3835-3853.
- [77] J. García-Amorós, D. Velasco, *Beilstein J. Org. Chem.* **2012**, *8*, 1003-1017.
- [78] H. Rau, E. Lueddecke, *J. Am. Chem. Soc.* **1982**, *104*, 1616-1620.
- [79] C. R. Crecca, A. E. Roitberg, *J. Phys. Chem. A* **2006**, *110*, 8188-8203.

- [80] H. M. D. Bandara, S. C. Burdette, *Chem. Soc. Rev.* **2012**, *41*, 1809-1825.
- [81] V. Balzani, M. Clemente-León, A. Credi, B. Ferrer, M. Venturi, A. H. Flood, J. F. Stoddart, *Proc. Natl. Acad. Sci. USA* **2006**, *103*, 1178-1183.
- [82] N. Tamai, H. Miyasaka, *Chem. Rev.* **2000**, *100*, 1875-1890.
- [83] O. Sadovski, A. A. Beharry, F. Zhang, G. A. Woolley, *Angew. Chem.* **2009**, *121*, 1512-1514; *Angew. Chem. Int. Ed.* **2009**, *48*, 1484-1486.
- [84] P. Gorostiza, E. Isacoff, *Mol. BioSyst.* **2007**, *3*, 686-704.
- [85] O. Srinivas, N. Mitra, A. Surolia, N. Jayaraman, *Glycobiology* **2005**, *15*, 861-873.
- [86] C. Dohno, K. Nakatani, *Chem. Soc. Rev.* **2011**, *40*, 5718-5729.
- [87] C. Dohno, S. N. Uno, K. Nakatani, *J. Am. Chem. Soc.* **2007**, *129*, 11898-11899.
- [88] C. Renner, L. Moroder, *ChemBioChem* **2006**, *7*, 868-878.
- [89] J. Bredenbeck, J. Helbing, J. R. Kumita, G. A. Woolley, P. Hamm, *Proc. Natl. Acad. Sci. USA* **2005**, *102*, 2379-2384.
- [90] J. A. Ihalainen, B. Paoli, S. Muff, E. H. G. Backus, J. Bredenbeck, G. A. Woolley, A. Caflisch, P. Hamm, *Proc. Natl. Acad. Sci. USA* **2008**, *105*, 9588-9593.
- [91] G. A. Woolley, *Acc. Chem. Res.* **2005**, *38*, 486-493.
- [92] J. R. Kumita, D. G. Flint, O. S. Smart, G. A. Woolley, *Protein Eng.* **2002**, *15*, 561-569.
- [93] B. F. Erlanger, *Annu. Rev. Biochem.* **1976**, *45*, 267-284.
- [94] P. Gorostiza, E. Y. Isacoff, *physiology* **2008**, *23*, 238-247.
- [95] E. Bartels, N. H. Wassermann, B. F. Erlanger, *Proc. Natl. Acad. Sci. USA* **1971**, *68*, 1820-1823.
- [96] L. Lien, D. C. J. Jaikaran, Z. Zhang, G. A. Woolley, *J. Am. Chem. Soc.* **1996**, *118*, 12222-12223.
- [97] C. J. Stankovic, S. H. Heinemann, S. L. Schreiber, *Biochim. Biophys. Acta*, **1991**, *1061*, 163-170.
- [98] M. Banghart, K. Borges, E. Isacoff, D. Trauner, R. H. Kramer, *Nat. Neurosci.* **2004**, *7*, 1381-1386.
- [99] M. Volgraf, P. Gorostiza, R. Numano, R. H. Kramer, E. Y. Isacoff, D. Trauner, *Nat. Chem. Biol.* **2006**, *2*, 47-52.
- [100] C. Wyart, F. D. Bene, E. Warp, E. K. Scott, D. Trauner, H. Baier, E. Y. Isacoff, *Nature* **2009**, *461*, 407-410.

- [101] X. Qian, S. J. Metallo, I. S. Choi, H. Wu, M. N. Liang, G. M. Whitesides, *Anal. Chem.* **2002**, *74*, 1805-1810.
- [102] N. Strömberg, P. G. Nyholm, I. Pascher, S. Normark, *Proc. Natl. Acad. Sci.* **1991**, *88*, 9340-9344.
- [103] O. Srinivas, N. Mitra, A. Surolia, N. Jayaraman, *J. Am. Chem. Soc.* **2002**, *124*, 2124-2125.
- [104] J. W. Wehner, M. J. Weissenborn, M. Hartmann, C. J. Gray, R. Sardzik, C. E. Eyers, S. L. Flitsch, T. K. Lindhorst, *Org. Biomol. Chem.* **2012**, *10*, 8919-8926.
- [105] J. W. Wehner, M. Hartmann, T. K. Lindhorst, *Carbohydr. Res.* **2013**, *371*, 22-31.
- [106] M. J. Weissenborn, R. Castangia, J. W. Wehner, R. Sardzik, T. K. Lindhorst, S. L. Flitsch, *Chem. Commun.* **2012**, *48*, 4444-4446.
- [107] J. C. Love, L. A. Estroff, J. K. Kriebel, R. G. Nuzzo, G. M. Whitesides, *Chem. Rev.* **2005**, *105*, 1103-1170.
- [108] R. Klajn, *Pure Appl. Chem.*, **2010**, *82*, 2247-2279.
- [109] C. Grabosch, M. Kleinert, T. K. Lindhorst, *Synthesis* **2010**, 828-836.
- [110] M. Kleinert, N. Röckendorf, T. K. Lindhorst, *Eur. J. Org. Chem.* **2004**, 3931-3940.
- [111] C. Grabosch, M. Kind, Y. Gies, F. Schweighöfer, A. Terfort, T. K. Lindhorst, *Org. Biomol. Chem.* **2013**, *11*, 4006-4015.
- [112] M. B. Thygesen, K. K. Sorensen, E. Cló, K. J. Jensen, *Chem. Commun.* **2009**, 6367-6369.
- [113] M. B. Thygesen, J. Sauer, K. J. Jensen, *Chem. Eur. J.* **2009**, *15*, 1649-1660.
- [114] N. C. Reichardt, M. Martin-Lomas, S. Penadés, *Chem. Soc. Rev.* **2013**, *42*, 4358-4376.
- [115] M. Marradi, F. Chiodo, I. García, S. Penadés, *Chem. Soc. Rev.* **2013**, in press.

Permissions for reprinting of Figures

In chapter 1 & 2, the figures are adapted with the permission from the cited journals/articles. A proof for the licenses can be found in this section.



RightsLink®

[Home](#)
[Account Info](#)
[Help](#)


Title: Multivalency as a Chemical Organization and Action Principle

Author: Carlo Fasting, Christoph A. Schalley, Marcus Weber, Oliver Seitz, Stefan Hecht, Beate Kokschi, Jens Dornedde, Christina Graf, Ernst-Walter Knapp, Rainer Haag

Publication: Angewandte Chemie International Edition

Publisher: John Wiley and Sons

Date: Sep 5, 2012

Copyright © 2012 WILEY-VCH Verlag GmbH & Co. KGaA, Weinheim

Logged in as:

vijayanand chandrasekaran

Account #:
3000676541

[LOGOUT](#)

Order Completed

Thank you very much for your order.

This is a License Agreement between vijayanand chandrasekaran ("You") and John Wiley and Sons ("John Wiley and Sons"). The license consists of your order details, the terms and conditions provided by John Wiley and Sons, and the [payment terms and conditions](#).

[Get the printable license.](#)

License Number	3194810024601
License date	Jul 23, 2013
Licensed content publisher	John Wiley and Sons
Licensed content publication	Angewandte Chemie International Edition
Licensed content title	Multivalency as a Chemical Organization and Action Principle
Licensed copyright line	Copyright © 2012 WILEY-VCH Verlag GmbH & Co. KGaA, Weinheim
Licensed content author	Carlo Fasting, Christoph A. Schalley, Marcus Weber, Oliver Seitz, Stefan Hecht, Beate Kokschi, Jens Dornedde, Christina Graf, Ernst-Walter Knapp, Rainer Haag
Licensed content date	Sep 5, 2012
Start page	10472
End page	10498
Type of use	Dissertation/Thesis
Requestor type	University/Academic
Format	Print and electronic
Portion	Figure/table
Number of figures/tables	1
Original Wiley figure/table number(s)	1
Will you be translating?	No
Total	0.00 USD

[ORDER MORE...](#)

[CLOSE WINDOW](#)

Copyright © 2013 [Copyright Clearance Center, Inc.](#) All Rights Reserved. [Privacy statement](#).
Comments? We would like to hear from you. E-mail us at customercare@copyright.com



RightsLink®

[Home](#)
[Account Info](#)
[Help](#)


Title: The Bacterial Lectin FimH, a Target for Drug Discovery – Carbohydrate Inhibitors of Type 1 Fimbriae-Mediated Bacterial Adhesion

Author: Mirja Hartmann, Thisbe K. Lindhorst

Publication: European Journal of Organic Chemistry

Publisher: John Wiley and Sons

Date: Jun 15, 2011

Copyright © 2011 WILEY-VCH Verlag GmbH & Co. KGaA, Weinheim

Logged in as:

vijayanand chandrasekaran

Account #:

3000676541

[LOGOUT](#)

Order Completed

Thank you very much for your order.

This is a License Agreement between vijayanand chandrasekaran ("You") and John Wiley and Sons ("John Wiley and Sons"). The license consists of your order details, the terms and conditions provided by John Wiley and Sons, and the [payment terms and conditions](#).

[Get the printable license.](#)

License Number	3194811105500
License date	Jul 23, 2013
Licensed content publisher	John Wiley and Sons
Licensed content publication	European Journal of Organic Chemistry
Licensed content title	The Bacterial Lectin FimH, a Target for Drug Discovery – Carbohydrate Inhibitors of Type 1 Fimbriae-Mediated Bacterial Adhesion
Licensed copyright line	Copyright © 2011 WILEY-VCH Verlag GmbH & Co. KGaA, Weinheim
Licensed content author	Mirja Hartmann, Thisbe K. Lindhorst
Licensed content date	Jun 15, 2011
Start page	3583
End page	3609
Type of use	Dissertation/Thesis
Requestor type	University/Academic
Format	Print and electronic
Portion	Figure/table
Number of figures/tables	1
Original Wiley figure/table number(s)	1
Will you be translating?	No
Total	0.00 USD

[ORDER MORE...](#)

[CLOSE WINDOW](#)

Copyright © 2013 [Copyright Clearance Center, Inc.](#) All Rights Reserved. [Privacy statement](#).
Comments? We would like to hear from you. E-mail us at customercare@copyright.com



RightsLink®

[Home](#)
[Account Info](#)
[Help](#)


Title: Fiber Formation across the Bacterial Outer Membrane by the Chaperone/Usher Pathway

Author: Han Remaut, Chunyan Tang, Nadine S. Henderson, Jerome S. Pinkner, Tao Wang, Scott J. Hultgren, David G. Thanassi, Gabriel Waksman, Huilin Li

Logged in as:
vijayanand chandrasekaran
Account #:
3000676541

[LOGOUT](#)

Publication: Cell

Publisher: Elsevier

Date: 16 May 2008

Copyright © 2008, Elsevier

Order Completed

Thank you very much for your order.

This is a License Agreement between vijayanand chandrasekaran ("You") and Elsevier ("Elsevier"). The license consists of your order details, the terms and conditions provided by Elsevier, and the [payment terms and conditions](#).

[Get the printable license.](#)

License Number	3194830301833
License date	Jul 23, 2013
Licensed content publisher	Elsevier
Licensed content publication	Cell
Licensed content title	Fiber Formation across the Bacterial Outer Membrane by the Chaperone/Usher Pathway
Licensed content author	Han Remaut, Chunyan Tang, Nadine S. Henderson, Jerome S. Pinkner, Tao Wang, Scott J. Hultgren, David G. Thanassi, Gabriel Waksman, Huilin Li
Licensed content date	16 May 2008
Licensed content volume number	133
Licensed content issue number	4
Number of pages	13
Type of Use	reuse in a thesis/dissertation
Portion	figures/tables/illustrations
Number of figures/tables /illustrations	1
Format	both print and electronic
Are you the author of this Elsevier article?	No
Will you be translating?	No
Order reference number	
Title of your thesis/dissertation	Sweet switches: Azobenzene glycosides as photosensitive lectin inhibitors in solution and on surfaces
Expected completion date	Jul 2013
Elsevier VAT number	GB 494 6272 12
Permissions price	0.00 EUR
VAT/Local Sales Tax	0.00 EUR
Total	0.00 EUR

ORDER MORE...

CLOSE WINDOW

Copyright © 2013 [Copyright Clearance Center, Inc.](#) All Rights Reserved. [Privacy statement](#).
Comments? We would like to hear from you. E-mail us at customercare@copyright.com



RightsLink®

[Home](#)
[Account Info](#)
[Help](#)


Title: Azobenzenes—synthesis and carbohydrate applications

Author: Florian Hamon, Florence Djedaini-Pilard, Francis Barbot, Christophe Len

Publication: Tetrahedron

Publisher: Elsevier

Date: 5 December 2009

Copyright © 2009, Elsevier

Logged in as:

vijayanand chandrasekaran

Account #:

3000676541

[LOGOUT](#)

Order Completed

Thank you very much for your order.

This is a License Agreement between vijayanand chandrasekaran ("You") and Elsevier ("Elsevier"). The license consists of your order details, the terms and conditions provided by Elsevier, and the [payment terms and conditions](#).

[Get the printable license.](#)

License Number	3195360875348
License date	Jul 24, 2013
Licensed content publisher	Elsevier
Licensed content publication	Tetrahedron
Licensed content title	Azobenzenes—synthesis and carbohydrate applications
Licensed content author	Florian Hamon, Florence Djedaini-Pilard, Francis Barbot, Christophe Len
Licensed content date	5 December 2009
Licensed content volume number	65
Licensed content issue number	49
Number of pages	19
Type of Use	reuse in a thesis/dissertation
Portion	figures/tables/illustrations
Number of figures/tables /illustrations	1
Format	both print and electronic
Are you the author of this Elsevier article?	No
Will you be translating?	No
Order reference number	
Title of your thesis/dissertation	Sweet switches: Azobenzene glycosides as photosensitive lectin inhibitors in solution and on surfaces
Expected completion date	Jul 2013
Elsevier VAT number	GB 494 6272 12
Permissions price	0.00 EUR
VAT/Local Sales Tax	0.00 EUR
Total	0.00 EUR

[ORDER MORE...](#)

[CLOSE WINDOW](#)

Copyright © 2013 [Copyright Clearance Center, Inc.](#) All Rights Reserved. [Privacy statement](#).
Comments? We would like to hear from you. E-mail us at customercare@copyright.com



RightsLink®

[Home](#)[Account Info](#)[Help](#)**Title:** Photoswitchable Molecular Glue for DNALogged in as:
vijayanand chandrasekaran**Author:** Chikara Dohno, Shin-nosuke Uno, and, and Kazuhiko Nakatani*Account #:
3000676541[LOGOUT](#)**Publication:** Journal of the American Chemical Society**Publisher:** American Chemical Society**Date:** Oct 1, 2007

Copyright © 2007, American Chemical Society

PERMISSION/LICENSE IS GRANTED FOR YOUR ORDER AT NO CHARGE

This type of permission/license, instead of the standard Terms & Conditions, is sent to you because no fee is being charged for your order. Please note the following:

- Permission is granted for your request in both print and electronic formats, and translations.
- If figures and/or tables were requested, they may be adapted or used in part.
- Please print this page for your records and send a copy of it to your publisher/graduate school.
- Appropriate credit for the requested material should be given as follows: "Reprinted (adapted) with permission from (COMPLETE REFERENCE CITATION). Copyright (YEAR) American Chemical Society." Insert appropriate information in place of the capitalized words.
- One-time permission is granted only for the use specified in your request. No additional uses are granted (such as derivative works or other editions). For any other uses, please submit a new request.

If credit is given to another source for the material you requested, permission must be obtained from that source.

[BACK](#)[CLOSE WINDOW](#)

Copyright © 2013 [Copyright Clearance Center, Inc.](#) All Rights Reserved. [Privacy statement.](#)
Comments? We would like to hear from you. E-mail us at customercare@copyright.com



RightsLink®

[Home](#)[Account Info](#)[Help](#)

Title: Photocontrolling Peptide α Helices

Logged in as:

vijayanand chandrasekaran

Author: G. Andrew Woolley*

Account #:

3000676541

Publication: Accounts of Chemical Research

Publisher: American Chemical Society

[LOGOUT](#)

Date: Jun 1, 2005

Copyright © 2005, American Chemical Society

PERMISSION/LICENSE IS GRANTED FOR YOUR ORDER AT NO CHARGE

This type of permission/license, instead of the standard Terms & Conditions, is sent to you because no fee is being charged for your order. Please note the following:

- Permission is granted for your request in both print and electronic formats, and translations.
- If figures and/or tables were requested, they may be adapted or used in part.
- Please print this page for your records and send a copy of it to your publisher/graduate school.
- Appropriate credit for the requested material should be given as follows: "Reprinted (adapted) with permission from (COMPLETE REFERENCE CITATION). Copyright (YEAR) American Chemical Society." Insert appropriate information in place of the capitalized words.
- One-time permission is granted only for the use specified in your request. No additional uses are granted (such as derivative works or other editions). For any other uses, please submit a new request.

If credit is given to another source for the material you requested, permission must be obtained from that source.

[BACK](#)[CLOSE WINDOW](#)

Copyright © 2013 [Copyright Clearance Center, Inc.](#) All Rights Reserved. [Privacy statement.](#)
Comments? We would like to hear from you. E-mail us at customercare@copyright.com



RightsLink®

[Home](#)[Account Info](#)[Help](#)

Title: Nanoengineering Ion Channels for Optical Control

Author: Pau Gorostiza, Ehud Y. Isacoff

Publication: Physiology

Publisher: The American Physiological Society

Date: Oct 1, 2008

Copyright © 2008, The American Physiological Society

Logged in as:

vijayanand chandrasekaran

Account #:

3000676541

[LOGOUT](#)

Permission Not Required

Permission is not required for this type of use.

[BACK](#)[CLOSE WINDOW](#)

Copyright © 2013 [Copyright Clearance Center, Inc.](#) All Rights Reserved. [Privacy statement.](#)
Comments? We would like to hear from you. E-mail us at customercare@copyright.com

Acknowledgement

It is really difficult to mention all the people who have helped me along the way during the long journey to achieve my academic goal.

Especially I hereby want to express my sincere thanks to,

My supervisor, Prof. Dr. Thisbe K. Lindhorst for her guidance, support, and also giving me the opportunity to pursue my graduate studies in her lab. Her enthusiasm, motivation and high standards in research always encouraged me to keep on pursuing interesting research.

Anu & Kashi (former members of Prof. Lindhorst research group) for referring me to join in Prof. Lindhorst group.

Prof. Dr. F. Sönnichsen for the fruitful NMR discussions and his team members for spectral analysis. Particularly, Frau Marion Höftmann and Frau Gitta Kohlmeyer-Yilmaz for their excellent NMR service.

COST office for my travel grant for short term scientific mission project (STSM) and Prof. Dr. Knud J. Jensen for allowing me to work in his group at University of Copenhagen, Denmark. Also, Mikkel B. Thygesen for supervising my work.

Frau Christine Haug for helping in official matters. I am very fortunate to have an english speaking secretary.

Frau Elwira for being kind and friendly throughout my stay in this group.

My colleagues Arne Stindt, Alexander Thrun, Kirsten Schwekendiek, Lena Fernando, Johannes Wehner, Carsten Grabosch, Mirja Hartmann, Martin Weissenborn, Eugen Johannes, Anna Ciuk, Sören Gutekunst, Bianca Kunz, Claudia Fessele, Michel Riese (still struggling to pronounce his name correctly) and Oksana Sereda. Especially, Femke Beiroth, Anne Müller for correcting my abstract (German version), Tobias Keller and Christian Müller for the very good lab atmosphere (which is really important) and for their constant helps. Computer expert Jörn Schmidt-Lassen (JSL) who is always kind in fixing my computer

related problems from the day I joined, Katharina Kolbe for the nice coffee breaks, my student Max Britz and finally Benjamin Sahlmann for building up the LED light for my irradiation experiments.

Award winning film crew members, Stefan Schwarzer, Frederike Tirre, Felix Wenning and Philip.

My friends in Kiel, Muthuraman, Mahesh, Sugumar, Venkat and Gopakumar`s family for their moral support.

My friends and family members in India, especially my parents, my brother Rajmohan (a) Babuji and my sister Radhika for their understanding and supports even from that long distance. My Akka Merlin for her help, support and proper guidance.

Finally, my lovely wife Kalpana and my cute daughter Diya (boss at home) for their love and constant support.

Curriculum Vitae

Personal data

Name : Vijayanand Chandrasekaran
Date of Birth : 19 June 1978
Place of Birth : Chennai, India
Marital status : Married
Nationality : Indian

Education

1996-1999 : B.Sc, R. K. M. Vivekananda College (Affiliated to University of Madras), Chennai, India
1999-2001 : M.Sc, R. K. M. Vivekananda College (Affiliated University of Madras), Chennai, India
2008-to present : Ph.D thesis under the supervision of Prof. Dr. Thisbe K. Lindhorst, Otto Diels Institute of Organic Chemistry, Christiana Albertina University of Kiel, Germany

Scientific Carrier

2002-2006 : Research Associate, Dr. Reddys Laboratories Ltd, Andhra Pradesh, India
2006-2008 : Research Scientist II, Albany Molecular Research, Singapore Science Park III, Singapore

Publications

1. V. Chandrasekaran, T. K. Lindhorst, Sweet switches: Azobenzene glycoconjugates by click chemistry. *Chem. Commun.* **2012**, 48, 7519-7521.
2. M. Hartmann, H. Papavlassopoulos, V. Chandrasekaran, C. Grabosch, F. Beiroth, T. K. Lindhorst, C.Röhl, Inhibition of Bacterial Adhesion to Live Human Cells: Activity and cytotoxicity of synthetic mannosides. *FEBS Lett.* **2012**, 586, 1459-1465.
3. V. Chandrasekaran, K. Kolbe, F. Beiroth, T. K. Lindhorst, Synthesis and testing of the first azobenzene mannobioside as photoswitchable ligand for the bacterial lectin FimH. *Beilstein J. Org. Chem.* **2013**, 9, 223–233.
4. V. Chandrasekaran, K. Kathirvel, F. Tuzcek, T. K. Lindhorst, Switchable azobenzene glyco-SAMs: Monitoring of *cis-trans* isomerization using infrared reflection absorption spectroscopy IRRAS. *J. Colloid Interface Sci. manuscript in preparation.*
5. V. Chandrasekaran, E. Johannes, H. Kobarg, F. D. Sönnichsen, T. K. Lindhorst, Sweet switches: Synthesis and photochemical properties of azobenzene glycosides. *Chem. Eur. J. manuscript in preparation.*
6. V. Chandrasekaran, M. B. Thygesen, K. J. Jensen, T. K. Lindhorst, Gold glyconanoparticles as a tool to investigate the photo-switchable, multivalent interaction of azobenzene glycoconjugates with the lectin Concanavalin A *Chem. Eur. J. manuscript in preparation.*
7. S. Kalyan, V. Chandrasekaran, E. S. Quabius, T. K. Lindhorst, D. Kabelitz, Neutrophils as mediators of human peripheral blood $\gamma\delta$ T cell loss observed with nitrogen-bisphosphonate use. *J. Bone. Miner. Res. submitted.*

Conference Contributions

- V. Chandrasekaran, T. K. Lindhorst, Switchable azobenzene glyco-SAMs, *16th European Carbohydrate Symposium 2011*, Sorrento - Naples, Italy.
- V. Chandrasekaran, T. K. Lindhorst, Sweet switches: Glycoazobenzenes in carbohydrate recognition, *26th International Carbohydrate Symposium 2012*, Madrid, Spain.
- V. Chandrasekaran, T. K. Lindhorst, Azobenzene glycoconjugates as inhibitors of type 1 fimbriae-mediated adhesion of *Escherichia coli* (*E. coli*), *ORCHEM 2012*, Weimar, Germany.
- F. Beiroth, V. Chandrasekaran, A. K. Ciuk, K. Kolbe, A. Müller, C. Müller, T. K. Lindhorst, Functional multivalent glycomimetics in the glycosciences, *2. International Symposium of the Collaborative Research Center (SFB-765) 2012*, Berlin, Germany. Poster award.
- J. Reverey, V. Chandrasekaran, M. Leippe, T. K. Lindhorst, C. Selhuber-Unkel, Carbohydrate Functionalization of nanostructured surfaces for biological adhesion applications, *2013 MRS Spring Meeting*, San Francisco, U.S.A